Regulation of the actin cytoskeleton in podocytes by the transcription factor LMX1B

DISSERTATION ZUR ERLANGUNG DES DOKTORGRADES DER NATURWISSENSCHAFTEN (DR. RER. NAT.) DER FAKULTÄT FÜR BIOLOGIE UND VORKLINISCHE MEDIZIN DER UNIVERSITÄT REGENSBURG

vorgelegt von

Markus Setzer

aus

Neumarkt i. d. OPf.

im Jahr

2018

Das Promotionsgesuch wurde eingereicht am:

Die Arbeit wurde angeleitet von:

Prof. Dr. Ralph Witzgall

_____

Markus Setzer

Table of Content

1. Introduction

1.1. Nail-patella syndrome

Nail-patella syndrome (NPS) is an autosomal-dominant hereditary disease with an incidence of approximately 1:50 000 (Bongers et al., 2002). While most patients suffer from dysplastic finger- and toenails (95 – 100%; Figure 1.1, A) and absent or hypoplastic patellae (74 - 93%; Figure 1.1, B), the occurrence of other symptoms is both interfamilial and intrafamilial quite diverse. These include iliac horns (68 – 81%), ocular symptoms like glaucoma (10 – 12%), ocular hypertension (4 – 7%) and iris hyperpigmentation (46 – 54%) and for the prognosis most important renal abnormalities (40%) (Witzgall, 2017). Renal symptoms often develop over years and range from mild proteinuria and hematuria to end-stage renal disease (Sweeney et al., 2003). In most cases of NPS, mutations of a gene encoding the LIM homeobox transcription factor 1 beta (LMX1B) is associated to the disease (Dreyer et al., 1998; McIntosh et al., 1998; Vollrath et al., 1998).

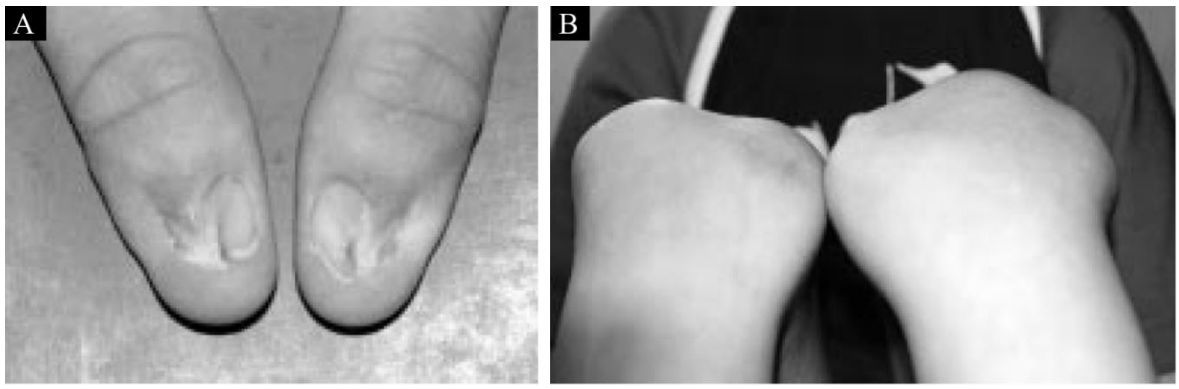

Figure 1.1: **Photographs of nails and knees of NPS patients.** [A] Dysplastic thumbnails. [B] Subluxation of the patellae on knee flexion (Sweeney et al., 2003).

1.2. Structural composition of the kidneys

The kidneys are two bean-shaped organs located retroperitoneal on both sides of the body. They take part in control of electrolyte concentrations, osmolality, acid-base balance and regulation of blood pressure, but most importantly they are responsible for blood filtration. The functional unit of the kidney is the nephron, consisting of the renal corpuscle and a tubular system, subdivided into the proximal and distal tubule (Figure 1.2). The average nephron number per human kidney is around 1 million, but numbers of individuals can differ widely (Bertram et al., 2011). The renal corpuscle is the place of the initial blood filtration resulting in 180 L primary urine per day, which is subsequently concentrated by the adjacent tubular system to 2 – 3 L per day. Histologically the kidney can be divided into the two major parts cortex and medulla. While renal corpuscles and both proximal and distal tubular segments are present in the cortex, the medulla is void of renal corpuscles.

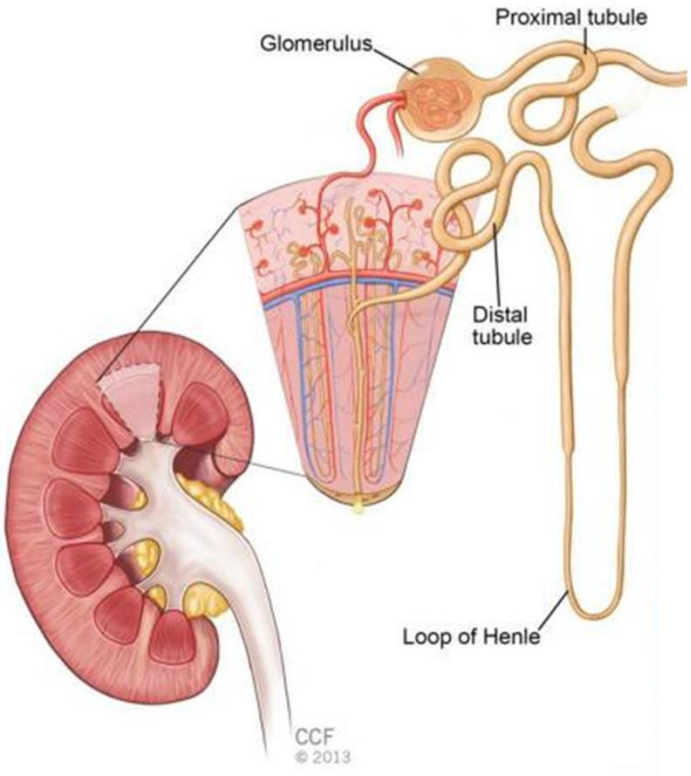

Figure 1.2: **Schematic overview of a kidney and more detailed illustrations of a kidney section and a nephron.** The glomerulus is a part of the renal corpuscle, where the blood is filtered to produce primary urine, which is resorbed to large parts by the following tubular system [modified from (Wessely et al., 2014)].

1.3. The renal corpuscle

The blood is filtered within the renal corpuscles, which are also called Malpighian corpuscles. As in this work, the term glomerulus is often used synonymously, although it describes more precisely the capillary tuft in the center of a renal corpuscle, composed of capillaries and the mesangium (Figure 1.3, A). The mesangium, which consists of the mesangial matrix and mesangial cells, stabilizes the tuft, while the endothelium of the capillary wall is fenestrated allowing the blood to flow through. The capillaries are covered by podocytes at the exterior (Figure 1.3, B), assembling the inner, visceral layer of the Bowman's capsule. The outer leaf of the Bowman's capsule is called parietal layer and is composed of parietal cells, enclosing the whole structure. Located in-between the podocytes and the fenestrated endothelium is the glomerular basement membrane (GBM), an extracellular matrix compartment secreted from both cell types (Figure 1.3, C). The entity of the fenestrated endothelium, the GBM and the podocytes is called glomerular filtration barrier (GFB). The blood enters and leaves the glomerulus through afferent and efferent arterioles at the vascular pole, while the primary urine leaves the renal corpuscle at the opposing urinary pole (Figure 1.3, A).

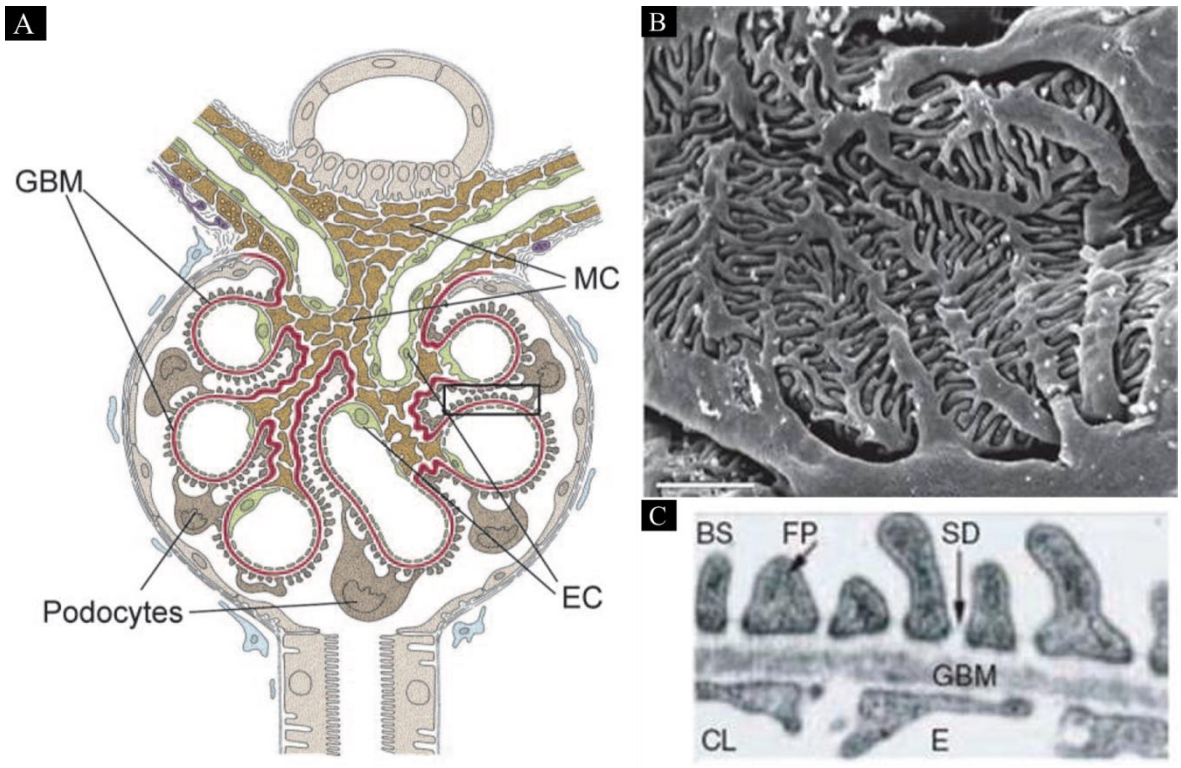

Figure 1.3: **Composition of the renal corpuscle and the glomerular filtration barrier (GFB).** [A] Schematic view of a renal corpuscle. Filtration takes place at the GFB composed of fenestrated endothelial cells (EC), the glomerular basement membrane (GBM, red) and interdigitating foot

processes extending from the podocyte bodies. Mesangial cells (MC) secrete the mesangial matrix, together forming a stabilizing backbone (Sugimoto et al., 2006). [B] SEM micrograph of interdigitating podocyte foot processes of a C57BL/6 mouse attached to the capillary loops; scale bar: 2 µm; (Burghardt et al., 2015) [C] TEM micrograph of a glomerular filtration barrier composed of the fenestrated endothelium (E), the glomerular basement membrane (GBM) and podocyte foot processes (FP). Slit diaphragms (SD) span the gap between adjacent foot processes. (BS), Bowman space; (CL), capillary lumen; (Mundel and Reiser, 2010)

1.4. The glomerular filtration barrier

The transition from blood to primary urine occurs at the glomerular filtration barrier within the renal corpuscle. It is composed of three layers: the fenestrated endothelium, the GBM and the podocytes (Figure 1.3, C). All three layers are thought to take part in blood filtration, but the exact mechanism is still unknown (Moeller and Tenten, 2013). Blood leaves the capillary lumen through the fenestrations and enters Bowman space after passing the GBM and the slit diaphragm of podocytes. Blood cells and most plasma proteins are not able to pass the size and charge selective filtration barrier (Jarad and Miner, 2009), but damage to any of these three layers can lead to protein and blood cell loss via the urine.

1.4.1. Endothelium

The fenestrated endothelium is the first part of the GFB (Figure 1.3, C). Fenestrations have a diameter of 60 - 80 nm, contain no diaphragm and occupy 30 – 40% of the capillary wall (Avasthi et al., 1980; Lea et al., 1989). As the diameter of fenestrations is by far larger than that of albumin, the most abundant plasma protein, it was long time thought that the endothelium does not contribute to blood filtration (Satchell, 2013). However, studies showing proteinuria without alterations of the GBM or the podocyte structure suggested an important role of the endothelium in blood filtration (Eremina et al., 2008; Friden et al., 2011; Sugimoto et al., 2003). These findings can possibly be explained by the glycocalyx covering the endothelial cells, which is comprised of proteoglycans, glycoproteins and sialic acids anchored at the cell surface (Reitsma et al., 2007; Weinbaum et al., 2007). These components serve as a backbone for the adsorption of plasma proteins and excreted soluble proteins like hyaluronic acid, building up a gel-like dynamic structure called the endothelial surface layer (Pries et al., 2000). This layer extends not only into the capillary lumen but also into the fenestrations (Avasthi and Koshy, 1988). Additionally, parts of the endothelial surface layer are sulfated resulting in a net negative charge. As of its gel-like structure and negative charge it is thought to act as a size-selective sieve on the one hand and also as an electrostatic barrier on the other hand (Jeansson and Haraldsson, 2003).

1.4.2. Glomerular basement membrane

The GBM is located between the fenestrated endothelium and the podocytes. Although the present extracellular matrix proteins can also be found in other basement membranes, its isoform composition is rather unique (Figure 1.4, B). The GBM is relatively thick, owed to the fact that it is excreted during nephrogenesis from both the endothelial cells and the podocytes (Abrahamson, 1985; St John and Abrahamson, 2001). The main components of the basement membrane are nidogen, heparin sulfate proteoglycans, laminin-521, collagen α3α4α5(IV) and to a lesser extent collagen α1α1α2(IV) (Lennon et al., 2014a; Paulsson, 1992). Ultra-resolution microscopy showed that the proteoglycan agrin and the C-terminal end of laminin-521 are located in the vicinity of podocytes, whereas collagen α1α1α2(IV) is located near the endothelial cells. Collagen α3α4α5(IV) and nidogen form the middle part of the membrane (Suleiman et al., 2013). Cell-matrix contacts of podocytes are mediated through α3β1-integrin binding to the C-terminal domain of laminin-521 (Figure 1.4, A).

In case of NPS patients, the GBM is thickened with both fibrillary deposits and electron-lucent areas (Ben-Bassat et al., 1971; Del Pozo and Lapp, 1970). This might contribute to renal symptoms, as the importance of a proper GBM structure for GFB function is given by the fact of two hereditary glomerular diseases caused by mutations of basement membrane proteins. One of them is Pierson syndrome, which is caused by mutations of the *LAMB2* gene encoding for the β2 chain of laminin (Zenker et al., 2004). The symptoms of patients vary greatly, dependent on the nature of the mutation, but invariably leads to death in childhood. Truncation mutations result generally in more severe phenotype than missense mutations (Matejas et al., 2010). Mice with *Lamb2* knock-out develop proteinuria and die within three weeks of age (Noakes et al., 1995). Interestingly, proteinuria is already present in week one, while the loss of slit diaphragms and changes in podocyte foot process structure appear in week two (Figure 1.4, C). This suggests a direct role of laminin-521 in blood filtration rather than a secondary effect (Jarad et al., 2006). Forced laminin-511 deposition in the basement membrane prevents nephrotic syndrome in *Lamb2* knock-out mice (Suh et al., 2011). The other hereditary GBM related disease, Alport syndrome, is caused by either mutations in the *COL4A3*, *COL4A4* or *COL4A5* gene coding for collagen type IV α3, α4 or α5 chains, respectively, leading to end-stage renal disease, hearing loss and lens defects (Chew and Lennon, 2018). During nephrogenesis initial collagen α1α1α2(IV) is replaced by collagen α3α4α5(IV) to a great extent, which is not the case in Alport syndrome patients (Kalluri et al., 1997). The altered glomerular basement membrane composition leads to membrane thickening and splitting (Figure 1.4, D). As the glomerular disease develops after years, it is assumed that collagen α3α4α5(IV) is not necessary for blood filtration itself, but may play a role in signaling to podocytes (Gross et al., 2004)..

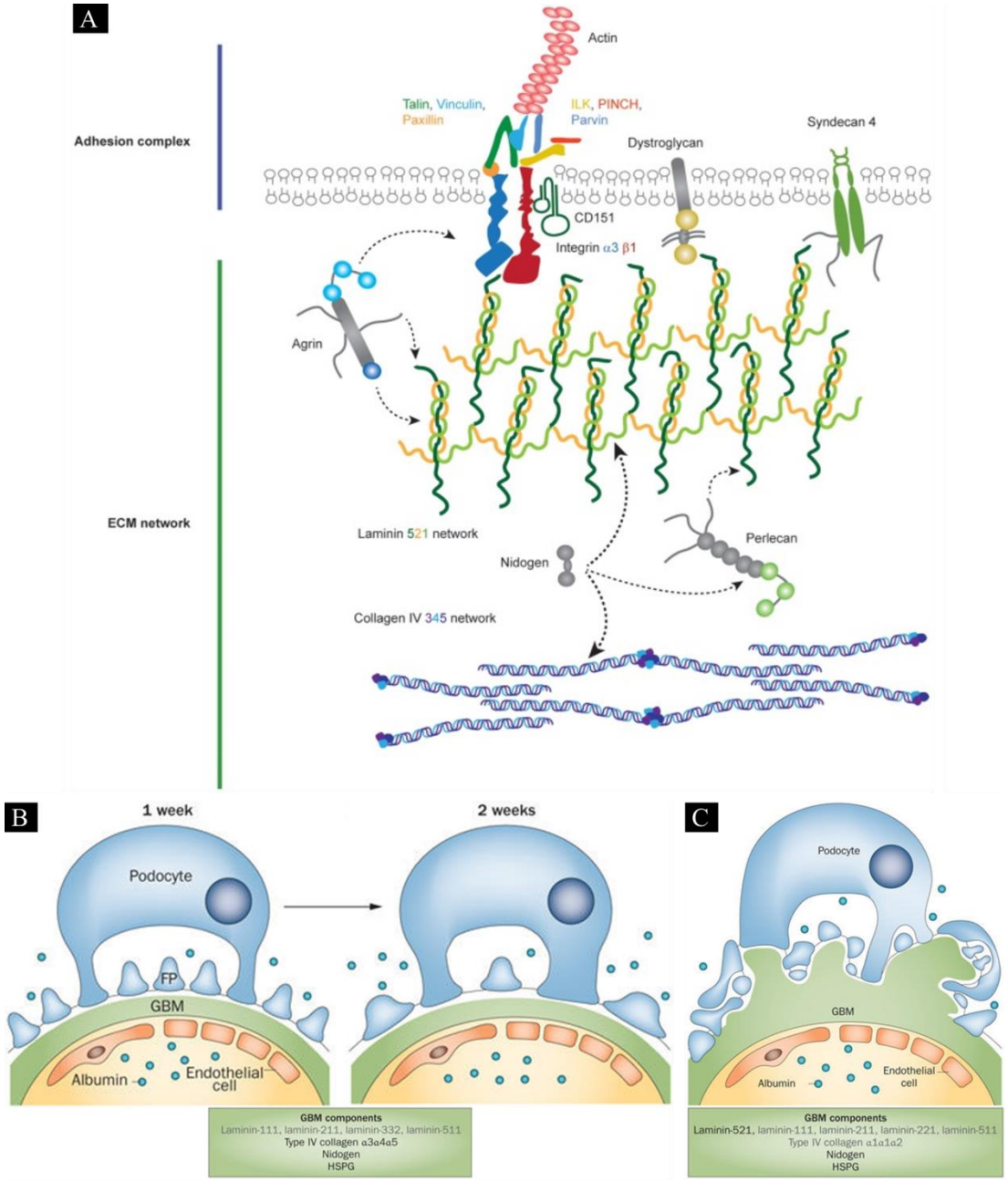

Figure 1.4: **Schematic illustrations of the GBM structure and composition in health and disease.** [A] Composition of the GBM and localization of its main components. Podocyte adhesion complexes are depicted on top. (Lennon et al., 2014b). [B] Pierson syndrome mice lack laminin-521, which is partly replaced by other laminins leading to proteinuria and delayed foot process effacement. [C] Alport syndrome mice in turn lack collagen α3α4α5(IV), which is compensated by increased collagen α1α1α2(IV) deposits, resulting in a split and thickened basement membrane and proteinuria [modified from (Suh and Miner, 2013)]. *Abbreviations:* (ECM), extracellular matrix; (FP), foot processes; (GBM), glomerular basement membrane; (HSPG) heparan sulfate proteoglycan; (ILK), integrin-linked kinase; (PINCH), Particularly interesting new cysteine-histidine-rich protein;

1.4.3. Podocytes

Architecture

Podocytes are specialized and terminally differentiated epithelial cells with a unique three-dimensional structure, covering the exterior of the glomerular capillaries (Pavenstadt et al., 2003). As these cells are not able to replicate by mitosis, dead or detached cells cannot be replaced. Compensation of podocyte loss may be achieved by hypertrophy of neighboring podocytes (Wiggins, 2007), but also parietal and progenitor cells may partly substitute podocytes (Appel et al., 2009; Shankland et al., 2014). Nowadays it is thought that podocytes play the most crucial role in renal filtration, as many mutations in podocyte genes lead to renal failure (Vivante and Hildebrandt, 2016), as summarized in Figure 1.5. Podocytes have also an impact on the other components of glomerular filtration barrier, as they excrete glomerular basement membrane proteins and also vascular endothelial growth factor (VEGF), a compound inducing the endothelial fenestrations (Sison et al., 2010). Primary processes extending from the floating podocyte cell body split up into secondary and tertiary so-called foot processes, anchoring the cell to the GBM (Figure 1.3, B). Those processes interdigitate and are always neighbored to processes from another podocyte, with the slit diaphragm located in-between (Burghardt et al., 2015; Tao et al., 2014). Slit diaphragms are specialized cell-cell junctions considered to play an important role in blood filtration. While primary processes are mainly stabilized by intermediate filaments and microtubules, the delicate foot processes are stabilized by a tightly regulated actin cytoskeleton (Andrews and Bates, 1984; Schell and Huber, 2017).

Podocyte damage and foot process effacement

There are different responses of podocytes to stress including hypertrophy and increased turnover of cell material, but the most general is the retraction of their foot processes to form a broad, uniform layer accompanied by loss of slit diaphragms. This retraction is termed as foot process effacement (FPE) and can be divided into two stages. First, the foot processes retreat to form short irregularly shaped cell protrusions without slit diaphragms. Second, the overall structure of the podocyte changes to form a disc-like cell without any processes covering the GBM (Kriz et al., 2013). It is described that FPE leads to proteinuria (Seefeldt et al., 1981). On the molecular level FPE is accompanied by a change in the expression of actin cytoskeleton-related proteins (Shirato et al., 1996; Smoyer et al., 1997) and by an altered actin cytoskeleton structure (Shirato, 2002). Additionally, genetic defects in actin-binding proteins like α-actinin-4 (Kaplan et al., 2000), myosin heavy chain 9 (Heath et al., 2001), and anillin (Gbadegesin et al., 2014) as well as genetic defects of actin-regulating proteins like inverted formin 2 (Brown et al., 2010) and ARHGAP24 (Gee et al., 2013) lead to podocyte defects und proteinuria (Figure 1.5). These findings underline the importance of the actin cytoskeleton for podocyte foot process structure and function.

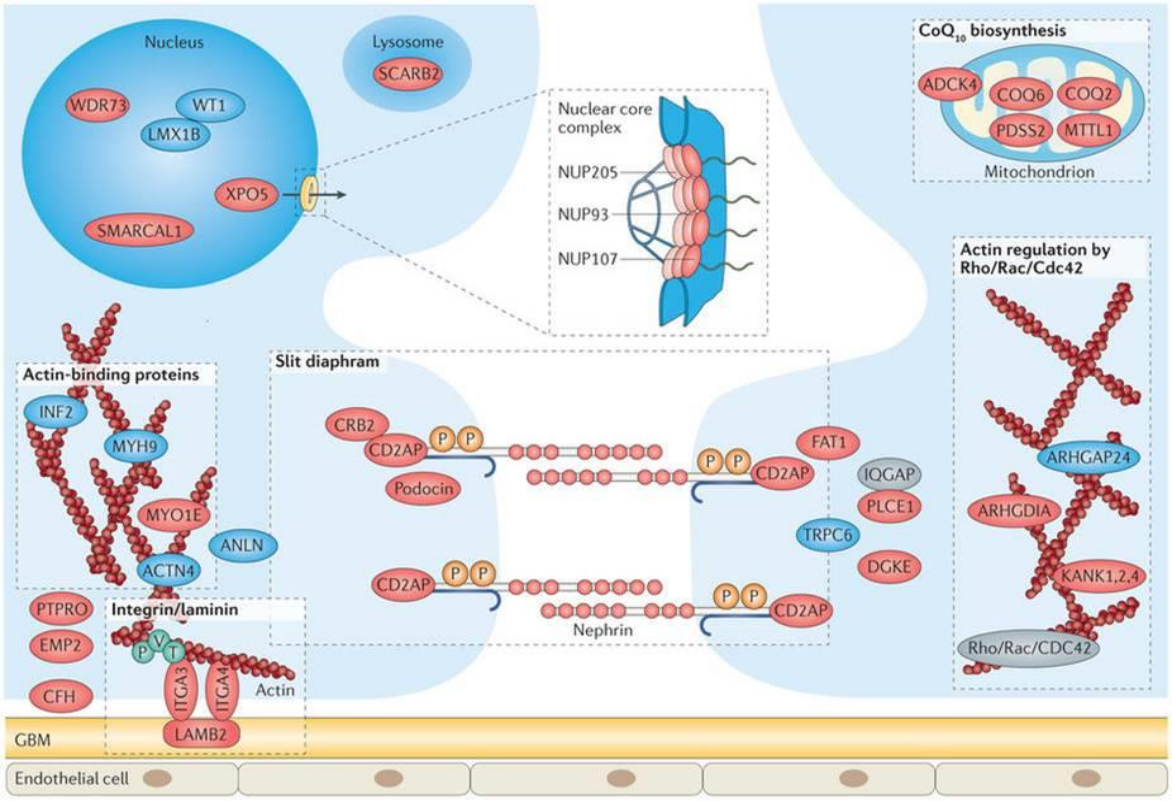

Figure 1.5: **Schematic localization of proteins encoded by genes which mutations cause monogenetic steroid-resistant nephrotic syndrome in a recessive (red) or dominant (blue) manner.** *Abbreviations:* (ACTN4), actinin alpha 4; (ADCK4), AarF domain containing kinase 4; (ANLN), anillin actin-binding protein; (ARHGAP23), Rho GTPase activating protein 23; (ARHGDIA), Rho GDP dissociation inhibitor alpha; (CD2AP), CD2 associated protein; (CDC42), cell division cycle 42; (CFH), complement factor H; (COQ2), coenzyme Q2, polyprenyltransferase; (COQ6), coenzyme Q6, monooxygenase; (CRB2), crumbs 2, cell polarity complex component; (DGKE), diacylglycerol kinase epsilon; (EMP2), epithelial membrane protein 2; (FAT1), FAT atypical cadherin 1; (GBM), glomerular basement membrane; (INF2), inverted formin 2; (IQGAP), IQ motif containing GTPase activating protein; (ITGA3), integrin alpha 3; (ITGA4), integrin alpha 4; (KANK1, 2, 4), KN motif and ankyrin repeat domains 1, 2, 4; (LAMB2), laminin beta 2; (LMX1B), LIM homeobox transcription factor 1 beta; (MTTL1), mitochondrially encoded TRNA leucine 1; (MYH9), myosin heavy chain 9; (MYO1E), myosin IE; (NUP93/107/205), nucleoporin 93/107/205; (PDSS2), decaprenyl diphosphatase synthase subunit 2; (PLCE1), phospholipase C epsilon 1; (PTPRO), protein tyrosine phosphatase, receptor type O; (Rac), Ras-related C3 botulinum toxin substrate; (Rho), Ras homology; (SCARB2), scavenger receptor class B member 2; (SMARCAL1), SWI/SNF related, matrix associated, actin dependent regulator of chromatin, subfamily A like 1; (TRPC6), transient receptor potential cation channel subfamily C member 3; (WDR73), WD repeat domain 73; (WT1), Wilms tumor 1; (XPO5), exportin 5; [modified from (Vivante and Hildebrandt, 2016)]

Cell-cell contacts: slit diaphragm

The slit diaphragms are unique cell-cell contacts exclusively established by podocytes between adjacent foot processes (Figure 1.6). Slit diaphragms are networks of transmembrane proteins originating from 40 nm distant adjacent foot processes forming pores of a size smaller than that of albumin (Wartiovaara et al., 2004). Originally thought to be organized in a zipper-like structure (Rodewald and Karnovsky, 1974), it has nowadays been shown by electron tomography that there is more than just one layer of cell-cell contacts (Burghardt et al., 2015; Grahammer et al., 2016). Although both studies show clearly that there are two types of cell-cell contacts at different basolateral positions, they are contrary to whether one of the contacts consists of a continuous layer or just single spots of filamentous structures.

The importance of slit diaphragms for filtration is given by the fact that mutations in many slit diaphragm related proteins lead to podocyte foot process effacement and proteinuria (Figure 1.5). Main components are nephrin (Holzman et al., 1999; Kestila et al., 1998) and the shorter but structurally related neph1 (Donoviel et al., 2001) spanning the gap between neighboring podocyte foot processes (Figure 1.6). Knock-out of either gene in mice leads to FPE, proteinuria and early death. Besides interacting with each other these slit diaphragm constituents interact with and regulate many actin-related proteins (Figure 1.7, A) (Faul et al., 2007). Other transmembrane proteins which are also reported to locate to filtration slits are P-cadherin (Reiser et al., 2000) and FAT1 (Inoue et al., 2001). The slit diaphragm is bound to the actin cytoskeleton via the adaptor protein CD2AP (Lehtonen et al., 2002). *Cd2ap* knock-out studies in mice showed renal defects leading to death within 6 to 7 weeks (Shih et al., 1999). Another important protein at slit diaphragms is podocin, encoded by *NPHS2* (Boute et al., 2000). It is almost exclusively expressed in podocytes and binds to nephrin (Huber et al., 2001), neph1 (Sellin et al., 2003) and CD2AP (Schwarz et al., 2001). Podocin is therefore important for signaling and slit diaphragm protein recruitment. *Nphs2* knock-out mice develop severe proteinuria and die within few days after birth from renal failure (Roselli et al., 2004).

Cell-matrix contacts

Podocytes anchor to the glomerular basement membrane via several transmembrane proteins located at their foot processes (Figure 1.6). As the podocyte body floats in the primary urine and podocyte foot processes are exposed to high shear stress at the exterior of the capillaries, decreased number or strength of cell-matrix contacts may lead to podocyte detachment and loss (Kriz et al., 2013). Additionally, disturbance of cell-matrix adhesions leads to altered signaling pathways and ultimately to foot process effacement and proteinuria (Sachs and Sonnenberg, 2013). The adhesion receptors are connected with the actin cytoskeleton via various adaptor and signaling proteins (Figure 1.7, B). The most

common adhesion proteins belong to the integrin family, which form αβ heterodimers. Podocytes express mainly α3β1-integrin (Sterk et al., 1998), but also low expression of other integrins is observed, e.g. αvβ3-integrin (Wei et al., 2008). Other adhesion receptors expressed in podocytes are dystroglycan (Durbeej et al., 1998) and syndecan-4 (Pyke et al., 1997) (Figure 1.6).

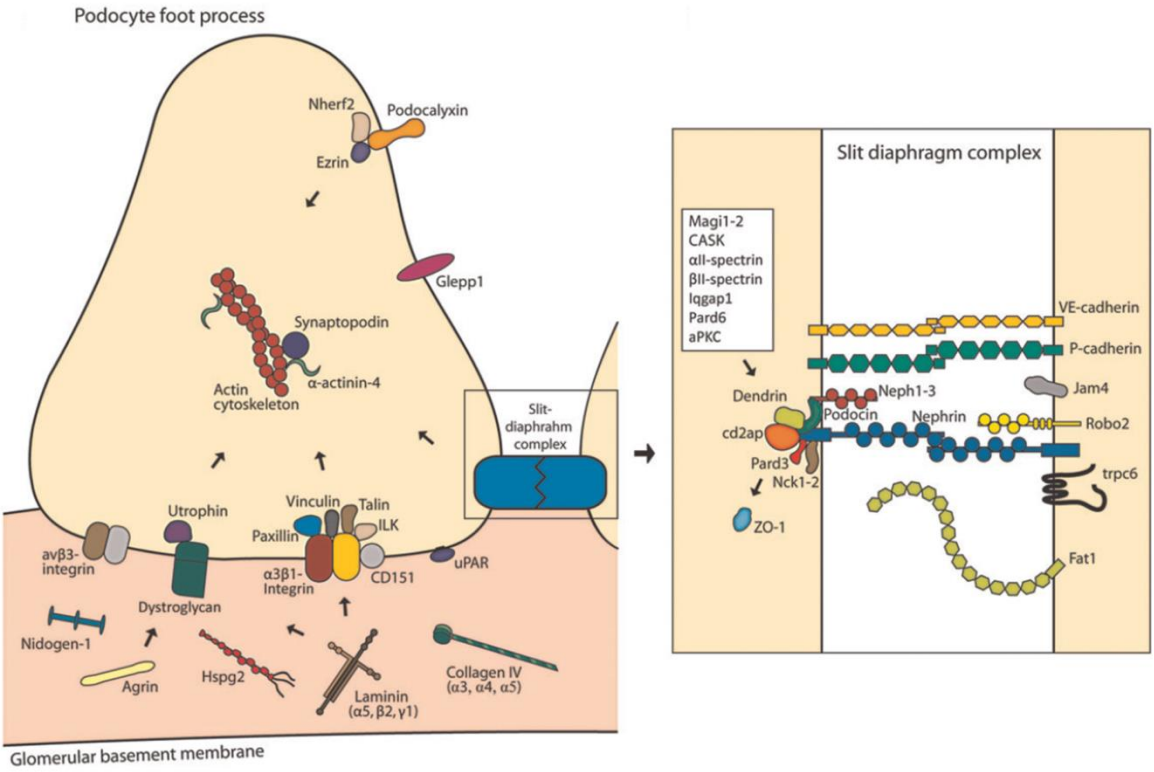

Figure 1.6: **Overview and localization of important podocyte cell junction proteins.** Slit diaphragm proteins are depicted on the right-hand side. *Abbreviations:* (aPKC), atypical protein kinase C; (CASK), calcium/calmodulin-dependent serine protein kinase; (CD151), cluster of differentiation 151; (cd2ap), CD2-associated protein; (Glepp1), glomerular epithelial protein 1; (HSPG), heparan sulfate proteoglycan; (ILK), integrin-linked kinase, (jam4), junctional adhesion molecule 4; (Magi1-2), membrane-associated guanylate kinase, WW and PDZ domain-containing protein 1/2; (Nck1-2), non-catalytic region of tyrosine kinase adaptor protein; (Robo2), roundabout guidance receptor 2; (trpc6), transient receptor potential cation channel, subfamily C, member 6; (uPAR), urokinase-type plasminogen activator receptor; (ZO-1), zonula occludens-1; [modified from (Finne et al., 2014)].

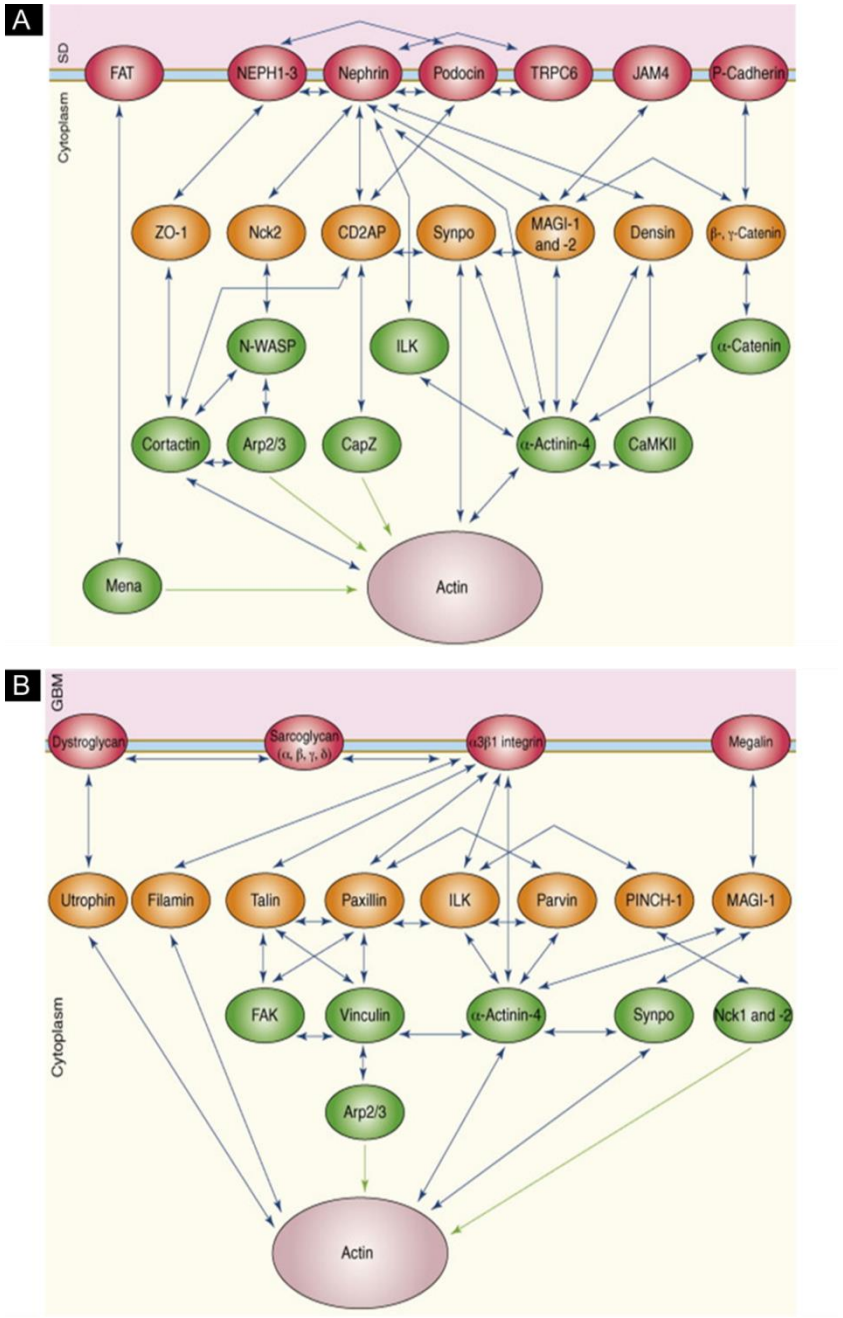

Figure 1.7: **Interactions and signaling pathways between [A] slit diaphragms or [B] cell-matrix adhesion molecules and the actin cytoskeleton**. *Abbreviations:* (CaMKII), Ca^{2+}/calmodulin-dependent protein kinase; (CapZ), capping protein (actin filament) muscle Z-line; (CD2AP), CD2-associated protein, (FAK), focal adhesion kinase; (ILK), integrin-linked kinase; (JAM4), junctional cell adhesion molecule 4; (MAGI-1/2), membrane-associated guanylate kinase, WW and PDZ domain-containing protein 1/2; (NCK1/2), non-catalytic region of tyrosine kinase adaptor protein 1/2; (N-Wasp), neural Wiskott-Aldrich syndrome protein; (PINCH-1), particularly interesting new cysteine-histidine-rich protein; (Synpo), synaptopodin; (TRPC6), transient receptor potential cation channel, subfamily C, member 6; (ZO-1), zonula occludens 1; [modified from (Faul et al., 2007)].

The integrin family is composed of 18 α and 8 β subunits in vertebrates, assembling into 24 different non-covalently bound heterodimers (Barczyk et al., 2010). The common structure of the α and β chains are depicted in Figure 1.8, but it has to be mentioned that only 9 out of 18 α chains contain an αI domain. In their function as adhesion receptors, integrins can bind to ligands at both the cytoplasmic and extracellular side and thus transmitting signals in both directions. On the cytoplasmic side binding to PTB domain-containing proteins (e.g. talin, kindlin) is mediated through two NPXY motifs of the β chain. Binding to extracellular ligands is mainly located at the βI and αI domains (Campbell and Humphries, 2011).

Distinct active and inactive states of heterodimers are known. In the bent conformation, access to the binding pocket is sterically hindered and the αI / βI domains are in an inactive conformation (Figure 1.8). Ligand binding to the cytoplasmic side induces an upright conformation and a conformational change in the binding pocket, enabling binding to extracellular matrix components (inside-out signaling). Binding to extracellular ligands and mechanical tension induces a conformational change in the αI/βI domains and a further "swing-out" of the hybrid domain, resulting in a clustering of integrins and formation of stable focal adhesions (outside-in signaling) (Askari et al., 2009). Antibodies recognizing active states mostly bind to epitopes on the β chain (Byron et al., 2009).

Focal adhesions are clusters of proteins linking the extracellular matrix to the actin cytoskeleton. Although integrins and integrin clustering are essential for focal adhesions, more than 150 proteins are known to assemble to focal adhesions, underlining their importance not only in mechanical anchoring but also in signal transduction (Geiger and Yamada, 2011).

The most important integrin heterodimer in podocytes is α3β1-integrin (Sachs and Sonnenberg, 2013), binding specifically to laminins (Barczyk et al., 2010). The α3 subunit does not contain an αI domain. Depletion of either of the two chains leads to severe proteinuria, foot process effacement, glomerular basement membrane defects and renal failure (Kanasaki et al., 2008; Kreidberg et al., 1996; Pozzi et al., 2008). Talin, an important focal adhesion protein, mechanically links integrins to the actin cytoskeleton. Podocyte-specific deletion of talin leads to foot process effacement and proteinuria (Tian et al., 2014). Also, other focal adhesion proteins have been shown to be essential for podocyte function and renal filtration, e.g. vinculin (Lausecker et al., 2018), integrin-linked kinase (El-Aouni et al., 2006) and CD151 (Sachs et al., 2006).

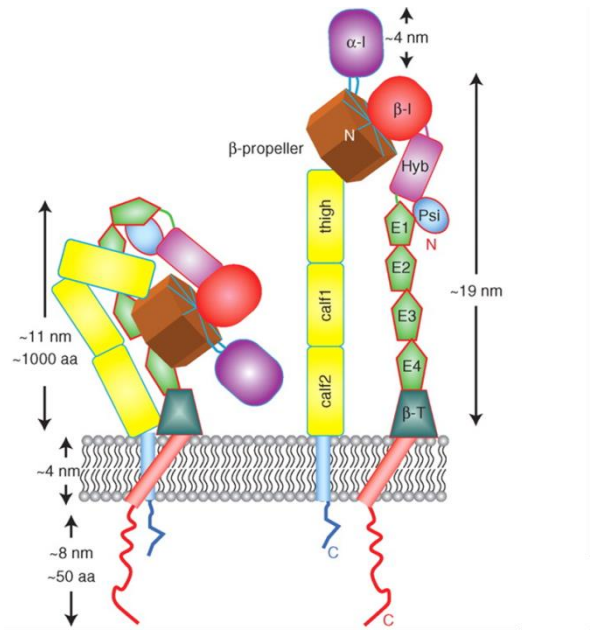

Figure 1.8: **Schematic illustration of the α and β subunits of integrin and their domains in different conformations.** Only 9 out of 18 α subunits contain an αI domain. Extracellular matrix compounds bind to the αI or βI domain, intracellular ligands to the C-terminal tail of the β-subunit. In the bent conformation (left side) the binding pocket is inactive. In the upright conformation (right side), integrin is ready to bind extracellular matrix proteins. *Abbreviations:* (aa), amino acids; (β-T), β-tail domain; (E1-4), epidermal growth factor modules 1-4; (Hyb), hybrid domain; (Psi), plexin-semaphorin-integrin; [modified from (Campbell and Humphries, 2011)]

The adhesion receptor dystroglycan is also expressed in podocytes besides integrins (Durbeej et al., 1998). It binds to extracellular laminin and links it to the actin cytoskeleton (Ervasti and Campbell, 1993). Dystroglycan is composed of a transmembrane β subunit and an extracellular α subunit, and the complex is connected to the actin cytoskeleton by dystrophin in muscle cells and utrophin in epithelial cells (Michele and Campbell, 2003). Although anchoring of the podocyte to the extracellular matrix is essential, dystroglycan is dispensable, as deletion in podocytes of mice does not result in any renal abnormalities both under normal conditions and stress (Jarad et al., 2011).

1.5. The actin cytoskeleton

1.5.1. Structure

The actin cytoskeleton is a dynamic network primarily composed of thin polymerized actin filaments (filamentous actin, F-actin) with a diameter of approximately 8 nm (Blanchoin et al., 2014). The actin monomer (globular actin, G-actin) is highly conserved among eukaryotic species (Gunning et al., 2015) and the most abundant protein in many eukaryotic cells. Actin locates all over the cytosol and also in the nucleus, but to a lesser extent (Belin and Mullins, 2013). It has a nucleotide-binding pocket for ATP/ADP, with ATP hydrolysis in filaments happening stochastically. ATP bound monomers associate with a higher binding constant to filaments than ADP bound actin does (Pollard, 2017). Actin assembles into double-helical filaments with all monomers orientated to the same direction, resulting in structural polarity with the more dynamic barbed (or plus) end and the less dynamic pointed (or minus) end. As a result of different binding constants at the filament ends and ATP hydrolysis, actin filaments can depolymerize at the pointed end and at the same time polymerize at the barbed end, a process termed “treadmilling”. There are a multitude of proteins binding to actin monomers or polymers, influencing actin filament nucleation, elongation, branching, capping, severing, bundling, cross-linking, etc. (Figure 1.9). While elongation of existing filaments is energetically favorable, nucleation is not and therefore only rarely happens spontaneously. Thus, the limiting step of nucleation is tightly regulated by nucleation factors (Siton-Mendelson and Bernheim-Groswasser, 2017).

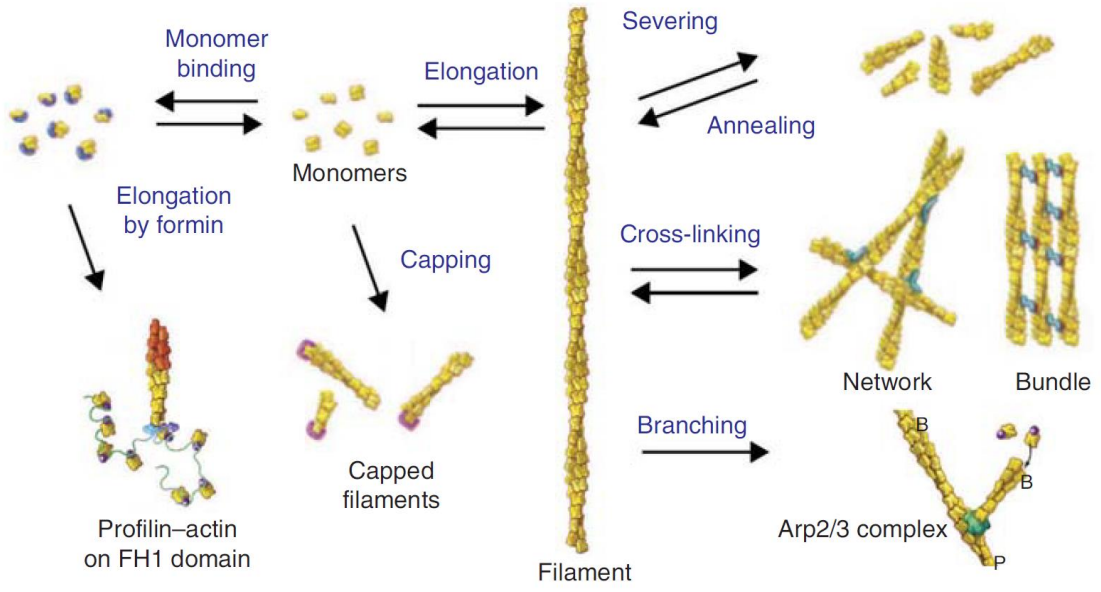

Figure 1.9: **Overview of actin-binding protein groups.** Actin monomers are depicted in yellow. *Abbreviations:* (B), barbed end; (FH1), formin homology 1; (P), pointed end; (Pollard, 2016)

1.5.2. Function

Actin filaments fulfill numerous functions within eukaryotic cells. As a part of the cytoskeleton, actin takes part in stabilizing the morphology of a cell. Podocyte foot processes for example are stabilized by a central actin bundle and additionally cortical actin filaments (Ichimura et al., 2007), and reorganization leads to foot process effacement (Shirato, 2002). Actin is also important in the separation of two daughter cells as the last step of the cell division process. For that purpose an accumulation of actin and myosin-2 filaments to a contractile ring applies force and constricts the cell membrane, which is essential for cytokinesis (Glotzer, 2005). The site for cleavage is marked by Rho GTPases (Chircop, 2014). As mentioned above, podocytes are not able to divide. Nevertheless, cell division is frequently observed in primary podocyte culture [unpublished observations]. Cell motility and protrusion generation is also dependent on the actin cytoskeleton. The force necessary to produce a protrusion is at least partly generated by actin filaments. A dense network of short and branched actin filaments nucleates at the cell edge, with each filament applying piconewton forces (Kovar and Pollard, 2004). Consecutive branch formation results in a front edge movement of up to 1 µm per second (Svitkina et al., 1997). Other cellular functions with participation of actin filaments are endocytosis, organelle transport and contraction of muscle cells (Pollard and Cooper, 2009). Nuclear actin is also described to take part in transcriptional regulation (Grosse and Vartiainen, 2013).

1.5.3. Important actin-binding proteins

Cofilin

Cofilin is an actin-binding protein important for actin turnover. The cofilin family consists of three members in mammals, non-muscle cofilin-1, muscle cofilin-2 and actin-depolymerizing factor (ADF, also known as destrin) (Poukkula et al., 2011). Cofilin preferably binds to ADP-F-actin, inducing a conformational twist resulting in cleavage of the actin filaments (Hawkins et al., 1993; Hayden et al., 1993; McGough et al., 1997). Those severed filaments are subsequently either depolymerized to refresh the pool of actin monomers (Kiuchi et al., 2007), or they serve as new cores for nucleation and branching (Chen and Pollard, 2013; Ghosh et al., 2004). High cofilin concentrations are also considered to facilitate debranching (Blanchoin et al., 2000), and very high concentrations are considered to promote actin nucleation (Andrianantoandro and Pollard, 2006). On the other hand, inactivation of cofilin slows actin turnover and retrograde flow down (Ohashi et al., 2011). These findings underline the central role of cofilin in actin dynamics.

The activity of cofilin is mainly controlled by phosphorylation at Ser-3, with being inactive when phosphorylated (Moriyama et al., 1996). The most important kinases for cofilin phosphorylation are the members of LIM domain-containing protein kinase (LIMK) family, LIMK1 and LIMK2 (Figure 1.10), while dephosphorylation is mediated by the slingshot phosphatase family (SSH) (Ohashi, 2015).

Mice with podocyte-specific deletion of *Cfl1*, encoding for cofilin-1, develop normally, but produce persistent proteinuria by 3 months and slight foot process effacement by 8 months of age. These mice are also more susceptible to protamine sulfate podocyte damage (Garg et al., 2010). Combined deletion of *Cfl1* and *Dstn*, encoding destrin, results in strong kidney developmental defects, demonstrating the importance of cofilin-dependent actin turnover in kidney development (Kuure et al., 2010).

Arp2/3 complex

The Arp2/3 complex consists of seven subunits, including actin-related proteins 2 and 3 (Arp2 and 3) and five scaffolding proteins named actin-related protein complex 1 - 5 (ARPC1 - 5). The complex is highly conserved, expressed by almost all eukaryotes and is essential for cellular function (Goley and Welch, 2006). The activated complex binds to an existing mother filament and induces the nucleation of a new daughter filament at a ~70° angle to the barbed end of the mother filament (Figure 1.9) (Amann and Pollard, 2001; Mullins et al., 1998). To achieve branch formation, the Arp2 and Arp3 proteins mimic an actin-nucleation core, orientated with the pointed end towards the preexisting filament (Rouiller et al., 2008). The explosive Arp2/3 complex induced actin nucleation generates the force required for cell movement (Kovar and Pollard, 2004), lamellipodia formation (Svitkina and Borisy, 1999) and endocytosis (Ferguson et al., 2009).

Arp2/3 initiated nucleation requires a conformational change of the complex achieved by binding of nucleation promoting factors (NPFs), such as Wiskott-Aldrich syndrome protein (WASP) or WASP-family verprolin homologous protein (WAVE) (Figure 1.10) as well as binding to an existing actin filament (Molinie and Gautreau, 2018; Rodnick-Smith et al., 2016; Rouiller et al., 2008).

Formins

Formins are a major class of homodimeric actin nucleators and elongators. They all share a formin homology 1 (FH1) and a formin homology 2 (FH2) domain. The FH2 domain resembles a doughnut-shaped structure binding to barbed ends of actin filaments and in case of some formins also to plus ends of microtubules. The FH1 domain binds to profilin-actin complexes increasing the local concentration of actin at the barbed end (Chesarone et al., 2010). Profilin is a ubiquitous G-actin-binding protein associated with most actin monomers in cells (Kaiser et al., 1999). Nucleation is a feature of the FH2 domain (Pring et al., 2003; Sagot et al., 2002), while the FH1 domain regulates elongation speed. Once bound to a barbed end of filaments, formins assemble new monomers and move along the growing end (Figure 1.9), preventing barbed end capping by other actin regulatory proteins (Pruyne et al., 2002; Zigmond et al., 2003).

Besides the FH1 and FH2 domains formins comprehend of varying additional domains, which are considered to be important for regulation of the formin activity (Chesarone et al., 2010). The important and well-studied formin diaphanous-related formin 1 (mDia1), for example, is autoinhibitory regulated and activated by binding of RhoA to the Rho GTPase binding domain (GBD) (Figure 1.10) (Li and Higgs, 2003).

In humans, mutations in the gene *INF2*, encoding for inverted formin 2, are reported to cause focal segmental glomerulosclerosis (FSGS) (Figure 1.5) (Brown et al., 2010). INF2 binds to mDia1 and modulates its activation via RhoA (Sun et al., 2011). Normal function of Inf2 in mice is not necessary for glomerular development, but mice with *Inf2* knock-out show impaired regeneration from protamine sulfate induced damage (Subramanian et al., 2016).

Myosin-2

The class 2 myosins, also called conventional myosins, are motor protein complexes composed of six subunits. Two identical heavy chains dimerize, forming two head regions at the one end and the extended rod domain at the other end. Two different light chains, regulatory light chain (RLC; also named myosin light chain, MLC) and essential light chain (ELC), bind to the neck region situated between the head and the tail domain of each heavy chain. The rod domain is an association of the two heavy chains into a long, α–helical coiled coil (Preller and Manstein, 2013). The head regions bind to F-actin and generate ATP-dependent force resulting in movement of the filament or of the myosin alongside the filament (Houdusse and Sweeney, 2016; Toyoshima et al., 1987). Therefore, myosin-2 takes part in multiple actions, including muscle contraction, cytokinesis, cell morphology and transport.

Smooth muscle and non-muscle myosin-2 are activated by phosphorylation of Ser-19 of the regulatory light chain (Newell-Litwa et al., 2015; Yu et al., 2016). Kinases phosphorylating RLC are p21-associated kinase (PAK) (Chew et al., 1998), myotonic dystrophy kinase-related Cdc42-binding kinase (MRCK) (Leung et al., 1998) and Rho kinase (ROCK). ROCK activates myosin-2 indirectly by inactivating myosin phosphatase (Figure 1.10) as well as directly by phosphorylation (Totsukawa et al., 2000).

Within the glomerulus, non-muscle myosin heavy chain IIA, encoded by *MYH9*, is mostly expressed in podocytes (Arrondel et al., 2002) and associated with FSGS (Figure 1.5) (Ghiggeri et al., 2003). Podocyte-specific deletion of *Myh9* in different mouse strains does not result in glomerular defects but influences the susceptibility of mice to some, but not all, glomerular damage models (Johnstone et al., 2013).

α-Actinin

α-actinins are rod-like proteins forming antiparallel homodimers, which crosslink actin filaments to bundles via their actin-binding domain (ABD) at the end of each rod (Sjoblom et al., 2008). In addition, α-actinins interact with numerous other proteins making them particularly important for cell adhesion, cell junction, and signaling (Figure 1.7) (Feng et al., 2015). In mammals, two (*ACTN1*, *ACTN4*) of the four *ACTN* genes are widely expressed in many different tissues, while expression of *ACTN2* and *ACTN3* is restricted to muscle tissues (Foley and Young, 2014).

Mutations of *ACTN4* / *Actn4* lead to renal symptoms in humans (Figure 1.5) (Kaplan et al., 2000) and mice (Henderson et al., 2008). Knock-out of *Actn4* in mice results in progressive proteinuria and typically death within several months (Kos et al., 2003). Furthermore, α-actinin-4 dysregulation is observed in several nephrotic syndromes (Goode et al., 2004; Smoyer et al., 1997).

Synaptopodin

Synaptopodin, encoded by the *SYNPO* gene, is a proline-rich actin-binding protein expressed in podocytes (Mundel et al., 1997). It has only little secondary and tertiary structure at physiological conditions (Chalovich and Schroeter, 2010). Synaptopodin interacts and regulates α-actinin-4 activity and therefore influences actin cytoskeleton organization (Figure 1.7) (Asanuma et al., 2005; Kremerskothen et al., 2005). The Rho GTPases RhoA and Cdc42 are also influenced by synaptopodin in an indirect manner, inducing stress fiber formation and suppression of filopodia formation (Asanuma et al., 2006; Yanagida-Asanuma et al., 2007).*Synpo* knock-out mice show normal ultrastructure of podocytes, but impaired recovery from protamine sulfate or liposaccharide-induced podocyte damage (Asanuma et al., 2005).

1.5.4. Key regulators: Rho family of GTPases

Structure and function

The Ras homologue (Rho) family of GTPases comprises a family of more than 22 small GTPases in humans (Chircop, 2014). Among them, the highly conserved RhoA, Rac1 and Cdc42 are best studied. Most Rho GTPases, including the three mentioned above, are active when bound to GTP and inactive when bound to GDP. The small GTPases have an intrinsic hydrolysis capacity but are moreover tightly regulated by guanine nucleotide exchange factors (GEFs), GTPase activating proteins (GAPs) and guanine nucleotide dissociation inhibitors (GDIs). While GEFs activate GTPases through promoting the exchange of GDP to GTP, GAPs and GDIs inactivate Rho GTPases by activating the intrinsic hydrolysis activity or sequestering the small GTPases in their inactive state, respectively (Tcherkezian and Lamarche-Vane, 2007). As GTPases can cycle between the active and inactive form, they are often referred to as molecular switches. Active, GTP bound Rho GTPases activate a variety of effectors, making them central players in regulating many cellular functions, such as cell morphology, adhesion, cytokinesis, cell polarity and membrane transport (Etienne-Manneville and Hall, 2002).

Signaling pathways

Rho GTPase signaling pathways are highly complex and yet not fully understood nor all interactions are discovered. Canonically, activation of RhoA leads to formation of actomyosin bundles called stress fibers, while Rac1 activation leads to formation of lamellipodia and Cdc42 activation to filopodia (Figure 1.10) (Nobes and Hall, 1995). GTP-RhoA is a direct activator of the formin mDia1 (Li and Higgs, 2003) and it also activates myosin-2 (Totsukawa et al., 2000), but moreover inactivates cofilin over ROCK and LIMK, leading to the assembly of long, unbranched actin filaments and stress fibers (Maekawa et al., 1999). Active Rac1, on the other hand, counteracts stress fiber formation by inhibiting myosin-2 activity. This inhibition is achieved by phosphorylation and inactivation of myosin light chain kinase (MLCK) over the Rac1 effector p21-activated kinase 1 (PAK1) (Sanders et al., 1999). Rac1 activation additionally leads to direct activation of the nucleation-promoting factor (NPF) WAVE (Chen et al., 2010), which in turn activates the Arp2/3 complex resulting in a branched actin network and lamellipodia formation. Like RhoA, Rac1 activation also leads to phosphorylation and inactivation of cofilin (Edwards et al., 1999). GTP-Cdc42, in turn, activates another NPF, the neuronal Wiskott-Aldrich syndrome protein (N-WASP), leading to actin filament nucleation and branch formation (Rohatgi et al., 1999). Active Cdc42 interacts with PAK4, which phosphorylates LIMK, finally leading to cofilin phosphorylation and inactivation (Rane and Minden, 2014).

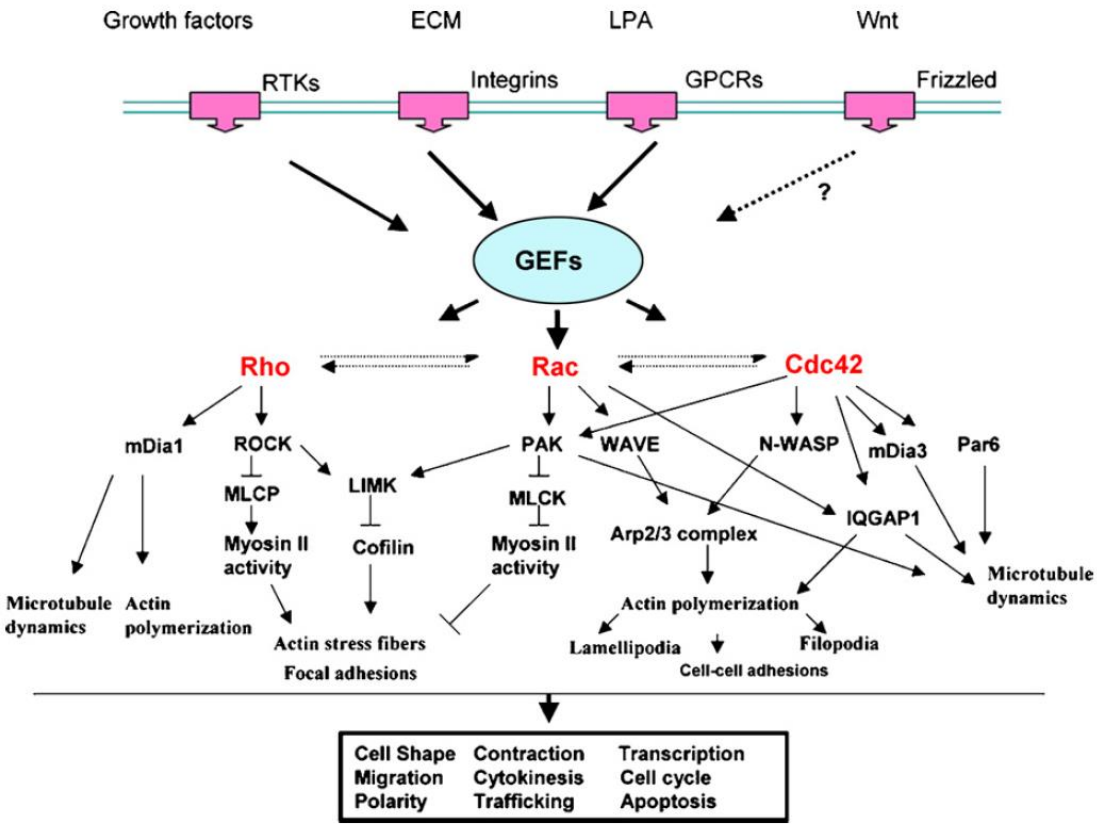

Figure 1.10: **Scheme depicting a part of the complex signaling pathways of actin regulation by RhoA, Rac1 and Cdc42**. Extracellular signals activate Rho GTPases via GEFs, which in turn regulate actin and microtubule dynamics. *Abbreviations:* (Arp2/3), actin related protein 2/3; (Cdc42), cell division control protein 42 homolog; (ECM), extracellular matrix; (GEF), guanine nucleotide exchange factor; (GPCR), G-protein coupled receptor; (IQGAP1), IQ motif-containing GTPase activating protein 1; (LIMK), LIM kinase; (LPA), lysophosphatidic acid; (mDia1/3), diaphanous related formin 1/3; (MLCK), myosin light chain kinase; (MLCP), myosin light chain phosphatase; (N-WASP), neuronal Wiskott-Aldrich syndrome protein; (PAK), p21-aktivated kinase; (Par6), partitioning defective 6 homolog; (Rac), Ras-related C3 botulinum toxin substrate 1; (Rho), Ras homologue; (ROCK), Rho kinase; (RTK), receptor tyrosine kinase; (WAVE), WASP-family verprolin homologous protein; (Wnt), wingless-type MMTV integration site family; (Rao and Maddala, 2006)

Role of Rho GTPases for podocyte health

Rac1 and Cdc42 are essential regulators, as knock-out of either encoding gene in mice leads to embryonic lethality (Chen et al., 2000; Sugihara et al., 1998). *RhoA* null mice, in turn, are not reported so far. Nevertheless, tissue-specific deletion of *RhoA* results in diverse abnormal phenotypes (Duquette and Lamarche-Vane, 2014), including embryonic lethality (Herzog et al., 2011). Podocyte-specific deletion of *Rac1* and *RhoA* in mice does not result in any overt phenotype, but *Cdc42* deletion in podocytes leads to foot process effacement, proteinuria and death (Blattner et al., 2013; Scott et al., 2012). Thus, Cdc42 expression is necessary for podocyte foot process development and maintenance, while RhoA and Rac1 are not essential. On the other hand, activation of RhoA and Rac1 over basal levels is reported in different damage models, and inhibiting RhoA or Rac1 signaling pathways reduces podocyte damage and proteinuria (Babelova et al., 2013; Gojo et al., 2007; Shibata et al., 2006). Moreover, podocyte-specific expression of constitutively active mutants of RhoA and Rac1 leads to podocyte damage and proteinuria (Robins et al., 2017; Wang et al., 2012a; Zhu et al., 2011). Additionally, mutations in *ARHGAP24*, encoding for a Rac1 inactivating GAP, are associated with familial FSGS in humans (Akilesh et al., 2011).

1.5.5. Effect of cytochalasin D on the actin cytoskeleton

Cytochalasin D is a cell-permeable fungal metabolite interacting with the actin cytoskeleton, without any reports of other interactions (Cooper, 1987). It binds actin filaments at the barbed end (K_d = 2 nM) and inhibits both polymerization and depolymerization at this end, but does not bind to the pointed end (Cooper, 1987; Sampath and Pollard, 1991). Additionally, it binds to monomeric G-actin with lower affinity (K_d = 2 - 20 µM) and induces actin dimerization (Goddette and Frieden, 1985; Nair et al., 2008). It is also reported to block cofilin binding to both actin monomers and filaments (Shoji et al., 2012). Treatment of cells with cytochalasin D leads to disruption of filament bundles and formation of actin filament aggregates, accompanied by a reduced cell stiffness (Wakatsuki et al., 2001).

1.6. LMX1B

1.6.1. Linkage to nail-patella syndrome

Genetical linkage of NPS to the ABO locus dates back to 1955 (Renwick and Lawler, 1955). More than 40 years later mutations of *LMX1B* were found to cause the syndrome (Dreyer et al., 1998; McIntosh et al., 1998; Vollrath et al., 1998). Though, there are rare cases of NPS without *LMX1B* mutations (Ghoumid et al., 2016). *LMX1B* is known to be responsible for establishing the dorsoventral pattern in limb development (Riddle et al., 1995; Vogel et al., 1995), which explains nail and skeletal abnormalities of NPS patients (Figure 1.1). Besides its importance in development LMX1B is also expressed in the anterior segment of the eye (Pressman et al., 2000), in the brain (Adams et al., 2000) and in the podocytes of the kidney (Dreyer et al., 1998; Morello et al., 2001). This expression pattern is reflected by NPS phenotypes (see chapter 1.1).

1.6.2. Structure and mutations

LMX1B contains two N-terminal LIM domains important for protein-protein interactions and a central homeodomain essential for DNA binding. The C-terminal glutamine- and serine-rich region is of unknown function (Bongers et al., 2002). On the genetic basis, *LMX1B* consists of 8 exons, whereof the LIM A domain is encoded by exon 2, LIM B by exon 3 and the homeodomain by exons 4, 5 and 6. In humans, two isoforms with a length of 395 and 402 aa are expressed by alternative splicing at the end of exon 7 (Witzgall, 2017). To date, more than 180 mutations are known to cause NPS, and the number is still growing (Ghoumid et al., 2016; Harita et al., 2017). The spectrum of mutations comprise missense, nonsense and frameshift mutations and complete or partial deletions (Harita et al., 2017), and the pathogenic mechanism is thought to be haploinsufficiency (Jiang et al., 2014). The vast majority of mutations are located within the two LIM domains and the homeodomain, raising the hypothesis that mutations within the conserved C-terminal region would lead to a distinct phenotype (Dunston et al., 2004). Genotype-phenotype correlation shows an increased frequency of renal symptoms of patients with mutations in the homeodomain, but no extra-renal correlation is observed (Bongers et al., 2005). In developing mice, Lmx1b is expressed in the kidney, brain, spinal cord, and the eye (Dunston et al., 2005). Within the kidney, Lmx1b is exclusively expressed in podocytes not only at embryonic stages but also in adult individuals (Morello and Lee, 2002).

1.6.3. Overview of target genes

As a transcription factor LMX1B regulates the expression of specific genes by binding to their promoter or enhancer regions. DNA binding is mediated through the homeodomain, which specifically binds to FAR linked AT-rich (FLAT) sequences (German et al., 1992).

In podocytes

Only a few Lmx1b target genes have been reported to date in podocytes, including *Col4a3*, *Col4a4* (chapter 1.4.2), *Cd2ap*, *Nphs2* (chapter 1.4.3), *Abra* (chapter 1.7.1), and *Arl4c* (chapter 1.7.2). The α3 and α4 chains of collagen IV are missing in the glomerular basement membrane of conventional *Lmx1b* knock-out mice, and LMX1B binds to FLAT elements within the first intron to both human and murine *COL4A4*/*Col4a4*. Furthermore, LMX1B activates a reporter construct containing six concatemerized binding sites from the *COL4A4* gene (Morello et al., 2001). In case of Cd2ap and podocin (encoded by *Nphs2*) both mRNA and protein levels are reduced in *Lmx1b* knock-out mice. LMX1B binds to promoter regions *in vitro* and activates transcription of a reporter construct containing 4 repeats of the *NPHS2* binding site and a minimal promoter in NIH 3T3 cells (Miner et al., 2002; Rohr et al., 2002). On the other hand, the α3 and α4 chains of collagen IV, Cd2ap and podocin are still present in podocyte-specific *Lmx1b* knock-out mice (Suleiman et al., 2007) and in human NPS patients (Heidet et al., 2003). The mRNA levels of *Abra*, *Arl4c* and *Sm22* are elevated in a time-dependent manner following doxycycline treatment of inducible podocyte-specific *Lmx1b* knock-out mice. In case of *ABRA* and *ARL4C*, LMX1B binds to FLAT elements in the respective promoter regions, as confirmed by gel shift assays and chromatin immunoprecipitation. No such binding could be shown for the promoter region of *SM22* (Burghardt et al., 2013).

In other cell types

Regulation of interleukin-6 (IL-6) and interleukin-8 (IL-8) by LMX1B was shown in HeLa cells stably transfected with an inducible *LMX1B* expression construct on the transcriptional level, and binding of LMX1B to the promoter regions was confirmed by chromatin immunoprecipitation (Rascle et al., 2009). A genome-wide analysis of Lmx1b binding to promoter regions of genes in the developing limbs of mice revealed several potential target genes by chromatin immunoprecipitation and next-generation sequencing. Promoter activity of growth differentiation factor 5 (*Gdf5*) was shown to overlap with Lmx1b expression in developing chick elbow, wrist, and digit joints (Haro et al., 2017).

1.6.4. Influence of Lmx1b on the actin cytoskeleton of podocytes

Glomerular outgrown cells from mice with an inducible and podocyte-specific knock-out of *Lmx1b* show an altered actin cytoskeleton behavior. While the fluorescence of phalloidin staining is increased in knock-out cells, the movement of fibronectin-coated nanobeads attached to the surface is decreased. Additionally, the spreading rate of primary *Lmx1b* knock-out podocytes after cytochalasin D treatment is reduced compared to control podocytes. Thus, a stiffer, less dynamic actin cytoskeleton was proposed (Burghardt et al., 2013).

1.7. LMX1B regulated proteins

1.7.1. Abra

Structure and expression

Actin-binding Rho-activating protein (Abra), also known as striated muscle activator of Rho signaling (STARS) or myocyte stress-1 (Ms1), is a 43 kDa protein expressed in cardiac, skeletal and smooth muscle (Arai et al., 2002; Mahadeva et al., 2002; Troidl et al., 2009). The subcellular localization of Abra is dependent on the developmental stage. In primary cardiomyocytes it is located at the I-bands and Z-disks (Arai et al., 2002), but in neonatal cardiomyocytes Abra localized to the nucleus (Zaleska et al., 2015). Structurally Abra comprises of two actin-binding domains (ABD1/2), with a higher affinity of ABD1 than ABD2 to bind F-actin (Fogl et al., 2012). ABD2, in conjunction with an AT-hook motif located in close proximity N-terminally of ABD2, is additionally able to bind to DNA (Zaleska et al., 2015). The expression of Abra is activated by the transcription factors estrogen-related receptor alpha (ERRα) (Wallace et al., 2011), serum response factor (SRF) (Chong et al., 2012) and myocyte enhancer factor 2 (MEF2) (Kuwahara et al., 2007). On the other hand, expression is restricted by the transcription factor GATA4 (Ounzain et al., 2012) and the miRNA miR-628-5p (Russell et al., 2017). Abra expression in skeletal muscle is decreased in older individuals, but mRNA levels increase after stress independent of age (Russell et al., 2017).

Interaction partners and signaling

Abra is an actin-associated protein inducing polymerization of actin, resulting in a reduction of the G-actin pool (Wallace and Russell, 2013). This, in turn, releases the transcriptional coactivator myocardin-related transcription factor-A (MRTF-A) from its inactive, G-actin bound state, followed by its translocation into the nucleus. As a final step of Abra signaling, the transcription factor SRF is activated by MRTF-A, leading to SRF-dependent protein expression (Figure 1.11) (Kuwahara et al., 2005). SRF is a transcriptional activator of the *SM22* gene, encoding for transgelin (Li et al., 1997). Downstream signaling of Abra is increased when a constitutively active mutant of RhoA is coexpressed, and inhibition of RhoA or ROCK partially blocks Abra signaling, leading to the assumption of a RhoA-dependent signaling pathway of Abra (Arai et al., 2002). However, evidence of the existence and nature of a direct interaction is missing. Abra interacts with actin-binding LIM protein-2 and -3 (ABLIM-2 and ABLIM-3), enhancing the downstream signaling of Abra (Barrientos et al., 2007). A negative regulator of the Abra pathway is calmodulin (CaM) in a Ca^{2+} dependent manner. The N-terminal region of Abra binds to CaM in the presence of Ca^{2+} ions, which in turn diminishes Abra signaling and SRF transcriptional activity (Furuya et al., 2016).

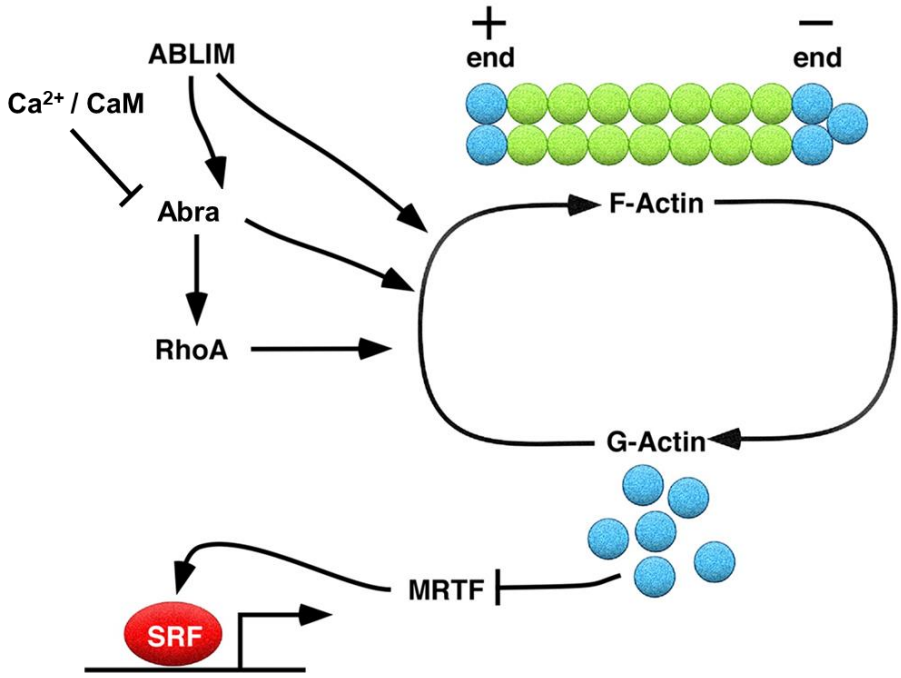

Figure 1.11: **Proposed model of Abra interactions and signaling** [modified from (Barrientos et al., 2007)]. *Abbreviations:* (ABLIM), actin-binding LIM protein; (Abra), actin-binding Rho-activating; (CaM), colmodulin; (MRTF), myocardin-related transcription factor; (RhoA), Ras homologue A; (SRF), serum response factor

1.7.2. Arl4c

Structure and expression

The small GTPase Arf-like 4c (Arl4c) is a member of the ADP-ribosylation factor (Arf) family and is also known as Arf-like 7 (Arl7). Like other small GTPases, Arl4c can cycle between an active GTP-bound state and an inactive GDP-bound state, but GEFs and GAPs are so far unknown (Matsumoto et al., 2017). In humans Arl4c has two isoforms, the shorter isoform comprises of 192 aa encoded by one exon and the longer isoform comprises of 201 aa encoded by two exons (Matsumoto et al., 2017). Arl4c expression is reported in human lung, brain, leukocytes, placenta, thymus, esophagus, stomach and intestine (Jacobs et al., 1999; Wei et al., 2009). In mouse embryos at embryonic day 15, Arl4c protein expression was observed in the brain, kidneys and in some epithelial rudiments (Matsumoto et al., 2014). Additionally, Arl4c is expressed in lung and colorectal cancer cells (Fujii et al., 2015). The subcellular localization is dependent on the activity state, as wild-type and constitutive active Arl4c are located at the plasma membrane, whereas a dominant negative form of Arl4c is distributed all over the cytosol (Engel et al., 2004; Hofmann et al., 2007). There are only few reports about the transcriptional regulation of Abra expression. Combined stimulation of cells with Wnt3a and epidermal growth factor (EGF) activates the β-catenin and mitogen-activated protein kinase (MAPK) pathways, leading to the formation of an Ets1/T-cell factor 4 (Tcf4)/CREB-binding protein (CBP) complex at the 3' untranslated region (UTR) of the *Arl4c* gene, and finally induces Arl4c expression (Matsumoto et al., 2014).

Interaction partners and signaling

Arl4c binds to α-tubulin independent of the GTP or GDP binding status, and active Arl4c accelerates the transferrin transport from early endosomes to recycling endosomes (Wei et al., 2009). Another function of Arl4c is the binding and recruitment of Arf nucleotide-binding site opener (ARNO) to the plasma membrane when Arl4c is in its active state. ARNO in turn recruits and activates ADP-ribosylation factor 6 (Arf6) (Hofmann et al., 2007). GTP-Arf6 then activates Rac1, potentially through kalirin and the dedicator of cytokinesis 1 (DOCK1)/engulfment and cell motility (ELMO) complex, followed by RhoA inhibition, leading to a reorganization of the actin cytoskeleton (Matsumoto et al., 2014). Arl4c additionally controls the actin cytoskeleton by the means of a distinct mechanism involving Cdc42. Active Arl4c binds to the actin regulator filamin-A (FLNa), which increases its association with the GEF FYVE, RhoGEF and PH domain-containing 6 (FDG6). This finally activates the small GTPases Cdc42, inducing filopodia formation and cell migration (Chiang et al., 2017). Other cellular functions with Arl4c involvement are osteogenesis (Wang et al., 2018), cholesterol efflux (Engel et al., 2004), and migration and invasion of gastric cancer cells (Hu et al., 2018).

1.7.3. Transgelin

Structure and expression

Transgelin, also known as smooth muscle 22 (SM22), is a 22 kDa protein encoded by the *SM22* gene. The gene comprises of 5 exons, while exon 1 and the first 12 base pairs of exon 2 and also the last 432 base pairs of exon 5 are not translated (Assinder et al., 2009; Camoretti-Mercado et al., 1998). The resulting 201 aa protein contains an N-terminal calponin homology domain (CH) and a C-terminal calponin like module (CLIK). In healthy, adult individuals transgelin is expressed mainly in smooth muscle cells (Shapland et al., 1988), but also in myofibroblasts and epithelial cells (Page et al., 1999; Yu et al., 2008). Additionally, transgelin is expressed during embryogenesis in mesenchymal, skeletal and cardiac muscle cells (Lawson et al., 1997; Li et al., 1996). Transgelin is also expressed in various types of cancer cells (Dvorakova et al., 2014) and in podocytes after glomerular damage (Marshall et al., 2011). On the subcellular level transgelin localizes in the cytosol and is also associated with actin filaments (Fu et al., 2000; Han et al., 2009). The expression of transgelin is regulated by multiple pathways. For instance, SRF, co-activated by MRTF-A, activates the *Sm22* promoter downstream of RhoA signaling (Li et al., 1997; Liu et al., 2003; Mack et al., 2001). Additionally, transforming growth factor β (TGF-β) signaling leads to an increase in Smad3 binding to the *Sm22* promoter and induces transgelin expression in cooperation with myocardin (Qiu et al., 2003; Qiu et al., 2005). A negative regulator of transgelin expression is gut-enriched Krüppel-like factor (GKLF) (Adams et al., 2000). A regulation of transgelin expression by mechanical tensions was shown for cultured fibroblast cell lines (Liu et al., 2017).

Interaction partners and function

Transgelin binds to actin at its C-terminal region including the CLIK module (Fu et al., 2000) at a ratio of one transgelin per six actin monomers and thereby bundles actin filaments *in vitro* and *in vivo* (Han et al., 2009; Shapland et al., 1993). Additionally, transgelin increases the ratio of F- to G-actin and the contractility of vascular smooth muscle cells (VSMC) (Han et al., 2009). On the other hand, transgelin inhibits calcium-independent contraction in VSMC (Je and Sohn, 2007) and it plays also a role in nuclear factor kappa-light-chain-enhancer of activated B-cells (NF-κB) signaling by binding to inhibitor of kappa B (IκBα) (Shu et al., 2015). Phosphorylation at serine residues inhibits transgelin binding to F-actin *in vitro* and *in vivo* (Fu et al., 2000; Rattan and Ali, 2015). In internal anal sphincter smooth muscle cells, the phosphorylation level is reduced after inhibition of ROCK in a dose-dependent manner (Rattan and Ali, 2015). Another interaction partner of transgelin, besides actin, is protein kinase C delta type (PKCδ), and this interaction is blocked by phosphorylation of transgelin (Lv et al., 2012).

Transgelin expression is not essential in mice, as *Sm22* knock-out mice are fertile and develop normally (Kühbandner et al., 2000; Zhang et al., 2001). Nevertheless, *Sm22* knock-out leads to a reduced contractility and actin content in arterial smooth muscle cells (Zeidan et al., 2004). Following glomerular damage, transgelin is expressed in podocytes of both rodents and humans (Marshall et al., 2011; Wang et al., 2012b). In an experimental crescentic glomerulonephritis model *de novo* transgelin expression in podocytes negatively affected the disease progression (Marshall et al., 2011).

1.8. Mouse lines and the human podocyte cell line (hPCL)

1.8.1. Podocyte-specific *Lmx1b* knock-out

Different mouse models are used to address the molecular pathways leading from knock-out of the *Lmx1b* gene to podocyte foot process effacement and proteinuria. These mouse models have in common that heterozygous *Lmx1b* knock-out does not display any overt phenotype of mice, in harsh contrast to the situation in human NPS patients. One of these mouse models is the podocyte-specific *Lmx1b* knock-out, illustrated in Figure 1.12.

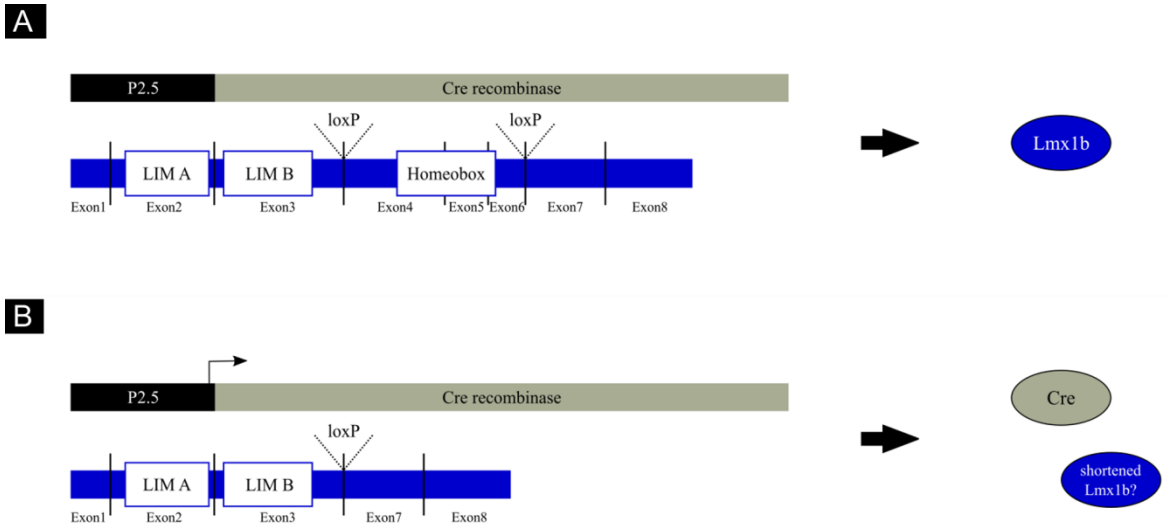

Figure 1.12: **Schematic illustration of the constructs leading to podocyte-specific inactivation of *Lmx1b*.** [A] In tissue aside of podocytes the 2.5 kbp promoter fragment of the *NPHS2* gene (named *P2.5*) is inactive, whereas full-length *Lmx1b* is transcribed and expressed (dependent on *Lmx1b* promoter activity). [B] The *P2.5* promoter is active in podocytes, leading to Cre recombinase expression. Cre recombines the *Lmx1b* gene at loxP sites located in intron 3 and 6, leading to a cut-out of the exons 4 - 6 containing the homeobox. The deletion is in-frame, but whether the shortened protein is still expressed is not known.

A 2.5 kbp promoter fragment of the human *NPHS2* gene (*P2.5*) encoding for podocin is cloned upstream of Cre recombinase, resulting in a Cre expression restricted to podocytes (Moeller et al., 2003). The *Lmx1b* gene is mutated to contain loxP sites for Cre-dependent recombination upstream of exon 4 and downstream of exon 6.

As the Cre recombinase expression is restricted to podocytes, the expression of Lmx1b in other cell types remains unchanged (Figure 1.12, A). Cre expression in podocytes leads to recombination of the *Lmx1b* gene, resulting in a cut-out of exons 4 – 6, including the homeobox. The deletion is in-frame, but whether a shortened protein is still expressed is unknown (Figure 1.12, B).

Mice containing loxP sites at both alleles (*Lmx1b fl/fl*) and *P2.5 Cre* show already some foot process effacement and proteinuria after 5 days of age, which progresses to heavy proteinuria and death at around an age of 14 days. The *Col4α3*, *Col4α4* and *Nphs2* genes are not downregulated in contrast to the situation in conventional *Lmx1b* knock-out mice (Suleiman et al., 2007).

1.8.2. Inducible podocyte-specific *Lmx1b* knock-out

"Quadruple transgenic mouse line"

As LMX1B is not only expressed in the developing kidney, but also in mature podocytes, it consequently plays a role in maintaining podocyte function. The role of Lmx1b in podocyte maintenance is mainly investigated with an inducible, podocyte-specific *Lmx1b* knock-out mouse model (Figure 1.13), which is generated by crossing of the four single transgenic mouse lines *P2.5 rtTA*, *LC-1*, *floxed Lmx1b*, and *mTmG*.

This model uses an enhanced version of the reverse tetracycline-controlled transcriptional transactivator (rtTA), which binds to tet operator sequences (*TetO*) in the presence of tetracycline/doxycycline (Tet-on system) (Urlinger et al., 2000). The tetracycline controlled regulatory system is derived from the *Escherichia coli* tetracycline-resistance operon (Gossen and Bujard, 1992). The *rtTA* gene is put under the control of the 2.5 kbp promoter fragment of *NPHS2* (*P2.5 rtTA*), resulting in podocyte-specific expression (Shigehara et al., 2003). The *LC-1* construct contains seven *TetO* repeats flanked by two cytomegalovirus minimal promoters, resulting in a bidirectional promoter. This promoter controls the expression of Cre recombinase and firefly luciferase dependent on rtTA binding (Schönig et al., 2002). Two *loxP* sites are introduced to *Lmx1b* upstream of exon 4 and downstream of exon 6, leading to a cut-out of the respective exons through Cre recombinase. Lastly, the *mTmG* reporter construct contains a modified version of *tdTomato* (*mT*) under the control of a chicken β-actin promoter and a cytomegalovirus enhancer (*pCA*) and a downstream polyadenylation sequence (*pA*), resulting in the ubiquitous expression of membrane-

targeted tdTomato. The combined *mT* and *pA* sequence is flanked by two *loxP* sites, which leads to a cut-out of this sequence in presence of Cre recombinase and an expression of the downstream membrane-targeted EGFP (mG) (Muzumdar et al., 2007).

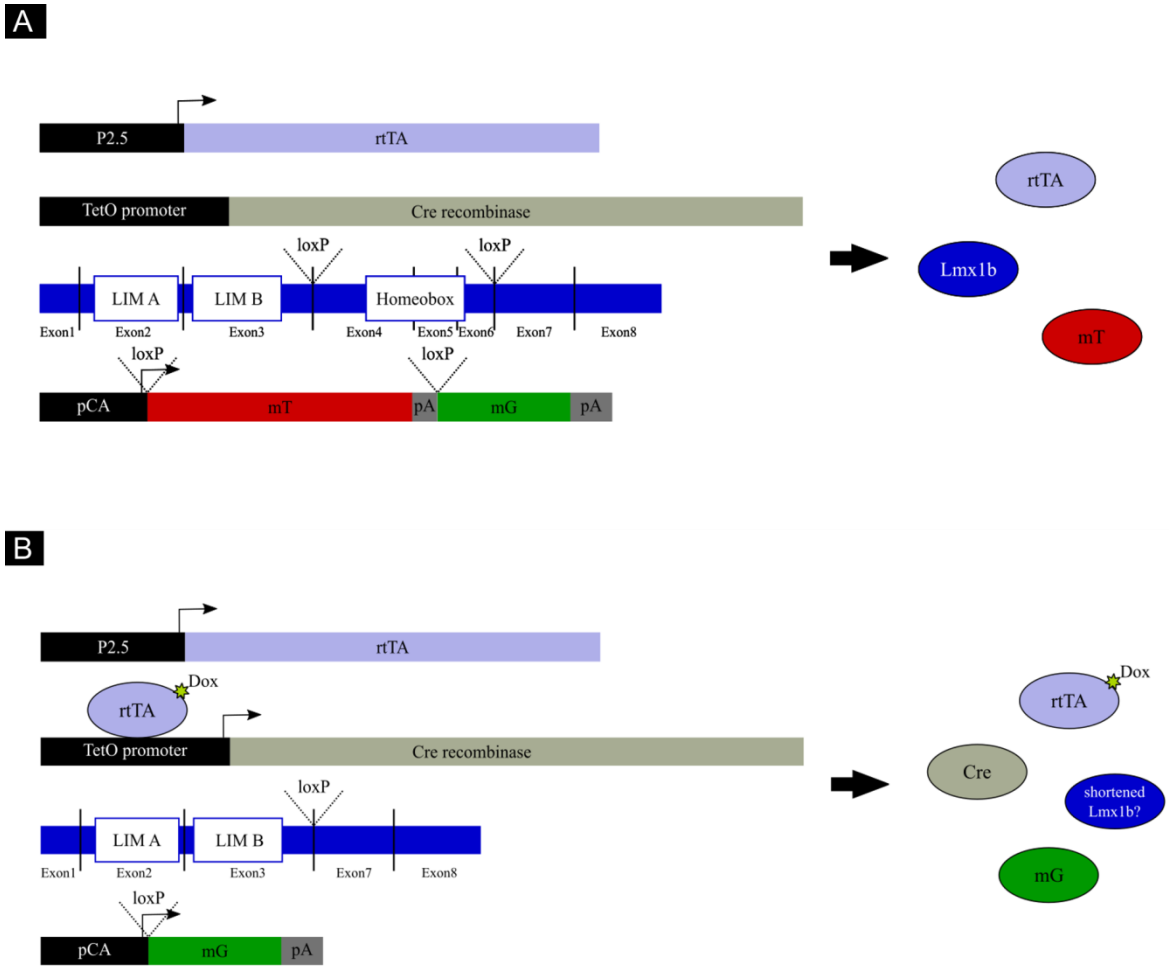

Figure 1.13: **Schematic overview of the inducible, podocyte-specific *Lmx1b* knock-out system in absence [A] and presence [B] of doxycycline.** Red fluorescent protein mT (a membrane-targeted tdTomato) is expressed in all cell types in absence of Cre recombinase. rtTA is under the control of the *P2.5* promoter and thus only expressed in podocytes. Upon doxycycline treatment of the animal, rtTA is able to bind to and activate the *TetO* promoter to induce Cre and luciferase expression (luciferase is not depicted). Cre expression drives the recombination of *Lmx1b* and the *mTmG* reporter construct, leading to a cut-out of exons 4 – 6 and the *mT* sequence, respectively. This results in expression of green fluorescent protein exclusively in podocytes expressing Cre and in an in-frame deletion of the homeobox of *Lmx1b*. Whether expression of a shortened Lmx1b protein still containing the LIM domains occurs, is so far unknown.

This transgene system leads to rtTA, Lmx1b and mT expression in the absence of doxycycline (Figure 1.13, A). Upon doxycycline treatment, rtTA binds to TetO promoter resulting in Cre expression in podocytes and therefore *mTmG* and *Lmx1b* recombination. The membrane targeted EGFP and potentially a shortened version of Lmx1b are expressed in the same podocytes (Figure 1.13, B). However, only ~60% of podocytes show recombination events, as estimated by *Lmx1b* mRNA levels (Burghardt et al., 2013).

Inducible podocyte-specific *Lmx1b* knock-out mice show an onset of proteinuria after 5 days of doxycycline treatment over the drinking water, which progresses and peaks at around two weeks. Thereafter proteinuria declines, but does not disappear, at four weeks. Mice survive doxycycline treatment for at least four weeks (Burghardt et al., 2013). Coincident with the podocyte-specific *Lmx1b* knock-out, *Col4α3*, *Col4α4* and *Nphs2* genes are not downregulated after one week of treatment although albuminuria is already present (Burghardt et al., 2013).

Green fluorescent podocytes

This mouse model is also useful for the isolation of glomeruli and *Lmx1b* knock-out podocytes, as renal damage is dependent on doxycycline treatment and not on the age of mice. Glomeruli are isolated by magnetic bead perfusion, and podocytes can either be digested off the glomeruli by proteases, or glomeruli can be plated onto cell culture flasks resulting in a grow-out of podocytes (referred to as "primary podocytes"). Primary outgrown cells are a mixture of green (with recombination events) and red fluorescent podocytes and possibly endothelial and mesangial cells. They do not establish foot processes and dedifferentiate within few days, but they attach to surfaces, proliferate and are suitable for many experiments. Recently, a culture medium was reported to induce foot process formation of primary podocytes cultured on laminin-521 (Yaoita et al., 2018), which expands the usefulness of this cell type. Podocytes digested off glomeruli do not adhere to surfaces, but are readily available without dedifferentiation and can be purified by fluorescence assisted cell sorting (FACS).

1.8.3. Human podocyte cell line

The human podocyte cell line (hPCL) is derived from a nephrectomy of a 3-year-old child with a unilateral antenatal obstructive/reflux nephropathy. Primary cells outgrown from glomeruli were infected with a simian virus large T antigen gene, selected and single clones were picked (Saleem et al., 2002). The resulting cells proliferate at permissive conditions (33 °C, 5% CO_2) and differentiate to a more podocyte like phenotype at non-permissive conditions (37 °C, 5% CO_2), as seen by expression of podocyte-specific proteins like nephrin and podocin (Saleem et al., 2002).

1.9. Aim of this study

Defects in the gene coding for the transcription factor LMX1B have been identified to cause NPS about 20 years ago, but the exact molecular mechanisms leading to the renal symptoms observed in some NPS patients remain elusive. As a previous study suggested an involvement of the podocyte actin cytoskeleton in disease progression (Burghardt et al., 2013), the main goal of this study was to identify and investigate possible links between the actin cytoskeleton, the transcription factor Lmx1b and renal defects. Therefore five different approaches were undertaken:

1) Validation of Lmx1b regulated genes on the protein level

Previously several genes were identified to be regulated by Lmx1b in murine glomeruli on the transcriptional level, among them *Abra*, *Arl4c*, and *Sm22*, encoding for actin cytoskeleton associated proteins (Burghardt et al., 2013). In order to validate the Lmx1b-dependent transcriptional regulation of those genes also on the protein level, it was planned to compare protein levels of knock-out and wild-type podocytes by western blotting. Therefore primary murine podocytes of the inducible, podocyte-specific mouse line should be collected by FACS.

2) Further investigation of a dysregulation of the actin cytoskeleton in *Lmx1b*-deficient podocytes

The dysregulation of the actin cytoskeleton in primary outgrown, murine green fluorescent podocytes following *Lmx1b* knock-out should be further confirmed by direct methods like determination of the F-actin content, but also by indirect methods monitoring actin-dependent processes like cell spreading and cell movement.

3) Investigation of molecular pathways linking Lmx1b and its target genes to the actin cytoskeleton

After confirming Lmx1b target genes and the involvement of the actin cytoskeleton in the disease, the signaling pathway(s) linking those should be discovered. This should be approached by investigation of the *Lmx1b* knock-out-dependent activity or phosphorylation of several well-known actin regulators and also by observation of the effect of inhibiting several actin-regulating pathways.

4) Determination of a potential dysregulation of focal adhesions in *Lmx1b*-deficient podocytes

As primary murine *Lmx1b* knock-out podocytes adhered stronger to laminin-111 compared to wild-type cells (Burghardt et al., 2013), the role of focal adhesions and its possible impact on the actin cytoskeleton should be investigated. Therefore the amount, localization and activation of the α3β1-integrin of primary wild-type and knock-out podocytes should be compared.

5) Investigation of the influence of the dysregulated protein transgelin on podocyte function and structure and on the actin cytoskeleton

The effect of transgelin, which expression was highest dysregulated in respect of *Lmx1b* knock-out (Burghardt et al., 2013), on podocyte health should be determined in more detail. Therefore a new mouse model should be established by crossing global *Sm22* knock-out mice with podocyte-specific *Lmx1b* knock-out mice. This mouse line should be investigated regarding survival, proteinuria, kidney histology and ultrastructure, and glomerular actin cytoskeleton organization.

2. Materials and Methods

2.1. Materials

2.1.1. Consumables

Equipment/Instrument	Source
µ-Dish, 35 mm, high, glass bottom	Ibidi
Autoclave tape	VWR
Bottle top filter 0.22 µm	Sarstedt
Cell culture dish, 100 mm	Sarstedt
Cell culture flask (25 cm², 75 cm²)	Sarstedt
Cell culture plate, (12-well, 24-well)	Sarstedt
Cell scraper, 39 cm	Sarstedt
Cell strainer, 100 µm	BD Falcon
Chromatography paper	Whatman
Cover glasses, 24 x 60 mm	Roth
CryoPure tube, 1.8 ml	Sarstedt
Dialysis cassette, Slide-A-Lyzer MWCO 3.5 kDa	Thermo Fisher
Dispenser tips (1.25, 2.5, 5, 12.5 mL)	VWR
Filters, folded 90 mm	Schleicher & Schull
Glass coverslips, 12 mm	R. Langenbrinck
Glass Pasteur pipettes	VWR
Gloves, latex	Kimtech
Gloves. nitrile	Kimtech
Gravity flow column	Promega
Hypodermic needles	B. Braun
Micro tube (0.2, 0.5, 1.5, 2.0 mL)	Sarstedt
Microscope slides	Roth
Microscope slides, SuperFrost® Plus	Thermo Fisher
Parafilm	Pechiney Plastic
Pipette filter tips	Sarstedt
Pipette tips	Sarstedt
Plate, 96-well	Sarstedt
PVDF transfer membrane, pore size 0.45 µm	Merck
Round bottomed tube with cell strainer, 35 µm	BD Falcon
Serological pipettes (5, 10, 25 mL)	Sarstedt
Syringes (1, 3 mL)	B. Braun
Task wipes	Kimtech
Tube (12, 15, 50 mL)	Sarstedt

2.1.2. Chemicals and reagents

Chemicals and reagents	Source
Acetic acid	Merck
Acrylamide, 30% / Bisacrylamide, 0.8% solution	Serva
Agarose, NEEO quality	Roth
Amido black 10B	Merck
Ampicillin sodium salt	Roth
Aprotinin	Roth
APS (Ammonium persulfate)	Fluka
Bacto agar	Becton Dickinson
Bacto tryptone	Becton Dickinson
Bacto yeast extract	Becton Dickinson
Bromophenol blue	Serva
BSA (Bovine serum albumim), fraction V	Sigma-Aldrich
Calcium chloride	Roth
Cantharidin	Sigma-Aldrich
Chloramphenicol	Sigma-Aldrich
Cyanogen bromide-activated Sepharose® 4B	Sigma-Aldrich
Cytochalasin D	AppliChem
DABCO (1,4 Diazabicyclo[2.2.2]octan)	Roth
DAPI (4',6-Diamidin-2-phenylindol)	Sigma-Aldrich
DePeX	Serva
Dipotassium hydrogen phosphate	Merck
di-Sodium hydrogen phosphate	Merck
DMP-30	Roth
DMSO (Dimethylsulfoxide)	Sigma-Aldrich
dNTPs (Deoxynucleotide triphosphates)	Fermentas
Doxycycline hyclate	AppliChem
Dynabeads M-450 tosylactivated	Invitrogen
EDTA, disodium salt (Ethylenediaminetetraacetic acid)	Roth
Eosin	Agar scientific
Epon embedding medium	Sigma-Aldrich
Epon hardener DDSA	Sigma-Aldrich
Epon hardener MNA	Sigma-Aldrich
Ethanol	Sigma-Aldrich
Ethidium bromide	Sigma-Aldrich
FCS (Fetal calf serum)	PAN Biotech
Ficoll™ 400	Serva
Glucose	Merck
Glutaraldehyde, 25%	Serva
Glycerol	Roth
Glycine	Sigma-Aldrich

Hematoxylin, Gill No. 3	Sigma-Aldrich
HEPES (4-(2-hydroxyethyl)-1-piperazineethanesulfonic acid)	Roth
His•Bind® resin	Merck
Hydrochloric acid, 1M	Fluka
Hydrochloric acid, 32%	Merck
Imidazole	Merck
Immersol 518 F	Zeiss
Immersol W2010	Zeiss
IPTG (Isopropyl-β-D-1-thiogalactopyranoside)	Fermentas
Isopropanol	Merck
ITS-G (Insulin-Transferrin-Selenium, 100x)	Gibco
Kanamycin sulfate	AppliChem
Laminin-521	BioLamina
Lead citrate, 3% (Ultrostain 2)	Leica
Leupeptin	Serva
LIM kinase Inhibitor I	Calbiochem
Magnesium chloride	Merck
Methanol	Roth
Narcoren	Merial
Nickel sulfate	Merck
Nonidet-P40	AppliChem
Paraplast Plus®	Leica
PEI (Polyethylenimine)	Polysciences Inc.
Penicillin-streptomycin	Sigma-Aldrich
PFA (Paraformaldehyde)	Merck
PI (Propidium iodide)	AppliChem
PMSF (Phenylmethane sulfonyl fluoride)	Sigma-Aldrich
Potassium chloride	Merck
Potassium dihydrogen phosphate	Merck
Puromycin	PAA
PVA (Poly(vinyl alcohol))	Sigma-Aldrich
Roti-Quant	Roth
SDS (Sodium dodecyl sulfate)	Serva
Skim milk powder	Sucofin
Sodium acetate	Roth
Sodium cacodylate trihydrate	Fluka
Sodium chloride	Merck
Sodium dihydrogen phosphate	Roth
Sodium hydroxide solution, 1 M	Fluka
Sucrose	Merck
SuperSignal West Pico	Thermo Fisher
TEMED (Tetramethylethylenediamine)	Roth
Thimerosal	Sigma-Aldrich

Tissue-Tek®	Sakura Finetek
Tris base (Tris(hydroxymethyl)aminomethane)	Sigma-Aldrich
Trisodium citrate	Merck
Triton-X-100	Roth
Tween 20	Roth
Uranyl acetate dihydrate	Merck
Urea	Merck
WesternBright ECL	advansta
Xylene cyanol FF	Serva
Xylol	Merck
Y-27632 dihydrochloride	Sigma-Aldrich
β-mercaptoethanol	Merck

2.1.3. Buffers, solutions and media

Commercial buffers and media

Buffer/Medium	Source
DMEM, high glucose	Sigma-Aldrich
DMEM / Ham's F12	Sigma-Aldrich
HBSS, premixed powder	Sigma-Aldrich
RPMI 1640	Sigma-Aldrich
10x Thermopol® buffer	NEB

Media/solutions for work with bacteria

Buffer/Solution	Ingredients		
LB	10 g/L 5g/L 10 g/L	Bacto tryptone Bacto yeast NaCl	autoclaved
Ampicillin stock solution	50 g/L	Ampicillin sodium salt	sterile filtrated
Chloramphenicol stock solution	34 g/L	Chloramphenicol	sterile filtrated
IPTG stock solution	1 M	IPTG	sterile filtrated, stored in the dark

Buffers/solutions for protein purification on Ni-NTA columns

Buffer/Solution	Ingredients		
2x Binding buffer	40 mM	Tris base	pH 7.9, HCl
	1 M	NaCl	
	10 mM	Imidazole	
	0.2%	Triton-X-100	
Urea binding buffer	6 M	Urea in 1x binding buffer	pH 7.9, HCl
2x Wash Buffer – His-Column	40 mM	Tris base	pH 7.9, HCl
	1 M	NaCl	
	120 mM	Imidazole	
	0.2%	Triton-X-100	
2x Elution Buffer	40 mM	Tris base	pH 7.9, HCl
	1 M	NaCl	
	2 M	Imidazole	
	0.2%	Triton-X-100	
2x Strip buffer	40 mM	Tris base	pH 7.9, HCl
	1 M	NaCl	
	200 mM	Na_2EDTA x 2 H	
8x Charge solution	400 mM	$NiSO_4$ x 6 H_2O	pH 7.9

Buffers for protein coupling to CNBr beads

Buffer/Solution	Ingredients		
Coupling Buffer	100 mM	$NaHCO_3$	pH 8.3
	500 mM	NaCl	
Blocking buffer	0.2 M	Glycine	pH 8.0
Wash buffer A	100 mM	NaAc	pH 4.0
	500 mM	NaCl	
Wash buffer B	100 mM	NaAc	pH 8.0
	500 mM	NaCl	
Storage buffer	0.4 g/L	Thimerosal in 1x PBS	pH 7.4

Buffers for antibody affinity purification

Buffer/Solution	Ingredients		
Wash buffer 1	10 mM	Tris base	pH 7.5, HCl
	170 mM	NaCl	
Wash buffer 2	10 mM	Tris base	pH 7.5, HCl
	170 mM	NaCl	
	0.02%	Tween 20	
Wash buffer 3	10 mM	Tris base	pH 7.5, HCl
	500 mM	NaCl	
	0.02%	Tween 20	
Elution buffer	0.2 M	Glycine	pH 2.0
	0.2 M	NaCl	
Neutralization buffer	1 M	Tris base	pH 8.8
	2.4 g/L	Thimerosal	

Buffers/solutions for SDS-PAGE

Buffer/Solution	Ingredients		
4x Stacking gel buffer	0.5 M	Tris base	pH 6.8, HCl
	4 g/L	SDS	
4x Separating gel buffer	1.5 M	Tris base	pH 8.8, HCl
	4 g/L	SDS	
5x SDS sample buffer	625 mM	Tris base	pH 6.7, HCl
	125 g/L	SDS	
	12.5 %	β-mercaptoethanol	
	0.5 g/L	Bromophenol blue	
	50%	Glycerol	
10x SDS running buffer	0.25 M	Tris base	
	1.9 M	Glycin	
	10 g/L	SDS	
Amido black staining solution	1.5 mM	Amido black 10B	
	50%	Methanol	
	10%	Acetic acid	

Buffers for western blotting

Buffer/Solution	Ingredients		
Transfer buffer	50 mM	Tris base	
	384 mM	Glycine	
	0.1 g/L	SDS	
	20%	Methanol	
10x TBS	0.25 M	Tris base	pH 7.4, HCl
	1.4 M	NaCl	autoclaved
	26.8 mM	KCl	
TBS-T	0.1%	Tween 20 in 1x TBS	
Blocking buffer	50 g/L	Skim milk powder	
	0.1%	Tween 20 in 1x TBS	

Solutions for mouse work

Buffer/Solution	Ingredients	
Induction solution	2 g/L	Doxycycline
	50 g/L	Sucrose
Physiological saline solution	9 g/L	NaCl
Narcoren working solution	1:50	dilution of Narcoren in physiological saline solution

Buffers/solutions for epon embedding

Buffer/Solution	Ingredients	
Epon	4.6 g	Epon embedding medium
	2.85 g	Hardener DDSA
	2,51 g	Hardener MNA
	0.15 g	Accelerator DMP-30
		Mix medium and hardeners and stir for 20 min, add DMP-30 and stir for another 20 min

Buffers for DNA isolation and genotyping

Buffer/Solution	Ingredients		
Tail buffer	100 mM	Tris base	pH 8.0, HCl
	200 mM	NaCl	autoclaved
	5 mM	$Na_2EDTA \times 2\ H_2O$	
	2 g/L	SDS	
TE buffer	10 mM	Tris base	pH 8.0, HCl
	1 mM	$Na_2EDTA \times 2\ H_2O$	autoclaved
50x TAE buffer	2 M	Tris base	pH 8.0,
	0.1 M	$Na_2EDTA \times 2\ H_2O$	acetic acid
5x DNA loading buffer	50 mM	$Na_2EDTA \times 2\ H_2O$	pH 8.0
	1.25 g/L	Bromophenol blue or xylene cyanol FF	
	1.5 g/L	Ficoll type 400	
	5 g/L	SDS	

Buffers for tissue and cell fixation

Buffer/Solution	Ingredients		
4% PFA	40 g/L	PFA solve in water with some drops of 1 mM NaOH added under heating to 60 °C; add 10x PBS after complete dissolving	pH 7.4
2% Glutaraldehyde	1:12.5	dilution of Glutaraldehyde, 25% in Caco buffer	pH 7.4
Caco buffer	0.1 M	Sodium cacodylate trihydrate	pH 7.4
Sucrose buffer	180 g/L	Sucrose in 1x PBS	pH 7.4

Buffers for immunofluorescence staining

Buffer/Solution	Ingredients		
Retrieval buffer	10 mM	$Na_3C_3H_5(COO)_3$ x 2 H_2O	pH 6.0
Histoblock buffer	20 g/L 0.1%	BSA Triton-X-100 in 1x PBS	pH 7.4
3% BSA buffer	30 g/L	BSA in 1x PBS	pH 7.4
Permeabilization buffer, cells	0.1%	Triton-X-100 in 1x PBS	pH 7.4
Permeabilization buffer, tissue	0.3%	Triton-X-100 in 1x PBS	pH 7.4
DAPI staining buffer	0.17 mg/L	DAPI in 1x PBS	pH 7.4
Mounting buffer	0.1 M 100 g/L 25 g/L 25%	Tris base PVA DABCO Glycerol Mix PVA in 50% glycerol o/n; solve at 50 °C after adding an equivalent amount of 0.2 M tris base the next day. Add DABCO, centrifuge (3 000 *g*, 15 min) and aliquot.	pH 8.0, HCl

Buffers/solutions for podocyte isolation and FACS

Buffer/Solution	Ingredients		
Bead slurry	40 µL in 8 mL	Dynabeads M-450 HBSS per mouse	pH 7.4
Digestion buffer	4 mg 4 mg 200 U in 4 mL	Pronase E Collagenase II DNase I stock solution HBSS per mouse	pH 7.4
Bead slurry in digestion buffer	10 µL in 2 mL	Beads M-450 tosylactivated Digestion solution per mouse	pH 7.4
FACS buffer	0.2%	FCS in 1x PBS	pH 7.4
PI stock solution	1 g/L	Propidium iodide	

Buffers and media for work with cells and coatings

Buffer/Solution	Ingredients		
10x PBS	1.27 M 27 mM 14.7 M 80.9 mM	NaCl KCl KH_2PO_4 Na_2HPO_4 x 2 H_2O	pH 7.4
Primary podocyte growth medium	90% 10% 10 mg/L 5.5 mg/L 0.67 ng/L 1000 unit 0.1 g/L	DMEM/Ham's F12 FCS Insulin Transferrin Sodium selenite Penicillin Streptomycin	
1x PBS^{++}	0.9 mM 0.5 mM	$CaCl_2$ $MgCl_2$ x 6 H_2O in 1x PBS	pH 7.4

Buffers for cell lysis

Buffer/Solution	Ingredients		
Lysis buffer A	150 mM	NaCl	pH 7.9
	20 mM	HEPES	
	0.6%	Nonidet-P40	
	10 µg/mL	Aprotinin	
	10 µg/mL	Leupeptin	
	100 µM	Cantharidin	
	1 mM	PMSF	
Lysis buffer B	690 mM	NaCl	pH 7.9
	80 mM	HEPES	
	3 mM	$MgCl_2$ x 6 H_2O	
	10 µg/mL	Aprotinin	
	10 µg/mL	Leupeptin	
	100 µM	Cantharidin	
	1 mM	PMSF	
	50%	Glycerin	
Urea lysis buffer	6 M	Urea	pH 7.4
	1%	Triton-X-100	
		in 1x PBS	

2.1.4. Enzymes, kits and markers

Enzymes

Enzyme	Source	
0:25% Trypsin-EDTA solution	Sigma-Aldrich	T4049
Accutase	Sigma-Aldrich	A6964
Collagenase IA	Sigma-Aldrich	C9891
Collagenase Type II	Worthington	LS004176
DNase I	AppliChem	A3778
Pronase E	Merck	1074330001
Proteinase K	Roth	7528.2
Taq DNA Polymerase	NEB	M0267L

Kits

Kit	Source
Plasmid Plus Midi Kit	Qiagen
RhoA/Rac1/Cdc42 G-LISA Activation Assay Bundle	Cytoskeleton

Markers

Marker	Source
2-log DNA ladder	NEB
PageRuler prestained protein ladder	Thermo Fisher

2.1.5. Antibodies and peptides

Primary antibodies and peptides

Name	Immunogen		Species	Dilution	Source
anti-Abra	Abra	m	Rabbit polyclonal	1:100 (WB)	Own Lab
anti-Arl4c	Arl4c	m	Rabbit polyclonal	1:100 (WB)	Own Lab
Cdc42 (P1)	Cdc42	h, m, r	Rabbit polyclonal	1:100 (WB)	Santa Cruz SC-87
Alexa Fluor™ 633 phalloidin	F-actin		/	1:40 (IF) 1:40 (IF-Cryo)	Invitrogen A-22284
Anti-GAPDH	GAPDH	h, m, r	Rabbit polyclonal	1:25000 (WB)	Sigma-Aldrich G9545
BMO8	Lmx1b	m	Rabbit polyclonal	1:1000 (WB)	Own Lab
Phospho-Myosin Light Chain 2 (Ser19)	Phospho-Myosin Light Chain 2 (Ser19)	h, m, r	Rabbit polyclonal	1:100 (IF)	Cell Signaling #3671
Podocin	Podocin	h, m, r	Rabbit polyclonal	1:500 (IF-P)	Sigma-Aldrich P0372
Rac1 (C-14)	Rac1	h, m, r	Rabbit polyclonal	1:100 (WB)	Santa Cruz SC-217

RhoA (67B9)	RhoA	h, m, r	Rabbit monoclonal	1:1 000 (WB)	Cell Signaling #2117
Anti-SM22 alpha	Transgelin	h, m, r	Goat polyclonal	1:500 (WB) 1:100 (IF) 1:200 (IF-P)	abcam ab10135
LEAF^{TM} Purified Rat IgG2a, κ isotype ctrl	Trinitrophenol + KLH	/	Rat monoclonal IgG2a, κ	1:320 (IF) 1:200 (FC)	BioLegend 400516
Anti-Integrin β_1 antibody, clone MB1.2	β1-integrin	h, m, r	Rat monoclonal	1:200 (FC)	Merck Millipore MAB1997
Purified Rat Anti-Mouse CD29 (9EG7)	β1-integrin, active	m	Rat monoclonal IgG2a, κ	1:50 (IF) 1:100 (FC)	BD Bioscience 550531

Secondary antibodies

Immunogen	Conjugate	Species	Dilution	Source
Goat IgG	Alexa 488	Donkey	1:600 (IF)	Invitrogen A-11055
Goat IgG	Alexa 568	Donkey	1:600 (IF)	Invitrogen A-11057
Goat IgG	HRP	Rabbit	1:80 000 (WB)	Sigma-Aldrich A5420
Rabbit IgG	Alexa 568	Donkey	1:600 (IF) 1:600 (IF-P)	Invitrogen A-10042
Rabbit IgG	HRP	Goat	1:200 000 (WB)	Sigma-Aldrich A0545
Rat IgG	Alexa 568	Goat	1:200 (IF)	Invitrogen A-11077
Rat IgG	Alexa 647	Goat	1:200 (FC)	Invitrogen A-21247

2.1.6. Oligonucleotides for genotyping

Gene	Primer	Sequence	Amplicon
Cre	forward	TGGACATGTTCAGGGATCGC	
	reverse	TCAGCTACACCAGAGACGGA	613 bp
Lmx1b, floxed	forward	AGGCTCCATCCATTCTTCTC	220 bp (WT)
	reverse	CCACAATAAGCAAGAGGCAC	330 bp (TG)
mTmG	forward	CTCTGCTGCCTCCTGGCTTCT	
	reverse wt	TCAATGGGCGGGGGTCGTT	330 bp (WT)
	reverse tg	CGAGGCGGATCACAAGCAATA	250 bp (TG)
P2.5 Cre	forward	GGTTGGCACCCCTCTAGCATGACATTAGGA	
	reverse	TCATCACTCGTTGCATCGACCGGTAATGCA	364 bp
rtTA	forward	GCAAGACTTTCTGCGGAACA	
	reverse	GAAAAGGAAGGCAGGTTCGG	340 bp
Transgelin (WT)	forward	CTCAGAGTGGAAGGCCTGCTT	
	reverse	CACACCATTCTTCAGCCACA	276 bp
Transgelin (KO)	forward	CTCAGAGTGGAAGGCCTGCTT	
	reverse	GGCGATCCCTGAACATGTCC	220 bp

2.1.7. Plasmids and cell lines

Plasmids

Plasmid	Bacterial strain	Resistance	Source
pcDNA3	DH5α	Amp	Invitrogen
pcDNA3/mAbra	DH5α	Amp	Own lab
pcDNA3/mArl4c	DH5α	Amp	Own lab
pET21a/mAbra-His	Rosetta pLysS	Amp/Cam	Own lab
pET21a/mArl4c-His	Rosetta pLysS	Amp/Cam	Own lab

Cell lines

Cell line/ bacterial strain	Description	Source
HEK239T	human embryonic kidney cell line Expression of SV40 large T-antigen	ATCC
hPCL pInducer-LMX1B clone#1	human podocyte cell line Transduced with pInducer-LMX1B in own lab; expression of Lmx1b upon doxycycline induction	hPCL from M.A. Saleem (University of Bristol); (Saleem et al., 2002)
DH5α	*Escherichia coli* strain Competent strain used for mammalian plasmid reproduction	DSMZ
Rosetta (DE3) pLysS	*Escherichia coli* strain Suitable for protein expression due to T7 polymerase, T7 lysozyme and rare tRNA expression	Thermo Fisher

2.1.8. Equipment and instruments

Equipment / Instrument	Source
Absorbance microplate reader "Sunrise"	TECAN
Agarose gel electrophoresis chamber "Horizon 58"	Gibco
Agarose gel electrophoresis chamber "Owl™ EasyCast™ B2"	Thermo Fisher
Autoclave "2540 ML"	Tuttnauer
Autoclave "5050 ELV"	Tuttnauer
Blotting chamber "Tank Blot SE 600"	Hoefer
Bunsen burner	Usbeck
Cell separation magnet "IMagnet™"	BD Bioscience
Cell sorter "FACSAria II"	BD Bioscience
Centrifuge "Avanti® J-26 XP" with rotor Ja-10	Beckman Coulter
Centrifuge "Heraeus Pico 17"	Thermo Fisher
Centrifuge "Hitachi himac CT15RE" with rotor T15A61-1041	VWR
Centrifuge "Multifuge 3 L-R" with rotor Ch. 2454	Heraeus
Centrifuge "Sigma-Aldrich 3K20" with rotor 12158	Sigma
Chemiluminescence system "Fusion-FX7"	Vilber Lourmat
CO_2 incubator "CB210"	Binder
Cryostat "CM3050s"	Leica
Digital slide scanner "NanoZoomer-SQ"	Hamamatsu
Freezers -20 °C	Privileg
Freezers -80 °C "Herafreeze™"	Thermo Fisher
Gel documentation system "GelDoc™ XR+"	Bio-Rad

Gel electrophoresis cell “Mini Protean 3”	Bio-Rad
Glassware (beakers, bottles, flasks)	Schott; VWR
Heating plate with a magnetic stirrer “MR 2002" and “MR 3001"	Heidolph
Hybridization oven “HB-1000”	UVP
Hybridization oven “OV3”	Biometra
Ice machine	Ziegra
Incubator “Kelvitron t"	Thermo Fisher
Incubator “Multitron standard”	Infors
Inverted microscope “Eclipse TS100”	Nikon
Laboratory pH Meter “CG 842"	Schott
Laminar flow bench “Lamin Air HA 2448 GS"	Heraeus
Liquid nitrogen container “Arpege TP 170"	Air Liquide Medical
Microtome “RM2255"	Leica
Microwave “8016 G"	Privileg
Multi-dispenser “HandyStep® electronic”	BRAND
Neubauer counting chamber (depth 0.1 mm)	Marienfeld
Paraffin embedding module “EG1150 H”	Leica
pH electrode “SenTix 60"	WTW
Pipettes	Gilson
Pipettor “IPS Pipetboy acu”	Integra Bioscience
Power supply “PS 608"	life technologies
Power supply “Standard Power Pack P25"	Biometra
Refrigerators	SEG, Privileg
Rocking platform shaker “Duomax 1030"	Heidolph
Rocking platform shaker “Polymax 2040”	Heidolph
Spectrophotometer “NanoDrop™ 2000”	Thermo Fisher
Spectrophotometer “U-2000"	Hitachi
Tissue processor “TP-1020”	Leica
Thermal cycler “Mastercycler gradient”	Eppendorf
Thermal cycler “MyCyclerTM”	Bio-Rad
Thermal cycler “T100”	Bio-Rad
Transmission electron microscope “EM Zeiss 902"	Zeiss
Ultrapure water unit “Seralpur PRO 90 CN”	Seral
Vacuum gas pump	VWR
Vertical gel electrophoresis cell “Mini Protean Tetra cell"	Bio-Rad
Vortexer	VWR
Weighing scale “BL 1500 S”	Sartorius
Weighing scale “Kern 770”	KERN & Sohn

Epifluorescence microscope

	Name	Source
Microscope	Axiovert 200M	Zeiss
Light source	LEJ (HXP-120)	Visitron Systems
Objectives	Ultrafluar, 40x/0.6	Zeiss
Camera	CoolSnap ES	Visitron Systems

Epifluorescence microscope with motorized x,y-stage

	Name	Source
Microscope	Observer.Z1	Zeiss
Light source	Colibri.2	Zeiss
Objectives	EC Plan-Neofluar 10x/0.30	Zeiss
Camera	Axiocam MR R3	Zeiss

Confocal microscope

	Name	Source
Microscope	Observer.Z1	Zeiss
Laser	405 nm, diode laser, LSM710	Zeiss
	488 nm, Argon multiline, LDN301	Lasos
	561 nm, DPSS laser, LSM710	Zeiss
	633 nm, HeNe laser, LSM710	Zeiss
Objectives	Plan-Apochromat 20x/0.8	Zeiss
	LD C-Apochromat 40x/1.1 W	Zeiss
	C-Apochromat 63x/1.20 W	Zeiss
Detection module	LSM BiG	Zeiss
Additional	Active gas mixer “The Brick”	Ibidi
equipment	Stage top incubator “HT 200”	Ibidi

2.1.9. Software and tools

Software

Software	Version	Purpose	Company
Bio 1D	15.07	WB quantification	Vilber Lourmat
EndNote	X7.1	Citation and references	Thomson Reuters
Excel	Office 2010	Data processing	Microsoft
FCS Express	6.05	Flow cytometry processing	De Novo Software
Fiji (ImageJ)	1.51s	Image processing	National Institutes of Health
FileMaker Pro	6	Database	FileMaker, Inc.
Fusion	15.18	WB imaging	Vilber Lourmat
ImageLab	5.2	Gel documentation	Bio-Rad
Inkscape	0.92.2	Image processing	/
Magellan™	7.2	Photometric measurement	TECAN
NanoDrop 2000/2000c Operating Software	1.6	Photometric measurement / DNA quantification	Thermo Fisher
OriginPro	9.0.0 SR2	Data processing, diagrams	OriginLab
SnapGene Viewer	4.1	Gene/plasmid handling	GSL Biotech, LLC
VisiView	2.1.4	Image recording	Visitron Systems
Word	Office 2010		Microsoft
ZEN 2011 SP3 (black edition)	8.1	Image recording	Zeiss MicroImaging

ImageJ plugins

Plugin	Version	Authors
ADAPT	1.185	(Barry et al., 2015)
JACoP	2.1.1	(Bolte and Cordelieres, 2006)
NDPI Tools	1.7.2	(Deroulers et al., 2013)
Scientifig	3.1	(Aigouy and Mirouse, 2013)

Internet databases and tools

Name	Internet address
BLAST	https://blast.ncbi.nlm.nih.gov/Blast.cgi
ensembl	http://www.ensembl.org/index.html
Primer 3	http://primer3.ut.ee/
PubMed	https://www.ncbi.nlm.nih.gov/pubmed/
UCSC Genome Browser	https://genome.ucsc.edu/

2.2. Working with bacteria and recombinant protein purification

2.2.1. Cultivation and recombinant protein expression

Long-term storage of bacteria was achieved by freezing cells in LB medium with glycerol (6:1) at -80 °C. All media and glass vessels were autoclaved while antibiotics and IPTG were sterile filtered before use. Inoculation of cultures was carried out under sterile conditions near the flame.

Cultures for plasmid isolation were directly inoculated with a small amount of bacteria and grown overnight at 37 °C under constant shaking in 50 mL LB medium supplemented with 0.5 mg/mL ampicillin.

In case of protein expression cultures, 5 mL of LB medium supplemented with appropriate antibiotics (0.5 mg/mL ampicillin, 34 µg/mL Chloramphenicol) was inoculated with a small amount of frozen bacteria and grown at 37 °C and constant agitation for approx. 5 h. Main cultures (450 mL) were inoculated with a dilution of 1:100 out of preparatory cultures. OD values were measured frequently with a spectrophotometer at 550 nm after diluting 0.5 mL of bacterial cultures 1:2 in LB medium. After reaching an OD of 0.5 the cultures were allowed to cool to RT and protein expression was induced by adding 1 mM IPTG. Protein expression was conducted at 37 °C (pET21a/mAbra-His) or 25 °C (pET21a/mArl4c-His) overnight.

2.2.2. Plasmid DNA isolation

Preparation of plasmid DNA was carried out with the Qiagen Plasmid Plus Midi Kit. At first, overnight cultures were centrifuged at 4 000 *g* for 15 min at 4 °C. The cell pellet was resuspended in 4 mL chilled buffer P1 by pipetting up and down. Afterwards, 4 mL of buffer P2 was added, mixed thoroughly and incubated for 3 - 5 min at RT. After adding buffer S3 (4 mL) and mixing, the lysate was immediately transferred into a sealed filter cartridge and incubated for 10 min. The lysate was filtered, 2 mL buffer BB was added and the clear solution was inverted several times. The solution was drawn through a spin column by applying vacuum. The bound DNA was washed with 0.7 mL buffer ETR and 0.7 mL buffer PE by centrifugation (10 000 *g*, 1 min). After spinning the dry column once more, the plasmid DNA was incubated for 1 min with 200 µL buffer EB and eluted by centrifugation. The DNA concentration was measured with the NanoDrop spectrophotometer.

2.2.3. Recombinant protein purification using His•Bind columns

After determination of the OD the cells were pelleted by centrifugation (4 000 *g*, 10 min, 4 °C) and resuspended in a volume of ice-cold 1x binding buffer calculated by equation (1).

$$V(binding\ buffer) = \frac{OD_{550} \times V(culture)}{50} \quad (1)$$

The cell suspension was lysed by five cycles of sonication (30 s each) and cooled in an ice bath between cycles. The lysate was centrifuged (10 000 *g*, 20 min, 4 °C), the supernatant was collected and stored. To dissolve the pellet, it was first washed 3x with 1x binding buffer and then resuspended in urea binding buffer with half the volume calculated with equation (1). The suspension was dissolved overnight while shaking on a rotating wheel at 4 °C. Remaining insoluble material was removed by centrifugation (10 000 *g*, 30 min, 4 °C).

For protein purification a His•Bind column was freshly prepared. 2 mL of resin slurry was filled into a pre-wetted gravity flow column and allowed to settle down to yield 1 mL bed volume. The column was never allowed to dry out and washed with 3x bed volume H_2O, activated with 5x bed volume charge solution and equilibrated with 3x bed volume urea binding buffer. To bind the His-tagged protein to the resin, the resin was removed from the column and incubated with the protein solution for 4 h at 4 °C on the rotating wheel. After centrifugation (1 000 *g*, 3 min, 4 °C) the resin pellet was resuspended in urea binding buffer and loaded again on the column. The column was washed with 10x bed volume urea binding buffer and 6x bed volume 1x wash buffer containing 6 M urea. Elution was carried out with 1x elution buffer supplemented with 6 M urea and six fractions were collected with 0.5x bed volume each. The column was washed and regenerated with 5x bed volume H_2O and 3x bed volume strip buffer and stored in strip buffer at 4 °C. To analyze which fractions contain the purified recombinant protein, SDS-PAGE was performed.

2.3. Working with proteins

2.3.1. Determination of protein mass concentration

Bradford assay was performed for fast estimation of whole protein content in solutions. The assay was conducted on 96-well plates. First, a BSA standard curve (160 mg/L, 80 mg/L, 40 mg/L, 16 mg/L and 8 mg/L) was diluted in water using a 10 g/L BSA stock solution. Samples to be analyzed and blanks containing only the sample buffer were diluted in the range of 1:10 and 1:200 in water. 50 µL/well of BSA dilutions, protein samples and blanks (buffer and water only blank) were pipetted in doublets on the 96-well plate. The diluted

Roti-Quant reaction solution (1:4 dilution, 200 µL/well) was added in fast succession with a multi-dispenser, air bubbles were removed and the absorbance was measured with 450 nm and 595 nm filters after a reaction time of 5 – 10 minutes. In case blank corrected 450/595 ratios of samples were not in the range of the standard curve, dilution was adjusted accordingly. To receive the mass concentration (β) of protein in the sample, ratios of absorbance at 450 nm to 595 nm was calculated and corrected by the respective blank ratio. Linear regression of the standard curve yielded a slope and y-intercept and the mass concentration could be obtained according to equation (2).

$$\beta(protein) = dilution\ factor \times \frac{corr.\ ratio \times y - intercept}{slope} \qquad (2)$$

2.3.2. Separation of proteins and peptides

Separation of proteins and peptides was achieved by SDS-PAGE. Different sizes and polyacrylamide concentrations were used according to the size and amount of the protein of interest. Small proteins < 20 kDa were separated on 15% gels, proteins between 20 and 50 kDa with 12% gels and larger proteins with 10% gels. Gels were cast at least one day before electrophoresis according to Table 2.1 for mini gels and Table 2.2 for maxi gels. TEMED and APS were added at last to the mixtures and separation gel was then immediately poured into the apparatus and covered with a small line of isopropanol. The gel was allowed to polymerize at least 45 min before isopropanol was decanted and stacking gel was added on top followed by insertion of a comb. After 45 min, gel was wrapped into wet paper towels and aluminum foil and stored at 4 °C.

Gels were mounted into separation chambers and filled with 1x running gel buffer. One part 5x loading buffer was added to four parts of protein solution and boiled for 10 - 15 min afterwards. After short cooling and centrifugation, a maximum of 30 µL for mini gels and 80 µL for maxi gels were loaded into gel pockets. For estimation of protein sizes 2 – 4 µL of pre-stained protein marker was used. Separation was conducted by applying a voltage of 150 V for mini gels and 500 V for maxi gels while stirring and in the case of maxi gels cooling to 10 °C. After the run, stacking gel was removed and gel was either used for western blotting or stained with amido black staining solution for 10 min. Destaining was conducted with water by several cycles of heating in the microwave and mild shaking for approx. 30 min. Gels were digitalized with a scanner.

Table 2.1: Amounts for the casting of mini gels. For separation gels, 7.2 mL was used and 2.5 mL for stacking gels.

Gel	Ingredients	
4% stacking gel	0.75 mL	4x stacking gel buffer
	1.82 mL	H_2O
	0.40 mL	Acrylamide, 30% / Bisacrylamide, 0.8% solution
	2.25 µL	TEMED
	22.5 µL	APS, 100 g/L solution
10% separation gel	2.50mL	4x separation gel buffer
	4.10 mL	H_2O
	3.33 mL	Acrylamide, 30% / Bisacrylamide, 0.8% solution
	5 µL	TEMED
	50 µL	APS, 100 g/L solution
15% separation gel	2.50mL	4x separation gel buffer
	2.44 mL	H_2O
	5.00 mL	Acrylamide, 30% / Bisacrylamide, 0.8% solution
	5 µL	TEMED
	50 µL	APS, 10% solution

Table 2.2: Volumes of components used for casting maxi gels. 25 mL were used for separation gels and 10 mL for stacking gels.

Gel	Ingredients	
4% stacking gel	3.00 mL	4x stacking gel buffer
	7.30 mL	H_2O
	1.6 mL	Acrylamide, 30% / Bisacrylamide, 0.8% solution
	9 µL	TEMED
	90 µL	APS, 100 g/L solution
12% separation gel	7.50mL	4x separation gel buffer
	10.33 mL	H_2O
	12 mL	Acrylamide, 30% / Bisacrylamide, 0.8% solution
	15 µL	TEMED
	150 µL	APS, 100 g/L solution
15% separation gel	7.50mL	4x separation gel buffer
	7.33 mL	H_2O
	15 mL	Acrylamide, 30% / Bisacrylamide, 0.8% solution
	15 µL	TEMED
	150 µL	APS, 100 g/L solution

2.3.3. Western blotting

Quantification of the relative amount of specific proteins was carried out by western blotting. Western blotting was carried out using wet blotting technique and a 0.45 µm pore size PVDF membrane. SDS-PAGE gel and six pieces of cropped Whatman 3MM papers were equilibrated in transfer buffer for 15 min. PVDF membrane was activated 1 min in pure methanol and afterwards also equilibrated. To transfer protein, a stack of 3 Whatman papers, the gel, the PVDF membrane and again 3 Whatman papers was build and air bubbles were removed. The stack was then put between porous sponges and mounted into the transfer chamber with the membrane orientated towards the anode.

The transfer was achieved under stirring of transfer buffer and cooling to 10 °C with a current of 1 A for 2:20 h. After the run, the membrane was cropped into several pieces if desired and marked at the right top edge of each fragment. For reduction of unspecific binding blocking was performed for 30 min with skim milk blocking buffer at RT. The primary antibody was diluted in blocking buffer and incubated with the membrane under constant agitation overnight. The next day membrane was swilled 2x and washed 4x with TBS-T (2x 5 min and 2x 10 min). The appropriate secondary antibody-HRP-conjugate was diluted in blocking buffer and incubated for 45 min at RT under constant agitation. After again 2x swilling and 4x washing (5 min) with TBS-T the blot was finally washed with 1x TBS for 5 min.

Protein was detected using chemiluminescence reactions catalyzed by HRP. Luminophore and oxidation reagent were freshly mixed 1:1 and incubated 1 min with the membrane. Afterwards, signal was measured with appropriate resolution and exposure time in the “Fusion-FX7” chamber. Signal was quantified with the software Bio 1D by measuring the intensity of bands within a defined area. After blank correction signals were normalized to glyceraldehyde-3-phosphate dehydrogenase (Gapdh) as an internal standard. In case the membrane was probed with several antibodies, chemiluminescent reagents were washed out with TBS-T and the next primary antibody was incubated for 2 h at RT followed by washing and incubation with secondary antibody as described above.

2.3.4. CNBr-activated Sepharose 4B coupling

Before proteins were covalently bound to CNBr-activated Sepharose 4B beads, interfering small molecules were washed out by dialysis. A dialysis cassette was wetted 2 min in H_2O and protein solution was injected with a syringe afterwards. After removing air bubbles the proteins were dialyzed three times against 0.4 L coupling buffer for 2 h, 4 h and overnight at 4 °C. The next day the dialyzed sample was transferred into a micro tube. As proteins at least partly precipitated, an appropriate amount of 100 g/L SDS in coupling buffer was added to yield 5 g/L SDS and boiled until all of the protein was dissolved. The solutions were allowed to cool down to RT.

A proper amount of beads was swollen in 10 mL HCl (1 mM) solution for 30 min and loaded into a gravity flow column. 1 mL bed volume of beads was used for 5 – 10 mg of protein. After washing beads 6x with 10 mL HCl (1 mM) solution and 1x with 2 mL coupling buffer supplemented with 5 g/L SDS, they were immediately mixed with the protein solution and put on the rotating wheel overnight at 4 °C. The next day bound protein was washed with 10 mL 1x coupling buffer containing 5 g/L SDS and afterwards with 10 mL coupling buffer without SDS. Remaining unreacted groups were blocked with blocking buffer for 2 h at RT. The column was washed in 3 cycles with 10 mL wash buffer A and 10 mL wash buffer B, followed by washing with 10 mL coupling buffer and 10 mL 1x PBS. Finally, the column was stored in 0.4 g/L thimerosal in 1x PBS at 4 °C.

2.3.5. Antibody affinity purification

For affinity purification of antibodies rabbit sera and the antigen bound CNBr sepharose columns were used. Both 9 mL of anti-Abra and anti-Arl4c serum was purified. The column was washed with 10x bed volume 1x PBS and mixed with the antibody serum. After incubation on the rotating wheel overnight at 4 °C unbound material was washed out with 10x bed volume buffer 1, 10x bed volume buffer 2, 10x bed volume buffer 3 and finally 10x bed volume buffer 1. The antibody was eluted in five cycles with 1x bed volume elution buffer into micro cups containing 0.2x bed volume neutralization buffer and stored at -20 °C. The column was washed with 10x bed volume 1x PBS and stored in 0.4 g/L thimerosal in 1x PBS at 4 °C. Elution fractions were analyzed by SDS-PAGE.

2.4. Working with mice

2.4.1. Mouse transgenes

LC-1

LC-1 is a transgene with direct control of luciferase and Cre recombinase expression under the promoter P_{tet}bi-1 (Schönig et al., 2002). This bidirectional promoter consists of seven *tetO* repeats flanked by two hCMV derived minimal promoters and is activated upon rtTA binding.

Lmx1b, floxed

In this transgenic mouse line, two loxP sites were introduced into introns downstream of exon 4 and upstream of exon 6 of the endogenous murine *Lmx1b* (Suleiman et al., 2007). Cre recombinase expression results in an in-frame deletion of exons 4 – 6, containing the homeobox sequence. Mice were kindly provided by R. Johnson.

mTmG

The reporter construct *mTmG* comprises of membrane-targeted versions of tdTomato (mT) and an EGFP (mG) under the control of a chicken β-actin core promoter with a CMV enhancer (Muzumdar et al., 2007). tdTomato and a downstream polyadenylation (pA) signal are flanked by loxP sites. This construct results in mT expression in all kinds of tissue under normal conditions. In case Cre recombinase is expressed, mT and the pA signal are cut-out and expression of mG starts. This construct enables to mark specific cell types with green fluorophores by specific promoter controlled Cre expression. Mice were kindly provided by T. B. Huber.

P2.5 Cre

The expression cassette for P1 bacteriophage Cre recombinase is regulated by a 2.5 kbp promoter fragment of the human *NPHS2* gene (Moeller et al., 2003) encoding the protein podocin. The *NPHS2* promoter is exclusively active in podocytes. The Cre recombinase excises flanked by loxP (floxed) gene sequences and for this reason, podocyte-specific gene deletions can be obtained.

P2.5 rtTA

The *rtTA* gene (reverse tetracycline-controlled transcriptional transactivator) is derived and modified from the *E. coli* tetracycline-resistance operon. The encoded protein is able to bind to *tetO* and activate transcription only if tetracyclines (e.g. doxycycline) are present. The gene was put under the regulatory control of a 2.5 kbp fragment of the human *NPHS2* promoter (Shigehara et al., 2003).

SM-CreER^{T2}(ki)

A construct encoding for the CreER^{T2}, an SV40 polyadenylation signal and a neomycin-resistance gene was integrated into the *Sm22* locus resulting in a *Sm22* promoter driven CreER^{T2} expression while transgelin expression is abolished (Kühbandner et al., 2000). CreER^{T2} is a Cre recombinase fused to a mutant estrogen ligand binding domain, resulting in an inactive protein in the absence of tamoxifen. In this work this mouse line was used as a knock-out mouse model, the CreER^{T2} protein was never activated with tamoxifen.

2.4.2. General handling and breeding

The mice are bred in euro standard type II and III cages in a conventional animal laboratory of the University of Regensburg. Offspring was marked by footpad tattoos and tail biopsied 4 – 21 days after birth and separated from the mother at 19 – 28 days of age. Animals had unlimited access to drinking water and complete food in a 12 h day/night cycle.

2.4.3. Genotyping

DNA isolation

Mouse biopsies were digested with 0.2 g/L proteinase K in 700 µL tail buffer overnight in a hybridization oven at 50 °C under rotation. The next day samples were vortexed and centrifuged (10 000 *g*, 30 min, 4 °C) to remove remaining insoluble material. Thereafter, 600 µL isopropanol was added to the supernatant in a fresh micro vial and it was vigorously inverted to precipitate DNA. After centrifugation (10 000 *g*, 30 min, 4 °C) supernatant was sucked off and 70% ethanol (500 µL) was added. The vial was inverted several times and centrifuged (10 000 *g*, 15 min, 4 °C) again. Finally, ethanol was discarded, DNA was completely dried at 40 °C for at least 30 min and resolved in 30 - 200 µL TE buffer overnight in a hybridization oven at 50 °C.

PCR

Mouse genotyping for all six transgenes was realized by PCR. In all cases, 0.5 µL DNA was diluted with DNA free water to 20 µL in a 0.2 mL micro tube. Additionally, a positive control of a known sample and a water control were also prepared. The master mix containing the appropriate primers was freshly prepared according to Table 2.3 and 5 µL was added to every sample. Immediately after a quick mix samples were put into a thermal cycler and the PCR program was started (Table 2.4 and Table 2.5). After the program finished samples were kept at 4 – 12 °C. A complete list of the primers can be found in chapter 2.1.6.

Table 2.3: Master mixes for genotyping mouse transgenes Cre, Lmx1b floxed, mTmG, P2.5 Cre, rtTA, and Sm22 (KO).

Ingredients	Volume for all transgenes except P2.5 Cre	Volume for transgene P2.5 Cre
10x Thermopol buffer	2.5 µL	2.5 µL
DMSO	/	0.75 µL
Primer (100 µM), each	0.15 µL	0.1 µL
dNTPs (10 mM)	0.5 µL	1.0 µL
Taq polymerase	0.25 µL	0.25 µL
H_2O	*ad* 5 µL	*ad* 5 µL

Table 2.4: PCR protocols for all transgenes except P2.5 Cre

Step	T	t		Comments
Melting DNA	94 °C	5 min		
Melting amplicon	94 °C	30 s	35 cycles	
Annealing	variable	1 min		58 °C: *Lmx1b floxed, rtTA* 61 °C: *mTmG, Cre* 63 °C: *Sm22 (*WT), *Sm22* (KO)
Elongation	72 °C	variable		45 s: *Lmx1b floxed, rtTA* 60 s: *mTmG, Cre* 20 s: *Sm22* (WT), *Sm22* (KO)
Final elongation	72 °C	5 min		

Table 2.5: PCR protocol for P2.5 Cre

Step	T	t	Comments
Melting DNA	94 °C	3 min	
Melting amplicon	94 °C	45 s	30 cycles
Annealing	55 °C	45 s	
Elongation	72 °C	2 min	
Final elongation	72 °C	10 min	

Agarose gel electrophoresis

5x DNA loading buffer was added to PCR samples and mixed well. In case the desired PCR amplicon was < 300 bp, xylene cyanol FF was used as a dye, for amplicons > 300 bp bromophenol blue. A 2% agarose gel was made by solving 3 g agarose in 150 mL 1x TAE buffer by heating in a microwave oven. For DNA visualization the intercalation dye ethidium bromide (60 µL/gel) was added. The liquid was cast in the apparatus, the combs were added and remaining air bubbles removed. After approx. 30 min of cooling at RT gel became solid and 12 µL PCR product with loading buffer was added per well. The 2-log DNA ladder was used for size estimation. Electrophoresis was conducted in 1x TAE buffer at a constant voltage of 150 V. DNA bands were visualized and documented by ultraviolet illumination in the GelDoc^{TM} system.

2.4.4. Collection and analysis of urine samples

Collection of urine

Urine samples of animals younger than 21 days and samples taken on the day of mouse perfusion were spontaneously voided urine samples (spot urine). At all other occasions, urine was taken over 24 h by keeping animals separately in a specialized cage for one day. Spot urine samples from animals tested for survival were taken (if possible) on day 4, 10 and 21 after birth. Additionally, 24 h urine was taken at the age of 6 and 13 weeks. Spot urine at the day of perfusion was taken from all animals regardless of experimental series.

Qualitative and quantitative urine analysis

For qualitative determination of urinary proteins, SDS-PAGE with 1 µL spot urine or a 1:500 volume dilution in water of 24 h urine was conducted. For a rough estimation of urine albumin content, different BSA amounts (1, 3, 10 and 30 µg) were loaded on the first four lanes. The protocol for SDS-PAGE is described in chapter 2.3.2.

The quantitative protein content was measured using the Bradford test with a sample dilution of 1:20, as described in chapter 2.3.1.

The urine creatinine mass concentration was determined by the Jaffe reaction. Because of urine volume limitations, urine creatinine was measured only once with 5 µL/well in a 96-well plate. Urine was diluted to 50 µL with water (1:10), whereas water blank (50 µL) and a creatinine standard curve (30, 15, 7.5 and 3.75 mg/L) were pipetted in doublets. 150 µL of the master mix (Table 2.6) was added in fast succession. After 10 min reaction time, the colorimetric product was measured spectrophotometrically at 540 nm. To calculate the mass concentration of samples, linear regression of the standard curve was calculated and mass concentration was obtained using equation (3).

$$\beta(creatinine) = dilution\ factor \times \frac{corr.A_{520} \times y - intercept}{slope} \qquad (3)$$

Table 2.6: Master mix for Jaffe reaction for one urine sample

Volume	Ingredients	
50 µL	1.2 M	Trichloroacetic acid
50 µL	35 mM	Picric acid
50 µL	1.6 M	Sodium hydroxide solution

2.4.5. Induction of *Lmx1b* knock-out

The inducible podocyte-specific *Lmx1b* knock-out mouse line received 2 g/L doxycycline in the drinking water to induce Cre expression. Normal drinking water was replaced by induction solution containing doxycycline and sucrose in the morning 7 days before animal perfusion. The solution was freshly prepared every two days and administered in lightproof bottles in excess.

2.5. Working with kidney sections

2.5.1. Kidney perfusion fixation

Mice were first weighed and spot urine was taken before anesthetizing by two intraperitoneal injections (0.07 -0.12 mg per gram body weight for 8-day old animals, 0.12 -0.15 mg per gram body weight for adult animals) of Narcoren working solution. Tail biopsies were taken for re-genotyping. After opening the *peritoneum*, *arteria* and *vena iliaca communis* and also the aorta below renal arteries were clamped. Abdominal aorta was cut horizontally halfway and the tubing was inserted and tightly fixed with a string. Finally, *vena cava inferior* was cut, the aorta clamp was removed and perfusion fixation was carried out with 4% PFA in 1x PBS at a constant pressure of 180 – 200 mbar for 3 min. Afterwards, the fixation tubing was removed and flushed with heparin. Kidneys were taken out and cut into two halves vertically to the longitudinal axis and further processed depending on embedding technique.

2.5.2. Embedding and slice preparation

Paraffin embedding and slice preparation

Kidney halves for paraffin embedding were additionally immersion fixed in 4% PFA in 1x PBS for 1 – 2 days at constant agitation. After fixation, the tissue was washed two times with 1x PBS and an alcohol series was conducted using an automated tissue processor with liquids and timings listed in Table 2.7. Paraffin-embedding was performed on a heated paraffin dispensing module with the cutting edge orientated towards the bottom of the block. Paraffin blocks were stored at RT. Tissue slices were prepared with a microtome at a thickness of 6 µm and relaxed in a 40 °C water bath. Two slices were taken up on one microscope slide and slice quality was controlled with a light microscope after drying on a heated plate at 40 °C. If slices should be used for immunofluorescence stainings, Superfrost™ Plus microscope slides were used. Finally, the slices were dried overnight at 37 °C.

Table 2.7: Liquids equipped and program of the automated tissue processor.

Liquid	Timings
Isopropanol, 50%	90 min
Isopropanol, 70%	90 min
Isopropanol, 80%	90 min
Isopropanol, 96%	90 min
Isopropanol, 100%	90 min
Isopropanol, 100%	90 min
Isopropanol, 100%	90 min
Xylol, 100%	90 min
Xylol, 100%	90 min
Melted paraffin (60 °C)	240 min
Melted paraffin (60 °C)	240 min
Melted paraffin (60 °C)	240 min

Cryo embedding and slice preparation

Perfusion-fixed kidney halves were processed in 18% sucrose in 1x PBS for 4 h under constant agitation. Afterwards, they were washed twice with 1x PBS, put into a cryomold® with the cutting edge orientated towards the bottom and embedded in Tissue-Tek®. After removing air bubbles the embedding medium was frozen in the gas phase above liquid nitrogen and stored at -80 °C. Tissue slices were taken with a cryostat at a thickness of 7 µm, dried at RT for 20 min and stored at -80 °C for a maximum of two weeks.

Table 2.8: Procedure for epon embedding of glutaraldehyde-fixed kidney pieces.

Liquid	Timings
0.1 M sodium cacodylate buffer	3x, 20 min
10 g/L Osmium tetroxide in 0.1 M sodium cacodylate buffer	2 h
0.1 M sodium cacodylate buffer	4x, 5 min
Ethanol, 50%	30 min
Ethanol, 70%	30 min
Ethanol, 90%	30 min
Ethanol, 96%	30 min
Ethanol, 100%	30 min
Acetone, 100%	3x, 15 min
Acetone / epon (1:1 mixture)	overnight
Epon	3 h (30 °C) and 2 d (60 °C)

Epon embedding and slice preparation

Perfused kidneys were post-fixed in 2% glutaraldehyde in 0.1 M sodium cacodylate buffer (pH 7.4) for at least 2 days at 4 °C under constant agitation. Thereafter, kidneys were cut into small chunks with a maximum edge length of 2 mm. Kidney pieces were washed with 0.1 M sodium cacodylate buffer and processed with osmium tetroxide at RT for better contrast and tissue conservation during dehydration. After another washing step samples were dehydrated in ethanol and acetone. Tissue was when treated with an acetone / epon mixture and finally with freshly made epon. Polymerization at 60 °C was finally conducted over two days. The complete procedure is listed in Table 2.8. Tissue slices were cut with an ultramicrotome at a thickness of 50 – 70 nm and placed on a grid for TEM examination.

2.5.3. Staining of paraffin sections

Deparaffinization and rehydration

To eliminate paraffin and to rehydrate the tissue section, slices were treated with a descending alcohol series according to Table 2.9. Thereto microscope slides were put into a glass holder and moved from one reservoir to the other. Slides were shortly stored in water until all slides were rehydrated.

Table 2.9: Descending alcohol series for deparaffinization and rehydration of paraffin sections and ascending alcohol series for dehydration after H&E staining.

Liquid	Timings	Timings
Xylol, 100%	10 min	10 min
Xylol, 100%	10 min	10 min
Isopropanol, 100%	2 min	2 min
Isopropanol, 100%	2 min	2 min
Isopropanol, 96%	2 min	2 min
Isopropanol, 80%	2 min	8 s
Isopropanol, 70%	2 min	3 s
Isopropanol, 50%	2 min	
bidest. H_2O	> 1 min	

H&E staining of paraffin sections

Prior to basophilic staining of deparaffinized and rehydrated sections with hematoxylin, the staining solution was filtered through a folded filter. Staining was conducted for 3 min at RT followed by short tap washing with H_2O. Afterwards, sections were differentiated 2x with 0.1% HCl in 70% isopropanol for few seconds to remove excess color followed by an additional tap water wash for 10 min. For acidophilic staining, a 1 g/L eosin solution was freshly prepared and a drop of acetic acid was added per 100 mL staining solution. Staining

was conducted for 40 s at RT and slides were washed with H_2O afterwards. To remove any water from the sections, an ascending alcohol series was performed according to Table 2.9. Fully dehydrated and stained sections were mounted with DePeX embedding medium. Slides were digitalized with a slide scanner equipped with a 40x objective.

Immunofluorescence staining of paraffin sections

To unmask epitopes of the desired proteins, sections were autoclaved in retrieval buffer for 10 min. After cooling down for 20 min, the container with the slides was removed from the autoclave and further cooled down at the bench for additional 20 min. Afterwards, slides were washed 1x with tissue permeabilization buffer in a glass reservoir. Before blocking with 30 µL histoblock buffer for 30 min at RT, a water-repellent circle was drawn around the sections with a pen. For incubation with primary antibodies the histoblock buffer was sucked off the slide and 25 µL antibody solution was added and incubated in a humidity chamber at 4 °C overnight. The antibody solution contained a dilution of all primary antibodies used in histoblock buffer. The next day slides were washed 3x with tissue permeabilization buffer in a glass reservoir. Subsequently, the water-repellent circle was dried carefully with a task wipe and sections were incubated with the 25 µL of secondary antibodies diluted in histoblock buffer for 45 min at RT in a humidity chamber in the dark. After incubation, the slides were washed 3x with 1x PBS and thereafter the liquid was removed from the slides by tapping. The sections were permeabilized with 30 µL tissue permeabilization buffer, stained with 25 µL DAPI for 5 min at RT and washed 3x with 1x PBS. Finally, sections were mounted air bubble free with mounting buffer and the viscous buffer was allowed to solidify overnight at 4 °C. Slides were examined using a confocal microscope.

2.5.4. Staining of cryosections

Phalloidin staining

Cryosections were used to stain F-actin with phalloidin conjugates. First, sections were washed 1x with tissue permeabilization buffer and subsequently slides were dried with task wipes before a water-repellant circle around each section was drawn. The cryosections were blocked with 30 µL histoblock buffer and after removing the blocking buffer, 25 µL phalloidin dilution was incubated for 20 min in a humidity chamber at RT. The slides were washed 3x with tissue permeabilization buffer in a glass reservoir and the water-repellent circle was dried with a task wipe thereafter. Nuclei were stained with 25 µL DAPI staining buffer and washed again 3x with 1x PBS. For better permanency sections were mounted with mounting buffer containing DABCO and kept at least overnight at 4 °C before inspection under the confocal microscope.

Quantification of phalloidin signal

The mean phalloidin intensity within a glomerulus was measured using ImageJ. The fluorescence picture was background subtracted by the "rolling ball" algorithm. Subsequently, the outline of the glomerulus was drawn by hand and the mean intensity of the phalloidin signal within the outlined glomerulus was measured. The complete procedure is listed in Appendix 8.1.

2.5.5. Contrasting of epon sections and quantification of filtration slits

The sections placed in the grid were washed with filtered double distilled H_2O (ddH_2O), negative stained with 1% uranyl acetate solution for 30 min in the dark, and washed again 10x with filtered ddH_2O. Finally, additional contrasting with 3% lead citrate solution for 1 min was conducted and sections were washed again 10x with filtered ddH_2O. TEM pictures of two glomeruli per mouse were taken at magnifications of 400x, 700x, 3 000x, 7 000x and 20 000x. To quantify the frequency of filtration slits, blinded 20 000x magnified micrographs were examined. The length of the basal membrane was measured at the border to neighboring podocytes using the software ImageJ and gaps between podocyte foot processes were counted to calculate the ratio slits/µm.

2.6. Isolation of glomeruli and primary podocytes

2.6.1. Isolation of glomeruli and outgrowth of primary podocytes

Isolation of glomeruli

Isolation of glomeruli by magnetic bead perfusion utilizes that beads perfused through the arteria renalis get stuck in the capillary loops of the glomeruli. After digestion glomeruli can be separated from other tissue with a magnet. Before perfusion, 50 µL bead stock slurry ($2x10^7$ beads) per mouse was washed 4 – 6 times with 1 mL HBSS using a magnet and beads are finally added to 10 mL warm HBSS and kept at 37 °C until perfusion. For podocyte isolation mice at the age of 3 – 5 months were used only. Mice were weighed and spot urine was collected, thereafter mice were anesthetized with two intraperitoneal injections of Narcoren working solution (0.12 -0.15 mg per gram body weight). A tail biopsy was taken for regenotyping before the peritoneum was opened to dissect kidneys. Kidneys were shortly washed in warm HBSS and subsequently perfused with tubing connected to a syringe over the *arteria renalis* with 1 mL HBSS followed by 2x 2.5 mL bead slurry each. The capsule was removed and the kidneys were cut into small pieces, split into two equal amounts and digested in two round bottomed 2 mL micro tubes prefilled with 1 mL collagenase IA (1 g/L) at 1200 rpm and 37 °C for 30 min. The following steps were all carried out on ice. The digested suspension was then filtered through a 100 µm cell

strainer into a 50 mL tube and rewashed with 7x 1 mL HBSS. The filtered solution was transferred to a 12 mL round-bottomed tube, rewashed with 2x 1.5 mL HBSS and glomeruli were collected with a magnet. The supernatant was carefully discarded and the remaining glomeruli were resuspended in 10 mL HBSS. After another washing step and resuspension in 6 mL HBSS, the suspension was filtered through a 100 µm cell strainer into a 12 mL round-bottomed tube and rewashed with 3x 2 mL HBSS. The glomeruli were then washed several times with 10 mL HBSS until the supernatant contained no more than 3 tubular fragments (7 – 9 washing steps). Isolated glomeruli were either lysed for Rho family activation assays or plated on culture flasks for outgrowth of podocytes.

Outgrowth of podocytes and podocyte harvesting

Glomeruli were resuspended in 6 mL pre-warmed primary podocyte growth medium and seeded on a cell culture flask. After four days of incubation at 37 °C and 5% CO_2 the medium was renewed. At this time point most glomeruli attached to the surface surrounded by outgrown glomerular cells, which are for the most part podocytes. The following day cells were washed 2x with 5 mL 1x PBS, incubated with 2 mL accutase for 10 min at 37 °C and vigorously tapped to detach all cells. To stop the enzymatic reaction 2 mL of primary podocyte medium was added. The suspension was filtered through a 35 µm cell strainer into a 15 mL tube. After rewashing 2x with 4 mL medium the cell suspension was centrifuged (260 *g*, 5 min, RT), the supernatant was discarded and the cells were resuspended in 3 mL primary podocyte growth medium. Cell amount was counted using a Neubauer chamber and cells were further processed depending on the planned experiment.

2.6.2. Isolation of glomeruli and podocytes using enzymatic digestion

Isolation of glomeruli

Podocytes detached from glomeruli by enzymatic digestion were exclusively used for FACS sorting followed by cell lysis, as they are not capable of attaching to surfaces in cell culture. The principle of glomeruli isolation is identical to the one described in chapter 2.6.1. Mice transgene for *mTmG*, which additionally expressed Cre recombinase podocyte-specific, were weighed and anesthetized with two intraperitoneal injections of Narcoren working solution (0.12 -0.15 mg per gram body weight) after spot urine collection. A tail biopsy was taken and kidneys were dissected and washed in warm HBSS. Each kidney was perfused over the *arteria renalis* with 1 mL HBSS, 2x 2 mL bead slurry and 1 mL digestion solution containing beads ($2x10^7$ beads in total per mouse). The capsule was removed and the kidneys were minced into small pieces. Thereafter, the tissue was transferred to a 3.5 mm cell culture dish and suspended in 2 mL digestion solution. The suspension was then incubated at 37 °C for 5 min under soft agitation, pipetted several times up and down and incubated for another 5 min. The digested suspension was filtered twice through

100 µm cell strainer and rewashed with approx. 20 mL ice-cold HBSS each. Tissue was pelleted by centrifugation (1500 rpm, 5 min, 4 °C) and the supernatant was decanted. Afterwards, the pellet was resuspended in 2 mL HBSS on ice, transferred into two round bottomed 2 mL micro tubes and rewashed with 2 mL HBSS. The glomeruli were washed 3 – 5 times to remove most of non-glomeruli tissue by collecting glomeruli with a magnet, removing the supernatant carefully and resuspending the remainder in ice-cold HBSS.

Detachment of podocytes by enzymatic digestion

Podocytes were detached from glomeruli by resuspending those in 1 mL digestion solution each round-bottomed micro tube, followed by incubation at 37 °C for 45 min in a thermomixer shaking at 1200 rpm. During incubation, the samples were treated according to Table 2.10. After digestion, green fluorescent podocytes and red fluorescent cells including podocytes without Cre expression, mesangial and endothelial cells were kept on ice. To remove the remaining glomerular and tubular fragments from the cell suspension the digestion was placed in the magnetic collector. The supernatant containing podocytes was collected and pooled, followed by a filtration through a 35 µm cell strainer and rewashing with HBSS. After centrifugation (1500 rpm, 5 min, 4 °C) the cell pellet was resuspended in 712 µL FACS buffer.

Table 2.10: Handling of glomeruli during incubation with digestion solution to detach podocytes.

Time	Procedure
5 min	Pipetted up and down with a glass pipet
10 min	Shortly vortexed, pipetted up and down with a glass pipet
15 min	Passed 3 - 5 times through a 27G needle
20 min	Shortly vortexed, pipetted up and down with a glass pipet
25 min	Pipetted up and down with a glass pipet
30 min	Shortly vortexed, passed through 200 µL pipette tip stuck on 1 mL pipette tip
35 min	Pipetted up and down with a glass pipet
40 min	Vigorously vortexed, passed through 200 µL pipette tip stuck on 1 mL pipette tip
45 min	Passed 3 - 5 times through a 27G needle

FACS sorting of green fluorescent podocytes

Immediately prior to FACS sorting the suspension was filtered again through a cell strainer and 38 µL PI stock solution was added to a final concentration of 50 mg/L. FACS sorting was carried out at the Department for Internal Medicine III, University Hospital Regensburg, Regensburg with the help of Jaqueline Dirmeier at a FACSAria II sorter (BD Biosciences). Green fluorescent podocytes were sorted using four gates listed in Table 2.11. Sorted cells were pelleted by centrifugation (260 *g*, 5 min, 4 °C), the supernatant was discarded and the dry pellet was snap frozen in liquid N_2 and stored at -80 °C.

Table 2.11: Gates and their description for FACS sorting of green fluorescent podocytes.

Gate	x-Axis	y-Axis	Purpose
1	FSC-A	SSC-A	Exclude debris
2	FSC-A	FSC-W	Exclude cell aggregates
3	FSC-A	PI	Exclude damaged or dead cells
4, 5	tdTomato	EGFP	Separation of green fluorescent (podocytes) and red fluorescent cells (glomerular and tubular cells)

2.7. Working with glomeruli

2.7.1. Rho family activation assays

For determination of the amount of active, GTP-bound RhoA, Rac1 and Cdc42 the G-LISA kits (cytoskeleton) were used. The kits utilize the specificity of Rho GTPase effectors to the active state. Effector domains are immobilized on the bottom of the wells to capture active GTPases, which themselves can be recognized by specific primary antibodies. Secondary antibody conjugates catalyze a chromogenic reaction which is then read out with a microplate spectrophotometer. The experiment was performed following the manufacturer's instructions.

Lysis of glomeruli

Freshly isolated glomeruli were pelleted and the supernatant was completely discarded. Ice cold lysis buffer (210 – 240 µL) included in the kit was added, glomeruli were resuspended and transferred to a pre-chilled micro tube. The suspension was immediately centrifuged (1 000 *g*, 1 min, 4 °C) and portions of the supernatant were aliquoted and snap frozen in liquid nitrogen. Afterwards, 20 µL of the remaining supernatant was transferred to a 1 mL cuvette. For protein content quantification Precision Red™ (1 mL) was added and the solution was well mixed. The absorbance at 600 nm was measured after 7 min and

corrected by blank (20 µL lysis buffer with 1 mL Precision Red™). The mass concentration could be calculated by a modified version of Beer-Lambert law (4) where A_{600} is the absorbance at 600 nm, l is the length of the solution the light passes in cm and ε is the extinction coefficient in mL/(mg × cm).

$$\beta = dilution\ factor \times \frac{A_{600}}{\varepsilon \times l} = 50 \times \frac{A_{600}}{10\ \frac{mL}{mg \times cm} \times 1\ cm} = 5\frac{mg}{mL} \times A_{600} \qquad (4)$$

As GTP bound to GTPases hydrolyzes rapidly only samples lysed in less than 7:30 min and with a protein mass concentration above 0.4 g/L were used for the G-LISA assays. Only one G-LISA assay per lysate could be carried out because of limited protein amounts.

G-LISA assay

Protocols for RhoA, Rac1 and Cdc42 G-LISA differ slightly (Table 2.12). Samples were kept on ice and processed rapidly until GTPases were bound to immobilized effector domains to limit GTP hydrolysis. All sample measurements were realized in duplicates. First, blanks and positive controls were diluted and cooled in an ice bath. G-LISA wells were cooled and 100 µL ice cold water was added each well to dissolve included powder. Glomerular lysates were rapidly thawed to 2/3 in an RT water bath, immediately put on ice thereafter and diluted with ice-cold lysis buffer to equalize lysate concentrations. In case of RhoA G-LISA, 60 µL of diluted samples were mixed with 60 µL ice-cold binding buffer. The solution from the G-LISA wells was removed by a series of vigorous pats onto paper towels, and immediately thereafter 50 µL of equalized lysates, blanks and positive controls there pipetted into duplicates. Samples were incubated on an orbital shaker (400 rpm, 4 °C) for a certain period stated in Table 2.12. Afterwards, wells were washed 2x with 200 µL wash buffer followed by incubation with 200 µL antigen presenting buffer for exactly 2 min at RT. After washing 3x with 200 µL wash buffer, primary antibody dilution (50 µL per well) was incubated on the orbital shaker (400 rpm, RT). Thereafter samples were washed 3x with 200 µL wash buffer and incubated with 50 µL secondary antibody dilution on the orbital shaker (400 rpm, RT). After another washing step (3x, 200 µL wash buffer) HRP detection mixture was freshly prepared by mixing equal volumes of reagent A and B and incubated in G-LISA wells. After the incubation time listed in Table 2.12 reaction was stopped by adding HRP stop solution. Absorption of bubble-free wells was measured at 490 nm using a microplate spectrophotometer. The blank corrected means of duplicates are proportional to the number of active GTPase species.

Table 2.12: Listing of volumes, mass concentrations, incubation times and antibody dilutions in which RhoA, Rac1 and Cdc42 G-LISA assays differ.

Step	RhoA	Rac1	Cdc42
Blanks	60 µL lysis buffer + 60 µL binding buffer	120 µL lysis buffer	120 µL lysis buffer
Positive controls	12 µL control protein + 48 µL lysis buffer + 60 µL binding buffer	36 µL control protein + 84 µL lysis buffer	24 µL control protein + 96 µL lysis buffer
Sample mass concentration after equalization	0.4 mg/mL	0.5 mg/mL	0.4 mg/mL
Addition of binding buffer	60 µL equalized samples + 60 µL binding buffer	/	/
Sample incubation on orbital shaker	30 min	30 min	15 min
Primary antibody diluted in antibody dilution buffer	1:250	1:50	1:20
Primary antibody incubation	45 min	45 min	30 min
Secondary antibody diluted in antibody dilution buffer	1:62.5	1:100	1:62.5
Secondary antibody incubation	45 min	45 min	30 min
Chromogenic reaction	50 µL detection reagent 37 °C, 13 min	50 µL detection reagent RT, 15 min	70 µL detection reagent 37 °C, 15 min
HRP stop buffer	50 µL	50 µL	140 µL

2.8. Working with cells

2.8.1. Mammalian cell culture

General handling

Aside from working in a laminar flow bench cells cultures were kept at 33 or 37 °C with 5% CO_2 and 95% relative humidity in a CO_2 incubator. For cultivation cell culture flasks with a filter cap at a size of 25 cm^2 or 75 cm^2 were used with 5 mL or 15 mL medium, respectively. All equipment was sterilized with 70% ethanol before putting into the bench, self-made liquids were autoclaved or sterile filtered before use. Consumables were bought sterile. Cell concentrations were determined by counting cells in all four quarters of a Neubauer chamber.

Subculture

Cells were passaged when they reached approx. 80% confluency estimated by light microscopy. For sub-culturing, cells were washed twice with 1x PBS and detached thereafter with 1 mL (T25 cell culture flask) or 2 mL (T75 cell culture flask) Trypsin/EDTA solution for 6 – 10 min. After full detachment of cells judged by light microscopy, at least 4 mL culture medium with FCS was added and cells were split 1:5 - 1:20 depending on cell growth rate and density.

Cell freezing

For freezing, cells were grown to 80% confluency, trypsinized and counted. After centrifugation (260 *g*, 5 min, 4 °C) the cell pellet was resuspended in 90% FCS and 10% DMSO as a cryoprotectant (1.8 mL per 1 – 2 million cells). The suspension was transferred to 1.8 mL cryovials and placed into polystyrene containers at -80 °C to ensure slow freezing at a rate of approx. 1 °C/min. For short-term storage cells were kept at -80 °C, for long-term storage cells were transferred to the gas phase of liquid nitrogen.

Cell thawing

Frozen cells were kept on ice until they were thawed by pipetting culture medium several times on top of the ice. The resulting cell suspension was diluted in culture medium to 10 mL and then immediately centrifuged (260 *g*, 5 min, 4 °C). Afterwards, the supernatant was discarded and the cell pellet was resuspended in the appropriate growth medium and plated in cell culture flasks.

HEK293T

HEK293T cells were cultured in DMEM supplemented with 10% FCS at 37 °C. Culture medium was exchanged twice a week and cells were passaged 1 or 2 times a week, depending on cell density.

hPCL pInducer-LMX1B clone#1

This cell line was cultured under permissive conditions at 33 °C and 5% CO_2 with RPMI 1640 medium supplemented with 10% FCS, 1x ITS-G and puromycin antibiotic (1 µg/mL). Cell culture medium was exchanged three times a week and passaging was carried out once a week. For differentiation, cells were seeded at a density of 7200 cells/cm^2 and kept at 33 °C for one day. Afterwards, they were shifted to 37 °C to induce differentiation for a total of 14 days. In the period of differentiation, the incubator was only opened for medium exchange three times a week and the medium contained no puromycin. Induction of LMX1B expression was performed by supplementing culture medium with 1 µg/mL doxycycline five days prior to the experiment. All experiments were performed with cells plated on laminin-521-coated coverslips placed in a 24 well cell culture dish.

Primary murine podocytes

Isolation of primary murine podocytes is described in chapter 2.6.1. Cells were cultivated in DMEM/Ham's F12 medium supplemented with 10% FCS, 1x ITS-G and penicillin (1000 units)/streptomycin (1 g/L) at 37 °C. After detachment with accutase and separation from glomeruli, cells were either directly stained for flow cytometry or seeded on laminin-521-coated glass substrates and subjected to experiments. Primary murine podocytes were not sub-cultured as differentiation markers diminish with cultivation duration.

2.8.2. Transient transfection

HEK293T cells were transiently transfected with polyethylenimine (PEI) as a polycationic DNA packaging agent. 1 million cells were plated on 100 mm cell culture dishes. The next day 6 µg plasmid DNA and 18 µg PEI were diluted in 1 mL DMEM without FCS and the mixture was incubated for 30 min at RT after vigorous vortexing. Shortly before transfection, the growth medium was exchanged with 4.6 mL fresh medium. The transfection mixture was pipetted dropwise evenly distributed over the culture dish. After 6 h of incubation at 37 °C and 5% CO_2, the transfection medium was replaced by 10 mL growth medium. Cells were lysed 24 h after transfection.

2.8.3. Coating with laminin-521

Coating with laminin-521 was conducted the evening before usage. The laminin-521 stock solution was slowly thawed in an RT water bath and diluted in PBS^{++} to a concentration of 5 µg/mL or 10 µg/mL. A volume of 300 µL was added to cover slides placed in 24-well plates and 400 µL was added to glass-bottomed µ-dishes. Thereafter culture plates or dishes were put in a refrigerator overnight to ensure even coating. Cells were seeded on coated surfaces after removal of PBS^{++} without washing. Coated surfaces were never allowed to dry out.

2.8.4. Fixation and immunofluorescence / phalloidin staining

Fixation and staining

Immunofluorescence staining was conducted on immortalized human and primary murine podocytes plated on laminin-521-coated cover slides in 24-well plates. First, cells were fixed by adding an equal volume of 4% PFA in 1x PBS to growth medium. After 15 min fixation at RT cells were washed 3x with 1 mL 1x PBS and permeabilized with 0.5 mL histoblock buffer for 30 min at RT. Primary antibodies diluted in histoblock buffer were pipetted on top of the cover slides placed on Parafilm® (20 µL/slide) and incubated for 2 h at RT in a humidity chamber. After washing 3x with 1 mL cell permeabilization buffer, cells were incubated with secondary antibodies or phalloidin diluted in histoblock buffer, for 30 min at RT in a humidity chamber. Thereafter, cells were washed again 3x with 1 mL cell permeabilization buffer and nuclei were stained with 0.5 mL DAPI staining buffer for 5 min at RT in the dark. After final washing steps with 3x 1 mL cell permeabilization buffer cover slides were mounted with mounting buffer on microscopy slides. The viscous buffer hardened at least overnight at 4 °C before confocal pictures were taken. Only in the case of pMLC stained hPCL pInducer-LMX1B clone#1 cells a conventional epifluorescence microscope was used.

Quantification of mean intensities of green fluorescent primary podocytes

Mean intensities of phalloidin, transgelin and active β1-integrin were quantified using ImageJ macros listed in Appendix 8.2 and Appendix 8.3. Pictures were only taken from podocytes without contact to other cells or the picture border. Cell borders were first determined using the green fluorescence of podocytes. Thereto the command “Find Edges” and a median filter were applied to the green channel to obtain a better signal to noise ratio. Signal was auto thresholded using “Triangle”, and “EDM Binary Operations” were performed to fill small gaps within signals. The cell edges were finally recorded by the command “Analyze Particles”. The mean intensity of stained protein within the cell boundary was measured in the corresponding channel after background subtraction.

Quantification of mean intensities in hPCL pInducer-LMX1B clone#1 cells

As hPCL cells do not express EGFP in contrast to primary podocytes the cells had to be stained. Transgelin is highly expressed in this cell type all over the cell and hence was used as a cell border marker. The mean intensity of pMLC was measured with ImageJ. Cells with contact to other cells or the picture edge were excluded from quantification. First, a median filter was used on the transgelin staining to sharpen cell borders and background was subtracted by the rolling ball algorithm. After thresholding with the auto threshold "Li" the cell boundary was extracted with the command "Analyze particles". Finally, the mean intensity of the pMLC signal was measured after background subtraction in the corresponding channel. The macro used is listed in Appendix 8.4.

Quantification of colocalization (Pearson correlation coefficient)

Colocalization of transgelin and phalloidin staining was quantified by calculating the Pearson correlation coefficient with the Costes' automatic threshold method. Both channels were background corrected by subtraction of the mean intensity of a background area. Pearson coefficient was calculated with the ImageJ plugin JACoP with the option "Costes' automatic threshold" enabled.

2.8.5. Cell lysis

HEK293T

For lysis of HEK293T cells, two buffers were subsequently used. Lysis buffer A contains the mild, nonionic and non-denaturing detergent Nonidet P-40 to break cell membranes open at low salt concentration. Lysis buffer B is a high salt buffer for nuclear protein extraction. Cultured cells were washed 24 h after transfection with 1x PBS and harvested with a cell scraper in 4 mL 1x PBS. After pelleting by centrifugation (300 *g*, 7 min, 4 °C), cells were resuspended in 50 µL ice-cold lysis buffer A and incubated 10 min on ice. Afterwards, the lysate was vortexed and 50 µL ice-cold lysis buffer B was added. This mixture was incubated for 20 min on ice and centrifuged (3 300 *g*, 15 min, 4 °C) to remove insoluble material. The supernatant was aliquoted, snap frozen in liquid nitrogen, and stored at -80 °C.

Primary murine podocytes

FACS sorted green fluorescent primary podocytes were lysed with high concentrations of urea and Triton X-100. Ice cold urea lysis buffer (70 µL) was added to snap-frozen cell pellets and incubated for 15 min on ice, vortexed, and incubated for further 10 min. Insoluble material was removed by centrifugation (10 000 *g*, 10 min, 4 °C) and the supernatant containing the denaturized proteins was snap frozen in liquid nitrogen.

2.8.6. Random movement of primary podocytes

Experimental procedure

Primary, green fluorescent murine podocytes were used to quantify random movement on laminin-521-coated dishes. Outgrown primary podocytes were harvested after five days as described in chapter 2.6.1 and plated on laminin-521-coated glass bottom µ-dishes at a density of 950 cells/cm^2. The next day the µ-dish was placed on the confocal microscope stage with heating (37 °C) and active gas regulation (5% CO_2) and equilibrated for 30 min. Thereafter a 5x4 tile scan (20x objective, 0.6 zoom) with 488 nm argon laser illumination was taken every 150 s over a period of 10 h. Tile scans were stitched using ZEN black software.

Quantification of mean velocity

Quantification of the mean velocity was realized using the ADAPT ImageJ plugin. Only the first 200 tiles (500 min) were analyzed due to RAM limitations. First, stitched time series were lateral drift corrected by aligning with the MultiStackReg (Transformation: Translation) command. After using the filter "despackle", drift corrected time series were then loaded into the ADAPT plugin and analysis was started with the options "Generate Morphology Data", "Auto Threshold (Li)" and "Minimum Object Size (1000)" enabled. The plugin calculates mean velocities for every green fluorescent specimen detected as a cell. To exclude artifacts only velocities of cells present at every time point were finally used for quantification.

2.8.7. Morphology of spreading and steady state podocytes

Experimental procedure

For examination of cell shape and area, green fluorescent primary podocytes were plated on laminin-521-coated cover slides (10 mm) placed in a 24-well plate (10 000 cells/well). Cells were allowed to settle at 37 °C and 5% CO_2 and fixed exactly after 20, 40 and 60 min (spreading cells) or after overnight growth (steady state cells) in an incubator. Nuclei of fixed cells were stained with DAPI and cells were mounted with mounting buffer on microscope slides. Fluorescence pictures of DAPI and the green channel were made by a tile scan of the whole cover slide with 30% overlap on an Observer.Z1 microscope and stitching with ZEN blue software.

Quantification of cell area, circularity and roundness

Quantification was achieved using a self-written macro for ImageJ (Appendix 8.5). As cells at the edge of the cover slides were often distorted, only the middle part (7 146 x 7 146 px, centered) was quantified. To reduce background and to sharpen cell edges a median filter and unsharpen mask was used. After background correction using the "rolling ball" algorithm the picture was converted to a binary using the auto threshold "triangle". Small holes in cells were closed by "EDM Binary Operations" followed by analyses of cell circularity, roundness or area with the command "Analyze Particles". Only signals with an area of at least 950 µm^2 and in case of area measurements with a circularity between 0.6 - 1.0 (0.1 – 1.0 in case of cells fixed after overnight incubation) were counted as a cell. Signals of remaining glomeruli, cells touching each other, and remaining artifacts were removed manually.

2.8.8. Cytochalasin D treatment of primary podocytes

Primary podocytes were treated with cytochalasin D to estimate the rate of F-actin depolymerization and subsequent polymerization by measuring the cell area. To examine the impact of specific signal pathways, cells were additionally incubated with inhibitors in some cases.

Shrinking of podocytes after cytochalasin D treatment

Outgrown green fluorescent podocytes were seeded on laminin-521-coated (10 µg/mL) glass bottom µ-dishes at a density of 3800 cells/cm^2. The next day cells were placed on the microscope stage equipped with a heating system (37 °C) and an active gas mixing unit (5% CO_2). After equilibrating 15 – 25 min growth medium was exchanged by warm (37 °C) growth medium supplemented with 10 µM cytochalasin D. Measurement was immediately started after focusing and the time between cytochalasin D treatment and begin of measurement was noted. A 5x4 tile scan with 20% overlap was recorded every minute over a period of 121 min. Resulting pictures were stitched using ZEN black edition.

Spreading of podocytes after wash-out of cytochalasin D

Outgrown green fluorescent podocytes plated on laminin-521-coated glass bottom µ-dishes (density: 3800 cells/cm^2) were treated with cytochalasin D (10 µM) six days after glomeruli isolation. After 23 h of cytochalasin D incubation growth medium was renewed including cytochalasin D and possibly an inhibitor. Addition of inhibitors is shown in Table 2.13. The µ-dish was placed 20 – 30 min prior cytochalasin D wash-out onto the heated (37 °C) and gas controlled (5% CO_2) microscope stage for equilibration. Exactly 24 h after the begin of cytochalasin D treatment, it was washed out twice with 2 mL growth medium possibly supplemented with an inhibitor and live cell imaging was started. Tile scans (5x4) with 20% overlap of the EGFP fluorescence were taken every minute over a period of 121 min.

Time between wash-out and start of the measurement was noted. Stitching was performed using the software ZEN black edition.

Table 2.13: Experimental setups for podocyte spreading experiments after cytochalasin D treatment

Experiment	Inhibitor name	Concentration	Inhibition target
Podocyte spreading	/	/	/
Podocyte spreading with ROCKi	Y-27632	5 µM	ROCK1 + ROCK2
Podocyte spreading with LIMKi	LIMKi 3	10 µM	LIMK1 + LIMK2

Quantification of the relative EGFP positive cell area

Stitched time series were corrected for lateral drift with the ImageJ tool "MultiStackReg" with the option "Transformation" set to "Translation". Thereafter a median filter was used to reduce noise and the background was corrected by the "rolling ball" algorithm. After contrast enhancement, pictures were tresholded with the auto threshold "Li". The EGFP-positive area was then measured within four non-overlapping ROIs with equal dimensions (Appendix 8.6). The macro to calculate EGFP positive areas is shown in Appendix 8.7. The resulting areas were then designated with the respective timespan past wash-out of cytochalasin D. As some focus fluctuations occurred mainly in the first few minutes of the experiment, EGFP positive area was normalized to the area at 10 min after wash-out.

Cytochalasin D treatment of podocytes for phalloidin staining

To show the effect of cytochalasin D on the actin cytoskeleton of podocytes outgrown primary podocytes were plated on laminin-521-coated cover slides (10 mm) placed in 24-well plates at a density of 3800 cells/cm^2. The next day, cells were treated with 10 µM cytochalasin D over a period of 24 h. After exactly 24 h half of the cover slides were fixed by adding an equal amount of 4% PFA in 1x PBS to the growth medium. After fixation for 15 min at RT cells were washed 3x with 1x PBS. The other half of cover slides was washed twice with growth medium. At exactly 2 h after the wash-out of cytochalasin D cells were fixed as described above. Podocytes were stained as described in chapter 2.8.4.

2.8.9. Analysis of β1-integrin activity of glomerular cells by flow cytometry

Freshly isolated glomeruli from 3 – 4 mice per genotype were resuspended in 6 mL podocyte growth medium and transferred to T25 cell culture flasks and incubated at 37 °C and 5% CO_2. After four days growth medium was renewed and podocytes were detached seven days past glomeruli isolation. To detach outgrown cells they were washed twice with 1x PBS (37 °C) and then incubated with 2 mL accutase (10 min, 37 °C). Enzymatic digestion was stopped by adding 4 mL growth medium and cells from mice with identical genotype were pooled. Cells and remaining glomeruli were pelleted by centrifugation (260 *g*, 5 min, 4 °C). Afterwards, the pellet was resuspended in 3.6 mL 1x PBS and split into three parts with equal volume. After another centrifugation step (260 *g*, 5 min, 4 °C) each third was incubated with 200 µL of a primary antibody (anti-active β1-integrin, anti-β1-integrin or isotype control) diluted in BSA blocking buffer (30 g/L BSA in 1x PBS) on a rotating wheel (30 min, 4 °C). Cells were washed twice with 1 mL ice-cold 1x PBS and incubated afterwards with 200 µL Alexa633-conjugated secondary antibody dilution on a rotating wheel (30 min, 4 °C). Thereafter, cells were pelleted and washed twice with ice cold 1x PBS and one time with FACS buffer. Finally, glomeruli and cell aggregates were sieved out by a 35 µm cell strainer, PI was added (50 µg/mL) and stained cells were immediately analyzed by flow cytometry. Flow cytometry was carried out at the Department for Internal Medicine III, University Hospital Regensburg, Regensburg with the help of Jaqueline Dirmeier at a FACSAria II sorter (BD Biosciences). Both green and red fluorescent glomerular cells were analyzed regarding Alexa633 signal intensity after gating out debris, cell aggregates and PI positive cells. Gates are depicted in Appendix 8.8.

3. Results

3.1. Validation of target gene expression

A previous study revealed several potential Lmx1b target genes in mouse glomeruli (Burghardt et al., 2013). The gene with the highest upregulation at the mRNA level following *Lmx1b* inactivation was *Sm22*, encoding for transgelin. Two additional promising candidates with mRNA upregulation were Abra and Arl4c, and binding of human LMX1B to the respective promoter regions could be confirmed for both (Burghardt et al., 2013). Although increased transgelin protein content could be shown by immunofluorescence staining in *Lmx1b* knock-out glomeruli, there were no data available regarding Abra and Arl4c regulation on the protein level. To address the question whether the amount of those proteins is increased specifically in green fluorescent *Lmx1b* knock-out podocytes, western blotting of FACS sorted murine podocytes was performed.

3.1.1. Affinity purification of rabbit antisera

Generation of specific antibodies against Arl4c and Abra was the first step towards protein expression validation. In case of transgelin, a commercial antibody was available. Antibodies were generated by injecting purified full-length mAbra or a peptide containing the C-terminal region of mArlc comprising of 60 aa in rabbits, as reported previously (Stepanova, 2016). In order to eliminate non-specific binding rabbit antisera were subjected to affinity purification. To generate affinity purification columns, *E. coli* strains (Rosetta pLysS) transfected with bacterial expression plasmids pET21a/mAbra-His or pET21a/mArl4c-His (containing the partial *Arl4c* sequence from 396 to 576 bp) were used to express recombinant mAbra and mArl4c. Recombinant proteins were purified on Ni^{2+} charged His•Bind columns. SDS-PAGE revealed protein elution mainly in fractions 2, 3 and 4 in case of mAbra (Figure 3.1, A) and in fractions 2 and 3 in case of mArl4c (Figure 3.1, B). After dialysis purified mAbra or mArl4c was coupled to CNBr Sepharose 4B beads and 9 mL rabbit antisera was affinity purified each.

In order to test the specificity of the affinity-purified antibodies and to determine the most suitable antibody dilution, western blotting using different antibody dilutions was performed. Therefore, lysates of HEK293T cells transfected with pcDNA3/mAbra, pcDNA3/mArl4c or control pcDNA3 plasmid were used. Western blotting showed specific binding of both anti-mAbra (Figure 3.2, A) and anti-mArl4c (Figure 3.2, B) in the full dilution range, but the highest signal was detected at a dilution of 1:100 in case of anti-mAbra and 1:300 in case of anti-mArl4c.

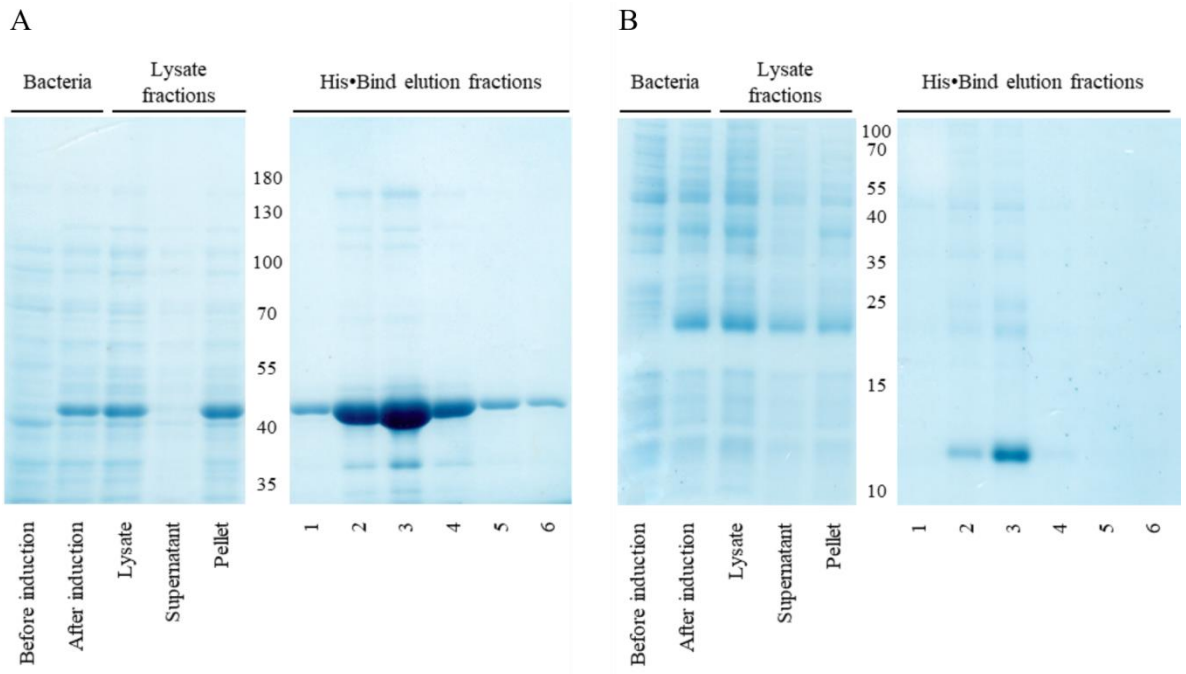

Figure 3.1: **SDS-PAGE showing different steps of the generation and purification of recombinant full-length mAbra [A] and the C-terminal 60 aa region of mArl4c [B].** Both constructs contained a C-terminal T7-tag and an N-terminal His-tag. The predicted molecular weights are 43.2 kDa (mAbra) and 8.5 kDa (mArl4c). The samples loaded on respective lanes were (from left to right): bacterial lysates before and after overnight induction with IPTG; the complete lysate, the supernatant and the pellet fraction after bacterial lysis. The elution fractions of the pellet purification on His•Bind columns were loaded right-hand side of the molecular weight marker. Marker weight is given in kDa.

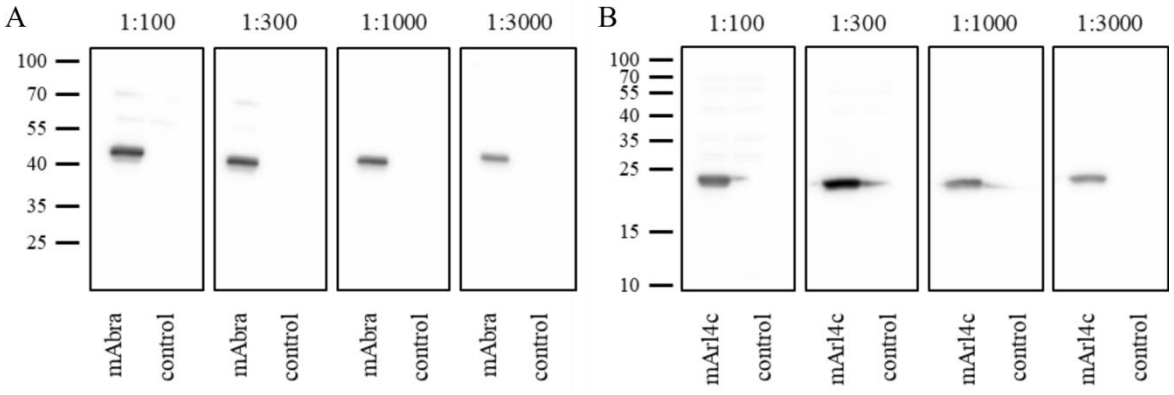

Figure 3.2: **Titration of the affinity purified anti-mAbra [A] and anti-mArlc [B] antibodies by western blotting.** Lysates of pcDNA3/mAbra, pcDNA3/mArl4c or control plasmid pcDNA3 transfected HEK293T cells were used (40 µg each lane) and probed with different dilutions of affinity purified antibodies. The predicted molecular weights are 42.4 kDa for HA-tagged mAbra and 22.2 kDa for HA-tagged mArl4c. Marker bands are depicted on the left in kDa.

3.1.2. Quantification of target gene expression by western blotting

To isolate podocytes, male inducible podocyte-specific *Lmx1b* knock-out and control mice at an age of 3 to 5 months were induced with doxycycline for one week. Primary podocytes were obtained by enzymatic digestion of freshly isolated glomeruli and FACS sorted (see chapter 2.6.2) to receive a fraction of podocytes with definite Cre expression and DNA recombination. Fewer podocytes per mouse could be obtained from *Lmx1b fl/fl* animals (~60 000 cells/mouse) compared to *Lmx1b +/fl* (~119 000 cells/mouse) and *Lmx1b +/+* (~121 000 cells/mouse) animals. A total of 24 *Lmx1b fl/fl*, 16 *Lmx1b +/fl* and 11 *Lmx1b +/+* mice were perfused with magnetic beads to gain a minimum of 1.3 million podocytes. Lysis of the podocytes resulted in at least 160 µg total protein each genotype, and two western blots with 80 µg protein each were carried out.

The knock-out of full-length Lmx1b could be confirmed on the protein level (Figure 3.3, B and C), but interestingly the shortened, homeodomain-lacking Lmx1b was still expressed and was not degraded (Figure 3.3, B and D). Incubation with the affinity purified Abra antibody resulted in only weak signals. Upon long exposure times two bands were identified, one stronger around 65 kDa and one weaker at around 39 kDa. The lower band might represent Abra protein with a predicted molecular weight of 43 kDa, but may also be of unspecific origin. Therefore, the signal was not quantified. Moreover, a 6-fold increase of the Arl4c protein content in *Lmx1b* knock-out podocytes compared to wild-type could be revealed, and also heterozygous *Lmx1b* knock-out podocytes showed a 2-fold increase (Figure 3.3, B and E). Transgelin was expressed in *Lmx1b fl/fl* podocytes, but not in *Lmx1b +/fl* or *Lmx1b +/+* controls (Figure 3.3, A and F), as previously indicated by glomerular mRNA content and immuno-fluorescence staining (Burghardt et al., 2013).

3.2. Dysregulation of the actin cytoskeleton

Besides the identification of Lmx1b target genes in glomeruli Burghardt *et al.* also presented data indicating an involvement of the actin cytoskeleton in the progression of podocyte damage after *Lmx1b* knock-out. These data were: (I) increased phalloidin staining of glomerular knock-out cells, (II) decreased spreading rate of primary *Lmx1b* knock-out podocytes after 24 h cytochalasin D treatment and (III) reduced movement of fibronectin-coated nanobeads attached to the surface of glomerular knock-out cells (Burghardt et al., 2013). However, these data are mainly based on cell mixtures of glomerular origin and not specifically on podocytes. Moreover, the GBM protein laminin-521 was not available at this time. Different experiments with green fluorescent podocytes were conducted to further examine the role of the actin cytoskeleton in podocytes following *Lmx1b* inactivation.

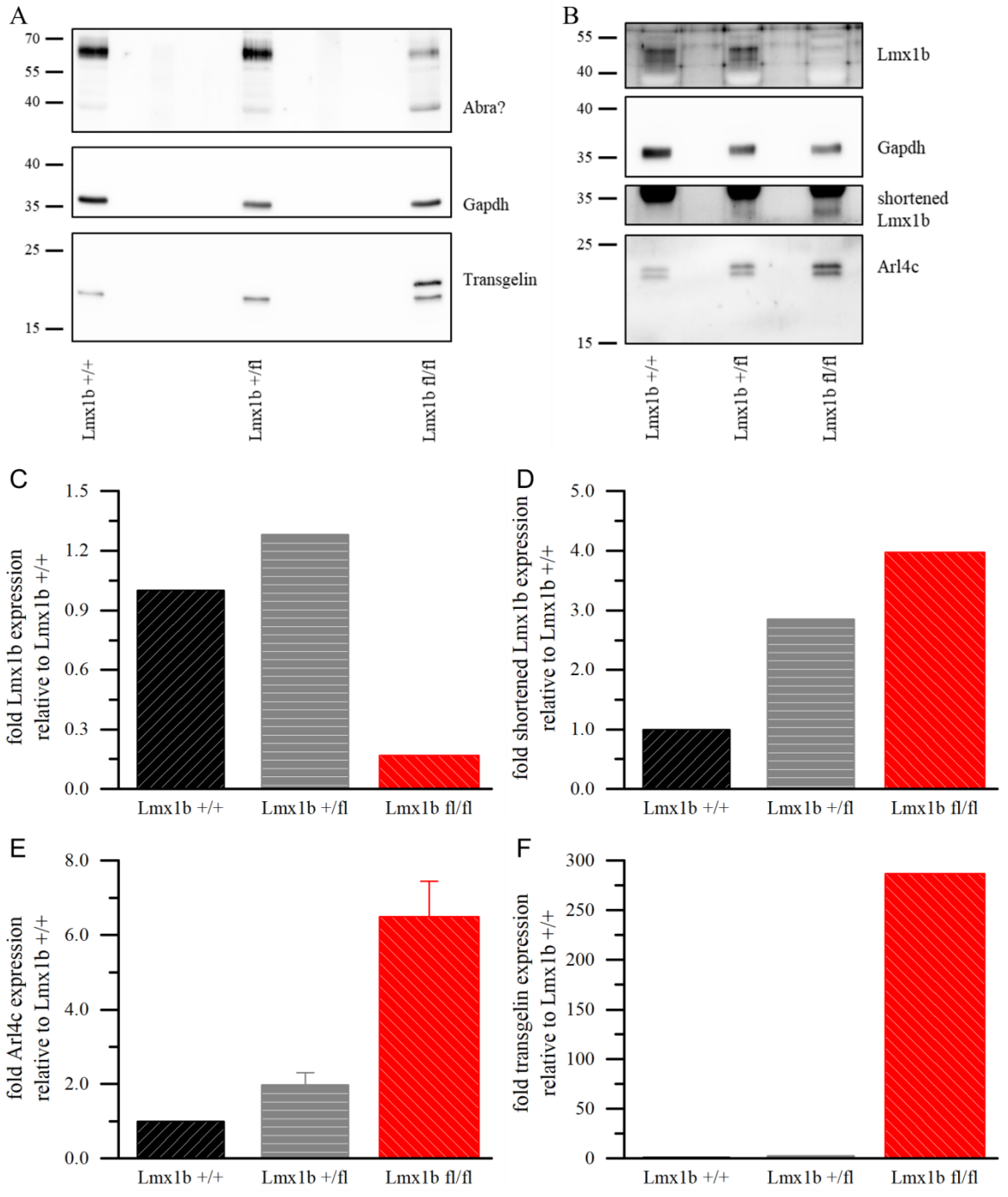

Figure 3.3: **Western blots using lysates of FACS sorted green fluorescent primary podocytes isolated from mice without (*Lmx1b +/+*) or with heterozygous (*Lmx1b +/fl*) and homozygous (*Lmx1b fl/fl*) podocyte-specific *Lmx1b* knock-out.** Lysates were generated from a total of 11 (*Lmx1b +/+)*, 16 (*Lmx1b +/fl*) and 24 (*Lmx1b fl/fl*) mice, and two western blots with 80 µg protein each lane were conducted. [A] Western blot against Arba (~43 kDa), Gapdh (~36 kDa) and transgelin (~22 kDa). The blot shows also an unspecific band of unknown nature. [B] Western blots showing Lmx1b (~42 kDa), Gapdh (~36 kDa), shortened Lmx1b (~29 kDa) and Arl4c (~21 kDa) expression. The band above that of the shortened Lmx1b corresponds to Gapdh.

[C - F] Quantification of the western blots. Signals were normalized to Gapdh and are presented as fold changes to wild-type. Arl4c was analyzed on both plots, shown are the mean values and SDs.

3.2.1. Mean phalloidin intensity

To analyze the amount of F-actin of primary podocytes, glomeruli were isolated from two 3 – 5-month-old male mice per genotype after doxycycline treatment for one week (see chapter 2.6.1). After 5 days of outgrowth, glomerular cells were plated on laminin-521-coated coverslips and fixed exactly 40 min after plating (spreading) or the next day (steady state). Fixed cells were stained with phalloidin to visualize F-actin, and the mean phalloidin fluorescence intensity per green fluorescent podocyte was analyzed on confocal images (see chapter 2.8.4).

The increased F-actin content of steady state *Lmx1b* knock-out podocytes could be confirmed (Figure 3.4) by analyzing exclusively Cre expressing podocytes seeded on laminin-521. Additionally, increased F-actin was already present on roundish spreading *Lmx1b fl/fl* cells fixed 40 min after plating, raising the possibility that a dysregulated actin cytoskeleton could impact dynamic actin-dependent processes like cell spreading.

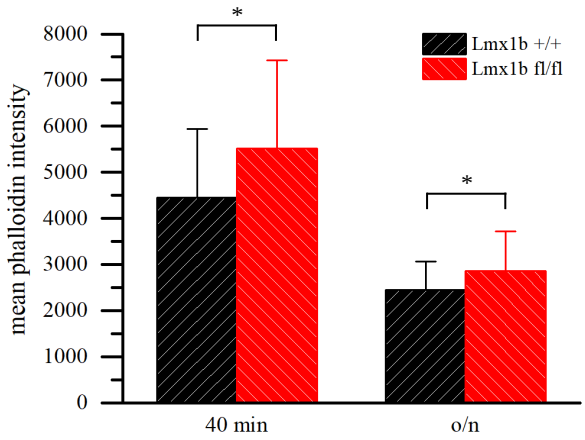

Figure 3.4: **Mean phalloidin intensity of green fluorescent primary podocytes isolated from two male mice per genotype of the inducible podocyte-specific *Lmx1b* knock-out line.** After 5 days of grow-out, the podocytes were plated on laminin-521-coated cover slides and fixed after the indicated time points and stained for F-actin. A total of 31 – 36 cells were analyzed per time point and genotype, and shown are mean values and SDs. *P < 0.05.

3.2.2. Random movement

As the actin cytoskeleton plays an important role in the cellular movement, the random movement of primary green fluorescent podocytes was another parameter of interest. Female inducible podocyte-specific Cre expressing mice were treated with doxycycline for one week, followed by isolation of glomeruli (see chapter 2.6.1). After 5 days outgrowth, glomerular cells were seeded on laminin-521-coated dishes and analyzed the following day by live cell imaging. Fluorescence pictures of the green channel were taken every 2.5 min over a period of 600 min (see chapter 2.8.6).

The membrane-targeted EGFP variant (mG), which is expressed only in induced podocytes, showed an even fluorescence signal throughout the cytosol and also in small cell protrusions (Figure 3.5, A). Therefore, it was suitable as a cell boundary marker. The mean velocity of primary podocytes of at least 3 mice per genotype was quantified using the ImageJ plugin ADAPT (Figure 3.5, B). There was no significant difference in the random movement of *Lmx1b* knock-out compared to wild-type podocytes.

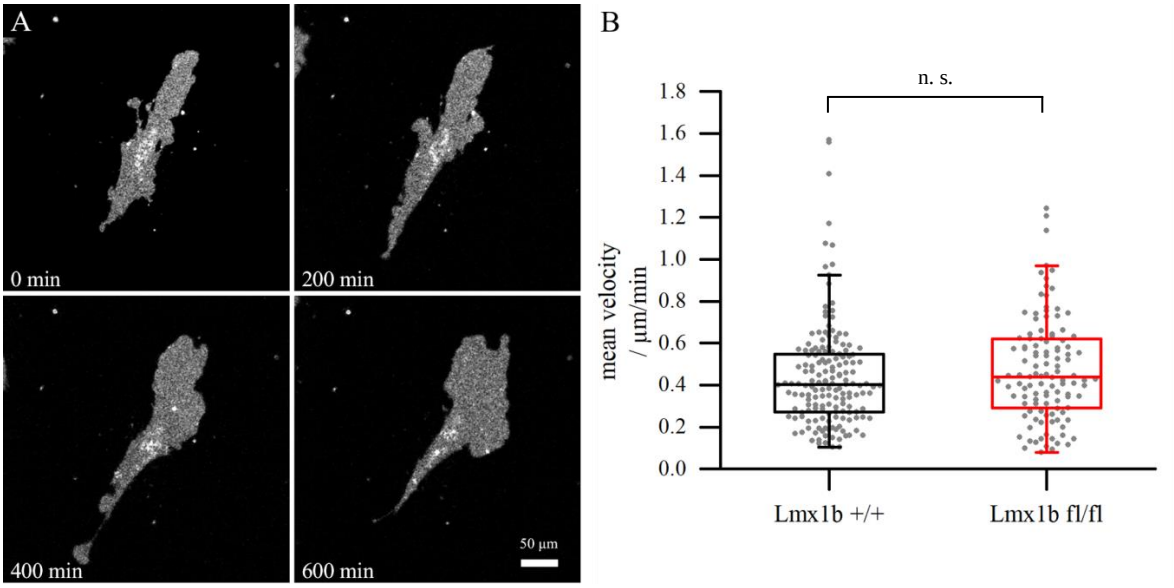

Figure 3.5: **Random movement of green fluorescent primary podocytes measured 6 days after the isolation of glomeruli.** Four female *Lmx1b* +/+ and three *Lmx1b fl/fl* mice were treated with doxycycline for one week, and primary podocytes were plated on laminin-521-coated culture dishes after 5 days of outgrowth. The next day cells were mounted on a live cell imaging stage with heating (37 °C) and CO_2 regulation (5%) and pictures were taken every 150 s over a period of 10 h. [A] Time series of a green fluorescent *Lmx1b* +/+ podocyte, visualizing the shape changes and random movement of the cell. [B] Quantification of the mean velocities of green fluorescent podocytes within 500 min. A total of 166 *Lmx1b* +/+ and 115 *Lmx1b fl/fl* podocytes were analyzed (gray dots), and shown are the median (middle line), the middle 50% percentile (box) and bars reaching to the last point within the range of 1.5 times the height of the box. n. s. not significant.

3.2.3. Morphology of spreading and steady state podocytes

The cytoskeleton is the backbone of the cells defining the cellular morphology. Particularly important is the actin cytoskeleton, as it applies the force to the membrane necessary for protrusion generation and cell movement (Pollard and Cooper, 2009). For this reason, the cell area, circularity and roundness of primary podocytes were determined at defined time points after cell plating. Therefore, three to four male mice each group were treated with doxycycline for 7 days, followed by the isolation of glomeruli and outgrowth of primary green fluorescent podocytes for 5 days (see chapter 2.6.1). Outgrown glomerular cells were plated on laminin-521-coated cover slides and fixed after 20, 40 and 60 min and on the next day. The green fluorescence, which marks primary podocytes expressing Cre recombinase, was used to examine the cell area, circularity and roundness (see chapter 2.8.7).

Primary podocytes attached already after 20 min to the laminin-521-coated cover slides and spread in the following time course on the surface (Figure 3.6). Attachment and spreading within the first 60 min showed no differences between murine *Lmx1b* knock-out and control podocytes regarding the cell area, as previously reported for glomerular cells on BSA- and fibronectin-coated surfaces (Burghardt et al., 2013). Nevertheless, steady state primary *Lmx1b* knock-out podocytes grown overnight were significantly larger (7 093 µm^2 ± 5 481 µm^2, 975 cells) than control podocytes (6 038 µm^2 ± 5 286 µm^2, 766 cells).

Circularity and roundness are two parameters both describing the shape of cells, but with different definitions. The values of the circularity range from 0 to 1, with 1 describing a perfectly circular cell. Circularity is defined as described in equation (5).

$$Circularity = 4\pi \frac{area}{(perimeter)^2} \tag{5}$$

As the area is divided by the square of the perimeter, any cell protrusions extending from the cell body lowers the circularity, but the shape of the cell body (round vs oblong) has low impact on that parameter. On the other hand, the roundness of a cell is a good parameter to characterize the shape of the cell body, as the cell area is divided by the square of the length of the major axis (equation (6)).

$$Roundness = 4 \times \frac{area}{\pi \times (major\ axis)^2} \tag{6}$$

Small protrusions like filopodia have low impact on the roundness, as they don't affect the length of the major axis. Just like the circularity, the maximum value of the roundness is 1 for a perfectly round cell and the minimum is 0.

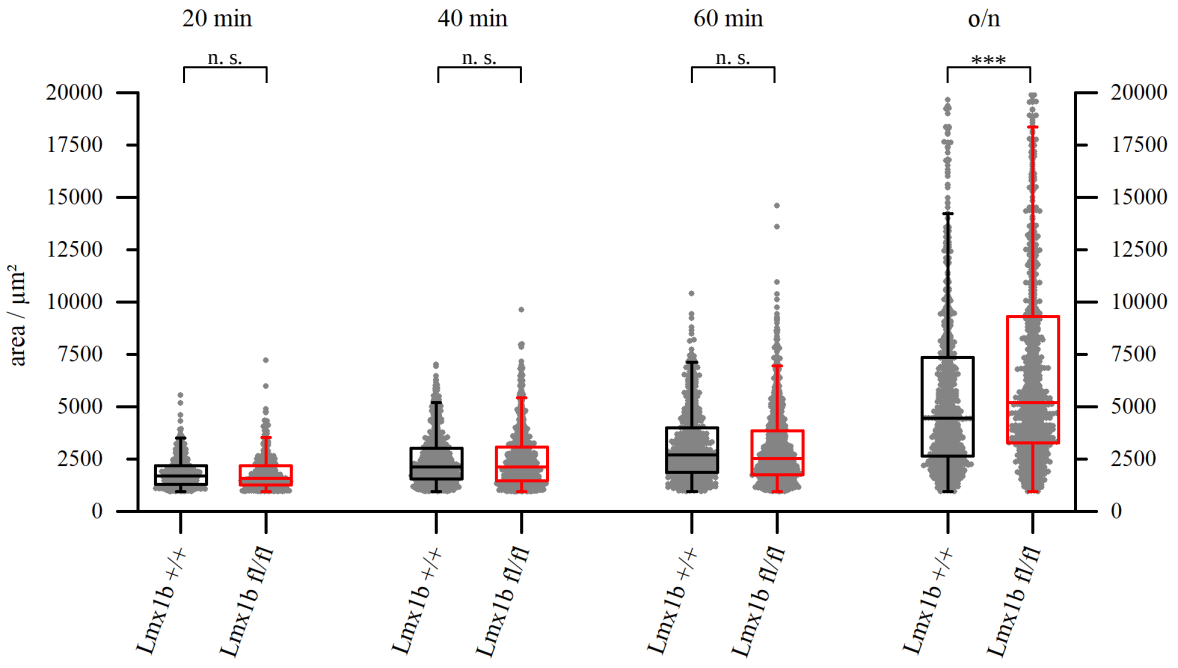

Figure 3.6: **Cell area of adherent green fluorescent podocytes at different discrete time points after plating on laminin-521-coated coverslips.** Glomerular cells were obtained by 5-day outgrowth of glomeruli isolated from doxycycline-induced quadruple transgenic mice. Cells were derived from 3 to 4 mice of each genotype, except for *Lmx1b* +/+ at 60 min, where cells from only 2 mice could be used. A minimum of 370 (maximum 1 099) cells were analyzed (gray dots) using the green fluorescence as a cell boundary marker. The data are presented in a box blot displaying the median (middle line), the lower and upper quartile (box) and the bars marking the last points within the range of 1.5 times the box height. n. s. not significant; ***P<0.001.

Primary green fluorescent podocytes were circular and round after attaching to the laminin-521-coated surface and in the early phase of cell spreading, regardless of the *Lmx1b* genotype (Figure 3.7). Within the course of the experiment, both circularity and roundness decreased. Already 60 min after plating of the cells, the cell shape differed between the two groups. Primary green fluorescent *Lmx1b fl/fl* podocytes showed a significantly higher circularity (0.80 ± 0.10) and roundness (0.86 ± 0.10, 1 220 cells) compared to *Lmx1b* +/+ podocytes (0.78 ± 0.10 and 0.84 ± 0.10, 555 cells). This difference was even higher in steady state podocytes, where both circularity (0.47 ± 0.21) and roundness (0.53 ± 0.22; 959 cells) of *Lmx1b* knock-out podocytes were significantly increased compared to control cells (0.37 ± 0.18 and 0.46 ± 0.20; 747 cells).

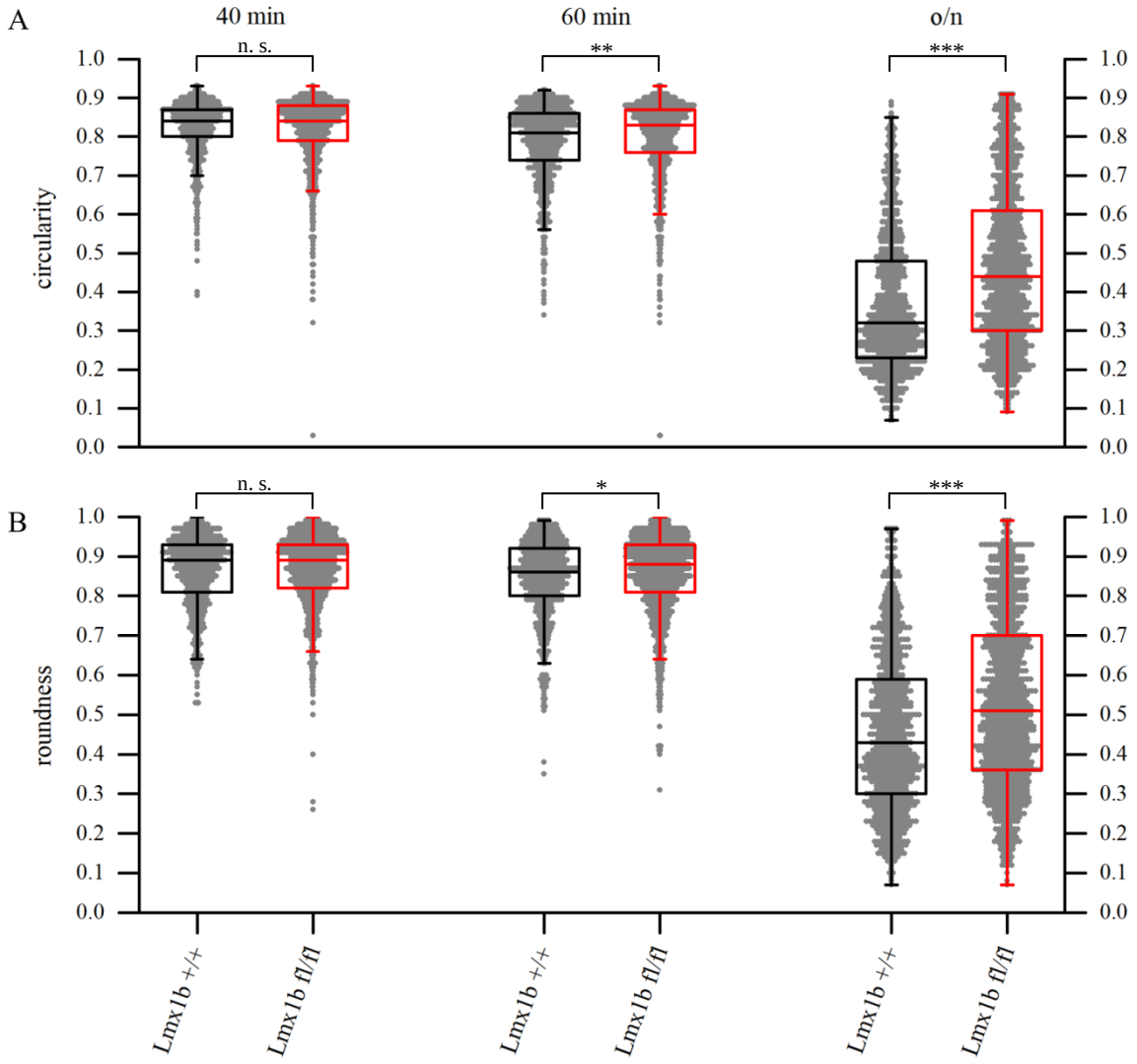

Figure 3.7: **Circularity [A] and roundness [B] of primary green fluorescent podocytes at different time points after plating on laminin-521-coated cover slides.** To isolate primary podocytes, at least 3 male quadruple transgenic mice (exception: *Lmx1b* +/+ podocytes at 60 min after plating were derived from only 2 mice) were induced with doxycycline for 7 days, followed by the isolation of glomeruli and outgrowth of podocytes for 5 days. The value of every single cell is depicted as a gray dot, while the box represents the lower and upper quartile. The median is shown as the horizontal line, and the bars reach to the furthest points within the range of 1.5 times the box height. n. s. not significant; *P<0.05; **P<0.01; ***P<0.001.

Taken together, the spreading rate of primary podocytes was not affected by *Lmx1b* knock-out, although some differences in the cell shape were observed in the late spreading phase. However, large morphological changes were present in steady state knock-out podocytes. *Lmx1b*-deficient podocytes were larger and exhibited a higher degree of circularity and roundness, arguing for less cellular protrusions maintained by the actin cytoskeleton.

3.2.4. Effect of cytochalasin D treatment on podocytes

A well-known and widely used toxin to depolymerize the actin cytoskeleton is cytochalasin D. As described in chapter 1.5.5, cytochalasin D has low side effects, but does not directly depolymerize F-actin, instead it rather caps the growing barbed end. Cytochalasin D was applied to primary podocytes to further investigate the dynamics of the actin cytoskeleton with respect to *Lmx1b* knock-out. Owing to the indirect mechanism of cytochalasin D induced F-actin depolymerization, the toxin was used to investigate the depolymerization by endogenous proteins. Moreover, F-actin polymerization following cytochalasin D wash-out was also examined.

Structure of the actin cytoskeleton after cytochalasin D treatment

In order to investigate the effect of cytochalasin D on the actin cytoskeleton of primary podocytes, F-actin was stained with phalloidin both after cytochalasin D treatment and after subsequent recovery for 2 h. Primary green fluorescent podocytes were obtained by outgrowth of podocytes from glomeruli isolated from 7 day induced female quadruple transgenic mice (see chapter 2.6.1). After 5 days of outgrowth, glomerular cells were plated on laminin-521-coated cover slides and treated with 5 µM cytochalasin D the next day for a period of 24 h. Thereafter, cells were fixed immediately or after wash-out of cytochalasin D and recovery for 2 h (see chapter 2.8.8). Five to six podocytes were investigated per mouse, and podocytes originated from two mice per genotype.

Treatment with cytochalasin D resulted in shrinkage of the cell body of primary podocytes, but many thin protrusions remained and did not retreat (Figure 3.8, A and B). Additionally, the actin cytoskeleton was in large parts destroyed, but some F-actin rich spots were located in proximity of the nucleus and at the base of cell protrusions, consistent with previous reports (Wakatsuki et al., 2001). No overt differences in the F-actin localization between *Lmx1b fl/fl* podocytes and *Lmx1b* +/+ controls were apparent judging from at least 11 confocal pictures.

Two hours past wash-out of cytochalasin D, the cells were spread again and showed a more typical podocyte structure with multiple broad and also some thin cell protrusions (Figure 3.8, C and D). The phalloidin staining revealed some actin fibers throughout the cell, mostly extending from F-actin-rich spots mentioned above. Those spots were neither seen in untreated spreading nor in steady state podocytes (see Figure 3.16). Again, the phalloidin staining showed no apparent differences regarding structure and localization between *Lmx1b* knock-out and control podocytes. Multiple nuclei in primary podocytes as seen in Figure 3.8 were frequently observed, but there was no difference in the nucleus count per podocyte after 5 days of outgrowth between *Lmx1b fl/fl* and *Lmx1b* +/+ podocytes (data not shown).

Taken together, cytochalasin D treatment resulted in shrinkage of primary podocytes and accumulation of short F-actin fibers into few aggregates, and wash-out of cytochalasin D led to a spreading of the cells, although the actin cytoskeleton remained structurally disturbed 2 h post wash-out.

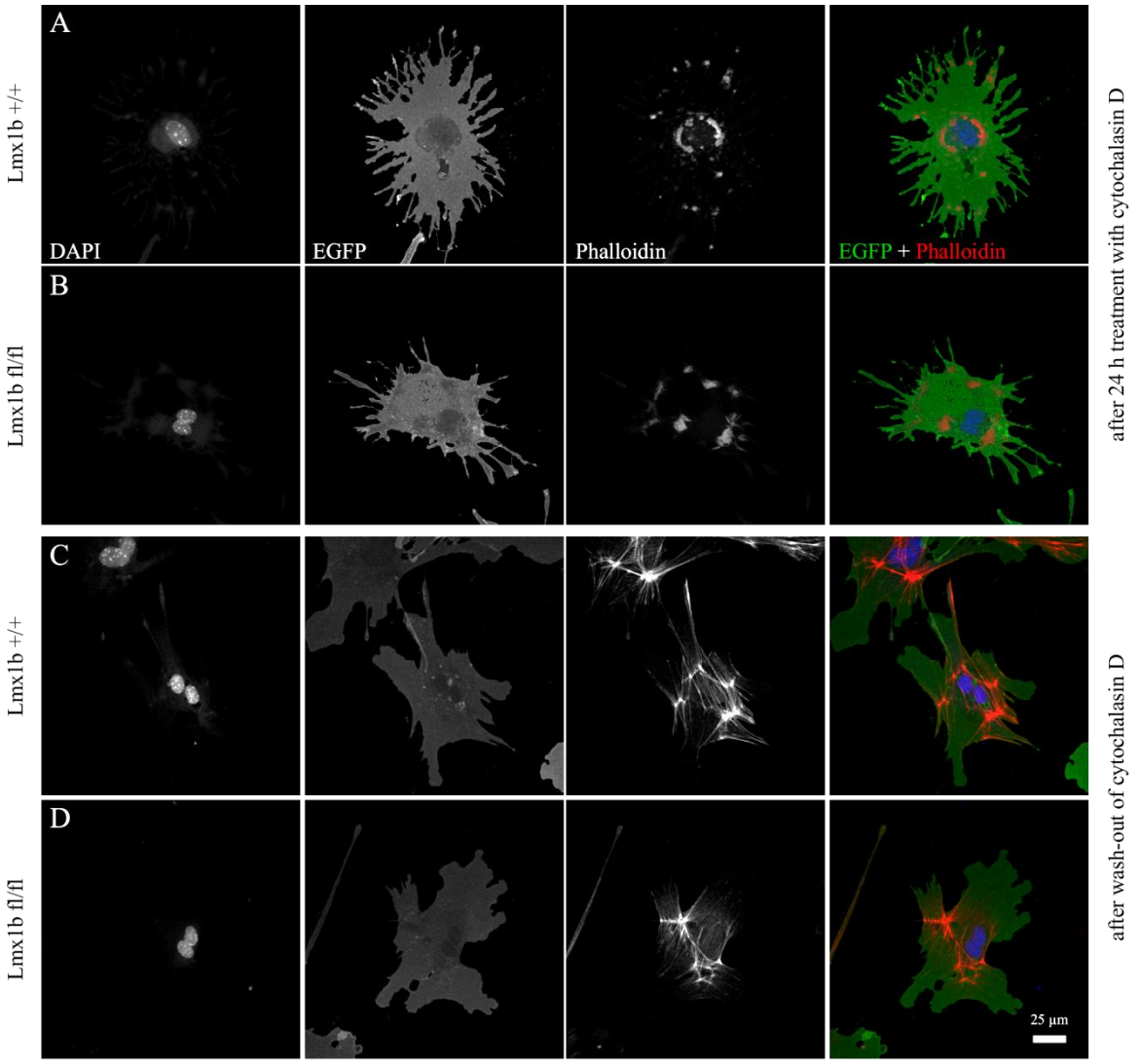

Figure 3.8: **Representative confocal pictures of primary green fluorescent podocytes stained with phalloidin to visualize F-actin.** Cells were treated with 5 µM cytochalasin D over a period of 24 h prior phalloidin staining [A, B] or were stained after subsequent wash-out of cytochalasin D and recovery for 2 h [C, D]. The primary podocytes originated from glomeruli of 7-day doxycycline-induced female quadruple transgenic mice. Two mice per genotype were investigated, and 5 - 6 confocal pictures of primary podocytes per mouse were taken.

Cytochalasin D induced cell shrinkage and post-cytochalasin D spreading

The capping of the barbed end of actin filaments drastically reduces the dynamic actin turnover and is therefore suitable to investigate the actin depolymerization or polymerization. Cytochalasin D was applied to primary green fluorescent podocytes to induce cell shrinkage and the podocyte area was taken as a parameter for F-actin depolymerization, as the direct observation of single actin filaments in live cell imaging experiments was not possible. Moreover, removal of cytochalasin D was taken as a starting point for newly actin filament growth and again the cell area was taken as an indicator of actin polymerization.

Female mice at an age between 3 and 5 months were induced with doxycycline for 7 days, followed by the isolation of glomeruli and the outgrowth of primary green fluorescent podocytes for 5 days (see chapter 2.6.1). The cells were plated on laminin-521-coated culture dishes. The next day fully expanded podocytes were treated with 5 µM cytochalasin D or solvent as a control. In shrinkage experiments, the green fluorescent surface area was immediately analyzed by taking fluorescence pictures every 60 s over a period of 121 min in a live cell imaging setup. For spreading experiments, cells were induced with cytochalasin D for a total of 24 h, and cytochalasin D was renewed 1 h prior wash-out (see chapter 2.8.8). Fluorescence pictures were taken immediately after the wash-out in the same way as described above. In both cases, 4 fields of view (FOVs) per experiment were analyzed regarding the green fluorescent surface area, and the value at 10 min after the start of the experiment was taken as 100%. The podocytes originated from one mouse per experiment, and a total of 24 FOVs (6 mice) were analyzed for every setting, except only 8 FOVs (2 mice) were used in the control experiments of cell shrinkage.

Following cytochalasin D treatment primary podocytes shrank slowly but constantly (Figure 3.9, A), while podocytes treated with ethanol shrank only within the first 30 min and regained their initial size within the course of the experiment. The reason for the initial cell shrinkage of control cells could either be the toxicity of the solvent ethanol or the cell stress accompanied by medium exchange. There was no difference in the cell area between *Lmx1b fl/fl* and *Lmx1b* +/+ podocytes after 121 min cytochalasin D treatment (Figure 3.9, C). This finding indicates that the depolymerization processes of the actin cytoskeleton are not influenced by *Lmx1b* knock-out. Nevertheless, as live visualization of the actin cytoskeleton was not possible, cell shrinkage could also be limited by focal adhesion disassembly. Although the difference between the control groups was significant, the number of experiments was in this case maybe too low for statistical analysis (8 FOVs).

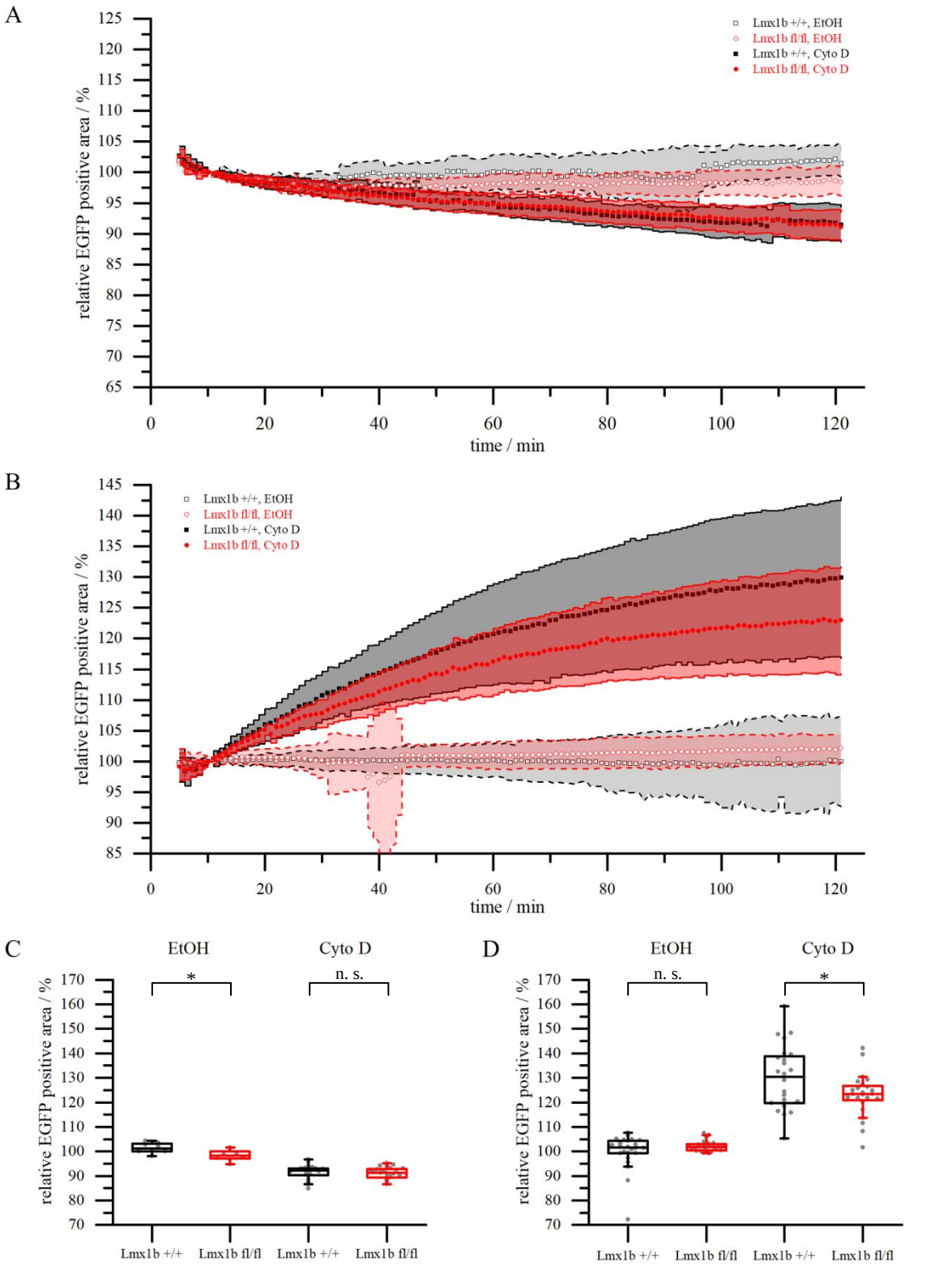

Figure 3.9: **Changes of the surface area covered with green fluorescent podocytes following cytochalasin D treatment or wash-out.** Outgrown primary podocytes were derived from female quadruple transgenic mice. The cells were plated on laminin-521-coated culture dishes and

subjected to live cell imaging experiments. Pictures of the green mG fluorescence were taken every 60 s over a period of 121 min. The area covered with green fluorescent podocytes was analyzed within 4 non-overlapping fields of view (FOVs) per mouse and the value at 10 min was defined as 100%. [A] Primary podocytes were treated with 5 µM cytochalasin D or solvent (ethanol) to induce cell shrinking. Shown are the mean values ± SD of 24 FOVs (cytochalasin D experiments) or 8 FOVs (ethanol controls). [B] Primary podocytes were incubated with 5 µM cytochalasin D or solvent for 24 h, and the spreading after wash-out of the toxin is depicted. Shown are the mean values ± SD of 24 FOVs per experiment. [C, D] Box plots of the relative EGFP positive area after 121 min cytochalasin D treatment [C] or after 121 min recovery post cytochalasin D wash-out [D]. The values are presented as gray dots, the median as the horizontal line and the box marks the lower and upper quartile. The bars reach to the last point within the range of 1.5 times the box height. n. s. not significant; *P<0.05.

After wash-out of cytochalasin D both *Lmx1b* knock-out and wild-type podocytes started to spread, while the spreading rate decreased over the course of the experiment (Figure 3.9, B). The wash-out of ethanol had no impact on the size of the podocytes, proving that cell spreading was a consequence of cytochalasin D wash-out. Interestingly, *Lmx1b* knock-out podocytes spread slower compared to wild-type podocytes, and the difference was significant at 121 min after removal of the toxin (Figure 3.9, D). As the actin cytoskeleton provides the force necessary for pushing the cell membrane, it is very likely that the assembly of actin filaments was disturbed or the number of assembling filaments was decreased.

Taken together, some actin-dependent processes like random movement, spreading of untreated cells and cytochalasin D induced cell shrinkage are not influenced by *Lmx1b* knock-out. Nevertheless, the cell area, circularity, and roundness of knock-out podocytes were increased, while the spreading after wash-out of cytochalasin D was decreased. Moreover, direct investigation of the actin cytoskeleton showed an increased F-actin staining in *Lmx1b* knock-out podocytes, arguing for an Lmx1b-dependent regulation of the actin cytoskeleton.

3.3. Dysregulation of signaling pathways regulating the actin cytoskeleton

The increased phalloidin intensity, cell area and roundness of *Lmx1b* knock-out podocytes and moreover the reduced spreading after removal of cytochalasin D demonstrated a dysregulation of the actin cytoskeleton. As the transcription factor Lmx1b is located within the nucleus, these observations cannot result from a direct interaction. It is more likely that Lmx1b regulated target genes impact the actin cytoskeleton. Indeed, Abra and transgelin are reported to directly interact with actin filaments (Arai et al., 2002; Fu et al., 2000), and furthermore, Arl4c influences Rho GTPases (Chiang et al., 2017; Matsumoto et al., 2014). For this reason, signaling pathways upstream of the actin cytoskeleton were investigated. For instance, the activation of Rho GTPases in glomerular lysates was checked, and additionally the phosphorylation of the myosin light chain in LMX1B expressing hPCL cells. Furthermore, the impact of different inhibitors on the spreading of podocytes was investigated.

3.3.1. Activity of Rho GTPases

As the Rho GTPases are master regulators of the actin cytoskeleton (Sadok and Marshall, 2014), the activities of the family members RhoA, Rac1 and Cdc42 were examined. Rho GTPases are active when bound to GTP and inactive when bound to GDP. Active Rho GTPases are short-lived species, as the intrinsic hydrolysis activity leads to GTP hydrolysis which is further catalyzed by GTPase activating proteins (GAPs). With this in mind, it was decided to analyze freshly isolated glomeruli and not FACS sorted detached podocytes or partly dedifferentiated outgrown glomerular cells.

Female podocyte-specific *Lmx1b* knock-out (*Lmx1b fl/fl*) mice and heterozygous controls (*Lmx1b +/fl*) were induced with doxycycline for 7 days before glomeruli were isolated (see chapter 2.6.1). Pure glomeruli fractions were immediately lysed in less than 8 min and snap frozen until the Rho GTPase activity was analyzed using G-LISA assays. Total protein content of glomerular lysates was equalized beforehand. Glomerular lysates from 5 mice per genotype were used in case of RhoA and Cdc42, and 4 in case of Rac1 G-LISA. The amount of active Rho-GTPases was detected by absorption measurements of a chromogenic reaction catalyzed by HRP-coupled antibodies (see chapter 2.7.1).

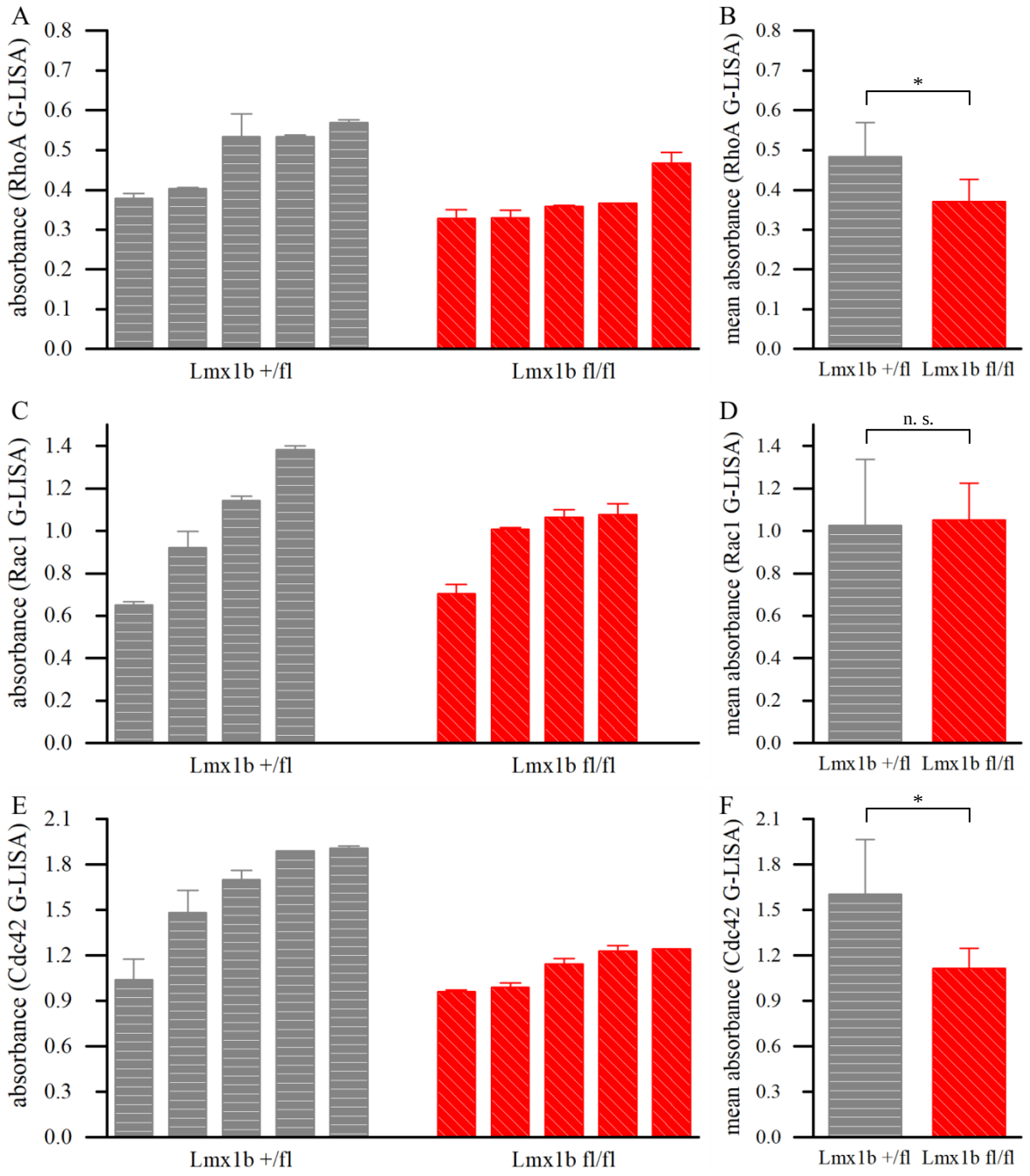

Figure 3.10: **Amount of active GTP-bound Rho GTPases as discovered by G-LISA assays.** Glomeruli were isolated from female quadruple transgenic mice induced with doxycycline for 7 days. The assays were conducted with equalized glomerular lysates after rapid lysis. Active Rho-GTPases were detected by HRP coupled antibodies catalyzing a chromogenic reaction. [A, C, E] Shown are the blank corrected means of doublets + SD per glomerular lysate for RhoA, Rac1 and Cdc42. [B, D, F] Shown are the mean Rho GTPase activity per genotype + SD. n. s. not significant; *P<0.05.

A statistically significant difference in the amount of active RhoA and Cdc42 between *Lmx1b fl/fl* and *Lmx1b +/fl* glomeruli was found. The amount of GTP-bound RhoA was decreased to 76% (Figure 3.10, B) and GTP-bound Cdc42 was decreased to 69% (Figure 3.10, F) in *Lmx1b*-deficient glomeruli compared to heterozygous knock-outs. The amount of active Rac1 was not dysregulated in respect to *Lmx1b* knock-out (Figure 3.10, D). A higher variance within *Lmx1b +/fl* controls was detected in all cases (Figure 3.10, A, C and E). Although these data show glomerular activity levels, podocytes were the only cells within the glomerulus with Cre expression and genomic recombination following doxycycline treatment, leading to the assumption that mostly podocytes contributed to changes in activity levels.

In summary, *Lmx1b* knock-out led to decreased levels of active RhoA and Cdc42, which might contribute to a dysregulation of the actin cytoskeleton of podocytes.

3.3.2. Phosphorylation of the myosin light chain 2

Myosin-2 is an actin-binding hexamer important for force generation alongside actin filaments which is activated by phosphorylation of Ser-19 of myosin light chain 2 (MLC) (see chapter 1.5.4). Rho GTPases regulate MLC phosphorylation, for instance, RhoA induces MLC phosphorylation over ROCK (Totsukawa et al., 2000) . This makes pMLC to an interesting target for deeper analyses regarding the influence of Rho GTPase signaling pathways on the actin cytoskeleton.

The hPCL pInducer-LMX1B cell line was used to investigate the amount of pMLC by immunofluorescence staining. As the hPCL cell line showed no LMX1B expression in proliferating and differentiated cells, the hPCL pInducer-LMX1B cell line was created by lentiviral transduction of hPCL cells. This cell line expressed human LMX1B after induction with doxycycline, as shown in Figure 3.11. Proliferating as well as differentiated cells showed low LMX1B protein in the absence of doxycycline, while induction with doxycycline for 5 days resulted in strong nuclear expression of LMX1B in nearly all proliferating cells. In differentiated cells, there was also LMX1B protein stained but to a lesser extent. The nuclei and cell area of differentiated cells were larger compared to proliferating hPCL pInducer-LMX1B.

To quantify the amount of pMLC in proliferating hPCL pInducer-LMX1B cells, cells were grown 5 days in the presence or absence of 1 mg/L doxycycline and were replated on laminin-521-coated cover slides thereafter. hPCL pInducer-LMX1B differentiation was conducted by culturing at 37 °C for 14 days. Within the last five days of differentiation some cells were additionally treated with doxycycline to induce LMX1B expression. Differentiated cells were replated on laminin-521-coated cover slides. Both proliferating

and differentiated cells were fixed 20, 40 and 60 min after replating and stained for pMLC and transgelin. The cell area was in both cases determined by immunofluorescence staining against transgelin, which located throughout the cytosol. Interestingly, transgelin was highly expressed both in induced and non-induced hPCL pInducer-LMX1B cells, at least after 5 days of doxycycline treatment.

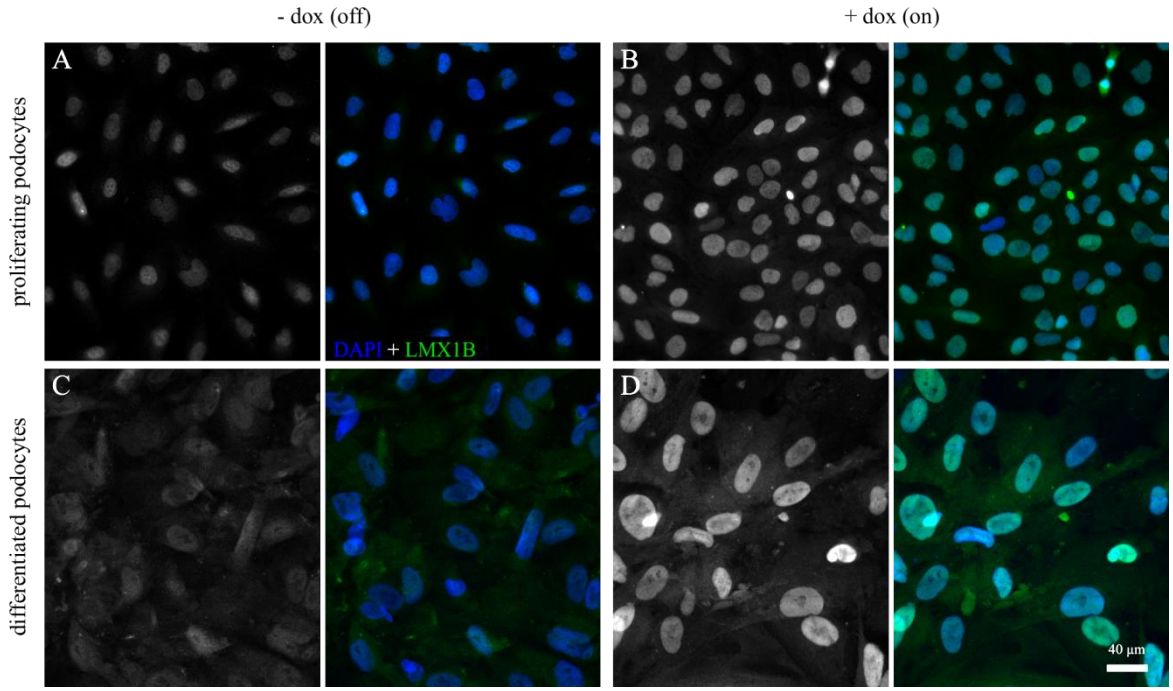

Figure 3.11: **LMX1B expression of the hPCL pInducer-LMX1B cell line in the presence or absence of doxycycline.** [A] Proliferating cells were plated on laminin-521-coated cover slides and stained for LMX1B after 5 days. [B] Proliferating cells induced with 1 mg/L doxycycline for 5 days. [C] Cells were plated on laminin-coated cover slides and differentiated over 14 days at 37 °C. [D] Differentiating cells were induced with 1 mg/L doxycycline the last five days of differentiation. For better visibility brightness of pictures C and D was increased compared to pictures A and B.

The expression of LMX1B influenced the amount of phosphorylated myosin light chain 2 in spreading hPCL pInducer-LMX1B cells. Proliferating podocytes showed significantly decreased pMLC fluorescence in doxycycline-induced LMX1B expressing cells both 20 and 40 min after plating (Figure 3.12, A). However, there was no difference after 60 min of cell spreading. A similar result was obtained when using differentiated cells (Figure 3.12, B). LMX1B expressing cells stained 40 min after plating had significantly reduced amounts of pMLC, while the difference at 60 min after plating was nearly significant. Nevertheless, there was again no difference at one time point, in this case at 20 min after plating.

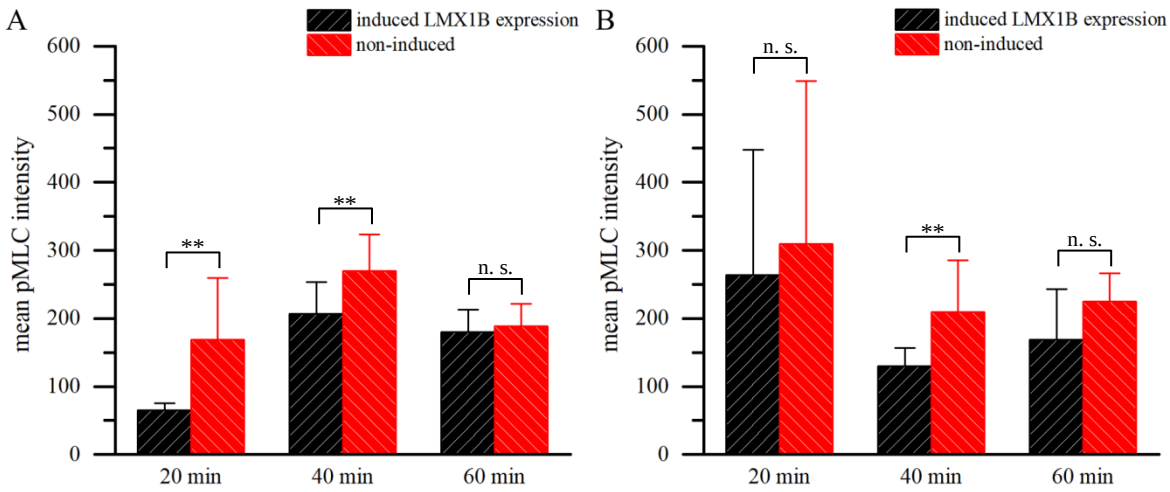

Figure 3.12: **Mean pMLC intensity of proliferating and differentiated hPCL pInducer-LMX1B cells in respect to doxycycline-induced LMX1B expression.** Proliferating and differentiated cells were fixed 20, 40 and 60 min after replating on laminin-521-coated cover slides and stained for pMLC and transgelin. Transgelin staining was used as a cell boundary marker. [A] Proliferating cells were treated with 1 mg/L doxycycline for five days prior replating. At least 10 cells were analyzed. [B] hPCL-pInducer-LMX1B cells were differentiated at 37 °C for 14 days and additionally induced with doxycycline within the last five days of differentiation. At least 8 cells were analyzed per setting. n. s. not significant; **P<0.01.

In summary, LMX1B expressing podocytes had reduced or equal levels of pMLC compared to control cells, but the pMLC amount was never increased. These data further hint towards a role of LMX1B in the regulation of the actin cytoskeleton, but the data are only preliminary as the experiment was performed only one time before the end of this thesis.

3.3.3. Influence of signaling cascades on the spreading of primary podocytes

It was shown in chapter 3.2.4 that primary *Lmx1b*-deficient podocytes spread slower after the removal of cytochalasin D. This experiment was used to narrow down the nature of the dysregulation of the actin cytoskeleton. The experimental setup and procedure remained unchanged, except for the addition of an inhibitor 1 h prior to the wash-out of cytochalasin D, and the inhibitor was also supplemented to the washing medium (see chapter 2.8.8). The effect of the inhibitor on the spreading of *Lmx1b* +/+ and *Lmx1b fl/fl* podocytes was then analyzed in comparison to untreated podocytes. Two inhibitors were used so far, Y-27632 (5 µM) and LIMKi 3 (10 µM), which inhibit the kinases ROCK1/2 and LIMK1/2, respectively. These kinases play an important role in the regulation of the actin cytoskeleton and act downstream of Rho GTPases.

The resulting spreading curves were interpreted as follows: In case the inhibited kinases are not part of the dysregulated signaling pathway, the inhibitor should act on the spreading of knock-out and wild-type podocytes in the same way. That means the spreading of *Lmx1b fl/fl* podocytes should remain slower. In case the inhibited kinases are dysregulated following *Lmx1b* knock-out, the inhibitor should nullify the differences in the actin regulation and in the spreading, at least as long as only one pathway is to most parts responsible for the dysregulation of the actin cytoskeleton.

Involvement of ROCK in the dysregulation of the actin cytoskeleton

When treated with ROCK inhibitor (ROCKi) Y-27632, the relative cell area of *Lmx1b fl/fl* podocytes 121 min after wash-out of cytochalasin D was significantly decreased (Figure 3.13, C). Unfortunately, there was only a slight and not significant difference in the spreading of control podocytes treated with the solvent of the inhibitor (H_2O), possibly because only half as many animals (3 mice, 12 FOVs) compared to the initial spreading experiment (Figure 3.9, B) were used. Nevertheless, the significant difference of ROCKi treated podocytes indicates that the kinase ROCK is not involved in the dysregulation of the actin cytoskeleton.

Involvement of LIMK in the dysregulation of the actin cytoskeleton

The spreading of green fluorescent *Lmx1b fl/fl* and *Lmx1b* +/+ podocytes treated with LIMKi was almost identical (Figure 3.13, B), and there was no difference in the relative EGFP positive area after 121 min of spreading (Figure 3.13, D). A marked difference in the spreading of control podocytes treated with solvent (DMSO) was noticeable, although it was not significant 121 min after wash-out of cytochalasin D. Again, the animal number was lower (3 mice, 12 FOVs) compared to the initial experiment, which explains this statistical finding. As the spreading curves of LIMKi treated podocytes were at the same level, it is hypothesized that LIMK is dysregulated in *Lmx1b* knock-out podocytes. Moreover, the spreading of knock-out podocytes in the presence or absence of LIMKi was similar, indicating that LIMK activity in *Lmx1b fl/fl* podocytes was already at a low level and therefore not influenced by the inhibitor.

Taken together, these results point towards a decreased activity of LIMK in *Lmx1b* knock-out podocytes, whereas the activity of ROCK is not affected.

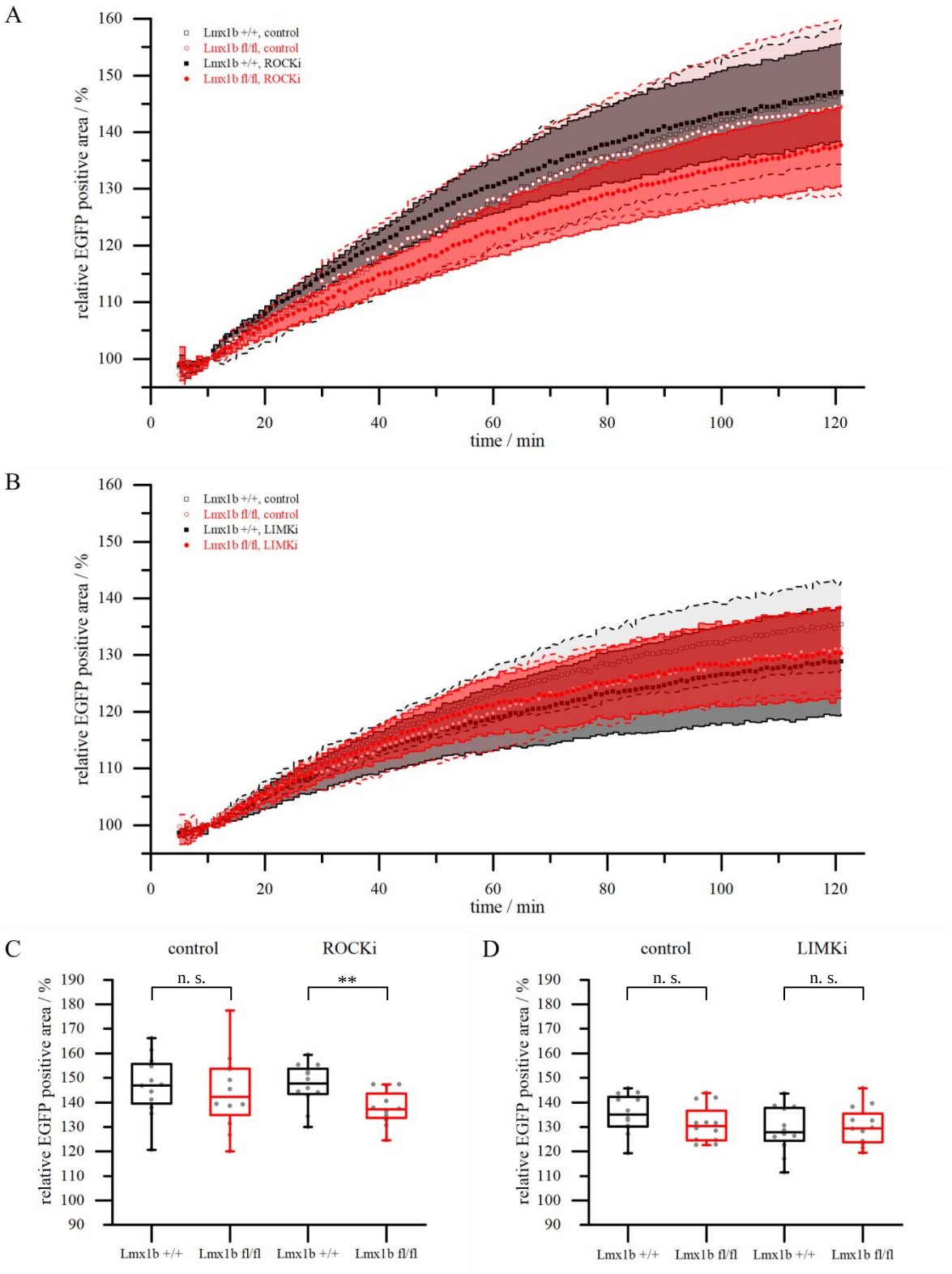

Figure 3.13: **Spreading of primary green fluorescent podocytes after wash-out of cytochalasin D in the presence or absence of inhibitors.** Primary podocytes derived from female quadruple transgenic mice after doxycycline induction for 7 days and were obtained by glomerular

outgrowth over 5 days. Podocytes were treated with cytochalasin D for 24 h and cell spreading was analyzed after wash-out of the toxin by live cell imaging (one picture every 60 s, 121 min observation time). The inhibitor treatment started 1 h before wash-out and continued in the course of the experiment. Data are presented as the green fluorescent cell area relative to the area 10 min post wash-out. Cells from one mouse per genotype were used per experiment, and 4 fields of view (FOVs) were analyzed per experiment. [A] Spreading of primary podocytes treated with 5 µM ROCK inhibitor or solvent (H_2O). Shown are the means and SDs from 3 experiments (12 FOVs). [B] Spreading of podocytes in the presence of 10 µM LIMK inhibitor or solvent (DMSO). Shown are the means and SDs from 3 experiments (12 FOVs). [C, D] Box plots of the relative podocyte area 121 min after cytochalasin D wash-out. Gray dots represent values of single FOVs, the boxes the lower and upper quartiles and the horizontal line the respective medians. Bars reach to the furthest points within 1.5 times the box height. n. s. not significant; **P<0.01.

3.4. Dysregulation of focal adhesions

The regulation of the actin cytoskeleton is influenced by extracellular signals, which are recognized by transmembrane receptors leading to an activation of signaling cascades. Two transmembrane compartments especially important in podocytes are focal adhesions and slit diaphragms (see chapter 1.4.3). Both are mechanically linked to the actin cytoskeleton and additionally regulate the actin cytoskeleton over signaling cascades (Faul et al., 2007). As the possibility to induce foot process and potentially slit diaphragm formation of cultured primary podocytes was reported only at the end of this thesis (Yaoita et al., 2018), the contribution of slit diaphragms to actin cytoskeleton dysregulation could not be investigated. On the other hand, some previous data hinted towards dysregulation of focal adhesions after *Lmx1b* knock-out. For instance, *Lmx1b* knock-out podocytes adhered stronger to laminin-111 (Burghardt et al., 2013) and FRAP experiments revealed slower recovery of α-actinin-1 and actin at focal adhesions in primary knock-out podocytes (Stepanova, 2016). Additionally, defects of focal adhesion proteins are known to cause podocyte damage and foot process effacement (Vivante and Hildebrandt, 2016). Focal adhesions were investigated to answer the question if dysregulation of the actin cytoskeleton in *Lmx1b* knock-out podocytes is already caused by dysregulated focal adhesions.

3.4.1. Activation of β1-integrin

Integrins are extracellular matrix receptors and the central proteins of focal adhesions. Within podocytes, the heterodimeric α3β1-integrin is the most abundant integrin (Sachs and Sonnenberg, 2013). Integrins are activated either to extracellular stimuli (outside-in signaling) or by intercellular binding of proteins (inside-out signaling) (Askari et al., 2009).

Owing to its importance for focal adhesions the activity of β1-integrin was investigated by fluorescence staining with an activation-state recognizing antibody.

Investigation by immunofluorescence staining of adherent podocytes

In a first experiment primary adherent podocytes were stained against active β1-integrin to visualize the localization and amount of active β1-integrin. To obtain primary podocytes, male quadruple transgenic mice were induced with doxycycline for 7 days, followed by isolation of glomeruli and outgrowth of podocytes for 5 days (see chapter 2.6.1). Outgrown podocytes were plated on laminin-521-coated cover slides and fixed after exactly 40 min or at the next day and stained against active β1-integrin. At least 26 green fluorescent primary podocytes originating from two male mice per genotype were analyzed.

The staining revealed the typical localization and shape of focal adhesions in spreading and steady state podocytes (Figure 3.14, A - H). This pattern was also frequently observed by paxillin staining of primary podocytes (data not shown). In roundish spreading podocytes, focal adhesions were commonly arranged in a ring near to the cell edge, but no difference between *Lmx1b +/+* and *Lmx1b fl/fl* podocytes was visible. The localization of active β1-integrin in steady state podocytes was more heterogeneous and was dependent on the cell shape, but again no overt differences between the two genotypes were recognizable. Isotype controls revealed some unspecific fluorescence signal primarily in the vicinity of the nucleus, especially in spreading cells. Quantification of the mean fluorescence intensity per cell showed equal levels of β1-integrin activation both in spreading and steady state podocytes when comparing *Lmx1b fl/fl* to *Lmx1b +/+* podocytes (Figure 3.14, I).

Investigation by flow cytometry

To reveal potential small differences in the activation of β1-integrin, a greater number of cells were investigated by flow cytometry. Female quadruple transgenic mice were induced with doxycycline for 7 days followed by isolation of glomeruli and podocyte outgrowth for additional 7 days (see chapter 2.6.1). Glomerular outgrown cells were detached from the surface and split into three equal parts. Each part was incubated either with anti-active β1-integrin, anti-total β1-integrin or isotype control antibodies (see chapter 2.8.9). As glomerular cells comprehended green fluorescent Cre expressing podocytes as well as red fluorescent podocytes without Cre expression and possibly red fluorescent endothelial and mesangial cells, an antibody coupled to the far-red fluorescent dye Alexa633 was chosen as a secondary antibody. Both green and red fluorescent cells were analyzed by flow cytometry regarding the Alexa633 intensity per cell. Total cell numbers are listed in Table 3.1, originating from 11 mice per genotype.

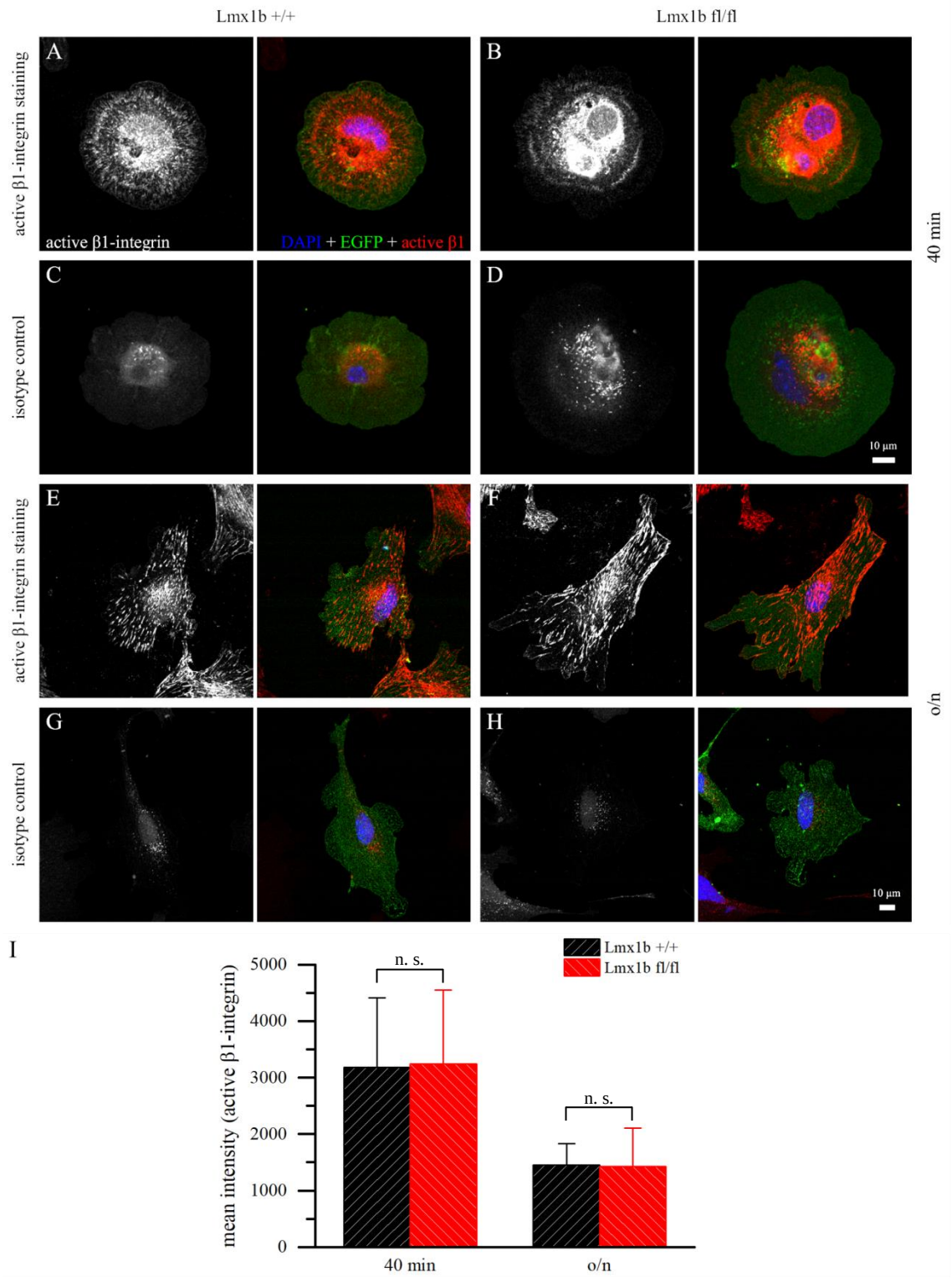

Figure 3.14: **Localization and quantification of the amount of active β1-integrin in primary green fluorescent podocytes.** Male quadruple transgenic mice were induced with doxycycline for 7 days followed by isolation of glomeruli and outgrowth of podocytes for 5 days. Outgrown cells were plated on laminin-521-coated cover slides and fixed after 40 min or the next day.

[A – H] Confocal pictures of spreading (top panels) and steady state (bottom panels) green fluorescent podocytes, stained for active β1-integrin. [I] Quantification of the mean fluorescence intensity within a cell. At least 26 cells isolated from 2 mice per genotype were analyzed. n. s. not significant.

A slight increase of active β1-integrin of green fluorescent *Lmx1b fl/fl* podocytes compared to *Lmx1b* +/+ podocytes was found, while the amount of total β1-integrin remained at the same level (Figure 3.15, A). The data were not compromised by unspecific binding of antibodies, judging from the low isotype control intensities.

Red fluorescent cells showed a different signal distribution (Figure 3.15, B). There were two peaks of active β1-integrin regardless of their origin, arguing for at least two different β1-integrin-expressing cell types. The right peak most likely corresponds to non-induced red fluorescent podocytes, as it showed similar fluorescence intensities compared to green fluorescent podocytes. Although there were differences in relative cell numbers of red fluorescent primary podocytes, the amount of active β1-integrin was at the same level between red fluorescent podocytes isolated from podocyte-specific *Lmx1b* knock-out and wild-type animals. The amount of total β1-integrin was increased in cells from *Lmx1b* knock-out animal origin. However, the broad signal argues again for overlapping signals from different cells types.

Taken together, green fluorescent but not red fluorescent podocytes from podocyte-specific *Lmx1b* knock-out mouse origin showed slightly increased β1-integrin activity, indicating that this difference was rather caused by intracellular processes than extracellular glomerular basement membrane alterations. On the other hand, the amount of total β1-integrin remained unchanged, at least in green fluorescent podocytes.

Table 3.1: Numbers of cells analyzed by flow cytometry regarding their active β1-integrin, total β1-integrin and isotype control staining intensity.

Primary antibody	Genotype	EGFP positive cells	tdTomato positive cells
active β1-integrin	*Lmx1b* +/+	107 193	196 206
	Lmx1b fl/fl	92 060	238 252
total β1-integrin	*Lmx1b* +/+	95 529	157 770
	Lmx1b fl/fl	76 532	243 888
isotype control	*Lmx1b* +/+	94 115	233 472
	Lmx1b fl/fl	92 788	250 893

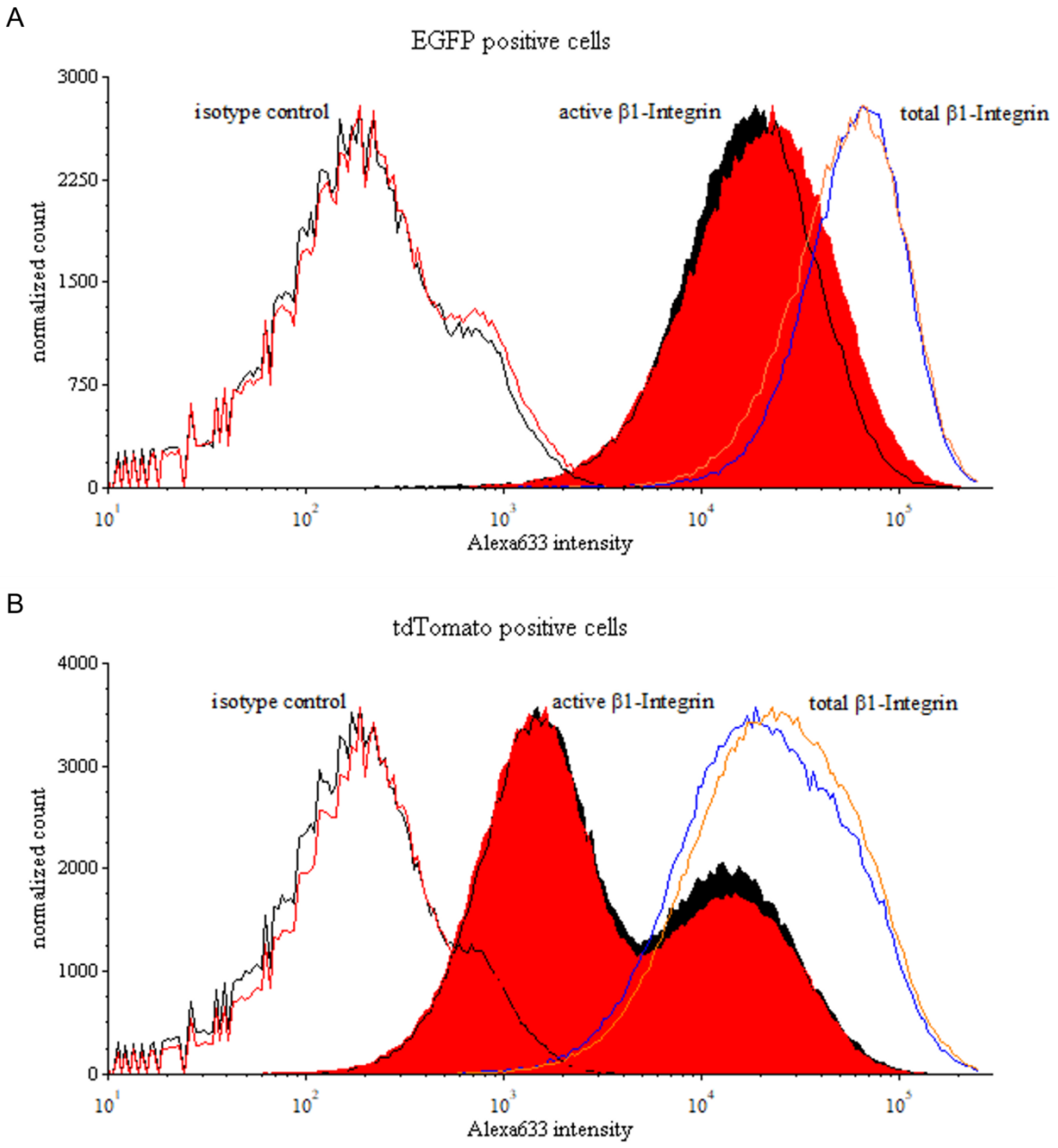

Figure 3.15: **Amount of active and total β1-integrin of green fluorescent podocytes and red fluorescent glomerular cells determined by flow cytometry.** Glomerular cells were obtained by 7-day lasting outgrowth from glomeruli isolated from a total of 11 female quadruple transgenic mice per genotype. Cells were incubated with monoclonal antibodies against active β1-integrin, total β1-integrin and an isotype control. An Alexa633 coupled secondary antibody was used and the Alexa633 intensity per cell was analyzed by flow cytometry. Red and orange color denotes curves of cells from *Lmx1b fl/fl* mouse origin and black and blue was used for curves of cells from *Lmx1b* +/+ mouse origin. The cell count was normalized for better comparability. [A] Alexa633 intensity histogram of green fluorescent podocytes with known Cre recombinase expression and activity. [B] Alexa633 intensity histogram of red fluorescent glomerular cells.

3.5. Investigation of transgelin in *Lmx1b* knock-out podocytes and mice

Transgelin revealed the strongest mRNA upregulation in podocyte-specific *Lmx1b* knock-out glomeruli identified by DNA microarray studies (Burghardt et al., 2013). Additionally, *de novo* transgelin expression in freshly isolated green fluorescent *Lmx1b fl/fl* podocytes was confirmed in chapter 3.1.2 at the protein level. Although upregulation of transgelin seems to be a common reaction of podocytes to damage, it is however an interesting study target owed to the observation that deletion of transgelin had beneficial effects in a crescentic glomerulonephritis model in mice (Marshall et al., 2011). The effect of transgelin in the progression of renal damage caused by *Lmx1b* homeobox deletion was mainly studied using a podocyte-specific *Lmx1b* knock-out mouse line crossed with a global transgelin deletion mouse line. Additionally, the subcellular localization and expression of transgelin in outgrown green fluorescent primary podocytes was investigated.

3.5.1. Subcellular localization of transgelin in primary podocytes

Transgelin localizes to the actin cytoskeleton in smooth muscle cells (Fu et al., 2000), but its localization in spreading and steady state podocytes was not reported so far. For this reason, primary podocytes were obtained from male 7 day induced quadruple transgenic mice by glomerular outgrowth for 5 days (see chapter 2.6.1). Those cells were replated on laminin-521-coated cover slides and fixed after exactly 40 min or at the next day and stained against transgelin. Confocal pictures of at least 31 green fluorescent podocytes per group were taken, and the cells originated from two male mice per genotype (see chapter 2.8.4).

Although transgelin was expressed only in freshly isolated *Lmx1b fl/fl*, but not in *Lmx1b* +/+ podocytes (see chapter 3.1.2), there was a strong transgelin expression in outgrown spreading and steady state podocytes of both genotypes (Figure 3.16). As the expression of transgelin in outgrown *Lmx1b* +/+ podocytes was unexpected, the mean transgelin intensity per cell was also quantified (Figure 3.17, B). Although there was no significant difference in spreading podocytes, steady state *Lmx1b* +/+ podocytes analyzed 6 days after isolation from mice had significantly lower levels of transgelin protein compared to *Lmx1b fl/fl* podocytes.

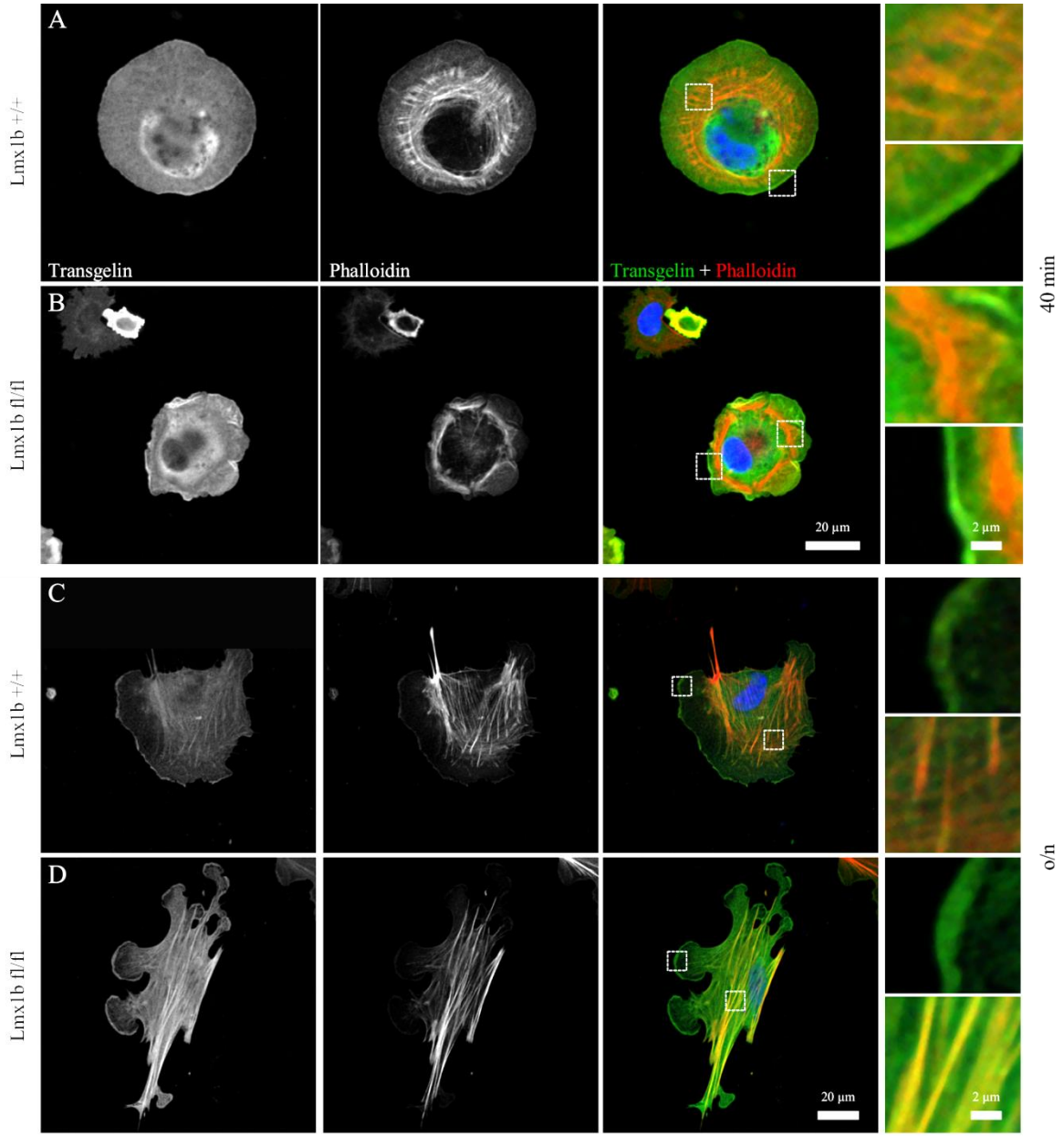

Figure 3.16: **Localization of transgelin and colocalization with actin in spreading and steady state podocytes.** The pictures show primary podocytes obtained by glomerular outgrowth for 5 days, which were replated on laminin-521-coated cover slides and fixed after 40 min [A, B] or the next day [C, D]. The podocyte sources were two male quadruple transgenic mice per genotype induced with doxycycline for 7 days. On the right-hand side are magnifications of the areas marked in the merge pictures displaying stress fibers and the leading edge.

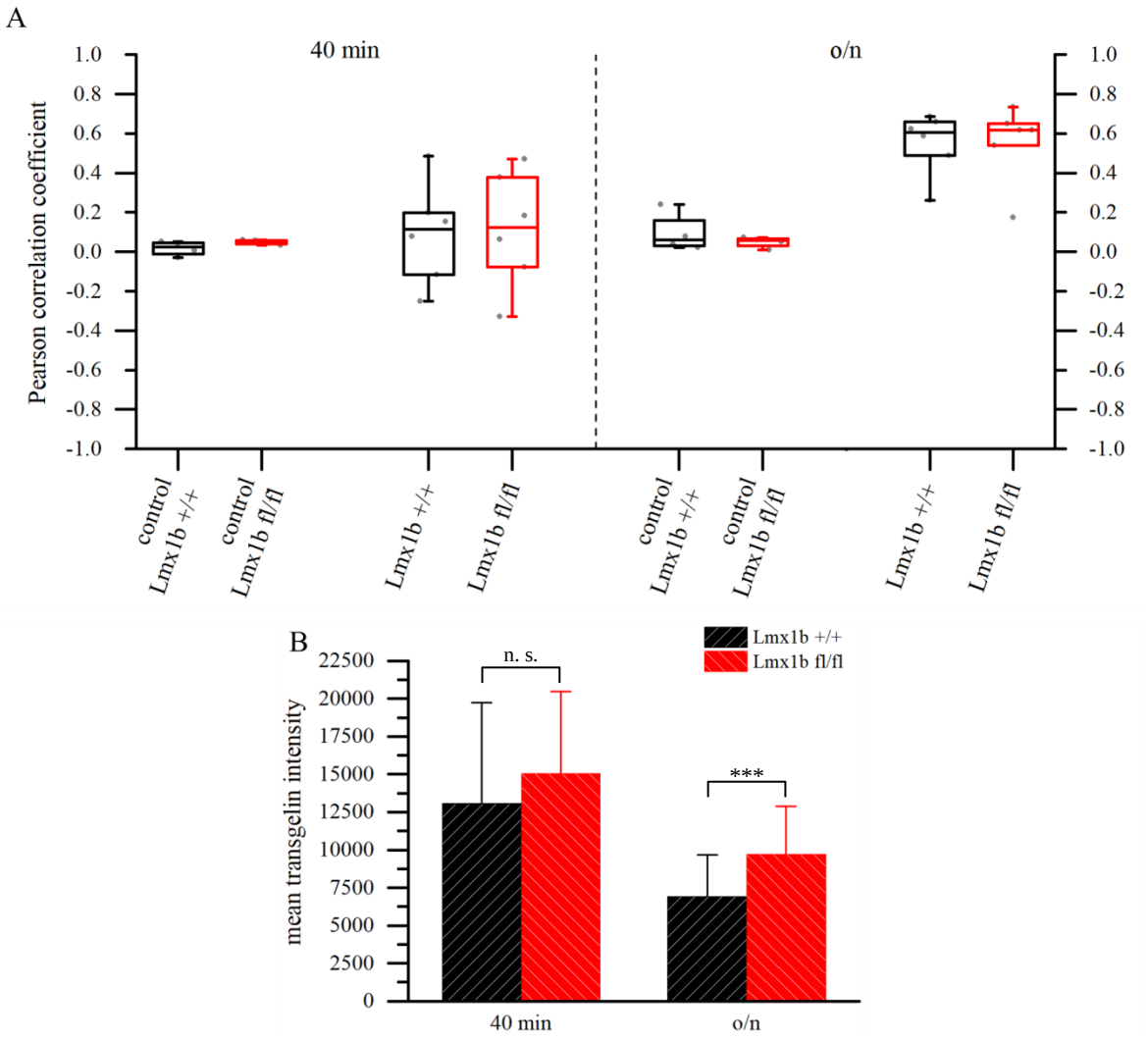

Figure 3.17: **Quantifications of actin-transgelin correlation and the amount of transgelin.** [A] Pearson correlation coefficient illustrating the colocalization of F-actin and transgelin. The coefficient was calculated by Costes' automatic threshold method for 4 control and 6 sample podocytes (gray dots) per genotype and time point. Controls were processed like sample cells apart from skipped anti-transgelin antibody incubation. The box represents the lower and upper quartile, the horizontal line within the box the median, and bars reach to the last points within 1.5 times the box height. [B] Mean transgelin intensity of at least 31 outgrown spreading and steady state podocytes. n. s. not significant; ***P<0.001.

In spreading podocytes, transgelin was localized throughout the cytosol (Figure 3.16, A and B). An increased fluorescence signal was noticed at the cell edge and at the perinuclear region, but not at phalloidin stained actin fibers. Actin fibers located in a belt between the nucleus and the cell edge similar to the localization of active β1-integrin stained focal adhesions (see Figure 3.14). No difference in the localization between knock-out and wild-type podocytes was obvious. In steady state podocytes, transgelin localized to the leading

edges of lamellipodia and to actin fibers regardless of the podocyte genotype (Figure 3.16, C and D), although the transgelin fluorescence in *Lmx1b* +/+ podocytes seemed to be weaker. Phalloidin staining was most prominent at stress fibers, but also weak staining of cortical actin was detectable.

Colocalization of transgelin and actin was quantified with the Pearson correlation coefficient (Figure 3.17, A). A value of 1 represents total positive correlation (colocalization), while 0 represents no correlation and -1 total negative correlation (exclusion). Cells treated with phalloidin and the secondary antibody, but without the primary antibody against transgelin served as controls. The coefficient was calculated for 6 cells per sample group and 4 cells per controls. The Pearson coefficient confirmed the finding of phalloidin and actin colocalization in steady state podocytes, but there was no colocalization in spreading podocytes. Colocalization was not influenced by *Lmx1b* knock-out.

In summary, transgelin colocalized with F-actin in steady state, but not in spreading podocytes. Transgelin was furthermore enriched at the leading edges and was generally expressed in dedifferentiated primary podocyte culture, although to a higher extent in *Lmx1b* knock-out podocytes.

3.5.2. Phenotypic characterization of *Lmx1b* and *Sm22* double knock-out mice

Podocyte-specific *Lmx1b* knock-out mice die from renal failure after around 14 days (Suleiman et al., 2007). Mice with global *Sm22* knock-out are healthy, fertile and show no overt abnormal phenotype (Kühbandner et al., 2000). To examine the effect of transgelin on the survival and proteinuria of *Lmx1b*-deficient mice, these mouse lines were crossed. As the probability of offspring of the desired genotype was low owing to three different transgenes, mice were bred in two different crossing schemes. Mice of both crossing schemes were of mixed C57BL/6 / 129/Sv genetic background.

The crossing schemes and frequencies of birth of the investigated genotypes are listed in Table 3.2. As the tail biopsies for genotyping were taken four days after birth, animals dying earlier were not included in statistics. As it was not possible to discriminate between hemizygous and homozygous *P2.5 Cre* mice by PCR genotyping, the expected probabilities are given as ranges. The birth rate of mice with both podocyte-specific *Lmx1b* knock-out and hetero- or homozygous *Sm22* knock-out were reduced, while the birth rate of *Lmx1b +/+, P2.5 Cre +, Sm22 -/-* mice was slightly increased. On the other hand, podocyte-specific *Lmx1b* knock-out mice had a birth rate similar to what was expected. The reason for the lower birth rate of double knock-out animals remained unclear.

Table 3.2: Frequencies of birth of mice with the denoted genotypes. Animals were obtained by two different crossing schemes, and a total of 367 mice in the upper and 130 mice in the lower case were genotyped 4 days after birth. Animal numbers are given in brackets.

Genotype	Expected offspring	Actual offspring
Lmx1b +/fl, P2.5 Cre +, Sm22 +/- x *Lmx1b +/fl, P2.5 Cre +, Sm22 -/-*		
Lmx1b +/+, P2.5 Cre +, Sm22 -/-	9.4 - 12.5%	14.2% (52)
Lmx1b fl/fl, P2.5 Cre +, Sm22-/-	9.4 - 12.5%	6.0% (22)
Lmx1b fl/fl, P2.5 Cre +, Sm22 +/-	9.4 - 12.5%	4.4% (16)
Lmx1b +/fl, P2.5 Cre +, Sm22 +/+ x *Lmx1b +/fl, P2.5 Cre +, Sm22 +/+*		
Lmx1b fl/fl, P2.5 Cre +, Sm22 +/+	18.8%	20.0% (26)

Nevertheless, Kaplan-Meier survival analysis (Figure 3.18, A) revealed a prolonged lifetime of a subset of double knock-out animals beyond 14 days. However, there was also one podocyte-specific *Lmx1b* knock-out mouse with comparable prolonged lifetime. The survival of *Lmx1b +/+, P2.5 Cre +, Sm22 +/-* mice was indistinguishable from podocyte-specific *Lmx1b* knock-out mice. Control *Sm22* knock-out mice showed no abnormal survival, at least within the observed time span of 17 weeks. Interestingly, most podocyte-specific *Lmx1b*-deficient mice died at around 14 days regardless of additional *Sm22* knock-out, but few mice survived longer. A possible explanation for this finding is the mixed genetic background, leading to birth of mice with different susceptibilities to renal damage caused by absent Lmx1b. But still, there was a higher degree of mice with a prolonged lifespan when *Sm22* was knocked-out. Unfortunately, there was no statistically significant influence of transgelin on the survival of podocyte-specific *Lmx1b* knock-out mice ($P = 0.189$, log-rank test) and also a direct comparison of the survival of double knock-out and podocyte-specific *Lmx1b* knock-out mice was not significant ($P = 0.105$, log-rank test).

Proteinuria was additionally determined for most animals (Figure 3.18, B). Urine samples were taken from mice at the age of 4, 10 and 21 days and 6, 13 and 17 weeks and analyzed by SDS-PAGE. As it was expected, *Sm22 -/-* mice had no proteinuria, including the two animals dying within the analyzed lifespan, hinting towards other causes of death apart from renal failure. All other animals, which could be analyzed for proteinuria at the last sample time point before death, had developed proteinuria. In general, mice which died at around 14 days showed proteinuria already at the age of 4 days, whereas mice with a prolonged lifespan had no proteinuria at that age. All podocyte-specific *Lmx1b* knock-out mice had developed proteinuria by 6 weeks, irrespective of additional *Sm22* knock-out.

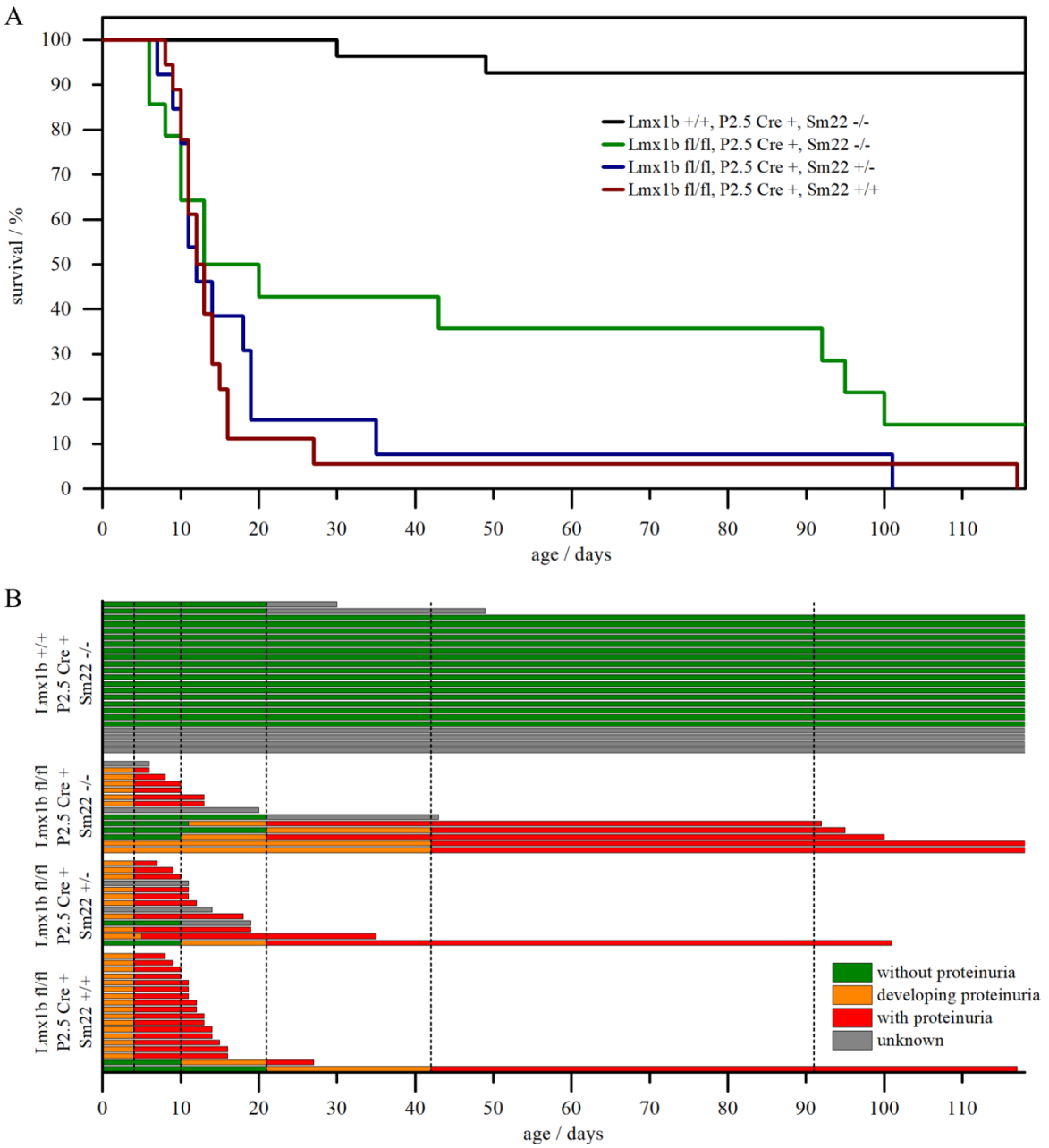

Figure 3.18: **Survival and onset of proteinuria of mixed C57BL/6 / 129/Sv mice with various combinations of podocyte-specific *Lmx1b* knock-out and global *Sm22* knock-out.** Mice were genotyped four days after birth, individuals dying earlier were excluded. A total of 27 *Lmx1b +/+, P2.5 Cre +, Sm22 -/-*, 14 *Lmx1b fl/fl, P2.5 Cre +, Sm22 -/-*, 13 *Lmx1b fl/fl, P2.5 Cre +, Sm22 +/-* and 18 *Lmx1b fl/fl, P2.5 Cre +, Sm22 +/+* mice were analyzed up to an age of 17 weeks. [A] Kaplan-Meier survival analysis. [B] Illustration of the survival and onset of proteinuria of each mouse. Proteinuria was determined by SDS-PAGE at the age of 4, 10, 21 days and 6, 13 and 17 weeks (dashed vertical lines). The lifetime until the last observation of no proteinuria is depicted in green and the lifetime after the first observations of proteinuria in red. The time span lying in-between is illustrated as orange, as proteinuria must have developed in this time frame. For some

mice it was not possible to obtain urine samples, and few mice died without any observation of proteinuria. Those times are depicted in gray, as proteinuria could potentially have developed before death.

In summary, a higher degree of double knock-out mice had a delayed onset of proteinuria and a prolonged lifespan compared to podocyte-specific *Lmx1b* knock-out mice, indicating that transgelin is one of multiple factors defining renal susceptibility to damage.

3.5.3. Investigation of *Lmx1b, Sm22* double knock-out mice 8 days postnatally

To further investigate the potential negative effect of *de novo* transgelin expression on podocyte health of *Lmx1b* knock-out mice, the kidneys of double knock-out mice and controls were perfusion fixed at the age of 8 days. Fixed kidneys were analyzed regarding kidney histology and ultrastructure in addition to immunofluorescence staining of selected proteins. As heterozygous *Sm22* inactivation had no effect on survival and proteinuria of podocyte-specific *Lmx1b* knock-out mice, those mice were excluded from further analyses.

Quantification of proteinuria, body weight and the density of filtration slits

Urine samples were taken and the weight was determined immediately prior to perfusion. The number of filtration slits per micrometer basement membrane was determined using electron micrographs of two glomeruli per mouse.

As expected, none of the 7 control mice (*Lmx1b* +/+, *P2.5 Cre* +, *Sm22* -/-) showed any sign of proteinuria, while all 6 podocyte-specific *Lmx1b* knock-out mice had developed proteinuria (Figure 3.19, A). Surprisingly, the protein to creatinine ratio of most double knock-out mice was increased compared to podocyte-specific *Lmx1b* knock-out animals. Nevertheless, one of the eight double knock-out mice showed no proteinuria 8 days after birth.

Consistent with those observations, the weight of some double knock-out mice was already markedly decreased, while the one without proteinuria (double-KO mouse 1) had a weight similar to controls (Figure 3.19, B). Again, the weight of podocyte-specific *Lmx1b* knock-out mice at the age of 8 days was still close to controls, indicating a milder phenotype.

Those observations were reflected on the subcellular level by the number of filtration slits per micrometer (Figure 3.19, C). Every gap between adjacent foot processes was counted as a filtration slit. The number of filtration slits was drastically reduced of both podocyte-specific *Lmx1b* knock-out and double knock-out animals, with the exception of the double-KO mouse 1.

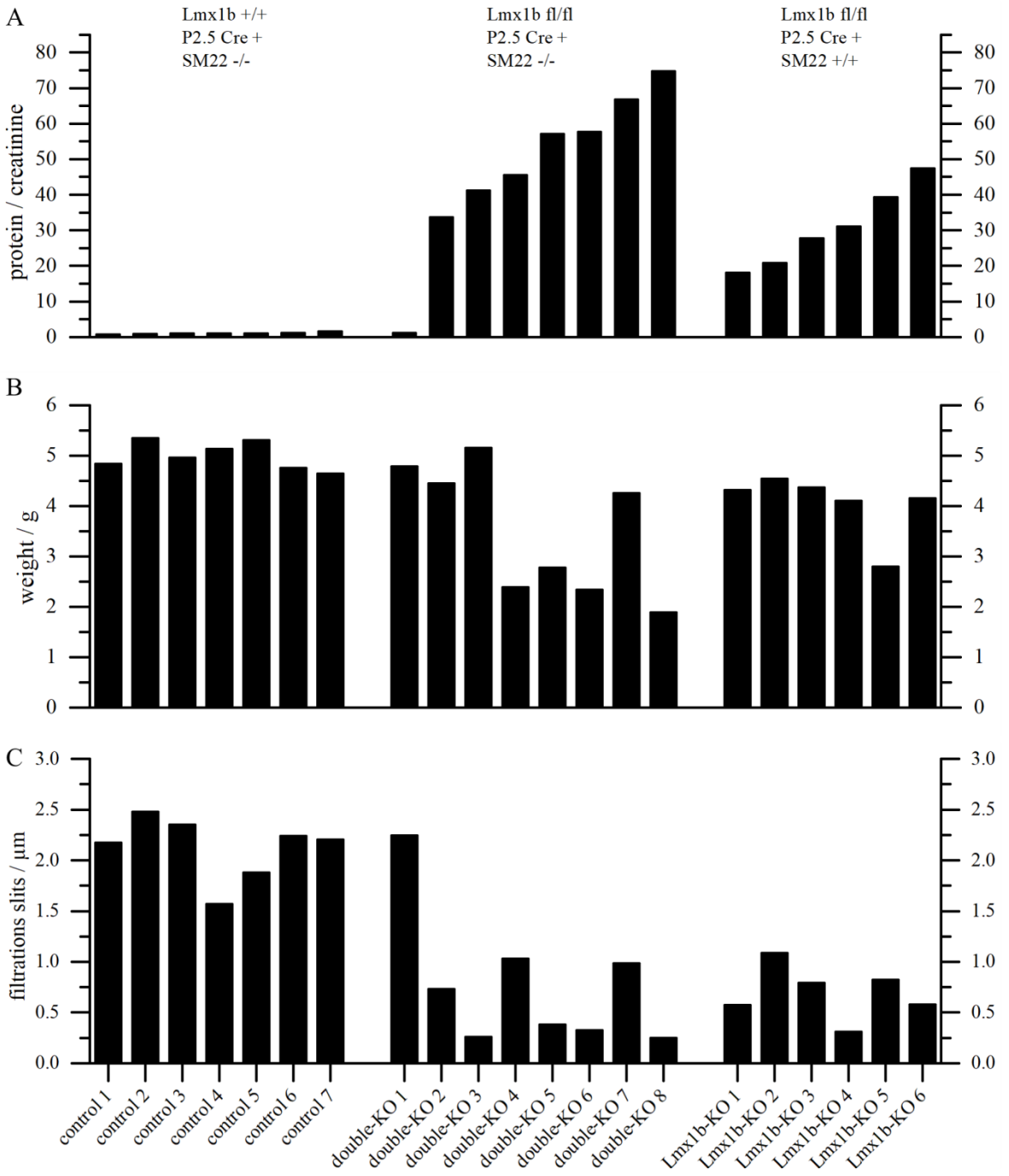

Figure 3.19: **Proteinuria, weight and filtration slits per micrometer basement membrane of 8-day old mice with combined podocyte-specific *Lmx1b* knock-out and global *Sm22* knock-out.** The values for individual animals are depicted, and every column represents one animal. [A] Urine protein to creatinine ratio determined by Bradford protein assay and Jaffe reaction. [B] Weight of individual mice at the time of perfusion. [C] Filtration slits per micrometer glomerular basement membrane. Slits were counted in electron micrographs of two glomeruli per mouse, and every gap between adjacent foot processes was counted as a filtration slit.

Glomerular expression of transgelin and podocin

To prove that transgelin is indeed absent in *Sm22* knock-out podocytes, paraffin embedded kidney sections were stained for transgelin and costained with podocin as a podocyte marker (Figure 3.20). Only juxtamedullary glomeruli were examined. Transgelin was solely expressed in the podocyte cell body of podocyte-specific *Lmx1b* knock-out mice without *Sm22* knock-out, confirming the successful deletion. Some remaining erythrocytes, visible as green spots, were located within the capillary loops central of the podocin stained foot processes.

Interestingly, the podocin expression in glomeruli of damaged kidneys was reduced, but still detectable. The pattern of podocin expression in healthy control glomeruli was a continuous line marking the foot processes at the exterior of the capillaries, while glomeruli, where only the shortened variant of Lmx1b was expressed, showed disruptions of this line. Staining of the kidney sections of the double-KO mouse 1 (Figure 3.20, C) revealed no alterations in the pattern of podocin expression.

Kidney histology

Kidney sections were investigated on the light microscopic level by hematoxylin / eosin staining of 6 µm thick paraffin sections (Figure 3.21). Kidneys of double knock-out animals, as well as podocyte-specific *Lmx1b* knock-out animals, appeared histological normal except for some tubular dilation and occasional eosinophilic casts within Bowman space and tubules (Figure 3.21, B and D). The eosinophilic casts were probably plasma proteins which were not adequately filtered by the glomerular filtration barrier and were therefore detectable in tubular segments and the urine. No overt abnormalities within glomeruli were detectable by light microscopy. The kidney of the double-KO mouse 1 was structurally normal without tubular dilations or protein casts (Figure 3.21, C).

Kidney ultrastructure

Kidney sections were further analyzed by electron microscopy to investigate glomerular ultrastructure and foot process effacement. Electron micrographs of control mice showed a regular glomerular filtration barrier with the fenestrated endothelium, the glomerular basement membrane and delicate foot processes (Figure 3.22, A). A broadening of foot processes in control animals was only rarely detectable. As expected, the double-KO mouse 1 showed no ultrastructural abnormalities (Figure 3.22, C). Podocyte-specific *Lmx1b* knock-out mice both with and without additional global *Sm22* deletion (Figure 3.22, B and D) showed markedly broadened foot processes accompanied by loss of filtration slits (quantified in Figure 3.19, C). In addition, kidneys of both genotypes frequently showed small segments of glomerular basement membrane splitting, with a bump always directing to the podocyte side.

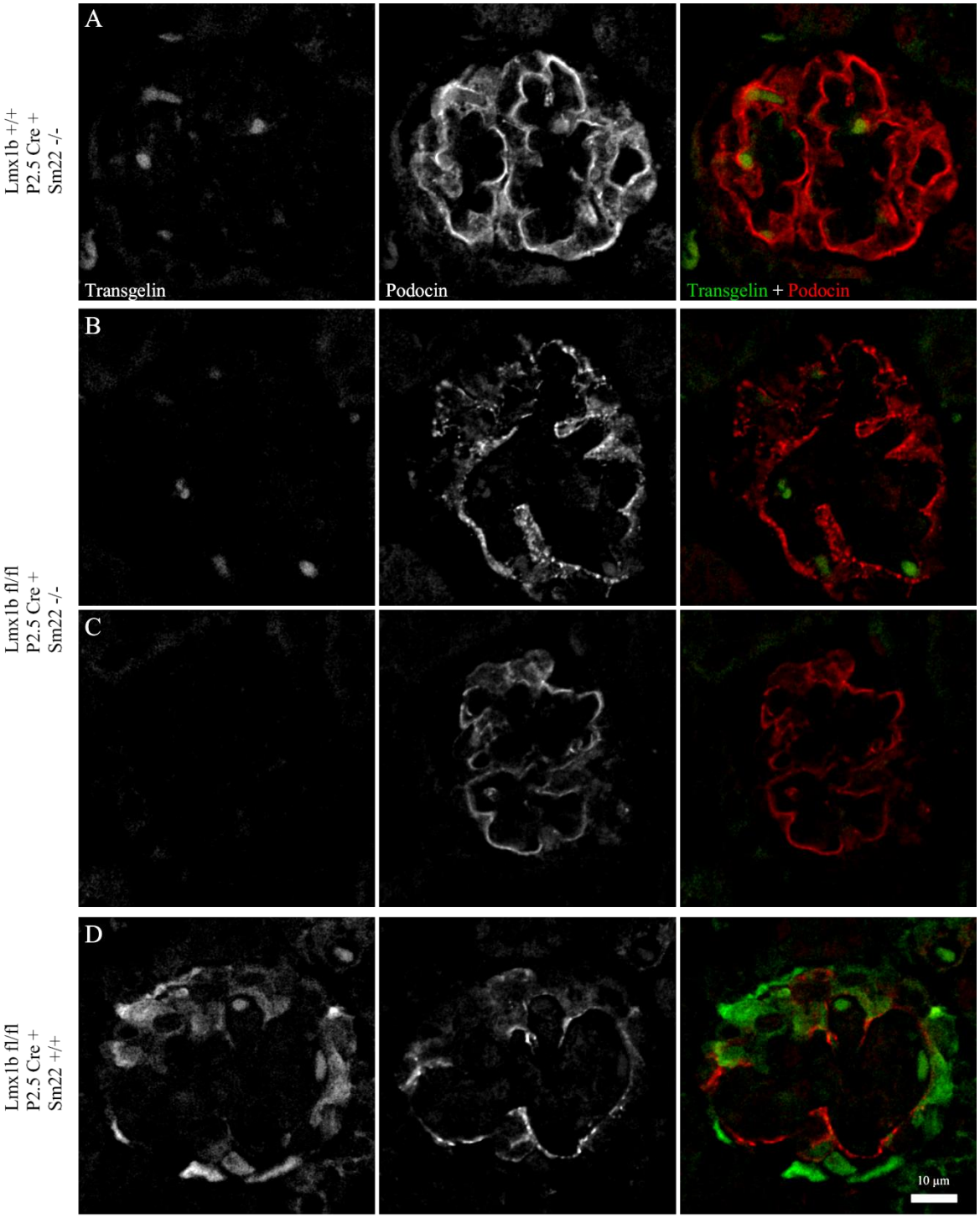

Figure 3.20: **Immunofluorescence staining against transgelin and podocin of paraffin-embedded kidney sections.** Mice were perfusion fixed 8 days postnatally and only juxtamedullary glomeruli were analyzed. Besides specific staining, the background fluorescence of some remaining erythrocytes was visible in the green channel. Shown are representative glomeruli of control animals [A], double knock-out animals with proteinuria [B], the double-KO mouse 1 [C] and podocyte-specific *Lmx1b* knock-out mice [D].

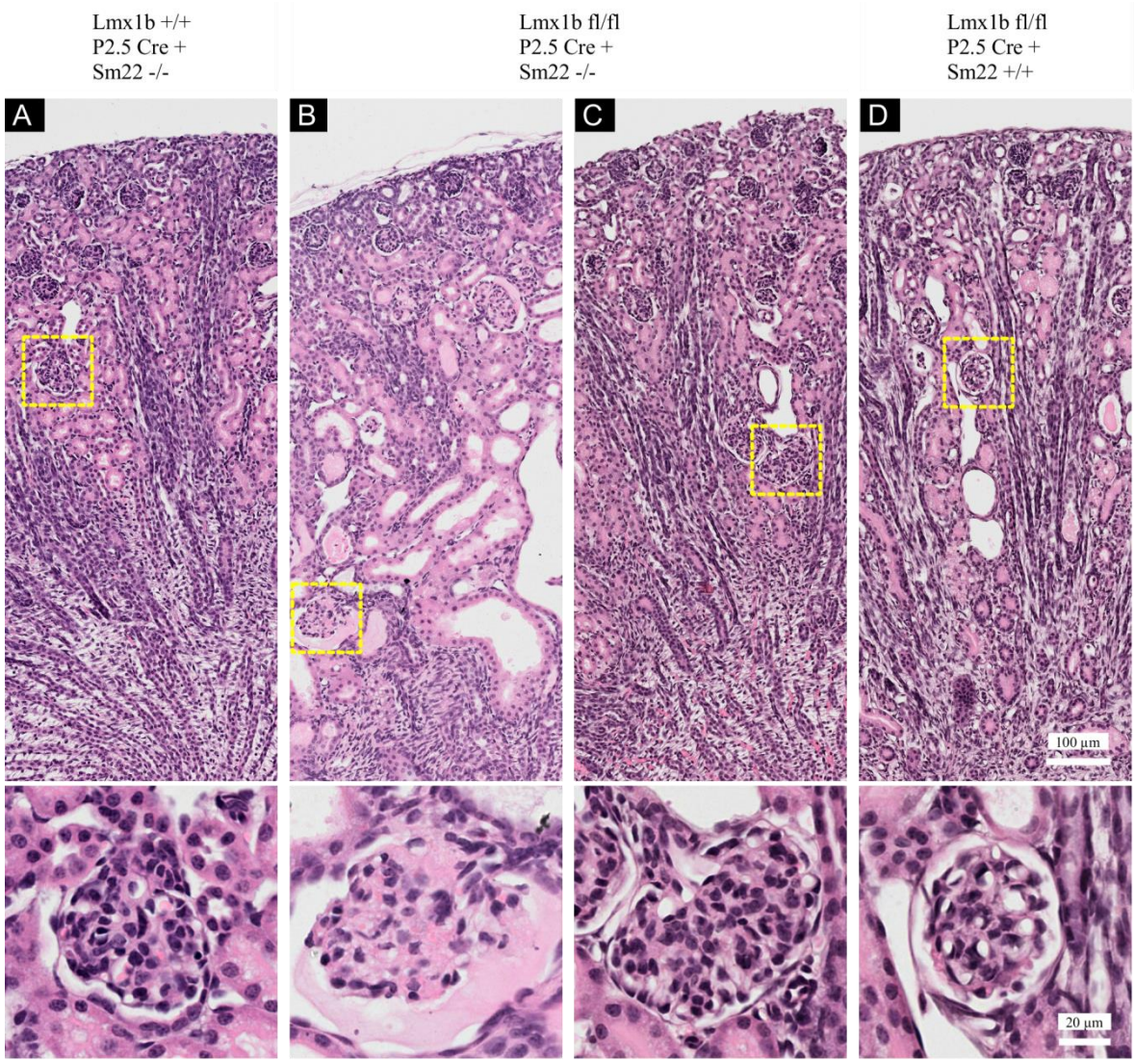

Figure 3.21: **Hematoxylin / eosin staining of 6 µm thick paraffin sections of kidneys from mice with combined podocyte-specific *Lmx1b* and global *Sm22* knock-out.** Boxes mark the magnified juxtamedullary glomeruli depicted in the bottom panel. Shown are representative pictures of control mice [A], double knock-out mice [B], the double-KO mouse 1 [C] and podocyte-specific *Lmx1b* knock-out mice [D].

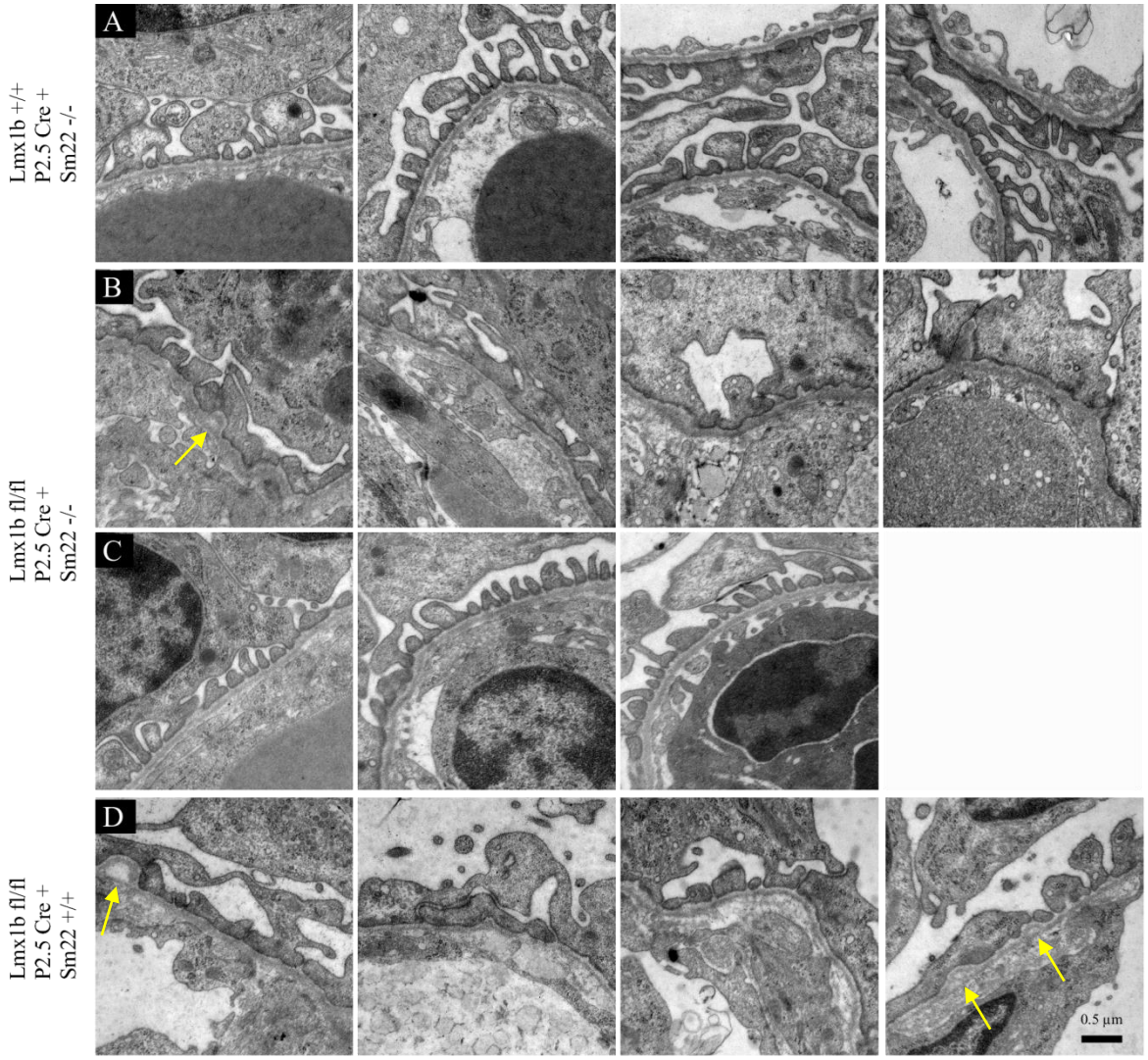

Figure 3.22: **Electron micrographs of the glomerular filtration barrier showing foot processes, the glomerular basement membrane and the fenestrated endothelium.** Shown are representative micrographs from global *Sm22* knock-out mice [A], podocyte-specific *Lmx1b* and global *Sm22* double knock-out mice [B], the double-KO mouse 1 which showed no renal abnormalities [C] and podocyte-specific *Lmx1b* knock-out mice [D]. Two animals per subgroup are depicted with 2 pictures each, except for C, which is only one animal. Arrows indicate sites of glomerular basement membrane splitting.

Structure and amount of filamentous actin within glomeruli

As transgelin binds and bundles actin filaments and also increases the F- to G-actin ratio (Han et al., 2009), structure and amount of F-actin were next investigated by phalloidin staining. On the light microscopic level no differences regarding the structure of actin was detectable (Figure 3.23, A – D). Strong staining aside from glomeruli was visible in the brush border of the proximal tubules. Quantification of the mean phalloidin intensity within glomeruli revealed no differences between the different genotypes (Figure 3.23, E), with the exception of one control animal.

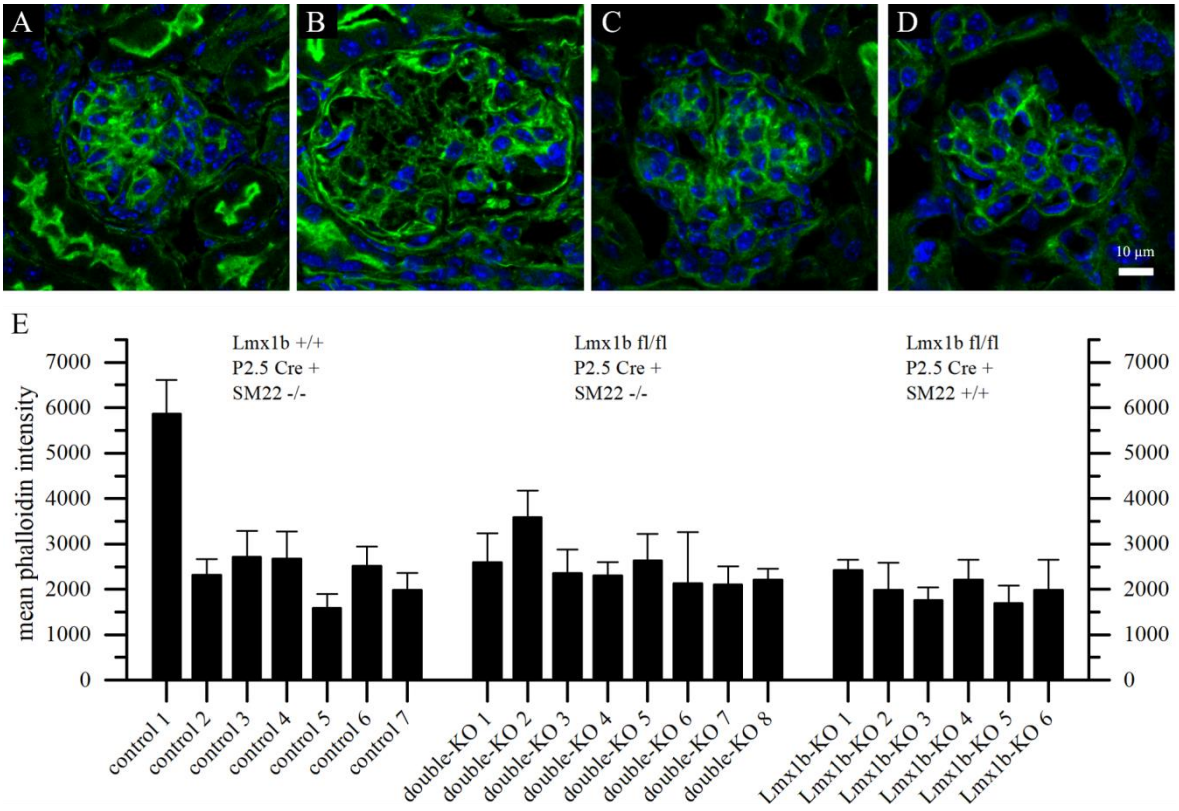

Figure 3.23: **Amount and structure of F-actin within glomeruli of 8-day old mice visualized by phalloidin staining of cryosections.** [A – D] From left to right: *Sm22* knock-out, podocyte-specific *Lmx1b* and *Sm22* knock-out, double-KO mouse 1 and podocyte-specific *Lmx1b* knock-out. [E] Quantification of the mean phalloidin intensity per glomerulus of 10 glomeruli per mouse. Values are means ± SD.

Taken together, no prominent differences of kidney physiology of most double knock-out mice compared to podocyte-specific *Lmx1b* knock-out mice were observed. Proteinuria and animal weight tended to be even a bit worse. But, on the other hand, there was one double knock-out animal which showed no sign of glomerular damage at all. The F-actin amount of whole glomeruli was not influenced by *Lmx1b* or *Sm22* knock-out.

4. Discussion

Nail-patella syndrome (NPS) is an autosomal-dominant hereditary disease, which incidence is frequently quoted as 1:50 000 (Bongers et al., 2002; Witzgall, 2017). The manifestation of the disease is heterogeneous, with skeletal, renal and ocular phenotypes. The renal phenotypes are most important for the prognosis of the patients. Around 40% of NPS patients suffer from renal symptoms (Witzgall, 2017), ranging from mild proteinuria and hematuria to end-stage renal disease (Sweeney et al., 2003). Mutations in a gene coding for the transcription factor LMX1B cause NPS (Dreyer et al., 1998; McIntosh et al., 1998; Vollrath et al., 1998).

Within the kidney, LMX1B is exclusively expressed in both developing and mature podocytes (Morello and Lee, 2002). In order to understand the molecular mechanisms and pathways leading from a mutated *LMX1B* gene to podocyte and renal dysfunction, three different *Lmx1b* knock-out mouse models were generated so far. Conventional *Lmx1b* knock-out mice died at the day of birth and exhibited a thickened glomerular basement membrane and reduced amounts of podocin, Cd2ap and the α3 and α4 chains of collagen IV (Chen et al., 1998; Miner et al., 2002; Morello et al., 2001). In contrast, there was no downregulation of those proteins in podocyte-specific *Lmx1b* knock-out mice, which died two weeks postnatally (Suleiman et al., 2007). In adult inducible podocyte-specific *Lmx1b* knock-out mice, the mRNA levels of Abra, Arl4c and Sm22 were upregulated. Binding of LMX1B to the promoter regions of *ABRA* and *ARL4C* was demonstrated, and Sm22 upregulation in murine glomeruli was also shown on the protein level. Moreover, first hints of a dysregulation of the actin cytoskeleton were evident in the same study (Burghardt et al., 2013). In the present study, further analyses of Lmx1b regulated genes, the actin cytoskeleton and actin regulatory pathways were conducted to establish a molecular linkage between LMX1B mutations and renal symptoms of NPS patients.

4.1. Investigation of Lmx1b and Lmx1b target gene expression on the protein level

As Lmx1b is a transcription factor, the identification of Lmx1b target genes is crucial for the discovery of the molecular pathways involved in renal dysfunction of NPS patients. Therefore, an inducible, podocyte-specific *Lmx1b* knock-out mouse line was used in a previous (Burghardt et al., 2013) and also in the present study (see chapter 1.8.2). In this mouse line *Lmx1b* knock-out is achieved by Cre/lox techniques, but although recombination of the floxed *Lmx1b* gene resulting in an in-frame deletion was already shown by PCR, it was so far unknown whether the homeodomain-lacking variant of Lmx1b is expressed on the protein level.

Abra, Arl4c and transgelin were previously identified to be upregulated on the transcriptional level in murine glomeruli following *Lmx1b* knock-out (Burghardt et al., 2013). Although binding of human LMX1B to FLAT elements upstream of *ABRA* and *ARL4C* could be shown (Burghardt et al., 2013), attempts to show an increased protein expression in murine podocytes via immunofluorescence staining failed (Stepanova, 2016). Hence, it was decided to investigate protein expression by western blotting using lysates from isolated and FACS sorted green fluorescent primary murine podocytes of quadruple transgenic mice (see chapter 3.1.2).

4.1.1. Validation of full-length Lmx1b deletion

The expression of endogenous Lmx1b protein (~42 kDA; see chapter 1.6) could be shown in wild-type and heterozygous, but not in homozygous *Lmx1b* knock-out podocytes (Figure 3.3), confirming the successful deletion of full-length *Lmx1b*. The quantification of a low amount of Lmx1b in knock-out podocytes might rather be a consequence of uneven background than remaining, full-length protein. This result additionally proves the reliability of the green fluorescence following *mTmG* recombination as a marker of *Lmx1b* recombination. The observed double band pattern of the Lmx1b protein might represent two different phosphorylation states. The unexpected detection of an increased amount of Lmx1b in *Lmx1b +/fl* compared to *Lmx1b +/+* podocytes might be explained by a negative feedback loop or a negative autoregulation of Lmx1b expression. Indeed, a cis-regulatory binding site of Lmx1b upstream of its gene was reported (Haro et al., 2017), although the authors argue for a positive autoregulation.

4.1.2. Expression of homeodomain-lacking Lmx1b

The homeodomain-lacking Lmx1b variant has a predicted molecular weight of ~29 kDa, and expression was indeed demonstrated in both *Lmx1b +/fl* and *Lmx1b fl/fl*, but not in

Lmx1b +/+ podocytes (Figure 3.3). This shows for the first time that the shortened variant lacking the homeodomain is still expressed. As there are no structural data, it is unclear whether the remaining domains of the shortened protein are correctly folded. Binding to DNA mediated by the homeodomain is certainly essential for Lmx1b to act as a transcription factor, but there might still be protein-protein interactions. Additionally, the C-terminal region of unknown function is also still present. This finding should be considered when comparing data of conventional *Lmx1b* knock-out mice with deletions of exons 3 - 7 (Chen et al., 1998) and transgene mice utilizing a the floxed Lmx1b construct with loxP sites flanking exons 4 – 6.

4.1.3. Potential regulation of Abra expression by Lmx1b

In case of the actin-regulating protein Abra (see chapter 1.7.1), a band with increased intensity in *Lmx1b* knock-out podocytes compared to wild-type podocytes was detected by the Abra antibody at around ~39 kDa (Figure 3.3). As the predicted molecular weight of Abra is slightly higher (~43 kDa) and the antibody produced also other unspecific bands, it is uncertain if the detected band represents Abra protein. Interestingly, the signal is increased following *Lmx1b* knock-out, which would be coincident with previous mRNA data. Abra was upregulated at the transcriptional level in glomeruli after *Lmx1b* knock-out, and binding of LMX1B to the promoter region could be shown (Burghardt et al., 2013). Additionally, Abra protein was detected in glomeruli by immunofluorescence staining of paraffin-embedded kidney sections of both *Lmx1b* +/+ and *Lmx1b fl/fl* mice, but the expression pattern of Abra in glomeruli did not resemble the typical podocyte pattern (Stepanova, 2016). With these data in mind there are two possibilities. Firstly, the detected bands correspond to Abra protein, and the expression of Abra in podocytes is repressively controlled by Lmx1b. Nevertheless, the resulting weak bands either indicate very low protein expression or low antibody affinity. Secondly, the detected bands do not represent Abra protein meaning that there is no Abra expression in podocytes but in other glomerular cells. Thus, upregulation of Abra expression could be a secondarily induced in endothelial or mesangial cells by an altered podocyte behavior, and *Abra* is not a target gene of Lmx1b.

4.1.4. Arl4c expression is regulated by Lmx1b

The small GTPase Arl4c (see chapter 1.7.2) could be confirmed as a target gene of Lmx1b (Figure 3.3). Expression of Arl4c in podocytes was not reported so far, but low expression in wild-type cells was detectable. Arl4c expression was 6-fold increased in *Lmx1b fl/fl* podocytes compared to *Lmx1b* +/+ podocytes. The observation of a slightly increased Arl4c expression in heterozygous knock-out podocytes isolated from mice without any renal phenotype further supports the theory of a direct regulation of *Arl4c* by Lmx1b. Binding of LMX1B to a FLAT element upstream of *ARL4C* was shown previously by ChIP

and gel shift experiments (Burghardt et al., 2013). In the case of Arl4c, Lmx1b acts as a transcriptional suppressor, which is in contrast to previous assumptions (Dreyer et al., 2000; Haro et al., 2017; Morello et al., 2001). Different modulating (activating or suppressing) mechanisms of Lmx1b can be explained by different cofactors and interaction partners. Indeed, a synergistic effect of the transcription factors Lmx1b and FoxC was reported to enhance *nphs2* promoter activity in zebrafish (He et al., 2014). On that basis, it is also imaginable that Lmx1b might inhibit other transcription factors by direct interaction or by blocking respective DNA-binding sites.

4.1.5. Transgelin is expressed in *Lmx1b* knock-out podocytes

Transgelin, an actin-binding protein mainly expressed in smooth muscle cells (see chapter 1.7.3), was not expressed in healthy *Lmx1b +/+* and *Lmx1b +/fl* podocytes, but a high expression was detected in *Lmx1b fl/fl* podocytes (Figure 3.3). Unlike Arl4c, transgelin expression is not increased in *Lmx1b +/fl* podocytes, hinting towards a secondary upregulation following podocyte damage. This observation is consistent with previous reports, which revealed high transgelin expression in human and rodent podocytes after glomerular damage (Marshall et al., 2011; Miao et al., 2009; Ogawa et al., 2007). Additionally, there is no FLAT element within 6 000 bp upstream of the *SM22* gene (Burghardt et al., 2013). Taken together, transgelin expression seems to be a general response of podocytes to damage, independently of Lmx1b. Transgelin expression is controlled by mechanical tension (Liu et al., 2017) and podocytes at the exterior of capillaries are constantly exposed to mechanical tension. Therefore, changes of the podocyte morphology (e.g. foot process effacement), the actin cytoskeleton or the focal adhesions may potentially trigger transgelin expression. Transgelin expression could also be more directly related to *Lmx1b* knock-out. The Lmx1b regulated protein Abra is reported to activate the transcription factor SRF via actin polymerization and translocation of MRTF-A to the nucleus (Figure 1.11) (Kuwahara et al., 2005), and SRF is reported to activate transgelin expression (Li et al., 1997). On the other hand, Abra expression in podocytes remains uncertain, and changes of the actin cytoskeleton independent of Abra may also activate this pathway (Mack et al., 2001). SRF is an important transcription factor for proper podocyte function and structure (Guo et al., 2018).

4.2. Dysregulation of the actin cytoskeleton of primary *Lmx1b*-deficient podocytes

An intact regulation of the actin cytoskeleton is important for podocyte structure and function (Perico et al., 2016). Mutations in genes coding for several proteins interacting with actin or regulating actin dynamics are known to cause pathological renal phenotypes (Schell and Huber, 2017). Evidence of a dysregulated actin cytoskeleton in primary, *Lmx1b*-deficient podocytes was previously reported (Burghardt et al., 2013). Knock-out glomerular cells had an increased F-actin content visualized by phalloidin staining, beads attached to the cell surface moved significantly slower and cells spread slower after removal of the toxin cytochalasin D from the culture medium. This finally led to the assumption of a stiffer and less dynamic actin cytoskeleton in *Lmx1b* knock-out podocytes (Burghardt et al., 2013).

This assumption was further investigated by several experiments with direct (F-actin staining) and indirect (shape and area of podocytes, random movement, cytochalasin D treatment) observation of the actin cytoskeleton. In comparison to the previous study (Burghardt et al., 2013), three experimental improvements were made described in the following. Firstly, the inducible, podocyte specific *Lmx1b* knock-out mouse line was crossed with the *mTmG* mouse line, allowing the exclusively investigation of podocytes with definite recombination and excision of the *Lmx1b* homeobox (see chapter 1.8.2). Secondly, all experiments were carried out with cells plated on laminin-521-coated substrates, which is a major glomerular basement membrane protein (Lennon et al., 2014a) and a ligand of the podocyte α3β1-integrin (Barczyk et al., 2010; Sterk et al., 1998). Finally, most experiments were carried out not only with steady state but also with spreading podocytes for a better understanding of the relevance of the findings in dynamic processes.

4.2.1. Dysregulations observed in untreated cells

Steady state as well as spreading *Lmx1b fl/fl* primary podocytes had a significantly higher mean phalloidin staining intensity compared to *Lmx1b* +/+ podocytes (Figure 3.4), as illustrated in Figure 4.1. This result does not only confirm previous findings with glomerular cells (Burghardt et al., 2013), it also shows that the dysregulation is already present in spreading podocytes 40 min after plating, making the finding relevant for dynamic cellular processes like cell spreading and migration. Nevertheless, the spreading of untreated podocytes within the first 60 min after plating on laminin-coated dishes is not affected by *Lmx1b* knock-out (Figure 3.6). This is in agreement with previous spreading experiments with glomerular cells plated on gold electrodes, where the spreading rate was analyzed by impedance sensing (Burghardt et al., 2013). Additionally, *Lmx1b* knock-out did not alter the mean velocity of random moving primary podocytes (Figure 3.5). Although the amount of F-actin is significantly increased in primary induced *Lmx1b fl/fl* podocytes, this does not affect the cell spreading rate and random movement. As the leading edge movement is controlled by many proteins and processes, the dysregulation of the actin cytoskeleton is possibly not the rate-limiting step.

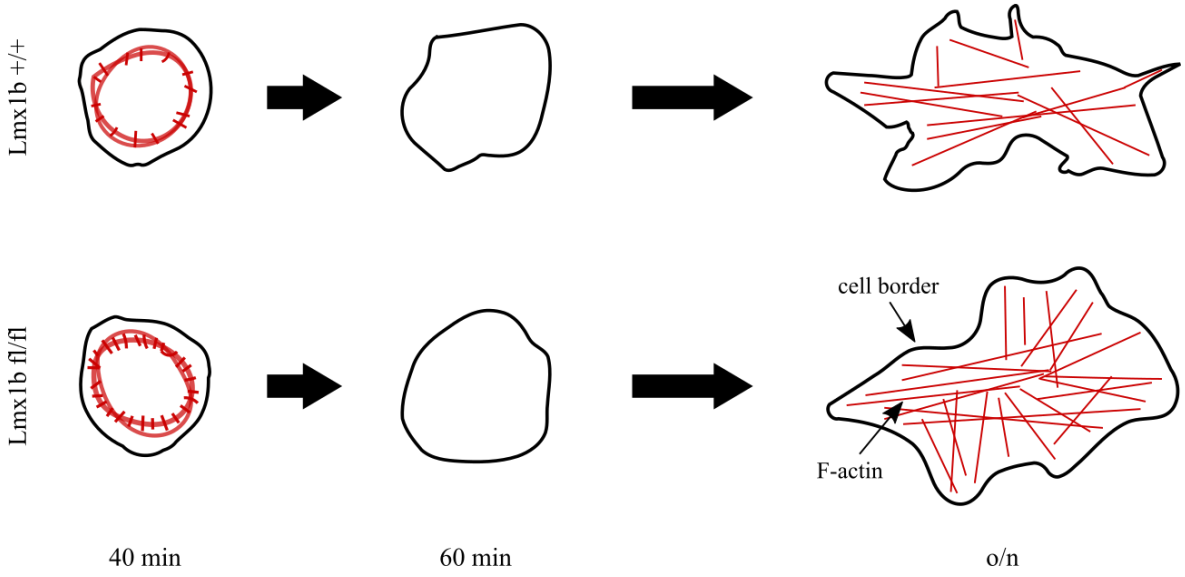

Figure 4.1: **Schematic view of adherent primary podocytes at different time points after plating on laminin-521-coated surfaces at a focal plane close to the growth surface.** The scheme illustrates the cell area which is increased only in steady state knock-out podocytes, the increased roundness and circularity of *Lmx1b* knock-out podocytes already 60 min after replating and the increased F-actin content of both *Lmx1b*-deficient spreading and steady state podocytes.

Even though the spreading rate was not affected, the cell area of adherent primary *Lmx1b* knock-out podocytes was highly significant increased after overnight growth (Figure 3.6), but not while spreading, also illustrated in Figure 4.1. As detached cells are round, a greater volume of cells would result in a greater cellular area right after attachment to the growth surface. The observation of identical cell areas early after plating argues for identical cell sizes. Moreover, primary podocytes, which were FACS sorted after 7 days of glomerular outgrowth, showed similar forward scatter (FSC) histograms independent of *Lmx1b* knock-out (data not shown). The forward scattered light is considered to be a measure of cell size (Herzenberg et al., 2002). This leads to the theory, that *Lmx1b fl/fl* knock-out does not affect the volume and spreading rate of untreated podocytes, whereas the endpoint of spreading is altered resulting in larger and flatter cells.

Aside from the cell area, two parameters describing the cell morphology were measured, circularity and roundness. The circularity is a good measure for small protrusions extending from the cell body. The roundness, on the other hand, is more robust to protrusions and is rather influenced by the shape of the cell body itself. As expected, both parameters had equally high values early after plating (Figure 3.7), as cells are nearly perfectly round soon after attachment. But already 60 min after plating *Lmx1b* knock-out podocytes had elevated values compared to wild-type podocytes, and this difference was even more evident after overnight growth (Figure 4.1). The morphological changes further hint towards a dysregulation of the actin cytoskeleton, as the cellular shape and structure are defined by the cytoskeleton (Fletcher and Mullins, 2010). Furthermore, differences in the cellular shape are already detectable in late spreading podocytes, indicating that podocyte spreading is more evenly distributed in knock-out podocytes, while the spreading rate of wild-type podocytes is locally different.

Summing up, the F-actin content, cell area, circularity, and roundness of murine primary podocytes were increased following on *Lmx1b* knock-out (Figure 4.1), whereas spreading and random movement are independent of Lmx1b. Since stress fiber, lamellipodia and filopodia formation are controlled by the Rho GTPases RhoA, Rac1 and Cdc42, respectively (Nobes and Hall, 1995; Ridley and Hall, 1992; Ridley et al., 1992), these results hint towards a dysregulation of those small GTPases.

4.2.2. Dysregulation observed in cytochalasin D treated cells

Treatment of primary podocytes with the toxin cytochalasin D resulted in cell shrinkage and accumulation of short F-actin bundles to spots near the nucleus and at the base of remaining cellular extensions (Figure 3.8). A multitude of small protrusions extended from the cell bodies, possibly because of remaining stable focal adhesions, which did not dissemble. The cytochalasin D induced shrinking rate was independent of *Lmx1b* knock-out

within two hours (Figure 3.9), and prolonged experiments indicated the same result for four hours (data not shown). The retraction of the cell membrane requires reorganization of the actin filaments (Cramer, 2013) and focal adhesion disassembly. This leads to the assumption that either depolymerization, severing and debranching of actin filaments is not influenced by *Lmx1b* knock-out, or another Lmx1b-independent step is rate-limiting.

However, the spreading of *Lmx1b* knock-out podocytes after wash-out of cytochalasin D was significantly slower compared to wild-type podocytes (Figure 3.9), again hinting towards a dysregulation of the actin cytoskeleton. This result is in contrast to what was observed in cell spreading after replating experiments (Figure 3.6). This discrepancy can be explained by different initial conditions, as the cell states at the beginning of the experiments differ substantially. Cytochalasin D treated cells are adherent and exhibit remaining focal adhesions, possibly even within the small cell protrusions, while detached cells are not adherent and void of focal adhesions. Furthermore, the actin cytoskeleton is differently organized. While F-actin is accumulated to dense spots in cytochalasin D treated cells (Figure 3.8), the F-actin in spreading podocytes early after plating is organized as a belt between the nucleus and the cell edge (Figure 3.16). Interestingly, two hours after wash-out of cytochalasin D the actin cytoskeleton still shows an unusual F-actin pattern (Figure 3.8), with spots of dense F-actin and stress fibers extending from them. It seems like the initial F-actin rich spots, which are a result of the cytochalasin D treatment (Wakatsuki et al., 2001), remain and serve as starting points for stress fiber formation. However, it is unknown to what extent this observation affects cell spreading, as branched filaments and not stress fibers are responsible for generating the pushing force (Pollard and Cooper, 2009). Nevertheless, the accumulation of F-actin might also influence the cellular distribution of the G-actin pool and associated proteins, and therefore affect actin nucleation and branching at the leading edges.

Taken together, there are several data demonstrating a dysregulation of the actin cytoskeleton in primary *Lmx1b*-deficient podocytes, but the exact nature of the dysregulation still remains unclear. The actin cytoskeleton is regulated by numerous different proteins fulfilling many different functions, like nucleation, branching, capping, severing, bundling, crosslinking and force generation (Figure 1.9) (Pollard, 2016). Each of the observed differences can be explained by dysregulation of more than one of these functions, for example spreading is dependent on nucleation and branching, but also on G-actin availability and actin turnover (Gardel et al., 2010). Therefore, the next aim was the identification of one or several dysregulated actin regulatory pathways causing these observations.

4.3. Influence of Lmx1b on actin-regulatory signaling pathways

For a better understanding of the nature of the dysregulation of actin cytoskeleton following the excision of the *Lmx1b* homeobox, different signaling pathways controlling the actin cytoskeleton were analyzed within this study. The master regulators of the actin cytoskeleton are the Rho GTPases (see chapter 1.5.4) (Steffen et al., 2017), controlling many important actin-dependent functions like cell morphology, polarization, migration and adhesion (Heasman and Ridley, 2008).

4.3.1. The activity of RhoA and Cdc42, but not Rac1, is influenced by Lmx1b

The activities of the best studied Rho GTPases RhoA, Rac1 and Cdc42 were analyzed using lysates of freshly isolated glomeruli. A significantly decreased amount of GTP-bound RhoA and Cdc42 was detected in *Lmx1b fl/fl* glomeruli, while the activity of Rac1 was at the same level (Figure 3.10). RhoA is known to induce F-actin polymerization and stress fiber formation, and a reduced activity would result in less phalloidin staining, which is in contrast to what was observed in podocytes (Figure 4.2). On the other hand, reduction of Cdc42 activity was more prominent. The role of Cdc42 in stress fiber formation is controversial. The Cdc42 effector protein family PAK induces MLC activation and stress fiber formation in neuronal cells, while it inactivates MLC and dissembles stress fibers in fibroblasts, endothelial and epithelial cells via a distinct pathway (Rane and Minden, 2014). Additionally, the myotonic dystrophy kinase-related Cdc42-binding kinases (MRCKs), another protein family activated by Cdc42, are also reported to induce stress fiber formation via MLC phosphorylation (Zhao and Manser, 2015). On this basis, it is hard to estimate if a reduced activity of Cdc42 could contribute to increased stress fiber formation in podocytes (Figure 4.2).

Active Cdc42 induces the generation of filopodia while depletion of Cdc42 abolishes filopodia generation (Nobes and Hall, 1995; Yang et al., 2006), and therefore the observed increased circularity and roundness of *Lmx1b fl/fl* podocytes may be a result of the reduced Cdc42 activity (Figure 4.2). Rho GTPases also impact cell spreading, more precisely, Rac1 and Cdc42 enhance cell spreading, while RhoA counteracts cell spreading (Arthur and Burridge, 2001; Price et al., 1998). The reduced spreading rate of *Lmx1b* knock-out podocytes after removal of cytochalasin D might thus also be a consequence of the reduced Cdc42 activity (Figure 4.2). Moreover, podocyte-specific knock-out studies in mice revealed that RhoA and Rac1 are dispensable for a proper function, while *Cdc42* knock-out resulted in severe proteinuria, foot process effacement and death (Blattner et al., 2013; Scott et al., 2012). This further underlines the relevance of the finding of reduced Cdc42 activity.

The Lmx1b target gene *Arl4c* encodes for a small GTPase, which was reported to act upstream of Rho GTPases (see chapter 1.7.2). In IEC-6 cells, Arl4c overexpression increased epidermal growth factor (EGF) induced activation of Rac1, while RhoA activity was decreased. Moreover, depletion of Arl4c by siRNA abolished EGF induced Rac1 activation and partly rescued RhoA activation (Matsumoto et al., 2014). In contrast, in a more recent study, it was shown that Arl4c interacts with filamin-A (FLNa) and activates Cdc42 and not Rac1 in HeLa cells (Chiang et al., 2017). The impact of Arl4c on Rho GTPase activity might be dependent on the cell type and in case of EGF treatment on additional, synergistically or antagonistically activated pathways. None of the studies examined the effect of constitutively active Arl4c on the activity of Rho GTPases. Therefore, the effect of Arl4c on Rho GTPases remains unclear in primary podocytes, and moreover it is unknown how the increased Arl4c expression in *Lmx1b*-deficient podocytes impacts Arl4c signaling, as downstream signaling pathways are dependent on Arl4c GTPase activation (Figure 4.2).

Abra was also reported to influence GTPase activities (see chapter 1.7.1). Abra and RhoA synergistically induced actin polymerization and SRF activation, and inhibition of RhoA blocked Abra induced SRF activation. For that reason, it was assumed that Abra acts upstream of RhoA (Arai et al., 2002). Nevertheless, the precise mechanism remains unclear. RhoA activation by Abra does not seem to play an important role in primary *Lmx1b* knock-out podocytes, as RhoA activity was decreased in glomeruli, although Abra protein expression is possibly increased (see chapter 4.1.3).

4.3.2. Increased MLC activity in *Lmx1b*-deficient hPCL

Myosin-2 is an actin-binding motor protein and together with actin a main constituent of stress fibers (see chapter 1.5.3). The increased phalloidin staining of *Lmx1b*-deficient podocytes pointed towards a higher amount of stress fibers compared to controls. The activity of myosin-2 is controlled by phosphorylation of its subunit MLC (Umemoto et al., 1989), and phosphorylation is controlled by a variety of kinases and phosphatases, many of them acting downstream of Rho GTPases (Newell-Litwa et al., 2015).

There is a clear tendency of decreased phosphorylation of MLC in both proliferating and differentiated, spreading hPCL cells when *de novo* Lmx1b expression was induced (Figure 3.11), although the data are only preliminary as the experiment was only done once. This result indicates that Lmx1b reduces MLC phosphorylation, and *vice versa Lmx1b* knock-out in podocytes leads to increased phosphorylation of MLC and therefore, to an increased amount of stress fibers, which is consistent with the observation of increased phalloidin staining (Figure 4.2).

4.3.3. LIMK, but not ROCK, is part of a dysregulated pathway

As the spreading of *Lmx1b* knock-out primary podocytes after the removal of cytochalasin D was decreased (Figure 3.9), this experiment was suitable to investigate different actin-dependent pathways. Cell spreading was analyzed in the presence of an inhibitor, and in case the inhibitor blocked the major pathway dysregulated by *Lmx1b* knock-out, the difference in the spreading was expected to be abolished. Following the assumption of a stiffer and less dynamic actin cytoskeleton in *Lmx1b* knock-out podocytes (Burghardt et al., 2013), a well-studied pathway controlling cofilin activity was investigated (Figure 1.10). Cofilin is an actin severing-protein and important for actin turnover and treadmilling (Kiuchi et al., 2007), and therefore is crucial for actin dynamics (see chapter 1.5.3). Cofilin is inactivated by phosphorylation via LIMK (Arber et al., 1998; Yang et al., 1998), and LIMK is activated by ROCK (Maekawa et al., 1999).

In the presence of LIMKi 3, a specific inhibitor of LIMK1 and LIMK2, the spreading curves of knock-out and wild-type podocytes were reproducible at the same level (Figure 3.13), arguing for a dysregulation of LIMK1/2 following *Lmx1b* knock-out. On the contrary, the specific ROCK1/2 inhibitor Y-27632 did not abolish the difference in the spreading rate. LIMK is not only phosphorylated and thereby activated by ROCK, but also by PAK (Edwards et al., 1999). While ROCK, in turn, is activated by RhoA (Nakagawa et al., 1996), PAK is an effector of Rac1 and Cdc42 (Edwards et al., 1999). Taken together, these results argue for a dysregulation of LIMK via PAK and not ROCK, indicating that Cdc42 rather than RhoA plays an important role in downstream signaling of Lmx1b and its target genes (Figure 4.2).

Moreover, inhibition of LIMK, resulting in decreased phosphorylation of cofilin and thereby increased activity, reduced the spreading of wild-type podocytes compared to DMSO treated cells, albeit not significantly due to a limited number of experiments (Figure 3.13). This was unexpected, as actin turnover by cofilin is important for replenishing the G-actin pool and therefore, spreading (Pollard and Borisy, 2003). This finding also contradicts the assumption that the reduced spreading of *Lmx1b* knock-out podocytes is a result of decreased actin cytoskeleton dynamics in podocytes, as this assumption implies that increased actin turnover leads to increased spreading.

4.3.4. Signaling relations of investigated proteins

The observed dysregulations following the inactivation of *Lmx1b* in mature podocytes are summarized in Figure 4.2 and are put into context of known signaling pathways. Green lines mark relationships that are consistent with the presented data, while red lines depict relations that are not coincident with observations made. Gray lines link observations where contrary or unspecified signaling connections were reported in the literature.

Nearly all actin-related dysregulations found in this thesis can be explained by the reduced Cdc42 activity in *Lmx1b* knock-out podocytes, but not by decreased RhoA activity. Moreover, podocyte-specific *Cdc42* null mice suffer from renal defects, while podocyte-specific *RhoA*-deficient mice are healthy (Scott et al., 2012), underlining the importance of this finding. The reduced activity of RhoA may potentially be a response of the cell to counteract the reduction of Cdc42 activity, as both GTPases have often contrary effects on the actin cytoskeleton. But still, it has to be considered that GTPase activity data accord to glomeruli with potential side effects of endothelial and mesangial cells, as FACS sorting was not an option as the enzymatic detachment and sorting procedure would impact GTPase activity. There is a recent report of re-differentiation of primary outgrown podocytes back to a more physiological state under specific conditions (Yaoita et al., 2018). This opens up the possibility of FACS sorting primary outgrown podocytes with subsequent re-differentiation and GTPase analysis.

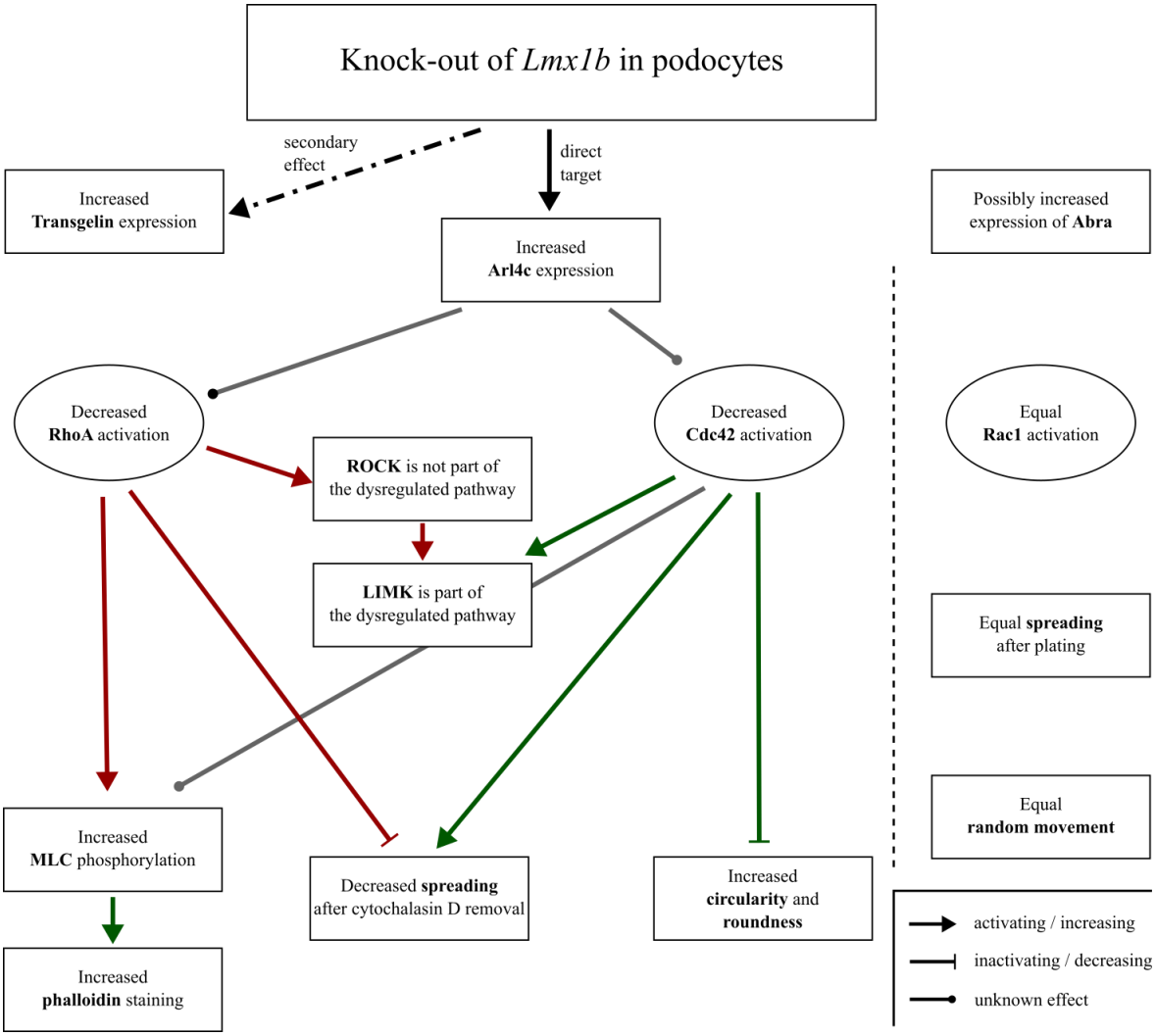

Figure 4.2: **Schematic overview of the observations made regarding the condition of the actin cytoskeleton and its regulation.** These observations are put into context of known signaling pathways, ranging from Lmx1b target genes to the actin cytoskeleton. Green lines show relationships, where the data are in agreement with reported signaling pathways. Red lines depict, on the other hand, relationships where the data cannot be explained by reported signaling pathways, and grey lines mark existing relations of unknown nature. Transgelin, Arl4c and possibly Abra are upregulated after *Lmx1b* knock-out in podocytes. Arl4c, in turn, is reported to influence the GTPases RhoA, Rac1 and Cdc42, but reports are contrary. The activity of the Rho GTPases RhoA and Cdc42, which are key regulators of the actin cytoskeleton, was found to be decreased in glomerular *Lmx1b* knock-out lysates. According to the literature, decreased RhoA activity should lead to decreased MLC phosphorylation, stress fiber formation and spreading (after cytochalasin D wash-out), but the opposite was observed. Moreover, ROCK, a direct effector of RhoA, does not seem to be dysregulated in knock-out cells. Decreased Cdc42 activity, on the other hand, can readily explain the decreased spreading and the increased circularity and roundness of podocytes. Additionally, the dysregulation of LIMK can be explained by decreased Cdc42 activity. Reports of the impact of Cdc42 on the phosphorylation of MLC are contrary.

4.4. Influence of Lmx1b on focal adhesions

Focal adhesions are aggregates of a multitude of proteins anchoring cells and the actin cytoskeleton to the extracellular matrix (see chapter 1.4.3). The most important proteins of focal adhesions are the integrin family of heterodimeric transmembrane proteins. Proper adhesion of podocytes is essential for regular blood filtration at the glomerular filtration barrier (Pozzi et al., 2008; Sachs et al., 2006). A loss of adhesion strength potentially results in podocyte detachment and loss, as the cell body itself is floating in the primary urine (Kriz et al., 2013). Focal adhesions are tightly connected with the actin cytoskeleton (Faul et al., 2007). Moreover, glomerular cells isolated from *Lmx1b* knock-out mice adhered stronger to laminin-111 (Burghardt et al., 2013), and the turnover of α-acintin-1 and actin was reduced at focal adhesions measured by FRAP (Stepanova, 2016). This made focal adhesions to an interesting target of investigation within the present work. The α3β1-integrin is the highest abundant and most important integrin in podocytes (Sachs and Sonnenberg, 2013; Sterk et al., 1998) and a selective laminin receptor (Nishiuchi et al., 2003). For this reason, the activity of integrin was analyzed with the help of the 9EG7 antibody selective for active β1-integrin (Lenter et al., 1993).

Immunofluorescence staining of adherent spreading and steady state primary podocytes visualized by confocal microscopy revealed no difference in the amount of active β1-integrin compared to control (Figure 3.14). Additionally, there was no abnormal pattern of focal adhesion localization. This is coincident with the observation of equal focal adhesion to cell area ratios visualized by paxillin staining (Burghardt et al., 2013).

The integrin activity was further analyzed by flow cytometry with increased cell numbers, and a slight increase in β1-integrin activation of *Lmx1b*-deficient cells was identified (Figure 3.15). The amount of total β1-integrin remained unchanged, further arguing for a constant amount and structure of focal adhesions. The slightly increased activity in knock-out cells is consistent with the previously reported increased adhesion to laminin-111 (Burghardt et al., 2013). A part of the podocytes did not show recombination of *Lmx1b* despite doxycycline treatment. Those and other glomerular cells exhibited β1-integrin activity independent of doxycycline-induced renal damage (Figure 3.15). This leads to the assumption that rather intracellular signaling pathways following *Lmx1b* knock-out cause increased β1-integrin activity than extracellular stimuli like an altered extracellular matrix composition or structure.

Taken together, a slightly increased activation of β1-integrin could be detected in *Lmx1b*-deficient podocytes, probably resulting in increased adhesion, while the amount and localization of focal adhesions remained unchanged. Actin is regulated downstream of integrin (Lawson and Burridge, 2014), but may also indirectly influence integrin activity via mechanical tension (Friedland et al., 2009).

4.5. Effect of *Sm22* deletion on *Lmx1b* knock-out podocytes and mice

Transgelin, encoded by the gene *Sm22*, is highly expressed in *Lmx1b*-deficient podocytes, but not in wild-type control cells (Figure 3.3). Although it is unlikely that *Sm22* is directly regulated by Lmx1b (see chapter 4.1.5), transgelin remained an interesting target of investigation as it associates with the actin cytoskeleton (Han et al., 2009) and may have a negative effect on the progression of renal symptoms (Marshall et al., 2011). For these reasons the localization of transgelin in primary outgrown podocytes was initially analyzed.

4.5.1. Transgelin colocalizes with actin in steady state podocytes

Surprisingly, transgelin was not only expressed in *Lmx1b* knock-out podocytes but also in wild-type controls, although to a lower extent (Figure 3.17). On the other hand it is known that outgrown podocytes do not assemble foot processes or slit diaphragms, and moreover lose expression of diverse podocyte-specific proteins, including Lmx1b (unpublished data). Therefore, *de novo* transgelin expression in outgrown podocytes may have various reasons, including Lmx1b depletion upon dedifferentiation or altered mechanical tension (Liu et al., 2017). Transgelin colocalized with actin in steady state podocytes at stress fibers and at the cell cortex (Figure 3.16). A strong association with actin stress fibers was previously reported (Shapland et al., 1993). Interestingly, there was no colocalization with actin in spreading podocytes, indicating that the increased amount of actin fibers (Figure 3.4) in spreading podocytes does not result from the actin bundling activity of transgelin.

Taken together, the significantly increased amount of transgelin and its localization to the actin cytoskeleton in steady state podocytes raises the possibility of an involvement of transgelin in actin dysregulation of *Lmx1b*-deficient podocytes, although its localization in spreading podocytes questions such an involvement in dynamic processes.

4.5.2. Survival and proteinuria of *Sm22* / *Lmx1b* double knock-out mice

To further elucidate the effect of transgelin on the progression of renal symptoms of NPS patients, a mouse line with podocyte-specific *Lmx1b* knock-out as well as global *Sm22* knock-out was created. As the podocyte-specific knock-out of *Lmx1b* in mice leads to early death at the age of two weeks (Suleiman et al., 2007), while deletion of *Sm22* results in no abnormal phenotype (Kühbandner et al., 2000), those double knock-out mice were firstly analyzed in terms of survival and proteinuria.

Consistent with previous reports, *Sm22*-deficient mice were phenotypically normal, while most *P2.5 Cre +, Lmx1b fl/fl* control mice developed proteinuria early in life and died at around two weeks (Figure 3.18). Interestingly, there was the exception of two podocyte-specific *Lmx1b* knock-out mice which showed no proteinuria 4 days postnatally, resulting in a prolonged lifetime. Similar observations were made when *Sm22* was additionally deleted. There was one population of mice with early onset of proteinuria and death, while the onset of proteinuria and death was delayed in another population. This high variance within experimental groups indicates that the prolonged lifetime is caused by additional genetic variances. Indeed, mice were of mixed C57BL/6 / 129/Sv genetic background, and influence of the genetic background on the severity of renal damage is reported in the literature (Lu et al., 2012; Sasaki et al., 2015). Nevertheless, there was a markedly increased percentage of double knock-out mice with prolonged survival compared to podocyte-specific *Lmx1b* knock-out mice.

4.5.3. Effect of *Sm22* deletion on *Lmx1b* knock-out kidney physiology

As additional *Sm22* knock-out led to an increased percentage of mice with prolonged lifetime (see chapter 4.5.2) and *Sm22* was identified to be detrimental in a model of crescentic glomerulonephritis (Marshall et al., 2011), *Sm22* / *Lmx1b* double knock-out mice were further investigated regarding proteinuria, body weight, kidney histology and ultrastructure at the age of 8-days.

At first, the expression of transgelin in podocyte-specific *Lmx1b* knock-out podocytes was confirmed (Figure 3.20), which was abolished by additional *Sm22* knock-out (Kühbandner et al., 2000). Interestingly, the expression pattern of podocin in both *Lmx1b*-deficient and double knock-out podocytes was altered compared to *Sm22 -/-* controls 8 days postnatally (Figure 3.20). This is in contrast to a previous report of comparable podocin expression 11 days postnatally (Suleiman et al., 2007), but may result from different genetic backgrounds, as the previous study used C57BL/6 mice.

Again, there was a great discrepancy of renal function within the *Lmx1b* and *Sm22* double knock-out group, but this time not in the podocyte-specific *Lmx1b* knock-out group (Figure 3.19). Except of one animal, all other double knock-out and *Lmx1b* knock-out mice exhibited strong proteinuria. This is consistent with the initial experiment, where also less podocyte-specific *Lmx1b* knock-out mice showed the phenomenon of delayed onset of proteinuria (Figure 3.18). The proteinuria of mice with combined *Sm22* and podocyte-specific *Lmx1b* knock-out tended to be stronger, while the body weight of some individuals was reduced compared to podocyte-specific *Lmx1b* knock-out animals (Figure 3.19).

No differences regarding the histology could be demonstrated, as dilated tubules and eosinophilic casts were present to comparable amounts in both genotypes (Figure 3.21). Electron microscopy led to the identification of GBM splitting found in both genotypes (Figure 3.22), which is characteristic for Alport syndrome (see chapter 1.4.2). Alport syndrome is caused by mutations of either α3, α4 or α5 chains of collagen type IV (Miner, 2012), but the observed splitting is not limited to this disease (Craver et al., 2014). Furthermore, the density of filtration slits was drastically reduced in animals exhibiting proteinuria, but again no difference between animals with or without additional Sm22 knock-out was detected (Figure 3.19).

Phalloidin staining of frozen kidney sections revealed similar mean glomerular phalloidin intensities (Figure 3.23), but potential differences within podocytes might be masked by other glomerular cells.

Taken together, the additional knock-out of *Sm22* tended to worsen the disease progression in terms of proteinuria and body weight within the population of mice with early onset of proteinuria. This is at first glance in conflict with a previous report (Marshall et al., 2011). But although Marshall et al. reported detrimental effects of transgelin in a model of crescentic glomerulonephritis, the proteinuria of *Sm22 -/-* mice was also significantly increased early after disease induction, arguing for a beneficial effect of transgelin on the actin cytoskeleton of podocytes. In the later progression of the disease, transgelin had detrimental effects possibly via impairment of proliferation pathways (Marshall et al., 2011). This leads to the hypothesis that transgelin is beneficial for individual podocytes via its action on the actin cytoskeleton at an early stage, but has also detrimental effects on proliferation and repopulation of the glomerular basement membrane at a later stage.

5. Summary

Mutations of *LMX1B* lead to the hereditary disease NPS, which is associated with renal symptoms (Witzgall, 2017). Within the kidney, the transcription factor LMX1B is exclusively expressed in podocytes and plays an essential role in the maturation and maintenance of the cell. Previous studies revealed not only the putative Lmx1b target genes *Abra*, *Arl4c* and *Sm22*, but also evidence of an impact of Lmx1b on the regulation of the podocyte actin cytoskeleton and focal adhesions (Burghardt et al., 2013; Stepanova, 2016). Therefore, the main purpose of the present work was to identify and investigate pathways linking Lmx1b and its target genes to the actin cytoskeleton and focal adhesions and to clarify the nature of actin and focal adhesion dysregulation in disease.

By the use of an inducible podocyte-specific *Lmx1b* knock-out mouse line with an *mTmG* reporter construct, knock-out of *Lmx1b* could be induced at a desired time point in podocytes of mature mice, and those podocytes could be separated from other glomerular cells. Analysis of the protein expression in podocytes by western blotting confirmed an increased expression of Arl4c and transgelin following *Lmx1b* knock-out. While *Arl4c* is most likely a direct target of Lmx1b, transgelin expression seems to be a general response to podocyte damage (Marshall et al., 2011). The expression of Abra in wild-type or knock-out podocytes could not be confirmed free of doubt.

Primary murine podocytes were used to clarify the impact of Lmx1b on the actin cytoskeleton. To better resemble the physiological conditions, cells were plated on laminin-521 in all of those experiments. As some effects of *Lmx1b* knock-out might only be visible during cell stress and not in the steady state, many experiments were performed with both spreading and also full-grown, steady state podocytes.

The knock-out of *Lmx1b* led to an increased F-actin staining in both spreading and steady state podocytes. Moreover, the circularity and roundness in the late phase of spreading and also at steady state were increased. The cell area of spreading podocytes and also the cell size measured by forward light scatter in FACS experiments was independent of *Lmx1b* knock-out, but the cell area of *Lmx1b*-deficient steady state podocytes was markedly increased. Thus, primary *Lmx1b* knock-out podocytes are flatter and rounder and contain more actin fibers.

Untreated podocytes revealed similar random movement velocities and spreading rates independent of Lmx1b expression. Treatment of podocytes with cytochalasin D induced cell shrinkage at similar rates and accumulation of short actin fibers at spots near the nucleus and at the base of small cell extensions. Removal of cytochalasin D, in turn, led to

cell spreading, which was reduced in the absence of Lmx1b. The cytoskeleton remained atypically organized two hours after wash-out of cytochalasin D in knock-out cells as well as wild-type controls. The different observations of cell spreading with or without prior cytochalasin D treatment can be explained by different initial states of the actin cytoskeleton and focal adhesions at the beginning of the experiment. Thus, only some actin-dependent dynamic processes are influenced by Lmx1b and its target genes.

As the impact of Lmx1b on the actin cytoskeleton was obvious, one of the main goals was to identify the signaling pathways involved. Therefore, two different strategies were carried out. One possibility was to examine the activities of proteins involved in signaling cascades. This was achieved either by specific binding of activated proteins to effectors or by analyzing the amount of phosphorylation utilizing specific antibodies. The other possibility was the investigation of the podocyte spreading after the removal of cytochalasin D in the presence of inhibitors blocking specific signaling proteins. In case the inhibitor would block a dysregulated protein, the spreading curves of knock-out and wild-type podocytes were expected to converge.

The Rho GTPases are key actin regulators (Sadok and Marshall, 2014) and therefore, were subject of investigation. The activity of RhoA and Cdc42 was significantly reduced in glomerular lysates of podocyte-specific *Lmx1b* knock-out mice, while the activity of Rac1 was equal to controls. Additionally, the phosphorylation of the myosin light chain and thereby activation of myosin-2 was decreased after *de novo* expression of LMX1B in a human podocyte cell line (hPCL). By the use of inhibitors in spreading experiments, LIMK but not ROCK could be identified to be dysregulated in primary murine *Lmx1b* knock-out podocytes. Many of the actin cytoskeleton related dysregulations of podocytes can be explained by the reduced activity of Cdc42, but not RhoA, including increased circularity and roundness, decreased spreading after removal of cytochalasin D and the dysregulation of LIMK. Nevertheless, further investigation of the Cdc42 pathway is required to prove this connection.

As *Lmx1b* knock-out podocytes revealed increased adhesion to laminin-111 (Burghardt et al., 2013), the potential role of focal adhesions downstream of Lmx1b was investigated. Moreover, outside-in signaling at focal adhesions impacts the actin cytoskeleton. Focal adhesions are accumulations of a multitude of proteins, which anchor cells to the extracellular matrix and establish a mechanical as well as a signaling link to the actin cytoskeleton. Transmembrane integrins are the most important proteins within focal adhesions, and $\alpha 3\beta 1$-integrin is the most abundant integrin in podocytes (Sachs and Sonnenberg, 2013).

Staining with an antibody specific for active β1-integrin revealed no differences between *Lmx1b* knock-out and wild-type control podocytes by confocal microscopy. On the other hand, a slightly increased activation of β1-integrin in knock-out podocytes was detectable by flow cytometry. The amount of total β1-integrin in podocytes and also the activity of β1-integrin in other glomerular cells remained unchanged, thus indicating primary intracellular rather than secondary extracellular causes for increased β1-integrin activation in podocytes. Further investigations regarding the pathway of increased integrin activation are of interest, for instance, talin or kindlin-2 expression and localization (Askari et al., 2009) as well as measurement of the mechanical tension at focal adhesions with FRET-based biosensors (Grashoff et al., 2010).

Transgelin is an actin-binding protein previously shown to be highly expressed in *Lmx1b*-deficient podocytes, but not in wild-type controls. Transgelin is localized to the cell cortex in both spreading and steady state podocytes, but colocalization with actin bundles was only observed in steady state podocytes. Surprisingly, podocyte outgrowth led to transgelin expression in wild-type controls, although to a lower extent when compared to steady state *Lmx1b* knock-out podocytes. To address the impact of *de novo* transgelin expression on the podocyte and on renal health, a double *Sm22* and *Lmx1b* (podocyte-specific) knock-out mouse line was created. Investigation of the survival and proteinuria of those mice revealed a strong dependence on the genetic background, but also an increased percentage of mice with prolonged lifetime and delayed onset of proteinuria compared to podocyte-specific *Lmx1b* knock-out control mice. A deeper analysis of double knock-out mice 8 days postnatally, on the other hand, demonstrated worse proteinuria of most mice, except for one animal without any pathological phenotype. No influence of additional *Sm22* knock-out on kidney histology, kidney ultrastructure, filtration slit density and glomerular phalloidin staining could be revealed. The body weight of some, but not all, double knock-out mice was reduced compared to controls. Supported by a previous report (Marshall et al., 2011), this led to the assumption of beneficial aspects of transgelin expression in early podocyte damage and detrimental effects in the later disease progression.

6. Bibliography

Abrahamson, D.R. 1985. Origin of the glomerular basement membrane visualized after in vivo labeling of laminin in newborn rat kidneys. *J Cell Biol*. 100:1988-2000.

Adams, K.A., J.M. Maida, J.A. Golden, and R.D. Riddle. 2000. The transcription factor Lmx1b maintains Wnt1 expression within the isthmic organizer. *Development*. 127:1857-1867.

Aigouy, B., and V. Mirouse. 2013. ScientiFig: a tool to build publication-ready scientific figures. *Nat Methods*. 10:1048.

Akilesh, S., H. Suleiman, H. Yu, M.C. Stander, P. Lavin, R. Gbadegesin, C. Antignac, M. Pollak, J.B. Kopp, M.P. Winn, and A.S. Shaw. 2011. Arhgap24 inactivates Rac1 in mouse podocytes, and a mutant form is associated with familial focal segmental glomerulosclerosis. *J Clin Invest*. 121:4127-4137.

Amann, K.J., and T.D. Pollard. 2001. Direct real-time observation of actin filament branching mediated by Arp2/3 complex using total internal reflection fluorescence microscopy. *Proc Natl Acad Sci USA*. 98:15009-15013.

Andrews, P.M., and S.B. Bates. 1984. Filamentous actin bundles in the kidney. *Anat Rec*. 210:1-9.

Andrianantoandro, E., and T.D. Pollard. 2006. Mechanism of actin filament turnover by severing and nucleation at different concentrations of ADF/cofilin. *Mol Cell*. 24:13-23.

Appel, D., D.B. Kershaw, B. Smeets, G. Yuan, A. Fuss, B. Frye, M. Elger, W. Kriz, J. Floege, and M.J. Moeller. 2009. Recruitment of podocytes from glomerular parietal epithelial cells. *J Am Soc Nephrol*. 20:333-343.

Arai, A., J.A. Spencer, and E.N. Olson. 2002. STARS, a striated muscle activator of Rho signaling and serum response factor-dependent transcription. *J Biol Chem*. 277:24453-24459.

Arber, S., F.A. Barbayannis, H. Hanser, C. Schneider, C.A. Stanyon, O. Bernard, and P. Caroni. 1998. Regulation of actin dynamics through phosphorylation of cofilin by LIM-kinase. *Nature*. 393:805-809.

Arrondel, C., N. Vodovar, B. Knebelmann, J.P. Grunfeld, M.C. Gubler, C. Antignac, and L. Heidet. 2002. Expression of the nonmuscle myosin heavy chain IIA in the human kidney and screening for MYH9 mutations in Epstein and Fechtner syndromes. *J Am Soc Nephrol*. 13:65-74.

Arthur, W.T., and K. Burridge. 2001. RhoA inactivation by p190RhoGAP regulates cell spreading and migration by promoting membrane protrusion and polarity. *Mol Biol Cell*. 12:2711-2720.

Asanuma, K., K. Kim, J. Oh, L. Giardino, S. Chabanis, C. Faul, J. Reiser, and P. Mundel. 2005. Synaptopodin regulates the actin-bundling activity of alpha-actinin in an isoform-specific manner. *J Clin Invest*. 115:1188-1198.

Asanuma, K., E. Yanagida-Asanuma, C. Faul, Y. Tomino, K. Kim, and P. Mundel. 2006. Synaptopodin orchestrates actin organization and cell motility via regulation of RhoA signalling. *Nat Cell Biol*. 8:485-491.

Askari, J.A., P.A. Buckley, A.P. Mould, and M.J. Humphries. 2009. Linking integrin conformation to function. *J Cell Sci*. 122:165-170.

Assinder, S.J., J.A. Stanton, and P.D. Prasad. 2009. Transgelin: an actin-binding protein and tumour suppressor. *Int J Biochem Cell Biol*. 41:482-486.

Avasthi, P.S., A.P. Evan, and D. Hay. 1980. Glomerular endothelial cells in uranyl nitrate-induced acute renal failure in rats. *J Clin Invest*. 65:121-127.

Avasthi, P.S., and V. Koshy. 1988. The anionic matrix at the rat glomerular endothelial surface. *Anat Rec*. 220:258-266.

Babelova, A., F. Jansen, K. Sander, M. Lohn, L. Schafer, C. Fork, H. Ruetten, O. Plettenburg, H. Stark, C. Daniel, K. Amann, H. Pavenstadt, O. Jung, and R.P. Brandes. 2013. Activation of Rac-1 and RhoA contributes to podocyte injury in chronic kidney disease. *PLoS One*. 8:e80328.

Barczyk, M., S. Carracedo, and D. Gullberg. 2010. Integrins. *Cell Tissue Res*. 339:269-280.

Barrientos, T., D. Frank, K. Kuwahara, S. Bezprozvannaya, G.C. Pipes, R. Bassel-Duby, J.A. Richardson, H.A. Katus, E.N. Olson, and N. Frey. 2007. Two novel members of the ABLIM protein family, ABLIM-2 and -3, associate with STARS and directly bind F-actin. *J Biol Chem*. 282:8393-8403.

Barry, D.J., C.H. Durkin, J.V. Abella, and M. Way. 2015. Open source software for quantification of cell migration, protrusions, and fluorescence intensities. *J Cell Biol*. 209:163-180.

Belin, B.J., and R.D. Mullins. 2013. What we talk about when we talk about nuclear actin. *Nucleus*. 4:291-297.

Ben-Bassat, M., L. Cohen, and J. Rosenfeld. 1971. The glomerular basement membrane in the nail-patella syndrome. *Arch Pathol*. 92:350-355.

Bertram, J.F., R.N. Douglas-Denton, B. Diouf, M.D. Hughson, and W.E. Hoy. 2011. Human nephron number: implications for health and disease. *Pediatr Nephrol*. 26:1529-1533.

Blanchoin, L., R. Boujemaa-Paterski, C. Sykes, and J. Plastino. 2014. Actin dynamics, architecture, and mechanics in cell motility. *Physiol Rev*. 94:235-263.

Blanchoin, L., T.D. Pollard, and R.D. Mullins. 2000. Interactions of ADF/cofilin, Arp2/3 complex, capping protein and profilin in remodeling of branched actin filament networks. *Curr Biol*. 10:1273-1282.

Blattner, S.M., J.B. Hodgin, M. Nishio, S.A. Wylie, J. Saha, A.A. Soofi, C. Vining, A. Randolph, N. Herbach, R. Wanke, K.B. Atkins, H. Gyung Kang, A. Henger, C. Brakebusch, L.B. Holzman, and M. Kretzler. 2013. Divergent functions of the Rho GTPases Rac1 and Cdc42 in podocyte injury. *Kidney Int*. 84:920-930.

Bolte, S., and F.P. Cordelieres. 2006. A guided tour into subcellular colocalization analysis in light microscopy. *J Microsc*. 224:213-232.

Bongers, E.M., M.C. Gubler, and N.V. Knoers. 2002. Nail-patella syndrome. Overview on clinical and molecular findings. *Pediatr Nephrol*. 17:703-712.

Bongers, E.M., F.T. Huysmans, E. Levtchenko, J.W. de Rooy, J.G. Blickman, R.J. Admiraal, P.L. Huygen, J.R. Cruysberg, P.A. Toolens, J.B. Prins, P.F. Krabbe, G.F. Borm, J. Schoots, H. van Bokhoven, A.M. van Remortele, L.H. Hoefsloot, A. van Kampen, and N.V. Knoers. 2005. Genotype-phenotype studies in nail-patella syndrome show that LMX1B mutation location is involved in the risk of developing nephropathy. *Eur J Hum Genet*. 13:935-946.

Boute, N., O. Gribouval, S. Roselli, F. Benessy, H. Lee, A. Fuchshuber, K. Dahan, M.C. Gubler, P. Niaudet, and C. Antignac. 2000. NPHS2, encoding the glomerular

protein podocin, is mutated in autosomal recessive steroid-resistant nephrotic syndrome. *Nat Genet*. 24:349-354.

Brown, E.J., J.S. Schlondorff, D.J. Becker, H. Tsukaguchi, S.J. Tonna, A.L. Uscinski, H.N. Higgs, J.M. Henderson, and M.R. Pollak. 2010. Mutations in the formin gene INF2 cause focal segmental glomerulosclerosis. *Nat Genet*. 42:72-76.

Burghardt, T., F. Hochapfel, B. Salecker, C. Meese, H.J. Grone, R. Rachel, G. Wanner, M.P. Krahn, and R. Witzgall. 2015. Advanced electron microscopic techniques provide a deeper insight into the peculiar features of podocytes. *Am J Physiol Renal Physiol*. 309:F1082-1089.

Burghardt, T., J. Kastner, H. Suleiman, E. Rivera-Milla, N. Stepanova, C. Lottaz, M. Kubitza, C.A. Boger, S. Schmidt, M. Gorski, U. de Vries, H. Schmidt, I. Hertting, J. Kopp, A. Rascle, M. Moser, I.M. Heid, R. Warth, R. Spang, J. Wegener, C.T. Mierke, C. Englert, and R. Witzgall. 2013. LMX1B is essential for the maintenance of differentiated podocytes in adult kidneys. *J Am Soc Nephrol*. 24:1830-1848.

Byron, A., J.D. Humphries, J.A. Askari, S.E. Craig, A.P. Mould, and M.J. Humphries. 2009. Anti-integrin monoclonal antibodies. *J Cell Sci*. 122:4009-4011.

Camoretti-Mercado, B., S.M. Forsythe, M.M. LeBeau, R. Espinosa, 3rd, J.E. Vieira, A.J. Halayko, S. Willadsen, B. Kurtz, C. Ober, G.A. Evans, R. Thweatt, S. Shapiro, Q. Niu, Y. Qin, P.A. Padrid, and J. Solway. 1998. Expression and cytogenetic localization of the human SM22 gene (TAGLN). *Genomics*. 49:452-457.

Campbell, I.D., and M.J. Humphries. 2011. Integrin structure, activation, and interactions. *Cold Spring Harb Perspect Biol*. 3.

Chalovich, J.M., and M.M. Schroeter. 2010. Synaptopodin family of natively unfolded, actin binding proteins: physical properties and potential biological functions. *Biophys Rev*. 2:181-189.

Chen, F., L. Ma, M.C. Parrini, X. Mao, M. Lopez, C. Wu, P.W. Marks, L. Davidson, D.J. Kwiatkowski, T. Kirchhausen, S.H. Orkin, F.S. Rosen, B.J. Mayer, M.W. Kirschner, and F.W. Alt. 2000. Cdc42 is required for PIP(2)-induced actin polymerization and early development but not for cell viability. *Curr Biol*. 10:758-765.

Chen, H., Y. Lun, D. Ovchinnikov, H. Kokubo, K.C. Oberg, C.V. Pepicelli, L. Gan, B. Lee, and R.L. Johnson. 1998. Limb and kidney defects in Lmx1b mutant mice suggest an involvement of LMX1B in human nail patella syndrome. *Nat Genet*. 19:51-55.

Chen, Q., and T.D. Pollard. 2013. Actin filament severing by cofilin dismantles actin patches and produces mother filaments for new patches. *Curr Biol*. 23:1154-1162.

Chen, Z., D. Borek, S.B. Padrick, T.S. Gomez, Z. Metlagel, A.M. Ismail, J. Umetani, D.D. Billadeau, Z. Otwinowski, and M.K. Rosen. 2010. Structure and control of the actin regulatory WAVE complex. *Nature*. 468:533-538.

Chesarone, M.A., A.G. DuPage, and B.L. Goode. 2010. Unleashing formins to remodel the actin and microtubule cytoskeletons. *Nat Rev Mol Cell Biol*. 11:62-74.

Chew, C., and R. Lennon. 2018. Basement Membrane Defects in Genetic Kidney Diseases. *Front Pediatr*. 6:11.

Chew, T.L., R.A. Masaracchia, Z.M. Goeckeler, and R.B. Wysolmerski. 1998. Phosphorylation of non-muscle myosin II regulatory light chain by p21-activated kinase (gamma-PAK). *J Muscle Res Cell Motil*. 19:839-854.

Chiang, T.S., H.F. Wu, and F.S. Lee. 2017. ADP-ribosylation factor-like 4C binding to filamin-A modulates filopodium formation and cell migration. *Mol Biol Cell*. 28:3013-3028.

Chircop, M. 2014. Rho GTPases as regulators of mitosis and cytokinesis in mammalian cells. *Small GTPases*. 5.

Chong, N.W., A.L. Koekemoer, S. Ounzain, N.J. Samani, J.T. Shin, and S.Y. Shaw. 2012. STARS is essential to maintain cardiac development and function in vivo via a SRF pathway. *PLoS One*. 7:e40966.

Cooper, J.A. 1987. Effects of cytochalasin and phalloidin on actin. *J Cell Biol*. 105:1473-1478.

Cramer, L.P. 2013. Mechanism of cell rear retraction in migrating cells. *Curr Opin Cell Biol*. 25:591-599.

Craver, R., J. Crespo-Salgado, and D. Aviles. 2014. Laminations and microgranule formation in pediatric glomerular basement membranes. *Fetal Pediatr Pathol*. 33:321-330.

Del Pozo, E., and H. Lapp. 1970. Ultrastructure of the kidney in the nephropathy of the nail--patella syndrome. *Am J Clin Pathol*. 54:845-851.

Deroulers, C., D. Ameisen, M. Badoual, C. Gerin, A. Granier, and M. Lartaud. 2013. Analyzing huge pathology images with open source software. *Diagn Pathol*. 8:92.

Donoviel, D.B., D.D. Freed, H. Vogel, D.G. Potter, E. Hawkins, J.P. Barrish, B.N. Mathur, C.A. Turner, R. Geske, C.A. Montgomery, M. Starbuck, M. Brandt, A. Gupta, R. Ramirez-Solis, B.P. Zambrowicz, and D.R. Powell. 2001. Proteinuria and perinatal lethality in mice lacking NEPH1, a novel protein with homology to NEPHRIN. *Mol Cell Biol*. 21:4829-4836.

Dreyer, S.D., R. Morello, M.S. German, B. Zabel, A. Winterpacht, G.P. Lunstrum, W.A. Horton, K.C. Oberg, and B. Lee. 2000. LMX1B transactivation and expression in nail-patella syndrome. *Hum Mol Genet*. 9:1067-1074.

Dreyer, S.D., G. Zhou, A. Baldini, A. Winterpacht, B. Zabel, W. Cole, R.L. Johnson, and B. Lee. 1998. Mutations in LMX1B cause abnormal skeletal patterning and renal dysplasia in nail patella syndrome. *Nat Genet*. 19:47-50.

Dunston, J.A., J.D. Hamlington, J. Zaveri, E. Sweeney, J. Sibbring, C. Tran, M. Malbroux, J.P. O'Neill, R. Mountford, and I. McIntosh. 2004. The human LMX1B gene: transcription unit, promoter, and pathogenic mutations. *Genomics*. 84:565-576.

Dunston, J.A., T. Reimschisel, Y.Q. Ding, E. Sweeney, R.L. Johnson, Z.F. Chen, and I. McIntosh. 2005. A neurological phenotype in nail patella syndrome (NPS) patients illuminated by studies of murine Lmx1b expression. *Eur J Hum Genet*. 13:330-335.

Duquette, P.M., and N. Lamarche-Vane. 2014. Rho GTPases in embryonic development. *Small GTPases*. 5:8.

Durbeej, M., M.D. Henry, M. Ferletta, K.P. Campbell, and P. Ekblom. 1998. Distribution of dystroglycan in normal adult mouse tissues. *J Histochem Cytochem*. 46:449-457.

Dvorakova, M., R. Nenutil, and P. Bouchal. 2014. Transgelins, cytoskeletal proteins implicated in different aspects of cancer development. *Expert Rev Proteomics*. 11:149-165.

Edwards, D.C., L.C. Sanders, G.M. Bokoch, and G.N. Gill. 1999. Activation of LIM-kinase by Pak1 couples Rac/Cdc42 GTPase signalling to actin cytoskeletal dynamics. *Nat Cell Biol*. 1:253-259.

El-Aouni, C., N. Herbach, S.M. Blattner, A. Henger, M.P. Rastaldi, G. Jarad, J.H. Miner, M.J. Moeller, R. St-Arnaud, S. Dedhar, L.B. Holzman, R. Wanke, and M. Kretzler. 2006. Podocyte-specific deletion of integrin-linked kinase results in severe glomerular basement membrane alterations and progressive glomerulosclerosis. *J Am Soc Nephrol*. 17:1334-1344.

Engel, T., A. Lueken, G. Bode, U. Hobohm, S. Lorkowski, B. Schlueter, S. Rust, P. Cullen, M. Pech, G. Assmann, and U. Seedorf. 2004. ADP-ribosylation factor (ARF)-like 7 (ARL7) is induced by cholesterol loading and participates in apolipoprotein AI-dependent cholesterol export. *FEBS Lett*. 566:241-246.

Eremina, V., J.A. Jefferson, J. Kowalewska, H. Hochster, M. Haas, J. Weisstuch, C. Richardson, J.B. Kopp, M.G. Kabir, P.H. Backx, H.P. Gerber, N. Ferrara, L. Barisoni, C.E. Alpers, and S.E. Quaggin. 2008. VEGF inhibition and renal thrombotic microangiopathy. *N Engl J Med*. 358:1129-1136.

Ervasti, J.M., and K.P. Campbell. 1993. A role for the dystrophin-glycoprotein complex as a transmembrane linker between laminin and actin. *J Cell Biol*. 122:809-823.

Etienne-Manneville, S., and A. Hall. 2002. Rho GTPases in cell biology. *Nature*. 420:629-635.

Faul, C., K. Asanuma, E. Yanagida-Asanuma, K. Kim, and P. Mundel. 2007. Actin up: regulation of podocyte structure and function by components of the actin cytoskeleton. *Trends Cell Biol*. 17:428-437.

Feng, D., C. DuMontier, and M.R. Pollak. 2015. The role of alpha-actinin-4 in human kidney disease. *Cell Biosci*. 5:44.

Ferguson, S.M., A. Raimondi, S. Paradise, H. Shen, K. Mesaki, A. Ferguson, O. Destaing, G. Ko, J. Takasaki, O. Cremona, O.T. E, and P. De Camilli. 2009. Coordinated actions of actin and BAR proteins upstream of dynamin at endocytic clathrin-coated pits. *Dev Cell*. 17:811-822.

Finne, K., H. Vethe, T. Skogstrand, S. Leh, T.D. Dahl, O. Tenstad, F.S. Berven, R.K. Reed, and B.E. Vikse. 2014. Proteomic analysis of formalin-fixed paraffin-embedded glomeruli suggests depletion of glomerular filtration barrier proteins in two-kidney, one-clip hypertensive rats. *Nephrol Dial Transplant*. 29:2217-2227.

Fletcher, D.A., and R.D. Mullins. 2010. Cell mechanics and the cytoskeleton. *Nature*. 463:485-492.

Fogl, C., L. Puckey, U. Hinssen, M. Zaleska, M. El-Mezgueldi, R. Croasdale, A. Bowman, A. Matsukawa, N.J. Samani, R. Savva, and M. Pfuhl. 2012. A structural and functional dissection of the cardiac stress response factor MS1. *Proteins*. 80:398-409.

Foley, K.S., and P.W. Young. 2014. The non-muscle functions of actinins: an update. *Biochem J*. 459:1-13.

Friden, V., E. Oveland, O. Tenstad, K. Ebefors, J. Nystrom, U.A. Nilsson, and B. Haraldsson. 2011. The glomerular endothelial cell coat is essential for glomerular filtration. *Kidney Int*. 79:1322-1330.

Friedland, J.C., M.H. Lee, and D. Boettiger. 2009. Mechanically activated integrin switch controls alpha5beta1 function. *Science*. 323:642-644.

Fu, Y., H.W. Liu, S.M. Forsythe, P. Kogut, J.F. McConville, A.J. Halayko, B. Camoretti-Mercado, and J. Solway. 2000. Mutagenesis analysis of human SM22: characterization of actin binding. *J Appl Physiol*. 89:1985-1990.

Fujii, S., S. Matsumoto, S. Nojima, E. Morii, and A. Kikuchi. 2015. Arl4c expression in colorectal and lung cancers promotes tumorigenesis and may represent a novel therapeutic target. *Oncogene*. 34:4834-4844.

Furuya, Y., M. Denda, K. Sakane, T. Ogusu, S. Takahashi, M. Magari, N. Kanayama, R. Morishita, and H. Tokumitsu. 2016. Identification of striated muscle activator of Rho signaling (STARS) as a novel calmodulin target by a newly developed genome-wide screen. *Cell Calcium*. 60:32-40.

Gardel, M.L., I.C. Schneider, Y. Aratyn-Schaus, and C.M. Waterman. 2010. Mechanical integration of actin and adhesion dynamics in cell migration. *Annu Rev Cell Dev Biol*. 26:315-333.

Garg, P., R. Verma, L. Cook, A. Soofi, M. Venkatareddy, B. George, K. Mizuno, C. Gurniak, W. Witke, and L.B. Holzman. 2010. Actin-depolymerizing factor cofilin-1 is necessary in maintaining mature podocyte architecture. *J Biol Chem*. 285:22676-22688.

Gbadegesin, R.A., G. Hall, A. Adeyemo, N. Hanke, I. Tossidou, J. Burchette, G. Wu, A. Homstad, M.A. Sparks, J. Gomez, R. Jiang, A. Alonso, P. Lavin, P. Conlon, R. Korstanje, M.C. Stander, G. Shamsan, M. Barua, R. Spurney, P.C. Singhal, J.B. Kopp, H. Haller, D. Howell, M.R. Pollak, A.S. Shaw, M. Schiffer, and M.P. Winn. 2014. Mutations in the gene that encodes the F-actin binding protein anillin cause FSGS. *J Am Soc Nephrol*. 25:1991-2002.

Gee, H.Y., P. Saisawat, S. Ashraf, T.W. Hurd, V. Vega-Warner, H. Fang, B.B. Beck, O. Gribouval, W. Zhou, K.A. Diaz, S. Natarajan, R.C. Wiggins, S. Lovric, G. Chernin, D.S. Schoeb, B. Ovunc, Y. Frishberg, N.A. Soliman, H.M. Fathy, H. Goebel, J. Hoefele, L.T. Weber, J.W. Innis, C. Faul, Z. Han, J. Washburn, C. Antignac, S. Levy, E.A. Otto, and F. Hildebrandt. 2013. ARHGDIA mutations cause nephrotic syndrome via defective RHO GTPase signaling. *J Clin Invest*. 123:3243-3253.

Geiger, B., and K.M. Yamada. 2011. Molecular architecture and function of matrix adhesions. *Cold Spring Harb Perspect Biol*. 3.

German, M.S., J. Wang, R.B. Chadwick, and W.J. Rutter. 1992. Synergistic activation of the insulin gene by a LIM-homeo domain protein and a basic helix-loop-helix protein: building a functional insulin minienhancer complex. *Genes Dev*. 6:2165-2176.

Ghiggeri, G.M., G. Caridi, U. Magrini, A. Sessa, A. Savoia, M. Seri, A. Pecci, R. Romagnoli, S. Gangarossa, P. Noris, S. Sartore, V. Necchi, R. Ravazzolo, and C.L. Balduini. 2003. Genetics, clinical and pathological features of glomerulonephritis associated with mutations of nonmuscle myosin IIA (Fechtner syndrome). *Am J Kidney Dis*. 41:95-104.

Ghosh, M., X. Song, G. Mouneimne, M. Sidani, D.S. Lawrence, and J.S. Condeelis. 2004. Cofilin promotes actin polymerization and defines the direction of cell motility. *Science*. 304:743-746.

Ghoumid, J., F. Petit, M. Holder-Espinasse, A.S. Jourdain, J. Guerra, A. Dieux-Coeslier, M. Figeac, N. Porchet, S. Manouvrier-Hanu, and F. Escande. 2016. Nail-Patella Syndrome: clinical and molecular data in 55 families raising the hypothesis of a genetic heterogeneity. *Eur J Hum Genet*. 24:44-50.

Glotzer, M. 2005. The molecular requirements for cytokinesis. *Science*. 307:1735-1739.

Goddette, D.W., and C. Frieden. 1985. The binding of cytochalasin D to monomeric actin. *Biochem Biophys Res Commun*. 128:1087-1092.

Gojo, A., K. Utsunomiya, K. Taniguchi, T. Yokota, S. Ishizawa, Y. Kanazawa, H. Kurata, and N. Tajima. 2007. The Rho-kinase inhibitor, fasudil, attenuates diabetic nephropathy in streptozotocin-induced diabetic rats. *Eur J Pharmacol*. 568:242-247.

Goley, E.D., and M.D. Welch. 2006. The ARP2/3 complex: an actin nucleator comes of age. *Nat Rev Mol Cell Biol*. 7:713-726.

Goode, N.P., M. Shires, T.N. Khan, and A.F. Mooney. 2004. Expression of alpha-actinin-4 in acquired human nephrotic syndrome: a quantitative immunoelectron microscopy study. *Nephrol Dial Transplant*. 19:844-851.

Gossen, M., and H. Bujard. 1992. Tight control of gene expression in mammalian cells by tetracycline-responsive promoters. *Proc Natl Acad Sci USA*. 89:5547-5551.

Grahammer, F., C. Wigge, C. Schell, O. Kretz, J. Patrakka, S. Schneider, M. Klose, S.J. Arnold, A. Habermann, R. Brauniger, M.M. Rinschen, L. Volker, A. Bregenzer, D. Rubbenstroth, M. Boerries, D. Kerjaschki, J.H. Miner, G. Walz, T. Benzing, A. Fornoni, A.S. Frangakis, and T.B. Huber. 2016. A flexible, multilayered protein scaffold maintains the slit in between glomerular podocytes. *JCI Insight*. 1.

Grashoff, C., B.D. Hoffman, M.D. Brenner, R. Zhou, M. Parsons, M.T. Yang, M.A. McLean, S.G. Sligar, C.S. Chen, T. Ha, and M.A. Schwartz. 2010. Measuring mechanical tension across vinculin reveals regulation of focal adhesion dynamics. *Nature*. 466:263-266.

Gross, O., B. Beirowski, S.J. Harvey, C. McFadden, D. Chen, S. Tam, P.S. Thorner, N. Smyth, K. Addicks, W. Bloch, Y. Ninomiya, Y. Sado, M. Weber, and W.F. Vogel. 2004. DDR1-deficient mice show localized subepithelial GBM thickening with focal loss of slit diaphragms and proteinuria. *Kidney Int*. 66:102-111.

Grosse, R., and M.K. Vartiainen. 2013. To be or not to be assembled: progressing into nuclear actin filaments. *Nat Rev Mol Cell Biol*. 14:693-697.

Gunning, P.W., U. Ghoshdastider, S. Whitaker, D. Popp, and R.C. Robinson. 2015. The evolution of compositionally and functionally distinct actin filaments. *J Cell Sci*. 128:2009-2019.

Guo, B., Q. Lyu, O.J. Slivano, R. Dirkx, C.K. Christie, J. Czyzyk, A.F. Hezel, A.G. Gharavi, E.M. Small, and J.M. Miano. 2018. Serum Response Factor Is Essential for Maintenance of Podocyte Structure and Function. *J Am Soc Nephrol*. 29:416-422.

Han, M., L.H. Dong, B. Zheng, J.H. Shi, J.K. Wen, and Y. Cheng. 2009. Smooth muscle 22 alpha maintains the differentiated phenotype of vascular smooth muscle cells by inducing filamentous actin bundling. *Life Sci*. 84:394-401.

Harita, Y., S. Kitanaka, T. Isojima, A. Ashida, and M. Hattori. 2017. Spectrum of LMX1B mutations: from nail-patella syndrome to isolated nephropathy. *Pediatr Nephrol*. 32:1845-1850.

Haro, E., B.A. Watson, J.M. Feenstra, L. Tegeler, C.U. Pira, S. Mohan, and K.C. Oberg. 2017. Lmx1b-targeted cis-regulatory modules involved in limb dorsalization. *Development*. 144:2009-2020.

Hawkins, M., B. Pope, S.K. Maciver, and A.G. Weeds. 1993. Human actin depolymerizing factor mediates a pH-sensitive destruction of actin filaments. *Biochemistry*. 32:9985-9993.

Hayden, S.M., P.S. Miller, A. Brauweiler, and J.R. Bamburg. 1993. Analysis of the interactions of actin depolymerizing factor with G- and F-actin. *Biochemistry*. 32:9994-10004.

He, B., L. Ebarasi, Z. Zhao, J. Guo, J.R. Ojala, K. Hultenby, S. De Val, C. Betsholtz, and K. Tryggvason. 2014. Lmx1b and FoxC combinatorially regulate podocin expression in podocytes. *J Am Soc Nephrol*. 25:2764-2777.

Heasman, S.J., and A.J. Ridley. 2008. Mammalian Rho GTPases: new insights into their functions from in vivo studies. *Nat Rev Mol Cell Biol*. 9:690-701.

Heath, K.E., A. Campos-Barros, A. Toren, G. Rozenfeld-Granot, L.E. Carlsson, J. Savige, J.C. Denison, M.C. Gregory, J.G. White, D.F. Barker, A. Greinacher, C.J. Epstein, M.J. Glucksman, and J.A. Martignetti. 2001. Nonmuscle myosin heavy chain IIA mutations define a spectrum of autosomal dominant macrothrombocytopenias: May-Hegglin anomaly and Fechtner, Sebastian, Epstein, and Alport-like syndromes. *Am J Hum Genet*. 69:1033-1045.

Heidet, L., E.M. Bongers, M. Sich, S.Y. Zhang, C. Loirat, A. Meyrier, M. Broyer, G. Landthaler, B. Faller, Y. Sado, N.V. Knoers, and M.C. Gubler. 2003. In vivo expression of putative LMX1B targets in nail-patella syndrome kidneys. *Am J Pathol*. 163:145-155.

Henderson, J.M., S. Al-Waheeb, A. Weins, S.V. Dandapani, and M.R. Pollak. 2008. Mice with altered alpha-actinin-4 expression have distinct morphologic patterns of glomerular disease. *Kidney Int*. 73:741-750.

Herzenberg, L.A., D. Parks, B. Sahaf, O. Perez, M. Roederer, and L.A. Herzenberg. 2002. The history and future of the fluorescence activated cell sorter and flow cytometry: a view from Stanford. *Clin Chem*. 48:1819-1827.

Herzog, D., P. Loetscher, J. van Hengel, S. Knusel, C. Brakebusch, V. Taylor, U. Suter, and J.B. Relvas. 2011. The small GTPase RhoA is required to maintain spinal cord neuroepithelium organization and the neural stem cell pool. *J Neurosci*. 31:5120-5130.

Hofmann, I., A. Thompson, C.M. Sanderson, and S. Munro. 2007. The Arl4 family of small G proteins can recruit the cytohesin Arf6 exchange factors to the plasma membrane. *Curr Biol*. 17:711-716.

Holzman, L.B., P.L. St John, I.A. Kovari, R. Verma, H. Holthofer, and D.R. Abrahamson. 1999. Nephrin localizes to the slit pore of the glomerular epithelial cell. *Kidney Int*. 56:1481-1491.

Houdusse, A., and H.L. Sweeney. 2016. How Myosin Generates Force on Actin Filaments. *Trends Biochem Sci*. 41:989-997.

Hu, Q., T. Masuda, K. Sato, T. Tobo, S. Nambara, S. Kidogami, N. Hayashi, Y. Kuroda, S. Ito, H. Eguchi, H. Saeki, E. Oki, Y. Maehara, and K. Mimori. 2018. Identification of ARL4C as a Peritoneal Dissemination-Associated Gene and Its Clinical Significance in Gastric Cancer. *Ann Surg Oncol*. 25:745-753.

Huber, T.B., M. Kottgen, B. Schilling, G. Walz, and T. Benzing. 2001. Interaction with podocin facilitates nephrin signaling. *J Biol Chem*. 276:41543-41546.

Ichimura, K., H. Kurihara, and T. Sakai. 2007. Actin filament organization of foot processes in vertebrate glomerular podocytes. *Cell Tissue Res*. 329:541-557.

Inoue, T., E. Yaoita, H. Kurihara, F. Shimizu, T. Sakai, T. Kobayashi, K. Ohshiro, H. Kawachi, H. Okada, H. Suzuki, I. Kihara, and T. Yamamoto. 2001. FAT is a component of glomerular slit diaphragms. *Kidney Int*. 59:1003-1012.

Jacobs, S., C. Schilf, F. Fliegert, S. Koling, Y. Weber, A. Schurmann, and H.G. Joost. 1999. ADP-ribosylation factor (ARF)-like 4, 6, and 7 represent a subgroup of the

ARF family characterization by rapid nucleotide exchange and a nuclear localization signal. *FEBS Lett*. 456:384-388.

Jarad, G., J. Cunningham, A.S. Shaw, and J.H. Miner. 2006. Proteinuria precedes podocyte abnormalities inLamb2-/- mice, implicating the glomerular basement membrane as an albumin barrier. *J Clin Invest*. 116:2272-2279.

Jarad, G., and J.H. Miner. 2009. Update on the glomerular filtration barrier. *Curr Opin Nephrol Hypertens*. 18:226-232.

Jarad, G., J.W. Pippin, S.J. Shankland, J.A. Kreidberg, and J.H. Miner. 2011. Dystroglycan does not contribute significantly to kidney development or function, in health or after injury. *Am J Physiol Renal Physiol*. 300:F811-820.

Je, H.D., and U.D. Sohn. 2007. SM22alpha is required for agonist-induced regulation of contractility: evidence from SM22alpha knockout mice. *Mol Cells*. 23:175-181.

Jeansson, M., and B. Haraldsson. 2003. Glomerular size and charge selectivity in the mouse after exposure to glucosaminoglycan-degrading enzymes. *J Am Soc Nephrol*. 14:1756-1765.

Jiang, S., J. Zhang, D. Huang, Y. Zhang, X. Liu, Y. Wang, R. He, and Y. Zhao. 2014. A microdeletion of chromosome 9q33.3 encompasses the entire LMX1B gene in a Chinese family with nail patella syndrome. *Int J Mol Sci*. 15:20158-20168.

Johnstone, D.B., O. Ikizler, J. Zhang, and L.B. Holzman. 2013. Background strain and the differential susceptibility of podocyte-specific deletion of Myh9 on murine models of experimental glomerulosclerosis and HIV nephropathy. *PLoS One*. 8:e67839.

Kaiser, D.A., V.K. Vinson, D.B. Murphy, and T.D. Pollard. 1999. Profilin is predominantly associated with monomeric actin in Acanthamoeba. *J Cell Sci*. 112 (Pt 21):3779-3790.

Kalluri, R., C.F. Shield, P. Todd, B.G. Hudson, and E.G. Neilson. 1997. Isoform switching of type IV collagen is developmentally arrested in X-linked Alport syndrome leading to increased susceptibility of renal basement membranes to endoproteolysis. *J Clin Invest*. 99:2470-2478.

Kanasaki, K., Y. Kanda, K. Palmsten, H. Tanjore, S.B. Lee, V.S. Lebleu, V.H. Gattone, Jr., and R. Kalluri. 2008. Integrin beta1-mediated matrix assembly and signaling are critical for the normal development and function of the kidney glomerulus. *Dev Biol*. 313:584-593.

Kaplan, J.M., S.H. Kim, K.N. North, H. Rennke, L.A. Correia, H.Q. Tong, B.J. Mathis, J.C. Rodriguez-Perez, P.G. Allen, A.H. Beggs, and M.R. Pollak. 2000. Mutations in ACTN4, encoding alpha-actinin-4, cause familial focal segmental glomerulosclerosis. *Nat Genet*. 24:251-256.

Kestila, M., U. Lenkkeri, M. Mannikko, J. Lamerdin, P. McCready, H. Putaala, V. Ruotsalainen, T. Morita, M. Nissinen, R. Herva, C.E. Kashtan, L. Peltonen, C. Holmberg, A. Olsen, and K. Tryggvason. 1998. Positionally cloned gene for a novel glomerular protein--nephrin--is mutated in congenital nephrotic syndrome. *Mol Cell*. 1:575-582.

Kiuchi, T., K. Ohashi, S. Kurita, and K. Mizuno. 2007. Cofilin promotes stimulus-induced lamellipodium formation by generating an abundant supply of actin monomers. *J Cell Biol*. 177:465-476.

Kos, C.H., T.C. Le, S. Sinha, J.M. Henderson, S.H. Kim, H. Sugimoto, R. Kalluri, R.E. Gerszten, and M.R. Pollak. 2003. Mice deficient in alpha-actinin-4 have severe glomerular disease. *J Clin Invest*. 111:1683-1690.

Kovar, D.R., and T.D. Pollard. 2004. Insertional assembly of actin filament barbed ends in association with formins produces piconewton forces. *Proc Natl Acad Sci USA*. 101:14725-14730.

Kreidberg, J.A., M.J. Donovan, S.L. Goldstein, H. Rennke, K. Shepherd, R.C. Jones, and R. Jaenisch. 1996. Alpha 3 beta 1 integrin has a crucial role in kidney and lung organogenesis. *Development*. 122:3537-3547.

Kremerskothen, J., C. Plaas, S. Kindler, M. Frotscher, and A. Barnekow. 2005. Synaptopodin, a molecule involved in the formation of the dendritic spine apparatus, is a dual actin/alpha-actinin binding protein. *J Neurochem*. 92:597-606.

Kriz, W., I. Shirato, M. Nagata, M. LeHir, and K.V. Lemley. 2013. The podocyte's response to stress: the enigma of foot process effacement. *Am J Physiol Renal Physiol*. 304:F333-347.

Kühbandner, S., S. Brummer, D. Metzger, P. Chambon, F. Hofmann, and R. Feil. 2000. Temporally controlled somatic mutagenesis in smooth muscle. *Genesis*. 28:15-22.

Kuure, S., C. Cebrian, Q. Machingo, B.C. Lu, X. Chi, D. Hyink, V. D'Agati, C. Gurniak, W. Witke, and F. Costantini. 2010. Actin depolymerizing factors cofilin1 and destrin are required for ureteric bud branching morphogenesis. *PLoS Genet*. 6:e1001176.

Kuwahara, K., T. Barrientos, G.C. Pipes, S. Li, and E.N. Olson. 2005. Muscle-specific signaling mechanism that links actin dynamics to serum response factor. *Mol Cell Biol*. 25:3173-3181.

Kuwahara, K., G.C. Teg Pipes, J. McAnally, J.A. Richardson, J.A. Hill, R. Bassel-Duby, and E.N. Olson. 2007. Modulation of adverse cardiac remodeling by STARS, a mediator of MEF2 signaling and SRF activity. *J Clin Invest*. 117:1324-1334.

Lausecker, F., X. Tian, K. Inoue, Z. Wang, C.E. Pedigo, H. Hassan, C. Liu, M. Zimmer, S. Jinno, A.L. Huckle, H. Hamidi, R.S. Ross, R. Zent, C. Ballestrem, R. Lennon, and S. Ishibe. 2018. Vinculin is required to maintain glomerular barrier integrity. *Kidney Int*. 93:643-655.

Lawson, C.D., and K. Burridge. 2014. The on-off relationship of Rho and Rac during integrin-mediated adhesion and cell migration. *Small GTPases*. 5:e27958.

Lawson, D., M. Harrison, and C. Shapland. 1997. Fibroblast transgelin and smooth muscle SM22alpha are the same protein, the expression of which is down-regulated in many cell lines. *Cell Motil Cytoskeleton*. 38:250-257.

Lea, P.J., M. Silverman, R. Hegele, and M.J. Hollenberg. 1989. Tridimensional ultrastructure of glomerular capillary endothelium revealed by high-resolution scanning electron microscopy. *Microvasc Res*. 38:296-308.

Lehtonen, S., F. Zhao, and E. Lehtonen. 2002. CD2-associated protein directly interacts with the actin cytoskeleton. *Am J Physiol Renal Physiol*. 283:F734-743.

Lennon, R., A. Byron, J.D. Humphries, M.J. Randles, A. Carisey, S. Murphy, D. Knight, P.E. Brenchley, R. Zent, and M.J. Humphries. 2014a. Global analysis reveals the complexity of the human glomerular extracellular matrix. *J Am Soc Nephrol*. 25:939-951.

Lennon, R., M.J. Randles, and M.J. Humphries. 2014b. The importance of podocyte adhesion for a healthy glomerulus. *Front Endocrinol (Lausanne)*. 5:160.

Lenter, M., H. Uhlig, A. Hamann, P. Jeno, B. Imhof, and D. Vestweber. 1993. A monoclonal antibody against an activation epitope on mouse integrin chain beta 1

blocks adhesion of lymphocytes to the endothelial integrin alpha 6 beta 1. *Proc Natl Acad Sci USA*. 90:9051-9055.

Leung, T., X.Q. Chen, I. Tan, E. Manser, and L. Lim. 1998. Myotonic dystrophy kinase-related Cdc42-binding kinase acts as a Cdc42 effector in promoting cytoskeletal reorganization. *Mol Cell Biol*. 18:130-140.

Li, F., and H.N. Higgs. 2003. The mouse Formin mDia1 is a potent actin nucleation factor regulated by autoinhibition. *Curr Biol*. 13:1335-1340.

Li, L., Z. Liu, B. Mercer, P. Overbeek, and E.N. Olson. 1997. Evidence for serum response factor-mediated regulatory networks governing SM22alpha transcription in smooth, skeletal, and cardiac muscle cells. *Dev Biol*. 187:311-321.

Li, L., J.M. Miano, P. Cserjesi, and E.N. Olson. 1996. SM22 alpha, a marker of adult smooth muscle, is expressed in multiple myogenic lineages during embryogenesis. *Circ Res*. 78:188-195.

Liu, H.W., A.J. Halayko, D.J. Fernandes, G.S. Harmon, J.A. McCauley, P. Kocieniewski, J. McConville, Y. Fu, S.M. Forsythe, P. Kogut, S. Bellam, M. Dowell, J. Churchill, H. Lesso, K. Kassiri, R.W. Mitchell, M.B. Hershenson, B. Camoretti-Mercado, and J. Solway. 2003. The RhoA/Rho kinase pathway regulates nuclear localization of serum response factor. *Am J Respir Cell Mol Biol*. 29:39-47.

Liu, R., M.M. Hossain, X. Chen, and J.P. Jin. 2017. Mechanoregulation of SM22alpha/Transgelin. *Biochemistry*. 56:5526-5538.

Lu, X., N. Li, N. Shushakova, R. Schmitt, J. Menne, N. Susnik, M. Meier, M. Leitges, H. Haller, F. Gueler, and S. Rong. 2012. C57BL/6 and 129/Sv mice: genetic difference to renal ischemia-reperfusion. *J Nephrol*. 25:738-743.

Lv, P., S.B. Miao, Y.N. Shu, L.H. Dong, G. Liu, X.L. Xie, M. Gao, Y.C. Wang, Y.J. Yin, X.J. Wang, and M. Han. 2012. Phosphorylation of smooth muscle 22alpha facilitates angiotensin II-induced ROS production via activation of the PKCdelta-P47phox axis through release of PKCdelta and actin dynamics and is associated with hypertrophy and hyperplasia of vascular smooth muscle cells in vitro and in vivo. *Circ Res*. 111:697-707.

Mack, C.P., A.V. Somlyo, M. Hautmann, A.P. Somlyo, and G.K. Owens. 2001. Smooth muscle differentiation marker gene expression is regulated by RhoA-mediated actin polymerization. *J Biol Chem*. 276:341-347.

Maekawa, M., T. Ishizaki, S. Boku, N. Watanabe, A. Fujita, A. Iwamatsu, T. Obinata, K. Ohashi, K. Mizuno, and S. Narumiya. 1999. Signaling from Rho to the actin cytoskeleton through protein kinases ROCK and LIM-kinase. *Science*. 285:895-898.

Mahadeva, H., G. Brooks, D. Lodwick, N.W. Chong, and N.J. Samani. 2002. ms1, a novel stress-responsive, muscle-specific gene that is up-regulated in the early stages of pressure overload-induced left ventricular hypertrophy. *FEBS Lett*. 521:100-104.

Marshall, C.B., R.D. Krofft, M.J. Blonski, J. Kowalewska, C.M. Logar, J.W. Pippin, F. Kim, R. Feil, C.E. Alpers, and S.J. Shankland. 2011. Role of smooth muscle protein SM22alpha in glomerular epithelial cell injury. *Am J Physiol Renal Physiol*. 300:F1026-1042.

Matejas, V., B. Hinkes, F. Alkandari, L. Al-Gazali, E. Annexstad, M.B. Aytac, M. Barrow, K. Blahova, D. Bockenhauer, H.I. Cheong, I. Maruniak-Chudek, P. Cochat, J. Dotsch, P. Gajjar, R.C. Hennekam, F. Janssen, M. Kagan, A. Kariminejad, M.J. Kemper, J. Koenig, J. Kogan, H.Y. Kroes, E. Kuwertz-Broking, A.F. Lewanda, A. Medeira, J. Muscheites, P. Niaudet, M. Pierson, A. Saggar, L. Seaver, M. Suri, A.

Tsygin, E. Wuhl, A. Zurowska, S. Uebe, F. Hildebrandt, C. Antignac, and M. Zenker. 2010. Mutations in the human laminin beta2 (LAMB2) gene and the associated phenotypic spectrum. *Hum Mutat*. 31:992-1002.

Matsumoto, S., S. Fujii, and A. Kikuchi. 2017. Arl4c is a key regulator of tubulogenesis and tumourigenesis as a target gene of Wnt-beta-catenin and growth factor-Ras signalling. *J Biochem*. 161:27-35.

Matsumoto, S., S. Fujii, A. Sato, S. Ibuka, Y. Kagawa, M. Ishii, and A. Kikuchi. 2014. A combination of Wnt and growth factor signaling induces Arl4c expression to form epithelial tubular structures. *EMBO J*. 33:702-718.

McGough, A., B. Pope, W. Chiu, and A. Weeds. 1997. Cofilin changes the twist of F-actin: implications for actin filament dynamics and cellular function. *J Cell Biol*. 138:771-781.

McIntosh, I., S.D. Dreyer, M.V. Clough, J.A. Dunston, W. Eyaid, C.M. Roig, T. Montgomery, S. Ala-Mello, I. Kaitila, A. Winterpacht, B. Zabel, M. Frydman, W.G. Cole, C.A. Francomano, and B. Lee. 1998. Mutation analysis of LMX1B gene in nail-patella syndrome patients. *Am J Hum Genet*. 63:1651-1658.

Miao, J., Q. Fan, Q. Cui, H. Zhang, L. Chen, S. Wang, N. Guan, Y. Guan, and J. Ding. 2009. Newly identified cytoskeletal components are associated with dynamic changes of podocyte foot processes. *Nephrol Dial Transplant*. 24:3297-3305.

Michele, D.E., and K.P. Campbell. 2003. Dystrophin-glycoprotein complex: post-translational processing and dystroglycan function. *J Biol Chem*. 278:15457-15460.

Miner, J.H. 2012. The glomerular basement membrane. *Exp Cell Res*. 318:973-978.

Miner, J.H., R. Morello, K.L. Andrews, C. Li, C. Antignac, A.S. Shaw, and B. Lee. 2002. Transcriptional induction of slit diaphragm genes by Lmx1b is required in podocyte differentiation. *J Clin Invest*. 109:1065-1072.

Moeller, M.J., S.K. Sanden, A. Soofi, R.C. Wiggins, and L.B. Holzman. 2003. Podocyte-specific expression of cre recombinase in transgenic mice. *Genesis*. 35:39-42.

Moeller, M.J., and V. Tenten. 2013. Renal albumin filtration: alternative models to the standard physical barriers. *Nat Rev Nephrol*. 9:266-277.

Molinie, N., and A. Gautreau. 2018. The Arp2/3 Regulatory System and Its Deregulation in Cancer. *Physiol Rev*. 98:215-238.

Morello, R., and B. Lee. 2002. Insight into podocyte differentiation from the study of human genetic disease: nail-patella syndrome and transcriptional regulation in podocytes. *Pediatr Res*. 51:551-558.

Morello, R., G. Zhou, S.D. Dreyer, S.J. Harvey, Y. Ninomiya, P.S. Thorner, J.H. Miner, W. Cole, A. Winterpacht, B. Zabel, K.C. Oberg, and B. Lee. 2001. Regulation of glomerular basement membrane collagen expression by LMX1B contributes to renal disease in nail patella syndrome. *Nat Genet*. 27:205-208.

Moriyama, K., K. Iida, and I. Yahara. 1996. Phosphorylation of Ser-3 of cofilin regulates its essential function on actin. *Genes Cells*. 1:73-86.

Mullins, R.D., J.A. Heuser, and T.D. Pollard. 1998. The interaction of Arp2/3 complex with actin: nucleation, high affinity pointed end capping, and formation of branching networks of filaments. *Proc Natl Acad Sci USA*. 95:6181-6186.

Mundel, P., H.W. Heid, T.M. Mundel, M. Kruger, J. Reiser, and W. Kriz. 1997. Synaptopodin: an actin-associated protein in telencephalic dendrites and renal podocytes. *J Cell Biol*. 139:193-204.

Mundel, P., and J. Reiser. 2010. Proteinuria: an enzymatic disease of the podocyte? *Kidney Int*. 77:571-580.

Muzumdar, M.D., B. Tasic, K. Miyamichi, L. Li, and L. Luo. 2007. A global double-fluorescent Cre reporter mouse. *Genesis*. 45:593-605.

Nair, U.B., P.B. Joel, Q. Wan, S. Lowey, M.A. Rould, and K.M. Trybus. 2008. Crystal structures of monomeric actin bound to cytochalasin D. *J Mol Biol*. 384:848-864.

Nakagawa, O., K. Fujisawa, T. Ishizaki, Y. Saito, K. Nakao, and S. Narumiya. 1996. ROCK-I and ROCK-II, two isoforms of Rho-associated coiled-coil forming protein serine/threonine kinase in mice. *FEBS Lett*. 392:189-193.

Newell-Litwa, K.A., R. Horwitz, and M.L. Lamers. 2015. Non-muscle myosin II in disease: mechanisms and therapeutic opportunities. *Dis Model Mech*. 8:1495-1515.

Nishiuchi, R., O. Murayama, H. Fujiwara, J. Gu, T. Kawakami, S. Aimoto, Y. Wada, and K. Sekiguchi. 2003. Characterization of the ligand-binding specificities of integrin alpha3beta1 and alpha6beta1 using a panel of purified laminin isoforms containing distinct alpha chains. *J Biochem*. 134:497-504.

Noakes, P.G., J.H. Miner, M. Gautam, J.M. Cunningham, J.R. Sanes, and J.P. Merlie. 1995. The renal glomerulus of mice lacking s-laminin/laminin beta 2: nephrosis despite molecular compensation by laminin beta 1. *Nat Genet*. 10:400-406.

Nobes, C.D., and A. Hall. 1995. Rho, rac, and cdc42 GTPases regulate the assembly of multimolecular focal complexes associated with actin stress fibers, lamellipodia, and filopodia. *Cell*. 81:53-62.

Ogawa, A., M. Sakatsume, X. Wang, Y. Sakamaki, Y. Tsubata, B. Alchi, T. Kuroda, H. Kawachi, I. Narita, F. Shimizu, and F. Gejyo. 2007. SM22alpha: the novel phenotype marker of injured glomerular epithelial cells in anti-glomerular basement membrane nephritis. *Nephron Exp Nephrol*. 106:e77-87.

Ohashi, K. 2015. Roles of cofilin in development and its mechanisms of regulation. *Dev Growth Differ*. 57:275-290.

Ohashi, K., S. Fujiwara, T. Watanabe, H. Kondo, T. Kiuchi, M. Sato, and K. Mizuno. 2011. LIM kinase has a dual role in regulating lamellipodium extension by decelerating the rate of actin retrograde flow and the rate of actin polymerization. *J Biol Chem*. 286:36340-36351.

Ounzain, S., S. Kobayashi, R.E. Peterson, A. He, A. Motterle, N.J. Samani, D.R. Menick, W.T. Pu, Q. Liang, and N.W. Chong. 2012. Cardiac expression of ms1/STARS, a novel gene involved in cardiac development and disease, is regulated by GATA4. *Mol Cell Biol*. 32:1830-1843.

Page, M.J., B. Amess, R.R. Townsend, R. Parekh, A. Herath, L. Brusten, M.J. Zvelebil, R.C. Stein, M.D. Waterfield, S.C. Davies, and M.J. O'Hare. 1999. Proteomic definition of normal human luminal and myoepithelial breast cells purified from reduction mammoplasties. *Proc Natl Acad Sci U S A*. 96:12589-12594.

Paulsson, M. 1992. Basement membrane proteins: structure, assembly, and cellular interactions. *Crit Rev Biochem Mol Biol*. 27:93-127.

Pavenstadt, H., W. Kriz, and M. Kretzler. 2003. Cell biology of the glomerular podocyte. *Physiol Rev*. 83:253-307.

Perico, L., S. Conti, A. Benigni, and G. Remuzzi. 2016. Podocyte-actin dynamics in health and disease. *Nat Rev Nephrol*. 12:692-710.

Pollard, T.D. 2016. Actin and Actin-Binding Proteins. *Cold Spring Harb Perspect Biol*. 8.

Pollard, T.D. 2017. What We Know and Do Not Know About Actin. *Handb Exp Pharmacol*. 235:331-347.

Pollard, T.D., and G.G. Borisy. 2003. Cellular motility driven by assembly and disassembly of actin filaments. *Cell*. 112:453-465.

Pollard, T.D., and J.A. Cooper. 2009. Actin, a central player in cell shape and movement. *Science*. 326:1208-1212.

Poukkula, M., E. Kremneva, M. Serlachius, and P. Lappalainen. 2011. Actin-depolymerizing factor homology domain: a conserved fold performing diverse roles in cytoskeletal dynamics. *Cytoskeleton (Hoboken)*. 68:471-490.

Pozzi, A., G. Jarad, G.W. Moeckel, S. Coffa, X. Zhang, L. Gewin, V. Eremina, B.G. Hudson, D.B. Borza, R.C. Harris, L.B. Holzman, C.L. Phillips, R. Fassler, S.E. Quaggin, J.H. Miner, and R. Zent. 2008. Beta1 integrin expression by podocytes is required to maintain glomerular structural integrity. *Dev Biol*. 316:288-301.

Preller, M., and D.J. Manstein. 2013. Myosin structure, allostery, and mechano-chemistry. *Structure*. 21:1911-1922.

Pressman, C.L., H. Chen, and R.L. Johnson. 2000. LMX1B, a LIM homeodomain class transcription factor, is necessary for normal development of multiple tissues in the anterior segment of the murine eye. *Genesis*. 26:15-25.

Price, L.S., J. Leng, M.A. Schwartz, and G.M. Bokoch. 1998. Activation of Rac and Cdc42 by integrins mediates cell spreading. *Mol Biol Cell*. 9:1863-1871.

Pries, A.R., T.W. Secomb, and P. Gaehtgens. 2000. The endothelial surface layer. *Pflugers Arch*. 440:653-666.

Pring, M., M. Evangelista, C. Boone, C. Yang, and S.H. Zigmond. 2003. Mechanism of formin-induced nucleation of actin filaments. *Biochemistry*. 42:486-496.

Pruyne, D., M. Evangelista, C. Yang, E. Bi, S. Zigmond, A. Bretscher, and C. Boone. 2002. Role of formins in actin assembly: nucleation and barbed-end association. *Science*. 297:612-615.

Pyke, C., P. Kristensen, P.B. Ostergaard, P.S. Oturai, and J. Romer. 1997. Proteoglycan expression in the normal rat kidney. *Nephron*. 77:461-470.

Qiu, P., X.H. Feng, and L. Li. 2003. Interaction of Smad3 and SRF-associated complex mediates TGF-beta1 signals to regulate SM22 transcription during myofibroblast differentiation. *J Mol Cell Cardiol*. 35:1407-1420.

Qiu, P., R.P. Ritchie, Z. Fu, D. Cao, J. Cumming, J.M. Miano, D.Z. Wang, H.J. Li, and L. Li. 2005. Myocardin enhances Smad3-mediated transforming growth factor-beta1 signaling in a CArG box-independent manner: Smad-binding element is an important cis element for SM22alpha transcription in vivo. *Circ Res*. 97:983-991.

Rane, C.K., and A. Minden. 2014. P21 activated kinases: structure, regulation, and functions. *Small GTPases*. 5.

Rao, P.V., and R. Maddala. 2006. The role of the lens actin cytoskeleton in fiber cell elongation and differentiation. *Semin Cell Dev Biol*. 17:698-711.

Rascle, A., T. Neumann, A.S. Raschta, A. Neumann, E. Heining, J. Kastner, and R. Witzgall. 2009. The LIM-homeodomain transcription factor LMX1B regulates expression of NF-kappa B target genes. *Exp Cell Res*. 315:76-96.

Rattan, S., and M. Ali. 2015. Role of SM22 in the differential regulation of phasic vs. tonic smooth muscle. *Am J Physiol Gastrointest Liver Physiol*. 308:G605-612.

Reiser, J., W. Kriz, M. Kretzler, and P. Mundel. 2000. The glomerular slit diaphragm is a modified adherens junction. *J Am Soc Nephrol*. 11:1-8.

Reitsma, S., D.W. Slaaf, H. Vink, M.A. van Zandvoort, and M.G. oude Egbrink. 2007. The endothelial glycocalyx: composition, functions, and visualization. *Pflugers Arch*. 454:345-359.

Renwick, J.H., and S.D. Lawler. 1955. Genetical linkage between the ABO and nail-patella loci. *Ann Hum Genet*. 19:312-331.

Riddle, R.D., M. Ensini, C. Nelson, T. Tsuchida, T.M. Jessell, and C. Tabin. 1995. Induction of the LIM homeobox gene Lmx1 by WNT7a establishes dorsoventral pattern in the vertebrate limb. *Cell*. 83:631-640.

Ridley, A.J., and A. Hall. 1992. The small GTP-binding protein rho regulates the assembly of focal adhesions and actin stress fibers in response to growth factors. *Cell*. 70:389-399.

Ridley, A.J., H.F. Paterson, C.L. Johnston, D. Diekmann, and A. Hall. 1992. The small GTP-binding protein rac regulates growth factor-induced membrane ruffling. *Cell*. 70:401-410.

Robins, R., C. Baldwin, L. Aoudjit, J.F. Cote, I.R. Gupta, and T. Takano. 2017. Rac1 activation in podocytes induces the spectrum of nephrotic syndrome. *Kidney Int*. 92:349-364.

Rodewald, R., and M.J. Karnovsky. 1974. Porous substructure of the glomerular slit diaphragm in the rat and mouse. *J Cell Biol*. 60:423-433.

Rodnick-Smith, M., Q. Luan, S.L. Liu, and B.J. Nolen. 2016. Role and structural mechanism of WASP-triggered conformational changes in branched actin filament nucleation by Arp2/3 complex. *Proc Natl Acad Sci USA*. 113:E3834-3843.

Rohatgi, R., L. Ma, H. Miki, M. Lopez, T. Kirchhausen, T. Takenawa, and M.W. Kirschner. 1999. The interaction between N-WASP and the Arp2/3 complex links Cdc42-dependent signals to actin assembly. *Cell*. 97:221-231.

Rohr, C., J. Prestel, L. Heidet, H. Hosser, W. Kriz, R.L. Johnson, C. Antignac, and R. Witzgall. 2002. The LIM-homeodomain transcription factor Lmx1b plays a crucial role in podocytes. *J Clin Invest*. 109:1073-1082.

Roselli, S., L. Heidet, M. Sich, A. Henger, M. Kretzler, M.C. Gubler, and C. Antignac. 2004. Early glomerular filtration defect and severe renal disease in podocin-deficient mice. *Mol Cell Biol*. 24:550-560.

Rouiller, I., X.P. Xu, K.J. Amann, C. Egile, S. Nickell, D. Nicastro, R. Li, T.D. Pollard, N. Volkmann, and D. Hanein. 2008. The structural basis of actin filament branching by the Arp2/3 complex. *J Cell Biol*. 180:887-895.

Russell, A.P., M.A. Wallace, M. Kalanon, E. Zacharewicz, P.A. Della Gatta, A. Garnham, and S. Lamon. 2017. Striated muscle activator of Rho signalling (STARS) is reduced in ageing human skeletal muscle and targeted by miR-628-5p. *Acta Physiol (Oxf)*. 220:263-274.

Sachs, N., M. Kreft, M.A. van den Bergh Weerman, A.J. Beynon, T.A. Peters, J.J. Weening, and A. Sonnenberg. 2006. Kidney failure in mice lacking the tetraspanin CD151. *J Cell Biol*. 175:33-39.

Sachs, N., and A. Sonnenberg. 2013. Cell-matrix adhesion of podocytes in physiology and disease. *Nat Rev Nephrol*. 9:200-210.

Sadok, A., and C.J. Marshall. 2014. Rho GTPases: masters of cell migration. *Small GTPases*. 5:e29710.

Sagot, I., A.A. Rodal, J. Moseley, B.L. Goode, and D. Pellman. 2002. An actin nucleation mechanism mediated by Bni1 and profilin. *Nat Cell Biol*. 4:626-631.

Saleem, M.A., M.J. O'Hare, J. Reiser, R.J. Coward, C.D. Inward, T. Farren, C.Y. Xing, L. Ni, P.W. Mathieson, and P. Mundel. 2002. A conditionally immortalized human podocyte cell line demonstrating nephrin and podocin expression. *J Am Soc Nephrol*. 13:630-638.

Sampath, P., and T.D. Pollard. 1991. Effects of cytochalasin, phalloidin, and pH on the elongation of actin filaments. *Biochemistry*. 30:1973-1980.

Sanders, L.C., F. Matsumura, G.M. Bokoch, and P. de Lanerolle. 1999. Inhibition of myosin light chain kinase by p21-activated kinase. *Science*. 283:2083-2085.

Sasaki, H., K. Marusugi, J. Kimura, H. Kitamura, K. Nagasaki, D. Torigoe, T. Agui, and N. Sasaki. 2015. Genetic background-dependent diversity in renal failure caused by the tensin2 gene deficiency in the mouse. *Biomed Res*. 36:323-330.

Satchell, S. 2013. The role of the glomerular endothelium in albumin handling. *Nat Rev Nephrol*. 9:717-725.

Schell, C., and T.B. Huber. 2017. The Evolving Complexity of the Podocyte Cytoskeleton. *J Am Soc Nephrol*. 28:3166-3174.

Schönig, K., F. Schwenk, K. Rajewsky, and H. Bujard. 2002. Stringent doxycycline dependent control of CRE recombinase in vivo. *Nucleic Acids Res*. 30:e134.

Schwarz, K., M. Simons, J. Reiser, M.A. Saleem, C. Faul, W. Kriz, A.S. Shaw, L.B. Holzman, and P. Mundel. 2001. Podocin, a raft-associated component of the glomerular slit diaphragm, interacts with CD2AP and nephrin. *J Clin Invest*. 108:1621-1629.

Scott, R.P., S.P. Hawley, J. Ruston, J. Du, C. Brakebusch, N. Jones, and T. Pawson. 2012. Podocyte-specific loss of Cdc42 leads to congenital nephropathy. *J Am Soc Nephrol*. 23:1149-1154.

Seefeldt, T., S.O. Bohman, H. Jorgen, H.J. Gundersen, A.B. Maunsbach, V.P. Petersen, and S. Olsen. 1981. Quantitative relationship between glomerular foot process width and proteinuria in glomerulonephritis. *Lab Invest*. 44:541-546.

Sellin, L., T.B. Huber, P. Gerke, I. Quack, H. Pavenstadt, and G. Walz. 2003. NEPH1 defines a novel family of podocin interacting proteins. *FASEB J*. 17:115-117.

Shankland, S.J., J.W. Pippin, and J.S. Duffield. 2014. Progenitor cells and podocyte regeneration. *Semin Nephrol*. 34:418-428.

Shapland, C., J.J. Hsuan, N.F. Totty, and D. Lawson. 1993. Purification and properties of transgelin: a transformation and shape change sensitive actin-gelling protein. *J Cell Biol*. 121:1065-1073.

Shapland, C., P. Lowings, and D. Lawson. 1988. Identification of new actin-associated polypeptides that are modified by viral transformation and changes in cell shape. *J Cell Biol*. 107:153-161.

Shibata, S., M. Nagase, and T. Fujita. 2006. Fluvastatin ameliorates podocyte injury in proteinuric rats via modulation of excessive Rho signaling. *J Am Soc Nephrol*. 17:754-764.

Shigehara, T., C. Zaragoza, C. Kitiyakara, H. Takahashi, H. Lu, M. Moeller, L.B. Holzman, and J.B. Kopp. 2003. Inducible podocyte-specific gene expression in transgenic mice. *J Am Soc Nephrol*. 14:1998-2003.

Shih, N.Y., J. Li, V. Karpitskii, A. Nguyen, M.L. Dustin, O. Kanagawa, J.H. Miner, and A.S. Shaw. 1999. Congenital nephrotic syndrome in mice lacking CD2-associated protein. *Science*. 286:312-315.

Shirato, I. 2002. Podocyte process effacement in vivo. *Microsc Res Tech*. 57:241-246.

Shirato, I., H. Hosser, K. Kimura, T. Sakai, Y. Tomino, and W. Kriz. 1996. The development of focal segmental glomerulosclerosis in masugi nephritis is based on progressive podocyte damage. *Virchows Arch*. 429:255-273.

Shoji, K., K. Ohashi, K. Sampei, M. Oikawa, and K. Mizuno. 2012. Cytochalasin D acts as an inhibitor of the actin-cofilin interaction. *Biochem Biophys Res Commun*. 424:52-57.

Shu, Y.N., F. Zhang, W. Bi, L.H. Dong, D.D. Zhang, R. Chen, P. Lv, X.L. Xie, Y.L. Lin, Z.Y. Xue, H. Li, S.B. Miao, L.L. Zhao, H. Wang, and M. Han. 2015. SM22alpha inhibits vascular inflammation via stabilization of IkappaBalpha in vascular smooth muscle cells. *J Mol Cell Cardiol*. 84:191-199.

Sison, K., V. Eremina, H. Baelde, W. Min, M. Hirashima, I.G. Fantus, and S.E. Quaggin. 2010. Glomerular structure and function require paracrine, not autocrine, VEGF-VEGFR-2 signaling. *J Am Soc Nephrol*. 21:1691-1701.

Siton-Mendelson, O., and A. Bernheim-Groswasser. 2017. Functional Actin Networks under Construction: The Cooperative Action of Actin Nucleation and Elongation Factors. *Trends Biochem Sci*. 42:414-430.

Sjoblom, B., A. Salmazo, and K. Djinovic-Carugo. 2008. Alpha-actinin structure and regulation. *Cell Mol Life Sci*. 65:2688-2701.

Smoyer, W.E., P. Mundel, A. Gupta, and M.J. Welsh. 1997. Podocyte alpha-actinin induction precedes foot process effacement in experimental nephrotic syndrome. *Am J Physiol*. 273:F150-157.

St John, P.L., and D.R. Abrahamson. 2001. Glomerular endothelial cells and podocytes jointly synthesize laminin-1 and -11 chains. *Kidney Int*. 60:1037-1046.

Steffen, A., T.E. Stradal, and K. Rottner. 2017. Signalling Pathways Controlling Cellular Actin Organization. *Handb Exp Pharmacol*. 235:153-178.

Stepanova, N. 2016. Identification and characterization of LMX1B target genes. *Universität Regensburg*.

Sterk, L.M., A.A. de Melker, D. Kramer, I. Kuikman, A. Chand, N. Claessen, J.J. Weening, and A. Sonnenberg. 1998. Glomerular extracellular matrix components and integrins. *Cell Adhes Commun*. 5:177-192.

Subramanian, B., H. Sun, P. Yan, V.T. Charoonratana, H.N. Higgs, F. Wang, K.V. Lai, D.M. Valenzuela, E.J. Brown, J.S. Schlondorff, and M.R. Pollak. 2016. Mice with mutant Inf2 show impaired podocyte and slit diaphragm integrity in response to protamine-induced kidney injury. *Kidney Int*. 90:363-372.

Sugihara, K., N. Nakatsuji, K. Nakamura, K. Nakao, R. Hashimoto, H. Otani, H. Sakagami, H. Kondo, S. Nozawa, A. Aiba, and M. Katsuki. 1998. Rac1 is required for the formation of three germ layers during gastrulation. *Oncogene*. 17:3427-3433.

Sugimoto, H., Y. Hamano, D. Charytan, D. Cosgrove, M. Kieran, A. Sudhakar, and R. Kalluri. 2003. Neutralization of circulating vascular endothelial growth factor (VEGF) by anti-VEGF antibodies and soluble VEGF receptor 1 (sFlt-1) induces proteinuria. *J Biol Chem*. 278:12605-12608.

Sugimoto, H., T.M. Mundel, M. Sund, L. Xie, D. Cosgrove, and R. Kalluri. 2006. Bone-marrow-derived stem cells repair basement membrane collagen defects and reverse genetic kidney disease. *Proc Natl Acad Sci U S A*. 103:7321-7326.

Suh, J.H., G. Jarad, R.G. VanDeVoorde, and J.H. Miner. 2011. Forced expression of laminin beta1 in podocytes prevents nephrotic syndrome in mice lacking laminin beta2, a model for Pierson syndrome. *Proc Natl Acad Sci U S A*. 108:15348-15353.

Suh, J.H., and J.H. Miner. 2013. The glomerular basement membrane as a barrier to albumin. *Nat Rev Nephrol*. 9:470-477.

Suleiman, H., D. Heudobler, A.S. Raschta, Y. Zhao, Q. Zhao, I. Hertting, H. Vitzthum, M.J. Moeller, L.B. Holzman, R. Rachel, R. Johnson, H. Westphal, A. Rascle, and R. Witzgall. 2007. The podocyte-specific inactivation of Lmx1b, Ldb1 and E2a yields new insight into a transcriptional network in podocytes. *Dev Biol*. 304:701-712.

Suleiman, H., L. Zhang, R. Roth, J.E. Heuser, J.H. Miner, A.S. Shaw, and A. Dani. 2013. Nanoscale protein architecture of the kidney glomerular basement membrane. *Elife*. 2:e01149.

Sun, H., J.S. Schlondorff, E.J. Brown, H.N. Higgs, and M.R. Pollak. 2011. Rho activation of mDia formins is modulated by an interaction with inverted formin 2 (INF2). *Proc Natl Acad Sci USA*. 108:2933-2938.

Svitkina, T.M., and G.G. Borisy. 1999. Arp2/3 complex and actin depolymerizing factor/cofilin in dendritic organization and treadmilling of actin filament array in lamellipodia. *J Cell Biol*. 145:1009-1026.

Svitkina, T.M., A.B. Verkhovsky, K.M. McQuade, and G.G. Borisy. 1997. Analysis of the actin-myosin II system in fish epidermal keratocytes: mechanism of cell body translocation. *J Cell Biol*. 139:397-415.

Sweeney, E., A. Fryer, R. Mountford, A. Green, and I. McIntosh. 2003. Nail patella syndrome: a review of the phenotype aided by developmental biology. *J Med Genet*. 40:153-162.

Tao, J., C. Polumbo, K. Reidy, M. Sweetwyne, and K. Susztak. 2014. A multicolor podocyte reporter highlights heterogeneous podocyte changes in focal segmental glomerulosclerosis. *Kidney Int*. 85:972-980.

Tcherkezian, J., and N. Lamarche-Vane. 2007. Current knowledge of the large RhoGAP family of proteins. *Biol Cell*. 99:67-86.

Tian, X., J.J. Kim, S.M. Monkley, N. Gotoh, R. Nandez, K. Soda, K. Inoue, D.M. Balkin, H. Hassan, S.H. Son, Y. Lee, G. Moeckel, D.A. Calderwood, L.B. Holzman, D.R. Critchley, R. Zent, J. Reiser, and S. Ishibe. 2014. Podocyte-associated talin1 is critical for glomerular filtration barrier maintenance. *J Clin Invest*. 124:1098-1113.

Totsukawa, G., Y. Yamakita, S. Yamashiro, D.J. Hartshorne, Y. Sasaki, and F. Matsumura. 2000. Distinct roles of ROCK (Rho-kinase) and MLCK in spatial regulation of MLC phosphorylation for assembly of stress fibers and focal adhesions in 3T3 fibroblasts. *J Cell Biol*. 150:797-806.

Toyoshima, Y.Y., S.J. Kron, E.M. McNally, K.R. Niebling, C. Toyoshima, and J.A. Spudich. 1987. Myosin subfragment-1 is sufficient to move actin filaments in vitro. *Nature*. 328:536-539.

Troidl, K., I. Ruding, W.J. Cai, Y. Mucke, L. Grossekettler, I. Piotrowska, H. Apfelbeck, W. Schierling, O.L. Volger, A.J. Horrevoets, K. Grote, T. Schmitz-Rixen, W. Schaper, and C. Troidl. 2009. Actin-binding rho activating protein (Abra) is essential for fluid shear stress-induced arteriogenesis. *Arterioscler Thromb Vasc Biol*. 29:2093-2101.

Umemoto, S., A.R. Bengur, and J.R. Sellers. 1989. Effect of multiple phosphorylations of smooth muscle and cytoplasmic myosins on movement in an in vitro motility assay. *J Biol Chem*. 264:1431-1436.

Urlinger, S., U. Baron, M. Thellmann, M.T. Hasan, H. Bujard, and W. Hillen. 2000. Exploring the sequence space for tetracycline-dependent transcriptional activators:

novel mutations yield expanded range and sensitivity. *Proc Natl Acad Sci USA*. 97:7963-7968.

Vivante, A., and F. Hildebrandt. 2016. Exploring the genetic basis of early-onset chronic kidney disease. *Nat Rev Nephrol*. 12:133-146.

Vogel, A., C. Rodriguez, W. Warnken, and J.C. Izpisua Belmonte. 1995. Dorsal cell fate specified by chick Lmx1 during vertebrate limb development. *Nature*. 378:716-720.

Vollrath, D., V.L. Jaramillo-Babb, M.V. Clough, I. McIntosh, K.M. Scott, P.R. Lichter, and J.E. Richards. 1998. Loss-of-function mutations in the LIM-homeodomain gene, LMX1B, in nail-patella syndrome. *Hum Mol Genet*. 7:1091-1098.

Wakatsuki, T., B. Schwab, N.C. Thompson, and E.L. Elson. 2001. Effects of cytochalasin D and latrunculin B on mechanical properties of cells. *J Cell Sci*. 114:1025-1036.

Wallace, M.A., M.B. Hock, B.C. Hazen, A. Kralli, R.J. Snow, and A.P. Russell. 2011. Striated muscle activator of Rho signalling (STARS) is a PGC-1alpha/oestrogen-related receptor-alpha target gene and is upregulated in human skeletal muscle after endurance exercise. *J Physiol*. 589:2027-2039.

Wallace, M.A., and A.P. Russell. 2013. Striated muscle activator of Rho signaling is required for myotube survival but does not influence basal protein synthesis or degradation. *Am J Physiol Cell Physiol*. 305:C414-426.

Wang, L., M.J. Ellis, J.A. Gomez, W. Eisner, W. Fennell, D.N. Howell, P. Ruiz, T.A. Fields, and R.F. Spurney. 2012a. Mechanisms of the proteinuria induced by Rho GTPases. *Kidney Int*. 81:1075-1085.

Wang, W., S. Wang, X. Liu, R. Gu, Y. Zhu, P. Zhang, Y. Liu, and Y. Zhou. 2018. Knockdown of ARL4C inhibits osteogenic differentiation of human adipose-derived stem cells through disruption of the Wnt signaling pathway. *Biochem Biophys Res Commun*. 497:256-263.

Wang, X., M. Sakatsume, Y. Sakamaki, S. Inomata, T. Yamamoto, and I. Narita. 2012b. Quantitative histological analysis of SM22alpha (transgelin) in an adriamycin-induced focal segmental glomerulosclerosis model. *Nephron Exp Nephrol*. 120:e1-11.

Wartiovaara, J., L.G. Ofverstedt, J. Khoshnoodi, J. Zhang, E. Makela, S. Sandin, V. Ruotsalainen, R.H. Cheng, H. Jalanko, U. Skoglund, and K. Tryggvason. 2004. Nephrin strands contribute to a porous slit diaphragm scaffold as revealed by electron tomography. *J Clin Invest*. 114:1475-1483.

Wei, C., C.C. Moller, M.M. Altintas, J. Li, K. Schwarz, S. Zacchigna, L. Xie, A. Henger, H. Schmid, M.P. Rastaldi, P. Cowan, M. Kretzler, R. Parrilla, M. Bendayan, V. Gupta, B. Nikolic, R. Kalluri, P. Carmeliet, P. Mundel, and J. Reiser. 2008. Modification of kidney barrier function by the urokinase receptor. *Nat Med*. 14:55-63.

Wei, S.M., C.G. Xie, Y. Abe, and J.T. Cai. 2009. ADP-ribosylation factor like 7 (ARL7) interacts with alpha-tubulin and modulates intracellular vesicular transport. *Biochem Biophys Res Commun*. 384:352-356.

Weinbaum, S., J.M. Tarbell, and E.R. Damiano. 2007. The structure and function of the endothelial glycocalyx layer. *Annu Rev Biomed Eng*. 9:121-167.

Wessely, O., D.M. Cerqueira, U. Tran, V. Kumar, J.M. Hassey, and D. Romaker. 2014. The bigger the better: determining nephron size in kidney. *Pediatr Nephrol*. 29:525-530.

Wiggins, R.C. 2007. The spectrum of podocytopathies: a unifying view of glomerular diseases. *Kidney Int*. 71:1205-1214.

Witzgall, R. 2017. Nail-patella syndrome. *Pflugers Arch*. 469:927-936.

Yanagida-Asanuma, E., K. Asanuma, K. Kim, M. Donnelly, H. Young Choi, J. Hyung Chang, S. Suetsugu, Y. Tomino, T. Takenawa, C. Faul, and P. Mundel. 2007. Synaptopodin protects against proteinuria by disrupting Cdc42:IRSp53:Mena signaling complexes in kidney podocytes. *Am J Pathol*. 171:415-427.

Yang, L., L. Wang, and Y. Zheng. 2006. Gene targeting of Cdc42 and Cdc42GAP affirms the critical involvement of Cdc42 in filopodia induction, directed migration, and proliferation in primary mouse embryonic fibroblasts. *Mol Biol Cell*. 17:4675-4685.

Yang, N., O. Higuchi, K. Ohashi, K. Nagata, A. Wada, K. Kangawa, E. Nishida, and K. Mizuno. 1998. Cofilin phosphorylation by LIM-kinase 1 and its role in Rac-mediated actin reorganization. *Nature*. 393:809-812.

Yaoita, E., Y. Yoshida, M. Nameta, H. Takimoto, and H. Fujinaka. 2018. Induction of interdigitating cell processes in podocyte culture. *Kidney Int*. 93:519-524.

Yu, H., S. Chakravorty, W. Song, and M.A. Ferenczi. 2016. Phosphorylation of the regulatory light chain of myosin in striated muscle: methodological perspectives. *Eur Biophys J*. 45:779-805.

Yu, H., M. Konigshoff, A. Jayachandran, D. Handley, W. Seeger, N. Kaminski, and O. Eickelberg. 2008. Transgelin is a direct target of TGF-beta/Smad3-dependent epithelial cell migration in lung fibrosis. *FASEB J*. 22:1778-1789.

Zaleska, M., C. Fogl, A.L. Kho, A. Ababou, E. Ehler, and M. Pfuhl. 2015. The Cardiac Stress Response Factor Ms1 Can Bind to DNA and Has a Function in the Nucleus. *PLoS One*. 10:e0144614.

Zeidan, A., K. Sward, I. Nordstrom, E. Ekblad, J.C. Zhang, M.S. Parmacek, and P. Hellstrand. 2004. Ablation of SM22alpha decreases contractility and actin contents of mouse vascular smooth muscle. *FEBS Lett*. 562:141-146.

Zenker, M., T. Aigner, O. Wendler, T. Tralau, H. Muntefering, R. Fenski, S. Pitz, V. Schumacher, B. Royer-Pokora, E. Wuhl, P. Cochat, R. Bouvier, C. Kraus, K. Mark, H. Madlon, J. Dotsch, W. Rascher, I. Maruniak-Chudek, T. Lennert, L.M. Neumann, and A. Reis. 2004. Human laminin beta2 deficiency causes congenital nephrosis with mesangial sclerosis and distinct eye abnormalities. *Hum Mol Genet*. 13:2625-2632.

Zhang, J.C., S. Kim, B.P. Helmke, W.W. Yu, K.L. Du, M.M. Lu, M. Strobeck, Q. Yu, and M.S. Parmacek. 2001. Analysis of SM22alpha-deficient mice reveals unanticipated insights into smooth muscle cell differentiation and function. *Mol Cell Biol*. 21:1336-1344.

Zhao, Z., and E. Manser. 2015. Myotonic dystrophy kinase-related Cdc42-binding kinases (MRCK), the ROCK-like effectors of Cdc42 and Rac1. *Small GTPases*. 6:81-88.

Zhu, L., R. Jiang, L. Aoudjit, N. Jones, and T. Takano. 2011. Activation of RhoA in podocytes induces focal segmental glomerulosclerosis. *J Am Soc Nephrol*. 22:1621-1630.

Zigmond, S.H., M. Evangelista, C. Boone, C. Yang, A.C. Dar, F. Sicheri, J. Forkey, and M. Pring. 2003. Formin leaky cap allows elongation in the presence of tight capping proteins. *Curr Biol*. 13:1820-1823.

7. List of abbreviations

In general, abbreviations of proteins and genes of human origin are written in capital letters, while murine genes and proteins start with a capital letter. Genes are moreover written in italics.

A

A	Absorbance
aa	Amino acid
ABD	Actin-binding domain
ABLIM	Actin-binding LIM protein
Abra	Actin-binding Rho-activating
ACTN	α-actinin
ADCK	AarF domain containing kinase
ADF	Actin-depolymerizing factor
ADP	Adenosine -5'-diphosphate
ANLN	Anillin actin-binding protein
aPKC	Atypical protein kinase C
APS	Ammonium persulfate
Arf	ADP-ribosylation factor
ARHGAP	Rho GTPase activating protein
ARHGDIA	Rho GDP dissociation inhibitor alpha
Arl4c	Arf-like 4c
Arl7	Arf-like 7 Synonym: Arl4c
ARNO	Arf nucleotide-binding site opener
ARP	Actin-related protein
ARPC	Actin-related protein complex
ATP	Adenosine-5'-triphosphate

B

B	Barbed end
β	Mass concentration
β-T	β-tail domain
bp	Base pairs
BS	Bowman space
BSA	Bovine serum albumin

C

$CaCl_2$	Calcium chloride
CaM	Calmodulin
CaMKII	Ca^{2+}/calmodulin-dependent protein kinase
CapZ	Capping protein (actin filament) muscle Z-line
CASK	Calcium/calmodulin-dependent serine protein kinase
CBP	CREB-binding protein
CD151	Cluster of differentiation 151
CD2AP	CD2 associated protein
Cdc42	Cell division cycle 42
CFH	Complement factor H
CH	Calponin homology
CL	Capillary lumen
CLIK	Calponin like module
CNBr	Cyanogen bromide
CO_2	Carbon dioxide
COL4	Collagen type IV
COQ2	Coenzyme Q2, polyprenyltransferase
COQ6	Coenzyme Q6, monooxygenase
CRB2	crumbs 2, cell polarity complex component
Cyto D	Cytochalasin D

D

DABCO	1,4 Diazabicyclo[2.2.2]octan
DAPI	4’,6-Diamidin-2-phenylindol
dd	Double distilled
DGKE	diacylglycerol kinase epsilon
DMEM	Dulbecco’s modified eagle medium
DMSO	Dimethylsulfoxide
DNA	Deoxyribonucleic acid
dNTP	Deoxynucleotide triphosphate
DOCK1	dedicator of cytokinesis 1
Dox	Doxycycline
DSTN	Destrin Synonym: ADF

E

ε	Extinction coefficient
E1-4	Epidermal growth factor modules 1-4
EC	Endothelial cells
ECM	Extracellular matrix
EDTA	Ethylenediaminetetraacetic acid
EGF	Epidermal growth factor
EGFP	Enhanced green fluorescent protein
ELC	Essential light chain
ELMO	Engulfment and cell motility
EMP	Epithelial membrane protein
ER	Estrogen receptor
ERRα	Estrogen-related receptor alpha
et al.	latin: et alia and others
etc.	latin et ceterea and so on
EtOH	Ethanol

F

FACS	Fluorescence assisted cell sorting
F-actin	Filamentous actin
FAK	Focal adhesion kinase
FAT1	FAT atypical cadherin 1
FC	Flow cytometry
FCS	Fetal calf serum
FDG6	FYVE, RhoGEF and PH domain-containing 6
FH	Formin homology
FLAT	FAR linked AT-rich
FLNa	Filamin-A
floxed / fl	Flanked by loxP
FOV	Field of view
FP	Foot processes
FPE	Foot process effacement
FRAP	Fluorescence recovery after photobleaching
FSC	Forward scatter
FSGS	Focal segmental glomerulosclerosis

G

G-actin	Globular actin
GAP	GTPase activating protein
Gapdh	Glyceraldehyde 3-phosphate dehydrogenase
GBM	Glomerular basement membrane
Gdf	Growth differentiation factor
GDI	Guanine nucleotide dissociation inhibitor
GDP	Guanosine-5'-diphosphate
GEF	Guanine nucleotide exchange factor
GFB	Glomerular filtration barrier
GKLF	Gut-enriched Krüppel-like factor
Glepp	glomerular epithelial protein
GPCR	G-protein coupled receptor
GTP	Guanosine-5'-triphosphate

H

h	Human (*homo sapiens*)
H_2O	Water
HA	Human influenza hemagglutinin
HBSS	Hanks' balanced salt solution
HCl	Hydrogen chloride
hCMV	Human cytomegalovirus
HEPES	4-(2-hydroxyethyl)-1-piperazineethanesulfonic acid
hPCL	Human podocyte cell line
HRP	Horseradish peroxidase
HSPG	Heparan sulfate proteoglycan
Hyb	Hybrid domain

I

-i	-inhibitor
IF (Cryo/P)	Immunofluorescence (cryosections/paraffin)
IL	Interleukin
ILK	Integrin linked kinase
INF2	Inverted formin 2
IPTG	Isopropyl-β-D-1-thiogalactopyranoside
IQGAP	IQ motif containing GTPase activating protein
ITGA	integrin alpha
ITS	Insulin-transferrin-selenium
IκBα	Inhibitor of kappa B

J

JAM4	Junctional cell adhesion molecule 4

K

KANK	KN motif and ankyrin repeat
KCl	Potassium chloride
K_D	Dissociation constant
KH_2PO_4	Potassium dihydrogen phosphate
KO	knock-out

L

l	Length
LAMB2	Laminin, beta 2
LB	Lysogeny broth
LC-1	Luciferase-Cre-1
LIMK	LIM domain-containing protein kinase
LMX1A	LIM homeobox transcription factor 1 alpha
LMX1B	LIM homeobox transcription factor 1 beta
LPA	Lysophosphatidic acid

M

m	Murine (*mus musculus*)
MAGI	Membrane-associated guanylate kinase, WW and PDZ domain-containing protein
MAPK	Mitogen-activated protein kinase
MC	Mesangial cells
mDia1	Diaphanous-related formin 1
MEF2	Myocyte enhancer factor 2
mG	Membrane-targeted EGFP
$MgCl_2$	Magnesium chloride
MLC	Myosin light chain
MLCK	Myosin light chain kinase
MLCP	Myosin light chain phosphatase
MRCK	Myotonic dystrophy kinase-related Cdc42-binding kinase
MRTF-A	Myocardin-related transcription factor-A
Ms1	Myocyte stress-1 Synonym: Abra
mT	Membrane-targeted tdTomato
MTTL1	Mitochondrially encoded TRNA leucine 1
MYH9	Myosin heavy chain 9
MYO1E	Myosin IE

N

n. s.	Not significant
Na_2HPO_4	Disodium hydrogen phosphate
$Na_3C_3H_5(COO)_3$	Trisodium citrate
NaAc	Sodium acetate
NaCl	Sodium chloride
$NaHCO_3$	Sodium hydrogen carbonate
NaOH	Sodium hydroxide
NCK	Non-catalytic region of tyrosine kinase adaptor protein
NF-κB	Nuclear factor kappa-light-chain-enhancer of activated B-cells
$NiSO_4$	Nickel sulfate
NPF	Nucleation promoting factor
NPHS2	Nephrosis 2, idiopathic, steroid-resistant (Podocin)
NPS	Nail-patella syndrome
NUP	Nucleoporin
N-Wasp	Neural Wiskott-Aldrich syndrome protein

O

o/n	Over night
OD	Optical density

P

P	Pointed end
p-	Plasmid- Phospho-
pA	Polyadenylation sequence
PAGE	Polyacrylamide gel electrophoresis
PAK	p21-associated kinase
Par6	Partitioning defective 6 homolog
PBS	Phosphate buffered saline
PBS^{++}	Phosphate buffered saline, supplemented with Mg^{2+} and Ca^{2+}
pCA	Cytomegalovirus enhancer
PCR	Polymerase chain reaction
PDSS2	Decaprenyl diphosphatase synthase subunit 2
PEI	Polyethylenimine
PFA	Paraformaldehyde
PI	Propidium iodide
PINCH	Particulary interesting new cysteine-histidine-rich protein
PKCδ	Protein kinase C delta type
PLCE1	Phospholipase C epsilon 1
PMSF	Phenylmethane sulfonyl fluoride
Psi	Plexin-semaphorin-integrin
PTB	Phosphotyrosine binding
PTPRO	Protein tyrosine phosphatase, receptor type O
PVA	Poly(vinyl alcohol)
PVDF	Polyvinylidene fluoride

R

r	Rat (*rattus norvegicus*)
Rac	Ras-related C3 botulinum toxin substrate
Rac	Ras-related C3 botulinum toxin substrate
Rho	Ras homology
RLC	Regulatory light chain
RNA	Ribonucleic acid
m-	messenger
mi-	micro
si-	small interfering
Robo2	Roundabout guidance receptor 2
ROCK	Rho kinase
RT	Room temperature
RTK	Receptor tyrosine kinase
rtTA	Reverse tetracycline-controlled transcriptional transactivator

S

SCARB2	Scavenger receptor class B member 2
SD	Slit diaphragm standard derivation
SDS	Sodium dodecyl sulfate
SEM	Scanning electron microscopy
Sm22	Smooth muscle 22 Synonym: transgelin
Smad3	Mothers against decapentaplegic homolog 3
SMARCAL 1	SWI/SNF related, matrix associated, actin dependent regulator of chromatin, subfamily A like 1
SRF	Serum response factor
SSH	Slingshot phosphatase
STARS	Striated muscle activator of Rho signaling Synonym: Abra
SV40	Simian virus 40
SYNPO	Synaptopodin

T

TAE	Tris, acetic acid, EDTA
TBS	Tris buffered saline
TBS-T	Tris buffered saline, supplemented with 0.1 % Tween 20
Tcf4	Ets1/T-cell factor 4
tdtomato	Tandem dimer tomato protein
TE	Tris-EDTA
TEM	Transmission electron microscopy
TEMED	Tetramethylethylenediamine
TetO	Tet operon
TG	Transgene
TGF-β	Transforming growth factor β
Tris base	Tris(hydroxymethyl)aminomethane
TRPC6	Transient receptor potential cation channel subfamily C member 3

U

uPAR	Urokinase-type plasminogen activator receptor
UTR	untranslated region

V

V	Volume
VEGF	Vascular endothelial growth factor
VSMC	Vascular smooth muscle cells

W

WASP	Wiskott-Aldrich syndrome protein
WAVE	WASP-family verprolin homologous protein
WB	Western blot
WDR73	WD repeat domain 73
Wnt	Wingless-type MMTV integration site family
WT	Wild-type
WT1	Wilms tumor 1

X

XPO5	Exportin 5

Z

ZO-1	Zonula occludens-1

8. Appendix

Appendix 8.1: ImageJ macro for measuring mean phalloidin intensity within an outlined glomerulus.

```
1  title = getTitle();
2  run("Set Measurements...", "area mean limit display redirect=None decimal=0");
3  run("Stack to Images");
4  selectWindow("Ch2-T3");
5  rename("Intensity - "+title+"");
6  run("Subtract Background...", "rolling=500");
7  run("Grays");
8  setTool("polygon");
9  waitForUser("Outline Glomerulus");
10 run("Measure");
11 run("Add Selection...");
12 selectWindow("ChS1-T2");
13 rename("Area - "+title+"");
14 run("Enhance Contrast...", "saturated=0.01 normalize");
15 run("Restore Selection");
16 run("Add Selection...");
17 run("Images to Stack", "name=+title+ title=[] use");
18 run("Grays");
19 saveAs("Tiff", "[Path]/"+title+"");
20 close();
```

Appendix 8.2: ImageJ macro for parallel quantification of mean phalloidin and mean transgelin intensities within green fluorescent podocytes

```
1  title = getTitle();
2  run("Options...", "iterations=1 count=1 black");
3  run("Set Measurements...", "area mean modal min limit display scientific redirect=None
   decimal=0");
4  run("Input/Output...", "jpeg=85 gif=-1 file=.tsv use_file copy_row save_column save_row");
5  run("Stack to Images");
6  selectWindow("Ch1-T1");
7  close();
8  selectWindow("ChS1-T2");
9  rename("Area - "+title+"");
10 run("Find Edges");
11 run("Median...", "radius=3");
12 run("8-bit");
13 run("Auto Threshold", "method=Triangle white");
14 run("EDM Binary Operations", "iterations=2 operation=open");
15 run("EDM Binary Operations", "iterations=5 operation=close");
16 run("Analyze Particles...", "size=1000-Infinity display exclude include add");
17 close();
18 selectWindow("ChS2-T3");
19 run("Subtract Background...", "rolling=1000");
20 rename("Transgelin - "+title+"");
21 roiManager("Measure");
22 close();
23 selectWindow("Ch2-T4");
24 run("Subtract Background...", "rolling=1000");
25 rename("Phalloidin - "+title+"");
26 roiManager("Measure");
27 close();
28 roiManager("Save", "[Path]/RoiSet - "+title+".zip");
29 roiManager("Delete");
```

Appendix 8.3: ImageJ macro for quantification of mean active β_1-Integrin intensity within green fluorescent podocytes.

```
1  title = getTitle();
2  run("Options...", "iterations=1 count=1 black");
3  run("Set Measurements...", "area mean modal min limit display scientific redirect=None
   decimal=0");
4  run("Input/Output...", "jpeg=85 gif=-1 file=.tsv use_file copy_row save_column save_row");
5  run("Stack to Images");
6  selectWindow("Ch1-T1");
7  close();
8  selectWindow("ChS1-T2");
9  rename("Area - "+title+"");
10 run("Find Edges");
11 run("Median...", "radius=3");
12 run("8-bit");
13 run("Auto Threshold", "method=Triangle white");
14 run("EDM Binary Operations", "iterations=2 operation=open");
15 run("EDM Binary Operations", "iterations=2 operation=close");
16 run("Analyze Particles...", "size=800-Infinity display exclude include add");
17 close();
18 selectWindow("Ch2-T3");
19 rename("9EG7 - "+title+"");
20 run("Subtract Background...", "rolling=1000");
21 roiManager("Measure");
22 close();
23 roiManager("Save", "[Path]/RoiSet - "+title+".zip");
24 roiManager("Delete");
```

Appendix 8.4: ImageJ macro for quantification of mean pMLC intensity within transgelin-marked hPLC cells.

```
1  title = getTitle();
2  run("Options...", "iterations=1 count=1 black");
3  run("Set Measurements...", "area mean modal min limit display scientific redirect=None
   decimal=0");
4  run("Input/Output...", "jpeg=85 gif=-1 file=.tsv use_file copy_row save_column save_row");
5  run("Stack to Images");
6  selectWindow("c:3/3 - mCherry/EGFP/Dapi");
7  close();
8  selectWindow("c:2/3 - mCherry/EGFP/Dapi")
9  rename("Area - "+title+"");
10 run("Median...", "radius=3");
11 run("Subtract Background...", "rolling=400");
12 run("8-bit");
13 run("Auto Threshold", "method=Li white");
14 run("Analyze Particles...", "size=50000-Infinity pixel exclude include add");
15 close();
16 selectWindow("c:1/3 - mCherry/EGFP/Dapi");
17 run("Properties...", "channels=1 slices=1 frames=1 unit=µm pixel_width=0.1612500
18 pixel_height=0.1612500 voxel_depth=1.0000000");
19 rename("pMLC - "+title+"");
20 run("Subtract Background...", "rolling=250");
21 roiManager("Measure");
22 close();
23 roiManager("Delete");
```

Appendix 8.5: Macro for determination of primary podocyte circularity and roundness.

```
1   title = getTitle();
2   run("Options...", "iterations=1 count=1 black");
3   run("Set Measurements...", "area shape limit redirect=None decimal=2");
4   run("Specify...", "width=7146 height=7146 x=5180 y=4267 slice=1 centered");
5   run("Duplicate...", "title=1");
6   run("Select None");
7   run("Median...", "radius=4");
8   run("Subtract Background...", "rolling=100");
9   run("Unsharp Mask...", "radius=2 mask=0.50");
10  run("8-bit");
11  run("Duplicate...", " ");
12  run("Auto Threshold", "method=Triangle white");
13  run("EDM Binary Operations", "iterations=1 operation=close");
14  run("Analyze Particles...", "size=950-Infinity show=Nothing display exclude clear add");
15  selectWindow("1");
16  run("Enhance Contrast...", "saturated=0.1 normalize");
17  run("From ROI Manager");
18  run("Flatten");
19  saveAs("Tiff", "[Path]\\Overlay - "+title+"");
20  saveAs("Results", "[Path]\\Results -"+title+".csv");
21  roiManager("Save", "[Path]\\Roi - "+title+".zip");
22  selectWindow("1");
23  close();
24  selectWindow("1-1");
25  close();
26  selectWindow(""+title+"");
27  close();
28  roiManager("Delete");
29  }
```

Please note that the macro for determination of the cell area is identical except that line 14 is replaced by *run("Analyze Particles...", "size=950-Infinity circularity=0.60-1.00 display exclude clear add");* or *run("Analyze Particles...", "size=950-Infinity circularity=0.10-1.00 display exclude clear add");* in case of fixation after overnight incubation.

Appendix 8.6: ROIs used for quantification of the EGFP positive area in cytochalasin D time series experiments.

Width	Height	Center x	Center y
2000	1500	1100	1000
2000	1500	3100	1000
2000	1500	1100	2500
2000	1500	3100	2500

Appendix 8.7: Macro to obtain the EGFP positive area of certain ROIs used for cytochalasin D experiments.

```
1  macro "Spreading/Shrinking [1]" {
2  title = getTitle();
3  run("Options...", "iterations=1 count=1 black");
4  run("Median...", "radius=2 stack");
5  run("Subtract Background...", "rolling=360 sliding stack");
6  run("Enhance Contrast...", "saturated=0.02 process_all");
7  run("Set Measurements...", "area limit redirect=None decimal=0");
8  run("Auto Threshold", "method=Li white stack");
9  roiManager("Open", "[Path]/RoiSet.zip");
10 roiManager("Multi Measure");
11 saveAs("Results", "[Path]\\Results -"+title+".csv");
12 run("Close");
13 roiManager("Delete");
14 close();
15 }
```

Appendix 8.8: Gate setup used for flow cytometric analysis of active β1-integrin of glomerular cells

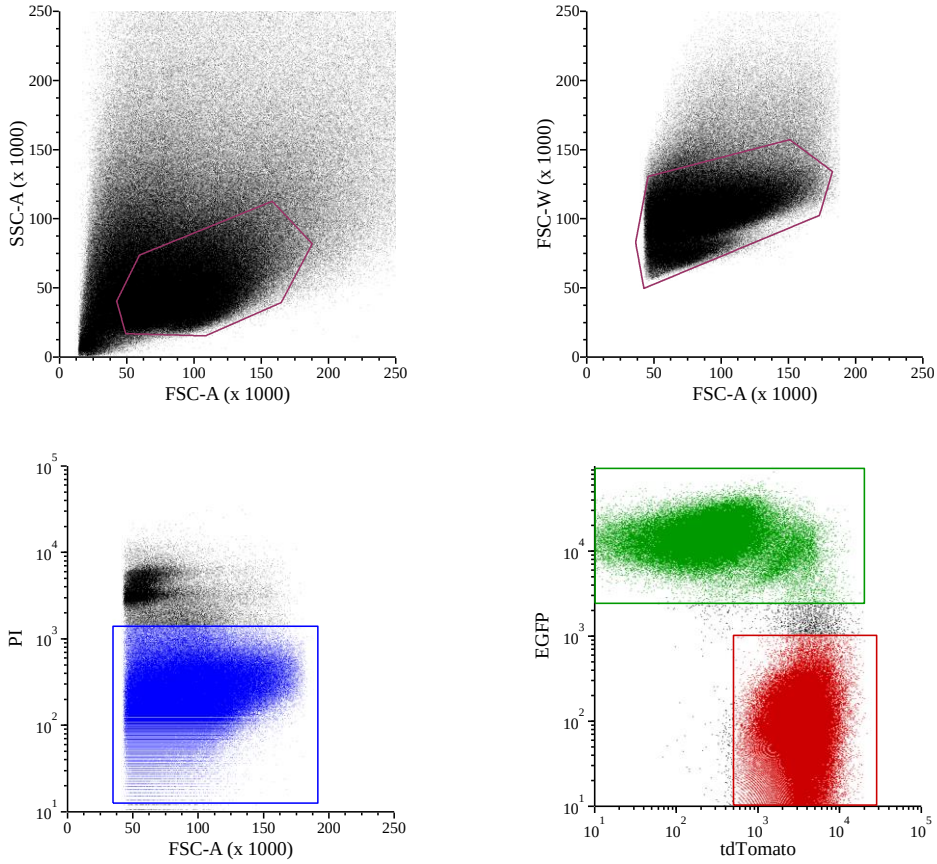

9. Acknowledgement

At the end of my thesis I want to thank all those peoples who helped and supported me during all the time from the very beginning to the end of this thesis.

Foremost, I want to thank Prof. Dr. Ralph Witzgall for giving me, as a chemist, the opportunity to work on the very interesting LMX1B project, and for his patience, support and advice throughout the thesis.

I am thankful to my mentoring team: Prof. Dr. Eugen Kerkhoff and Prof. Dr. Thomas Dresselhaus for their valuable advice and suggestions.

Special thanks to Dr. Tillmann Burghardt, who helped me a lot to learn all the background knowledge and techniques. Also special thanks to Dr. Melanie Zaparty, who always was open for discussions about the topic and provided lots of good suggestions and ideas.

I am deeply grateful for all the help of Marion Kubitza in everyday laboratory work and the great support in technical questions. I am also very thankful to Marina Wuttke who assisted me a lot at the laboratory work. Both of them were of great help especially in glomeruli isolation and tissue preparation.

I also want to express my gratitude to Kerstin Hermann, Olga Maier, and Helga Othmen for help and support.

I want to thank my current and former fellow PhD students Dr. Susanne Baumgarten, Dr. Natalya Stepanova, Nenja Bauer, Korbinian Bürger, Markus Dietz, Lisa Lucke, Sandra Meißinger, Kathrin Pohl, and Benjamin Salecker for creating a great atmosphere and moral support. Special thanks to Dr. Susanne Baumgarten for answering all of my questions.

My gratitude is extended to all the current and former members of Prof. Witzgalls group for the pleasant atmosphere I experienced in the past four years: Prof. Dr. Reinhard Rachel, Dr. Karin Barbinger, Dr. Melanie Grosch, Dr. Kerstin Schmidt, Anita Hecht, Edeltraud Lautenschlager, Ton Maurer, Christine Meese, Carina Mirbeth, Larissa Osten, Karin Schadendorf, Ludwig & Petra Utz, Uwe de Vries, Yulia Zaytseva, and Antje Zenker.

Last but not least I want to thank my parents, Heidi and Konrad Setzer, and most of all Nadine Schwab for all her love, support and patience throughout all of these years.

Eidesstattliche Erklärung

Ich erkläre hiermit an Eides statt, dass ich die vorliegende Arbeit ohne unzulässige Hilfe Dritter und ohne Benutzung anderer als der angegebenen Hilfsmittel angefertigt habe; die aus anderen Quellen direkt oder indirekt übernommenen Daten und Konzepte sind unter Angabe des Literaturzitats gekennzeichnet.

Bei Auswahl und Auswertung folgenden Materials haben mir die in der Arbeit genannten Personen in der jeweils beschriebenen Weise unentgeltlich geholfen.

Weitere Personen waren an der inhaltlich-materiellen Herstellung der vorliegenden Arbeit nicht beteiligt. Insbesondere habe ich hierfür nicht die entgeltliche Hilfe eines Promotionsberaters oder anderer Personen in Anspruch genommen. Niemand hat von mir weder unmittelbar noch mittelbar geldwerte Leistungen für Arbeiten erhalten, die im Zusammenhang mit dem Inhalt der vorgelegten Dissertation stehen.

Die Arbeit wurde bisher weder im In- noch im Ausland in gleicher oder ähnlicher Form einer anderen Prüfungsbehörde vorgelegt.

……

Markus Setzer